UNIVERSITY OF CRANFIELD

BERNARD O'CONNOR

High Strain Deformation and Ultimate Failure of HIPS and ABS Polymers

SCHOOL OF INDUSTRIAL AND MANUFACTURING SCIENCE

PhD THESIS

1997

CRANFIELD UNIVERSITY

SCHOOL OF INDUSTRIAL AND MANUFACTURING SCIENCE

PhD THESIS

1997

BERNARD O'CONNOR

High Strain Deformation and Ultimate Failure of HIPS and ABS Polymers

Supervisor: Prof. Clive Brian Bucknall

This thesis is submitted in partial fulfilment of the requirements for the degree of PhD.

ABSTRACT

The role of the rubber particle in the ultimate failure of High Impact Polystyrene and Acrylonitrile Butadiene Styrene was investigated by modifying the rubber content and the shear modulus of the rubber phase in the materials. The rubber content in a commercial grade HIPS and a commercial grade ABS, both with 8 wt. % rubber, was varied by blending with general purpose polystyrene and general purpose poly(styrene-acrylonitrile) respectively. The shear modulus of the rubber phase was varied through blending the materials with sulfur or irradiating the materials with gamma irradiation. Dynamical mechanical thermal analysis confirmed that the T_g of the rubber phase increased with increasing sulfur content. It was found that with decreasing rubber content or increasing rubber shear modulus, the yield, flow and breaking stresses and the elastic modulus of the composite increased, while the failure strain decreased.

In a similar experiment to Sjoerdsma and Boyens (1994), the statistics of failure of the materials were investigated with respect to rubber content and rubber shear modulus. Batches of specimens numbering not less than 20 were extended under a constant applied stress until failure occurred. A custom designed creep rig was built to carry out several long term creep tests simultaneously. From these tests it was concluded that the probability of failure increased as the stress on the rubber increased and underpinning this, is a novel discussion of the high strain deformation and the mechanism controlling failure in HIPS and ABS. This conclusion was discussed in terms of rubber content and rubber shear modulus and a model was developed which describes the maximum failure strain in terms of these variables. The level of applied stress was also found to have an effect on the probability of failure.

It was found that the success achieved by Sjoerdsma and Boyens (1994), in correlating failure strain data for a single grade of HIPS, could not be repeated when their model was applied to another grade of HIPS. The two–parameter Weibull equation gave an improved correlation between the failure of HIPS and the strain on the material. Analysis of the relationship between the experimental failure strain distribution and the Weibull distribution revealed that the mean stress on the rubber phase at failure may be a better basis for achieving a Weibull distribution.

ACKNOWLEDGEMENTS

This thesis would not have been possible without the support and assistance of the following people. Dr. Jerry Hahnfeld and the Dow Chemical company are gratefully acknowledged for the support of this program and the donation of materials. The technical advice and assistance of Mr. Peter Logan and Mr. Don Woolnough was invaluable to the success of the program, and the friendship extended from these and the rest of the polymer group was instrumental in my enjoyment of the last three years. I would like to thank Herr Joachim Laatsch and Dr. Robert Cieslinski for permission to use some of their micrographs, and Mr. Keith Lovell for irradiating specimens at short notice. I would especially like to thank an understanding supervisor, Prof. Clive Bucknall, whose patience and insight guided me past the many obstacles encountered, and for endeavouring to improve my technical writing.

The support and reassurance, in their many forms, of my parents, family and friends are also gratefully acknowledged. In particular I wish to thank my girlfriend, Sara Hayden, to whom this thesis is dedicated, for the sacrifices she has made, and the love and encouragement she has given me throughout the last three years.

TABLE OF CONTENTS:

TABLE OF FIGURES:

TABLES:

LIST OF SYMBOLS:

A_{eff}	effective area
α	Weibull scale parameter
β	Weibull shape parameter
C_r	concentration of rubber
C_f	concentration of rubber unfibrillated
C_{risk}	concentration of rubber at risk
χ	fraction of rubber which dilatates and initiates crazes
δ_r	fractional contribution of rubber dilatation to total dilatation
δ_c or δ_{cr}	fractional contribution of craze dilatation to total dilatation
ΔC_f	fractional change in the volume of the composite due to dilatation of the rubber
ΔH	enthalpy barrier
ΔV_t	total change in volume
ΔV_r	change in volume of rubber phase
ΔV_c	change in volume due to crazing
ε_{cr}	craze strain
ε_p	plastic strain
ε_{fr}	plastic strain at failure
ε_{max}	maximum recorded failure strain
ε_{min}	minimum recorded failure strain
ε_{rm}	mean strain on the rubber phase
E	elastic modulus
ϕ or ϕ_r	rubber particle volume fraction
γ	stress concentration factor
G_r	rubber shear modulus
k	Sjoerdsma and Boyens proportionality constant
k	rubber fibrillation conversion constant
λ	extension ratio
λ_{max} or λ_{rx}	maximum extension ratio of rubber
Γ	specific surface energy
η	concentration of rubber to sulfur

K_r	bulk modulus
μ	arithmetic mean
P_{nf}	probability of survival (non-failure)
P_f	probability of failure
σ_{app}	stress applied to composite
σ_y	yield stress
σ_f	flow stress
σ_r	stress on the rubber phase
σ_m	stress on the matrix
T_{fr}	time to fracture
τ	induction time
T_g	glass transistion temperature
U_v	volumetric stored energy in the rubber particle
U_D	energy potential between craze propagation and initiation
U_P	energy to thicken a craze
U_I	energy to nucleate a craze
V_r	volume of rubber
V_{uf}	volume of rubber unfibrillated
V_m	volume of matrix
V_r	volume of rubber
V_t	total volume
V_L	primordial volume of layer of rubber fibrils

1. Introduction

While rubber toughened polymers are used in many applications in everyday life, the exact role of the rubber particle in enhancing the fracture toughness of the material is still not fully understood. Polymers such as polystyrene and poly(styrene-acrylonitrile) are typically glassy, and fracture at strains of about 0.02. The addition of rubber particles to the material, while compromising the flow stress, greatly increases the strain at failure. However the mechanisms through which failure is delayed are not clear. Modification of parameters such as rubber content and cross-link density, particle morphology and size, and the rubber/matrix interfacial adhesion, can significantly affect the mechanical behaviour of the material (Bucknall, 1977 and Kinloch and Young, 1983).

High Impact Polystyrene (HIPS) and Acrylonitrile Butadiene Styrene (ABS) are two of the most renowned and commonly used rubber toughened polymers in existence. These materials deform through dilatational mechanisms such as multiple crazing of the matrix (Bucknall and Smith, 1965) and fibrillation of the rubber particles (Buckley, 1991), but also, more in the case of ABS, deform through shear deformation of the matrix. These mechanisms interact in a complicated manner to produce the observed mechanical behaviour of the composite. Crazing and rubber fibrillation are evident in Figure 1-1. The dark rings consist of rubber, which surround hard matrix inclusions. The bright white areas, are voids within the rubber and these voids are separated by rubber fibrils, thus maintaining the structure of the particle. The area separating the rubber particles, in this case, is polystyrene, and crazes are evident within the polystyrene as the long thin crack-like structures.

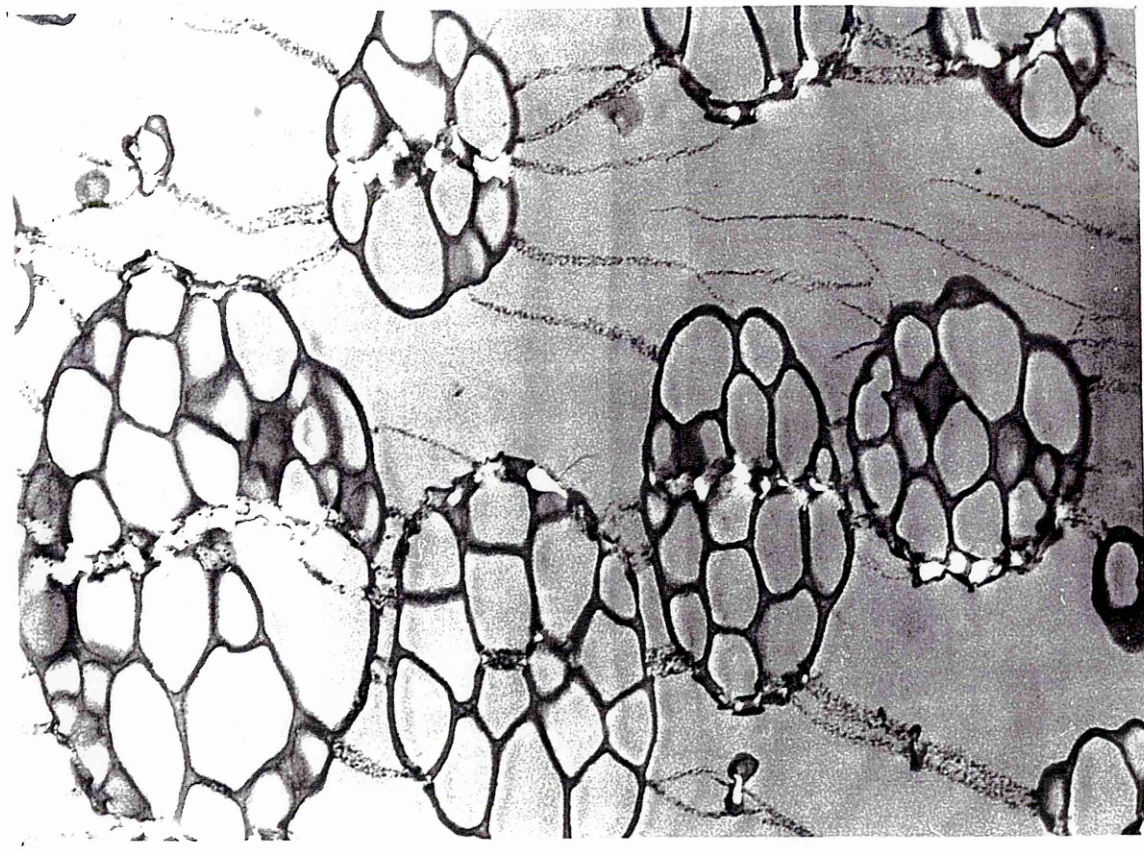

Figure 1-1. Post-mortem section of HIPS8. (0.5μm ———) (σ_{app} ↓)

There were two objectives in this study. One was to gain insight into high strain deformation of HIPS and ABS through changing one or more of the aforementioned material parameters, and the other objective was to identify the mechanism controlling final rupture of these materials. One of the difficulties in changing one of the material parameters, is that the other parameters may not remain constant. For example increase in the rate of agitation during manufacture will reduce the average particle size, but it may also change the morphology of the particle. The material parameters varied in this study were rubber content and rubber cross-link density. The variation in rubber content was achieved through compounding neat rubber toughened polymer with an unfilled

resin of similar molecular weight. As the rubber in the parent material is slightly cross-linked, the particles remain intact during the compounding process (Correa, 1990). The rubber cross-link density was varied in two ways. The principal way was to blend the composite with sulfur, and the second way was to gamma irradiate the composite. In this way the rubber morphology, size, content etc. remain unchanged, but the rubber cross-link density is increased. The effects of introducing these variables to the system, were examined with respect to high strain deformation of the materials. A third material was also investigated, namely Advanced Impact Modifier (AIM), which consists of a polystyrene matrix toughened with core shell rubber particles.

The structure of the thesis is as follows. The literature is reviewed in Chapter 2, followed by an account of the experimental procedures in Chapter 3. Presented in Chapters 4 and 5, are results demonstrating the effects of decreasing rubber content and increasing rubber cross-link density respectively, on the constant strain rate, creep and probability of failure behaviour of HIPS. Chapter 6 illustrates the effects of both preloading and irradiation, on the fracture probability of HIPS. Chapters 7 and 8 introduce the effects of decreasing rubber content and increasing rubber cross-link density respectively, on the constant strain rate, creep and probability of failure behaviour of ABS. Chapter 9 presents results for AIM. This leads to a discussion of the results. It was thought simpler to discuss the mechanisms controlling deformation initiation and percolation in terms of the well known standard tensile test, and so this is done in Chapter 10. This underpins the discussion in Chapter 11 of deformation percolation under creep conditions and the mechanism controlling failure in HIPS, ABS and AIM. Some models and methods describing the failure mechanisms observed in HIPS and ABS are illustrated in Chapter 12.

2. LITERATURE REVIEW

2.1 Crazing

Crazes are formed in tension at strains between 0.3 and 0.7 % depending on strain rate (Bucknall, 1967). The craze is oriented approximately normal to the tensile stress, and the material in the craze (as evidenced by Sauer et al. in Kambour and Robertson, 1972) is highly oriented parallel to the tensile axis. The term crazing comes from the middle English term 'crasen' - to break, a term long associated with complex networks of cracks in ceramics and glasses. Early interpretation of the observation of reflecting crack-like structures in glassy polymers, resulted in workers using the terms 'craze cracking' and 'microcracking'. The earliest description of the morphology and growth of crazes was made in 1941 by Klemperer (in Kambour, 1973), but the clearest distinction between crazes and cracks was made in 1949 by Sauer et al. (in Kambour, 1973), who pointed out that crazes, even when formed across the whole cross-section of the specimen, can support loads of 20 MPa. Further clarification was achieved in the 1960's, when the development of optical and electron microscopy techniques led to a new understanding of the morphology of crazes. Crazes were still termed craze cracks until the workers Lebedev and Kevshinskii in 1961 and Spurr and Niegisch in 1962 revealed through light microscopy, that crazes consist of continuous polymer interconnecting the two interfaces of the craze (Kambour, 1973).

2.1.1 Craze tip nucleation and growth

Kambour and Robertson (1972) suggested that while craze initiation can occur at defects such as scratches and dirt particles in the material, imperfections are not

necessary for their initiation. They suggest that the uniformity of the structure of the craze produced under given conditions, together with the small size of holes in the early stages of craze growth, infer that the fundamental origin of this phenomenon might lie in the way the molecules are grouped together and their ability to undergo large amounts of plastic flow. These authors proposed that under triaxial tension, holes would spring open while the neighbouring molecules flow around them, resulting in the observed craze structure.

However, crazes are usually observed to nucleate at the surface of the sample, at defects such as surface grooves (Argon and Hannoosh, 1977), steps or dust particles (Kramer, 1983). Argon and Hannoosh also found that for highly perfect samples of polystyrene, the stress required to nucleate crazes increased substantially, indeed several specimens deformed by shear yielding and necking before crazing. The factors affecting craze formation include: temperature, stress, molecular orientation of the sample and thermal history of the material (Bucknall, 1977).

Sternstein and Ongchin (in Bucknall, 1977) proposed the earliest criterion for craze formation on the basis of biaxial stressing of PMMA. The criterion expressed in terms of a stress bias, incorporates two temperature dependent material parameters and the third principal stress is zero. Oxborough and Bowden in 1973, modified the Sternstein and Ongchin analysis and developed a more useful strain criterion incorporating the familiar material parameters of Young's modulus and Poisson's ratio. Matsuo et al. in 1972, investigated strain and strain energy criteria, and found that the strain criterion was more satisfactory in correlating the craze formation results. However these authors did not investigate a stress bias criterion and none of the aforementioned criteria has gained general acceptance (McCrum et al., 1988).

Gent (1970) proposed a craze initiation process whereby the applied tensile stress, when magnified by a flaw or nick in the material, is such that the material is transformed to its rubbery state through a reduction in its T_g. Cavitation and subsequent craze growth of this softened region, takes place under the action of the same dilatational stress component that formed it. Gent proposed that if the deformations were large enough prior to the material transforming to its rubbery state, then ductile yielding would take place.

Argon in 1975, proposed that craze formation occurs through the generation of 'microcavities' at surface grooves and imperfections. These voids are produced when microshear bands, initiated by shear stress and thermal motion, are restricted at molecular level plastic heterogeneities. When they are of a sufficient density to produce interactions, the cavities, undergo large scale plastic growth, coalesce through the elastically strained surroundings, and produce a visible craze nucleus. Argon and Hannoosh (1977) proposed that surface imperfections and flaws such as trapped dust particles were not necessary for craze nucleation, and only serve to accelerate the process.

The activated nature of craze initiation, growth and fracture was first shown by Regel in 1956 (in Bucknall, 1977), and later in 1973 by Kambour, who both showed that craze kinetics could be described using the Eyring relationship. Bucknall (1977) showed using the data of Maxwell and Rahm, that overall rates of crazing can be described using the Eyring relationship. This analysis revealed an estimated true activation energy of 175 kJ/mol, which when compared with 230 kJ/mol for the activation energy of thermal bond rupture in polystyrene, raised the question of whether stress-activated chain scission is a rate determining step in craze initiation and propagation. Other workers have also used the Eyring relationship to describe stress and temperature activated crazing and shear

processes, including Dekkers and Heikens (1985) who used it to describe the stress dependant strain rate of PS, PSAN and PC, all filled with glass beads.

Brown and Fisher (1975) however, showed that not all craze formation and growth rates could be described using the Eyring theory. They found in tests on polychlorotrifluoroethylene under constant stress in a liquid nitrogen environment, that the number of crazes formed increased rapidly with applied stress, but the relationship was not linear as predicted by Eyring theory. Also there was no indication of a time dependent initiation of crazes.

It is now generally accepted that the mechanism that correctly describes craze tip advance, is that proposed by Argon and Salama (1977). This mechanism is based on the Taylor (1950) meniscus instability mechanism, which was originally formulated to describe the behaviour of a liquid between two rigid plates when the plates are subsequently forcibly separated. In an earlier paper, Argon (1975) suggested that tip advance occurred through the repeated nucleation of micropores ahead of the craze tip, which plastically expand to form the craze structure. This proposal, when examined further, was found to have several shortcomings, and the process was found to be more completely described by the meniscus instability mechanism. Described qualitatively, the meniscus instability mechanism holds that as the craze tip extends, material enters the plastic zone at the craze tip, advances forward through the ever-increasing stress field until it reaches the polymer/air interface, where it undergoes a convolution process. The convolution process is one in which the yielded material at the polymer/air interface, is unstable to perturbations of a well-defined wavelength, breaks up and through repeated convolutions, results in the fibrillated structure. This process was modelled by Argon and Salama (1977) and has received general acceptance.

2.1.2 Craze fibril extension

In 1964(a,b) Kambour estimated using surface scratches on the specimen, elongations of 50 to 60 % for an unstressed craze. Further, using critical angles for internal reflection, this worker estimated polymer volume fractions of 40 to 60 % for an unstressed craze. The polymer content is closely approximated by $1/\lambda$, where λ is the extension of the craze; therefore polymer contents of 40 to 60 % correspond to extensions of 2.5 to 1.67. However in 1979 Lauterwasser and Kramer, in an exceptional piece of work, showed that for an isolated air craze grown at room temperature in thin solvent cast films of polystyrene, the craze fibril volume fraction was between 0.34 and 0.17, in good agreement with that quoted earlier the same year by Brown. These values, when averaged to 0.27 correspond to a λ of 3.7, have achieved general acceptance as the range of extension ratios of polystyrene air craze fibrils.

2.1.3 Craze fibril diameters

In 1979 Lauterwasser and Kramer quoted craze fibril diameters of about 15 nm. This was contrary to previous transmission electron microscopic measurements by Kambour and Holik (1969), Kambour and Russell (1971), Kambour and Robertson (1972) and Kambour (1973) on microtomed impregnated crazes, and by Beahan et al. (1971, 1972 and 1975) on crazes in thin (approx. 100 nm.) polystyrene films. These workers measured craze fibril diameters of 20 to 40 nm. Lauterwasser and Kramer attributed these larger fibril diameters to the impregnation of the crazes with liquid sulfur or iodine eutectic in the case of the experiments by Kambour and co-workers, and in the case of the thin film experiments, the absence of plastic constraint.

The difficulty in measuring fibril diameters is also heightened by the overlapping of fibril images in 'thick' films. This could be overcome by reducing

the film thickness, but as evidenced by Donald, Chan and Kramer (1981), crazes in films with thicknesses below ~ 150 nm, have a coarse perforated sheet structure which is unrepresentative of crazes in the bulk material. These workers measured fibril diameters in air crazes in polystyrene films of thickness > 150 nm using the method of Donald and Kramer (1981), who found that through tilting the specimen in the TEM, individual fibrils could be resolved. They measured fibril diameters of between 4 and 8 nm which when averaged to 6 nm, are in agreement with small angle X-ray scattering (SAXS) measurements of fibrils in air crazes in bulk specimens of polystyrene (Brown and Kramer, 1981).

2.1.4 Craze Thickening

While craze tip advance is responsible initially for generating very short fibrils, the majority of the fibril length must be generated by craze thickening. There are two main mechanisms of craze thickening, craze fibril creep and surface drawing. Craze fibrils arise through the convolution of the polymer/air interface, producing tufts of polymer joining the upper and lower surfaces of the craze. These fibrils, of diameter 6 nm, are extended and are load bearing (Donald, Chan and Kramer, 1981). As the craze thickens, these fibrils can extend further while maintaining the same primordial thickness, or they can pull fresh material out of the walls of the craze. The primordial thickness of the craze, is the original thickness of the slab of material which has been transformed into crazed material.

Lauterwasser and Kramer in their ground breaking paper in 1979, showed that measurement of any two of the quantities: craze thickness, craze primordial thickness, craze surface displacement or craze fibril volume fraction, allows the calculation of the other two. They found in experiments on thin films of polystyrene, that the primordial thickness of the craze increased approximately linearly with distance from the craze tip. This was reiterated in a later paper,

where Chan, Donald and Kramer (1981) examined the effects of film thickness on craze micromechanics. They again found, for the three film thicknesses they examined, that the thickness of the primordial profile increased with distance from the craze tip, and the fibril extension ratio decreased with distance from the craze tip.

A surface drawing mechanism would produce the observed extension ratio and primordial thickness profile. The extension ratios of the fibrils range from 3 at the centre of the craze, to 6 at the craze tip. This suggested the additional hypothesis, that the extension ratio of the fibrils is determined by the stress on them at the time they were drawn. This would explain the phenomenon of the craze midrib, the less dense region along the mid-plane of the craze. Beahan et al. (1972) proposed that the midrib is formed by an extra large set of holes at the craze tip, but it is rather more likely to be a result of the higher stress on the fibril when it is drawn from the bulk near the craze tip. The stress decreases with distance from the craze tip, resulting in lower fibril extension ratios in the centre of the craze.

Kramer et al. suggested that surface drawing of the craze occurs through drawing material from a thin strain-softened layer of material, denoted the 'active zone', located at the interface of the craze with the bulk material (Lauterwasser and Kramer, 1979 and Kramer, 1983). (The importance of the active zone became more apparent later with respect to craze breakdown). They were able to investigate the width of this layer, using a gold decoration technique previously used to detail polymer crystal surfaces. The process involved creating a sandwich of polymer/gold/polymer, the gold consisted of uniformly spaced particles approximately 8 nm in diameter. The sandwich was subsequently crazed in tension and the width of the 'active zone', was determined as the distance from the craze/bulk interface over which the gold interparticle spacings increased. The

width of the active zone was observed with respect to temperature and strain rate and was seen to increase with decrease in strain rate, and increase in temperature. Kramer and Berger (1990) quoted active zone thicknesses of the order of a fibril diameter (5-10 nm).

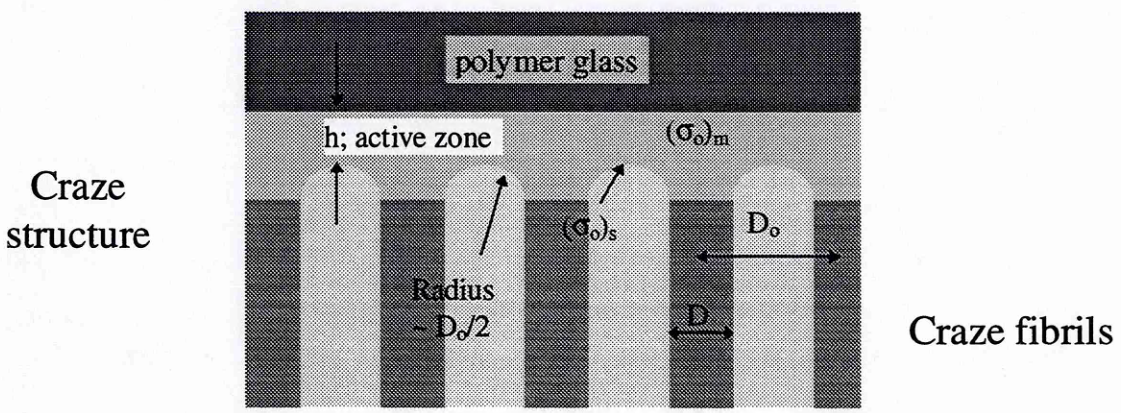

Figure 2-1. Schematic drawing showing the geometry of the craze/bulk interface. Kramer and Berger (1990).

The craze microstructure is directly affected by the craze drawing mechanism, in particular the mean fibril spacing D_o. Kramer and Berger (1990) modelled the material in the active zone as a strain-softened non-Newtonian fluid, and formulated the following equation for the velocity of the void surface between fibrils:

$$v = \frac{\dot{\varepsilon}_f \, h\sqrt{3}}{2(n+2)} \left(\frac{h\sqrt{3}}{2\sigma_{fc}} \right)^n |\nabla \sigma_o|^n$$

where σ_{fc} is the flow stress of the fluid at a strain rate of $\dot{\varepsilon}_f$, n is a material parameter, h is the width of the active zone, usually of the order of 6 nm, and

$\nabla\sigma_o$ is the gradient of pressure at this point in the fluid. The gradient of pressure can be approximated by:

$$\nabla\sigma_o \approx \frac{2[(\sigma_o)_m - (\sigma_o)_s]}{D_o}$$

where $(\sigma_o)_m$ and $(\sigma_o)_s$ are the hydrostatic tensions in the active zones, at the position directly above the fibril and at the surface of the void ceiling between the fibrils, respectively. The hydrostatic stress $(\sigma_o)_m$ above the fibrils is directly related to the average tensile stress on the craze interface S, through a proportionality constant β. Kramer et al. (1991) proposed that for the observed microstructure to result, the craze interface velocity must be related to the craze interface stress through the following equation:

$$S = \frac{4}{\beta}\left[\frac{2(n+2)v}{\dot{\varepsilon}_f h\sqrt{3}}\right]^{\frac{1}{2n}} \sqrt{\frac{\sigma_{fc}\Gamma}{h\sqrt{3}}}$$

where Γ is the surface tension of the void surface.

2.1.5 Craze Breakdown

Craze formation ahead of the crack tip is now known to enhance the fracture toughness of the polymer glass by a factor of 10^4 (Donald and Kramer, 1982b). However from Transmission Electron Microscopy studies on crazes, it is evident that crazes are precursors to crack propagation and failure (Beahan et al., 1971, 1972, Kambour and Robertson, 1972). So called "brittle fracture" in tension is now known to occur by the following sequence of events:

- under tension crazes are formed,
- at a somewhat higher stress a crack is initiated, invariably by breakdown of craze fibrils,
- the crack grows by further breakdown of craze fibrils until it reaches a critical size, and fracture occurs.

When the stress on the fibrils becomes high enough, craze breakdown can occur, through either chain reptation or chain scission (Donald and Kramer, 1982a). Chain reptation is the process whereby a chain travels in a snake-like manner, through a 'tube' created by the surrounding chains in the three dimensional network. These authors suggested, through work by Fellers and Kee (1974) and Kita (Donald et al., 1982a) on the effect of molecular weight on critical applied stress to fracture, that chain reptation has an influence on fibril failure.

Early workers (Beahan et al., 1973) noted from some of their results, that craze breakdown often occurs in the midrib. Other workers, Trassaert and Schirrer (1983), Verheulpen-Heymanns (1984), and Kramer and Hart (1984), suggested that craze breakdown occurs through localised creep along the craze fibril. Lauterwasser and Kramer (1979) suggested that because of the large extensions in the midrib, very little creep would be required for failure to occur at this point in the craze.

However the work of Yang et al. (1986a,b) and Berger (1990) showed that breakdown of craze fibrils always initiates at the interface between the craze and the bulk material, the so called active zone. Yang et al. prepared specimens from filtered and unfiltered samples. The process of filtering was carried out to decrease the number of extrinsic imperfections such as dust particles in the

material. In the case of the unfiltered specimens, breakdown was associated with dust particles, but at higher strains morphologically similar breakdowns were found in the filtered specimens. In both cases the breakdowns always consisted of pear shaped voids, which initiated at the interface. Kramer and Berger advanced fractographic observations by Beahan et al. (1975) and Hull (1970), as confirmation that fibril breakdown mechanisms observed in thin films, were characteristic of those in bulk polystyrene. Berger (1990) has observed similar craze breakdown morphologies in polystyrene-acrylonitrile (PSAN), polymethylmethacrylate (PMMA) and poly(α-methylstyrene) (PαMS).

A craze breakdown model was proposed by Zhurkov and Korsukov (1974) based on overloaded interatomic bonds, and models based on craze fibril breakdown have been suggested by Prentice (1983), Yang et al. (1986), Plummer and Donald (1991) and Berger (1990). Prentice investigated the molecular weight effects of the polymer glass on the fracture energy. He proposed the following model: under tensile stress crazes are formed, and through surface drawing the chain segments between entanglements become fully extended. Two mechanisms are now feasible, namely chain scission or chain pull out. The time for chain reptation to occur is dependent on the molecular weight, and if this time exceeds the time of the local fracture event, then chain scission will become the sole remaining mechanism through which the craze fibril will fail.

As mentioned earlier, Yang et al. (1986) prepared specimens from unfiltered samples and filtered samples, and measured the craze stability, taken as the difference between the strain to form the craze and the strain at which the craze fails. They found that craze strain breakdown statistics follow a Weibull distribution. The Weibull distribution, which is discussed in Chapter 4, is a versatile distribution which can relate the number of possible sites for breakdown to material properties such as stress or strain. A fundamental aspect of the

Weibull treatment, is that the probability of failure scales with the number of possible failure sites, i.e. the larger the volume of material, the greater the chance of failure. Yang et al. (1986) incorporated the size of the specimen as a separate parameter into the probability of failure model to account for this size effect. This forces the Weibull parameters to be purely material parameters unrelated to the specimen geometry. These workers also developed a microscopic statistical model incorporating the Weibull treatment of the breakdown probability, in which craze fibrils fail by random disentanglement of molecules at the craze/matrix interface. This treatment explains the well known molecular weight dependence of the craze stability, through assuming that, although some disentanglement and chain scission is assumed to occur in the formation of the craze fibrils, the critical event in craze fibril breakdown is the disentanglement of the molecular strands in the active region.

Other workers have utilised and developed this model, such as Plummer and Donald (1991) who investigated the effects of temperature on the fibril stability, and Berger (1990) who stated that Yang et al. were incorrect in their method of calculating n_e, the number of effectively entangled strands per unit cross section that had survived the fibrillation process, and published a revised model.

2.2 Rubber Toughening

In 1977 Bucknall asked the question *"How do small quantities of rubber produce such dramatic increases in the fracture resistance of brittle plastics ?"* The fundamental problem is well illustrated by comparing the extension behaviour of polystyrene and high impact polystyrene. Polystyrene in tension extends to strains of approximately 0.03, before fracturing in a brittle manner at a stress of over 40 MPa. HIPS on the other hand, extends to strains of over 0.50 depending

mainly on the volume, size and morphology of the rubber particles, before fracturing in a ductile manner.

Current understanding of the deformation of rubber toughened polymers attributes the enhanced toughness to one or a combination of the following:

- widespread crazing and/or shear yielding, both initiate at rubber particles. The rubber particles act as stress concentrators, increasing the stress on the matrix locally, in the same manner as a crack tip magnifies the stress locally (Bucknall, 1977).
- The importance of widespread rubber voiding and cavitation has recently been examined quantitatively (Bubeck et al., 1986, 1990. and 1991 and Buckley, 1991).
- Microscopic shear of the interparticle matrix ligaments has been proposed to operate in HIPS (Gilbert and Donald, 1986 and Buckley, 1991).
- So called 'dilatation bands' have recently been investigated in rubber toughened nylon (Lazzeri, 1991), and have been explained as an interaction of rubber cavitation and matrix shear yielding.

2.2.1 Theories of rubber-toughening

The earliest theory of rubber toughening was proposed by Merz, Claver and Baer (in Bucknall, 1977). This was based on the premise that the thousands of reflecting surfaces observed extending through the matrix and rubber particles were microcracks, and the rubber particles stretched to bridge these microcracks. The load bearing rubber particles strain-hardened and prevented rapid crack propagation. While this explained several experimental observations, its principle weakness was that it inferred that the rubber particles were supporting the majority of the load. Newman and Strella (1965) calculated that the percentage

energy absorbed by the rubber part of styrene-acrylonitrile (SAN) blended with polybutadiene, was 10 % of the impact energy. These authors attributed the remaining energy absorption to shear yielding of the matrix.

The multiple crazing theory, proposed by Bucknall and Smith in 1965, resolved the question of the structure of the reflecting surfaces. They found by stretching a thin section (5 to 10 μm) of HIPS under an optical microscope, they could observe and photomicrograph the material under increasing tensile strain. Earlier, Kambour (in Bucknall, 1977) showed that crazes were almost always precursive to cracks, and were responsible for the high fracture surface energies in PS and PMMA (as measured by Berry in 1961). Bucknall and Smith logically deduced that these 'microcracks' in rubber filled composites, were in fact crazes and based on this conclusion, developed the Merz et al. (1956) theory. They found the number of crazes in their material was much higher than that observed in unfilled materials, and to this they attributed their material's larger impact strength. This lead them to highlight the role of the matrix, (as opposed to the rubber, Merz et al., 1956) in the increased toughness of rubber filled composites.

Matsuo in 1966, examined HIPS and ABS under the electron microscope, and arrived at the same conclusions as Bucknall and Smith had. Matsuo observed that the 'microcracks' Merz et al. had observed, were crazes branching between particles, with the overall average direction perpendicular to the applied tensile stress. He also noted that the rubber particles elongate in the direction of tensile stress, resulting in lens shaped particles, but the diameter of the rubber particles in the direction perpendicular to the tensile axis, did not change. This underlines the well documented importance of good interfacial adhesion between the particles and the matrix. The importance of good adhesion also indicates that the rubber particles must sustain some load at some stage in the deformation process (Bucknall and Smith, 1965). Subsequent investigations, mainly based on TEM

analysis, revealed that crazes form in HIPS, ABS, toughened PVC, toughened PMMA and toughened epoxy resin (for a review of workers see Bucknall, 1977).

This also raises the issue of other filler systems such as glass beads. Lavengood et al. (1973) blended glass beads with SAN. It was found that glass beads, and particles which have a higher modulus than the matrix, can cause yielding, but the fracture strains of these composites are very low. This suggests an important role for the rubber in post yield deformation. In 1972, Bucknall and Clayton performed volume strain measurements on HIPS in tension, and showed that the deformation of the material was almost entirely dilatational. These authors described three stages in the deformation of HIPS:

- instantaneous dilatation: due to the hydrostatic component of the tensile stress on the material. This was thought to be a completely recoverable elastic response.
- Slow dilatation: attributed to crazing.
- Rapid dilatation: also due to crazing, but the rate of crazing was of a much higher rate and was constant up to the strain level tested.

The authors assumed on the basis of microscopic evidence, that almost all dilatation was due to crazing. Stage 2 was denoted the 'induction period', its duration is defined in the volume strain versus time curve, through extrapolation of the high strain linear portion of the curve, back to the point at which the volume strain is equal to the instantaneous volume strain. This will be referred to later in Chapter 4 .

The strain in the lateral direction, i.e. the direction perpendicular to the tensile axis, was very small, approximately – 0.001 on a specimen extended to a longitudinal strain of 0.05. This strain was attributed to shear yielding and

viscoelastic effects, and indicates the small role shear yielding plays in the dilatation of HIPS. Bucknall and Clayton proposed that approximately 75 % of the longitudinal strain was due to crazing, the remainder being the elastic response of the material. The same authors proposed a model for the kinetics of crazing.

Bucknall and Clayton's model was developed to describe two periods in the crazes' growth. The first stage relates to the period of craze growth and the other stage relates to the period of craze control/termination. The existence of craze control/termination was based on the premise that craze tip advance is terminated when it encounters a rubber particle, or when the stress at the craze tip drops below a critical value. In a succeeding paper, Bucknall, Clayton and Keast (1972) analysed blends of HIPS and poly(phenyloxide) PPO, and found two deformation mechanisms dominated, crazing and shear. The authors showed that with increasing fractional content of PPO, creep rates were reduced, and they accredited this to the termination of crazes through interaction with shear bands. Kambour (1973) also advanced this hypothesis and commented that the larger optimum particle size necessary in HIPS compared with ABS, may partially arise from the absence of shear banding acting as a craze terminating mechanism in the former material. Donald and Kramer (1982d) rejected these theories, questioning the assumption that rubber particles and shear bands do in fact act as craze terminators. These workers dismissed the presumption by Bucknall and co-workers (1972), that a long craze is weaker than a short craze. This latter rejection was based on the new evidence that crazes grow mainly by surface drawing and not craze fibril creep (Lauterwasser and Kramer 1979).

Quantitative transmission electron and optical microscopic techniques were used to study mechanisms of craze initiation and growth in thin films of HIPS and ABS (Donald and Kramer, 1982c). HIPS was diluted with PS to reduce

the number of crazes formed and therefore reduce craze-craze interactions. It was observed that while there was a strong size effect, crazes rarely nucleate from particles with diameters less than 1 μm. The internal morphology had little effect, craze nucleation being only slightly favourable at occluded particles. Argon (1975) suggested that additional stress concentrations which result from the rippled structure of the outer shell of an occluded particle, might superimpose on the stress enhancement already present due to the low modulus particle. This worker advanced a model, which showed that this effect would be most pronounced for large inhomogenous particles.

Craze tip nucleation and advance was proposed to occur as a consequence of the elastic stress enhancement initially at the rubber particle, and subsequently at the tip of the craze. For craze nucleation to occur, Donald and Kramer (1982c) proposed that this stress enhancement must exceed the stress concentration existing at a static craze tip, and it must also extend at least a distance corresponding to 3 fibril spacing (75 nm for PS) from the particle into the matrix. The spatial extent of the rubber induced stress enhancement increases with rubber particle diameter, thus neatly explaining the particle size effect as observed in the same study by Donald and Kramer and as discussed by Bucknall in 1977. However as they used the Goodier analysis to compute the stresses around the particles, they had to study a material containing a much lower volume fraction of rubber than generally added in common commercial materials. This was to ensure particles could be considered non-interacting, and implies limitations on the use of this analysis.

Donald and Kramer (1982c) found that crazes, provided they are of sufficient length, which initiate from rubber particles in HIPS, can be adequately modelled as crazes at crack tips through use of the Dugdale model. The issue of the applicability of the Dugdale model only to long crazes, originates in the

treatment of the rubber particles as spherical holes, when in fact the Dugdale model assumes that the plastic zone is grown from a planar crack. Donald and Kramer found that with a sufficient craze length, the shape of the initiating 'crack' becomes insignificant and the treatment is then valid. This implies that this analysis also might not be valid for commercial materials, with their generally higher concentration of rubber particles and resultant shorter crazes.

While the issue of the effect of the internal morphology of the rubber particle on the nucleation of crazes remains controversial, work by Donald and Kramer (1982a) has shown the internal structure does effect the breakdown of HIPS. The material considered was embedded with a distribution of particle sizes; particles less than 1μm were solid rubber and larger particles contained sub-inclusions of PS. It was observed that when crazes formed around the smaller solid rubber particles, significant lateral contraction of the particle took place at its equator. This caused failure of the rubber/matrix interface, resulting in void formation and craze breakdown. Conversely, occluded particles can accommodate the tensile displacements by local fibrillation of the rubber shells surrounding each sub-inclusion in the particle. As a result, the lateral contraction does not occur, and large craze displacements can be accommodated without void formation.

In a separate paper, Donald and Kramer (1982d) investigated the changes in the deformation of ABS which result from the addition of small solid rubber particles or large occluded rubber particles. They found in a blend with only small solid particles, only cavitation of the particles and matrix shear deformation resulted. However in the blends containing larger particles, cavitation of the larger particles and crazing dominated. Within the larger particles, while large voids formed, typically 0.7 μms in diameter, craze breakdown did not result. The authors attributed this to the lower true stress on SAN craze fibrils as opposed to

PS craze fibrils, indicating that the stress concentration resulting from a void is more damaging in HIPS than in ABS.

2.2.2 Concentration and Size of Second Phase Particles

Many workers have correlated the concentration and size of the dispersed particles with the composite's toughness. For a review of workers see Kinloch et al. (1983). There are several problems associated with the correlation of quantitative material parameters with toughness and fracture behaviour. The most salient issue is that resulting from the considerable difference between the initially added rubber, and the actual second phase volume fraction present after polymerisation. This difference is due to phase inversion in the material, which creates particles with matrix sub-inclusions surrounded by a rubber shell. In commercial materials the concentration of rubber might be 8 % whereas the rubber particle volume fraction may be 40 % or higher. Further complications arise when trying to find interrelations between morphological aspects of the material and fracture behaviour. Features such as rubber particle volume fraction, particle size, particle size distribution and internal structure are all often interrelated so making it very difficult to change one feature independently of others.

Studies by Wagner and Robeson (1970), Keskkula et al. (1971), Silberberg and Han (1978) and Turley and Keskkula (1980) investigated some effects arising from different rubber particle volume fractions. These workers, appreciating that slower rates results in increased rubber phase volume fractions, applied different rates of agitation to the polymerising solution. This was presumed to be a result of rupture of the rubber membranes during agitation. Wagner and Robeson found that impact strength and fracture strain both passed through a maximum at a rubber phase volume fraction of 0.22, coinciding with

commercial material volume fractions. This work indicates that the rubber particle volume fraction has to be optimised, because a balance exists between the lower limitation that the particles need to be a critical size or larger, and the upper desire to maximise the number of deformation initiating sites. Keskkula et al. (1971) correlated dynamical mechanical results for PS blended with differing quantities of SBR, with its notched Izod impact strength. Silberberg and Han (1978) found an increase in energy absorption with increasing rubber particle diameter in impact tests, but found the converse at low test speed. Turley and Keskkula (1980) observed the notched Izod impact strength increase, and the tensile strength decrease with increasing rubber particle volume fraction.

Hobbs (1986) proposed a model based on the premise that large rubber particles retard craze growth, and that failure occurs when a critical craze length is reached. Hobbs investigated the notched impact strength of HIPS, through varying the ratio of small particles to large particles. A non-linear increase in fracture energy was recorded with increasing fraction of large particles, followed by a more progressive decrease at larger fractions. Wu (1988) found through varying particle diameters for three different rubber contents, that a brittle-tough transition occurred at a critical rubber particle diameter, which was dependent on the rubber content in the material. This worker found however, when surface-to-surface interparticle distance was considered, a single brittle-tough transition occurred, regardless of rubber content. Wu attributed this transition to be a result of yielding of the interparticle ligaments and concluded that this is the critical factor in rubber toughening, not phase morphology, particle size or rubber particle volume fraction. Buckley (1991) performed creep and impact tensile tests simultaneously with Real Time Small Angle X-ray Scattering (RTSAXS) on ABS with various average particle sizes and rubber levels. He found the toughness of the material increased with increasing mean particle diameter up to 0.3 μm, but subsequently decreased. This worker, having employed impact rates of 50 $sec.^{-1}$

and creep rates of approximately 0.01 $sec.^{-1}$, found this effect to be moderately rate dependent.

Bucknall and co-workers (1986a,b) studied the effects of material parameters on mechanical properties of rubber toughened polymers, and in 1986(a) examined the effects of rubber particle volume fraction. They found that varying the volume fraction of rubber particles in HIPS had a direct effect on the Young's modulus and tensile and compressive yield stresses. They also performed tensile creep on the materials, and used the Eyring rate equation to describe the relationship between the maximum rate of volume increase and applied stress. Variations in the slope of this relationship resulting from changes in the rubber particle volume fraction, led the authors to conclude that different stress concentration factors were acting on the rate-controlling step in the deformation of the material. They proposed that the stress concentration at the particle interface would be greater than that predicted by the Goodier equations for an isolated void, or particle of low modulus. Further enhancement would occur in regions of large area fractions of rubber, estimated using the Ishai-Cohen effective area model, which in turn would improve the rate of generation of crazes.

2.2.3 Matrix/Particle Adhesion

As mentioned earlier, the addition of hard inclusions to polymers does initiate yielding, however small. The inability of fillers like glass beads to reproduce the large increase in fracture strain observed when rubber particles are added to polystyrene, does to some extent, elucidate the importance of interfacial adhesion in increasing the toughness of filler reinforced polymers. Studies on hard inclusion filled materials and rubber particle filled materials, have shown that good interfacial adhesion is required for many reasons, some of which include:

(a) in order that particles can prevent premature craze breakdown and crack initiation; (b) in order that particles can absorb energy in front of a crack tip through cavitation/fibrillation; (c) in order that particles can absorb energy behind a crack tip through crack pinning. In some of the early HIPS materials, composites were prepared through melt blending rubber with polystyrene. This resulted in rubber particles which were poorly bonded to the matrix. When the styrene was polymerised in the presence of the rubber, well bonded particles resulted along with much improved toughness values (Kinloch and Young, 1983).

Other workers such as Cook et al. (1993) and Fowler et al. (1987) have shown the importance of good rubber/matrix adhesion. Cook et al. showed that higher toughness values resulted, when the particle/matrix adhesion was strong enough to ensure that the particle did not debond from the matrix, thus forcing the propagating crack to travel through the particle, and not around it.

2.2.4 Rubber particle cavitation

Rubber cavitation, a process of voiding within the elastomeric particles, was noticed by electron microscopists at an early stage, but experimenters were tentative about interpreting the occasional voids as actual damage introduced during testing, and not microtoming artefacts. In 1977, Breuer et al. used optical microscopy, TEM and light scattering, to investigate the structure property relationship for blends of PVC filled with grafted rubber particles. They found through electron microscopy, that stress whitened zones contained a large number of cavities formed through rupture of the rubber particles. It was found from TEM that reflecting bands coincided with bands of ruptured particles, which led the authors to conclude that cavitation of the rubber particles improved the material's toughness not through the generation of crazes, but through the initiation of shear bands.

Donald and Kramer (1982d) in investigations of the effects of rubber particle size on the deformation of ABS, found that for both solid and occluded particles, internal voiding and cavitation was of primary importance. They observed that in blends with only small solid rubber particles (~ 1 μm diameter), crazing was not readily initiated, deformation instead occurring through shear yielding promoted by particle cavitation. In blends with larger particles, crazing was seen to readily form at the large particles, while shear deformation was not observed.

This mechanism of toughening based on particle cavitation in conjunction with matrix shear yielding, was proposed independently by Kinloch et al. (1983) and Pearson and Yee (1986), both from work on epoxies, and is now generally accepted as the most congruous with experimental data and observations. Since the early 1980's, there has been a growing understanding of the importance of rubber cavitation in the deformation of rubber filled polymers. Possibly one of the most important aspects of this understanding, is the order of events. Many workers believed particle cavitation occurred invariably as a consequence of other toughening mechanisms, such as crazing or shear. However there is growing evidence that rubber cavitation occurs **before** matrix damage. Wu and Mai (1993) found through SEM and TEM investigations of blends of poly(butylene terphthalate) (PBT) with polycarbonate (PC) and a rubber impact modifier (IM), that rubber cavitation occurs before crazing. Bubeck et al. (1986) showed, using real time small angle X-ray scattering (RTSAXS) to study failure mechanisms in HIPS and ABS, that the dilatation due to non-crazing mechanisms, occurred before the dilatation due to crazing. Borggreve et al. (1989) in studies on rubber toughened nylon, found a correlation between voiding in the material and its impact toughness. They proposed that voiding

occurs through cavitation and not debonding of the particles, and that the stress at which particles cavitate will be dependent on the modulus of the rubber.

Another aspect of the role of rubber particle cavitation in the deformation of rubber toughened polymers, is its ability to absorb energy. Bubeck et al. (1990 and 1991) and Buckley (1991) using RTSAXS techniques on HIPS and ABS, found that crazing accounts for at most only half of the total plastic strain in these materials. The authors attributed the remaining dilatation to rubber particle cavitation and microscopic shear deformation of interparticle ligaments. Wu and Mai (1993) also stated that widespread rubber cavitation was responsible for a considerable fraction of the energy absorbed in deformation of blends of PBT/PC/IM.

The aforementioned evidence gives an indication of the role of rubber cavitation in deformation processes. Correlations between impact toughness and rubber cavitation stress, coupled with the evidence that cavitation occurs before the formation of shear bands and crazing, at least suggests the possibility that rubber cavitation might be the rate determining step in the deformation of the material.

Recently, cavitation criterion models have been advanced by workers such as Lazzeri and Bucknall (1993), Bucknall, Karpodinis and Zhang (1994) and Dompas et al. (1994) based on an energy balance approach, Fond et al. (1996) based on a rubber fracture surface energy criterion for void formation and Kinloch and Guild (1996) based on finite element analysis to predict the toughness of an already cavitated system. Lazzeri and Bucknall's model is based on a study done by Gent and Wang (1991) on macroscopic rubber blocks, which assumes that in a large block of rubber, there exists voids ranging from about 0.5 μm in diameter. Gent and Wang's treatment could not be immediately construed

for rubber toughened polymers, because in most of these materials the particle diameters are of the order of 1 μm. Lazzeri and Bucknall proposed a model based on the assumptions that the largest voids within a typical rubber particle under triaxial tension, are of the order of a few nanometres, and that these voids will expand only if the resulting release of stored strain energy is sufficient both to increase the surface area of the void, and to stretch the surrounding shell of rubber. This prerequisite is the basis of the energy balance which exists between the volumetric strain on the particle and the size of the void. In modelling the thermodynamics required to grow a void within the particle, the authors demonstrated the relationship between the stored energy in the particle and the cavity size. For a rubber particle of radius R and bulk modulus K_r, at volume strain Δ_v, the volumetric stored energy $U_v(0)$ is

$$U_v(0)=\frac{2}{3}\pi R^3 K_r \Delta_v^2$$

and the volumetric stored energy of the cavitated particle is:

$$U_v(r)=\frac{2}{3}\pi R^3 K_r \left(\Delta_v^2-\frac{r^3}{R^3}\right)^2+4\pi r^2\Gamma+2\pi r^3 G_r F(\lambda_f)$$

Following cavitation, the volumetric strain energy is reduced through the formation of a void which required stretching of the surrounding rubber of shear modulus G_r, to form a new surface of specific surface energy Γ. $F(\lambda_f)$ is a function relating to the work done in stretching the rubber surrounding the void. This model reveals that for a constant volume strain (or applied stress), for cavity growth, the rubber particle diameter has to be greater than a critical value. Using this thermodynamic approach, it was possible to define, for a given volume

strain, if it was feasible that cavitation could take place. This approach has explained some observed effects in rubber toughened composites.

In proposing rubber cavitation as the rate determining step, the effects of such parameters as particle size, rubber modulus and temperature on the yielding behaviour of rubber toughened materials, can be explained. The growth of the void will therefore be dependent on factors such as rubber shear and bulk moduli, particle volume strain, size of initial void etc.

The conclusions of Fond et al. (1996) concerning the influence of the particle size on the onset of cavity formation are similar to those by Lazzeri and Bucknall (1993), Bucknall et al. (1994) and Dompas et al. (1994); their different criterion arises from the treatment of the stability of the void once it is created. In contrast with the work of the former authors, who described the void growth in terms of a spherical void expanding concentrically, Fond et al. described the cavities as voids with a complicated closed crack surface, opening to an approximately spherical shape. However all three approaches are currently limited in their correlation with macroscopic materials, and further work is required in this area in order to fully describe and explore the importance of rubber cavitation in toughened polymers.

2.2.5 Failure of HIPS and ABS

While much work has been done in the field of craze fibril breakdown in untoughened glassy polymers, as was reviewed in the section **Craze Breakdown**, few studies have been done to determine whether the same mechanisms are dominant in the failure of rubber toughened polymers. In most ABS polymers, stress-whitening and yielding are followed by localised necking. The specimen neck becomes profoundly white, and due to the increased stress in the neck, the

specimen fails at a lower strain than a comparable HIPS. Stress whitening becomes apparent in HIPS at strains of approximately 0.03 and becomes more intense as the specimen extends. It is especially noticeable in HIPS, that the specimen cross-sectional area remains unchanged to a large extent during the test, i.e. macroscopic necking does not occur (Bucknall, 1977). It is now well established that multiple crazing is one of the dominant reasons for stress whitening in HIPS. This indicates an increase of the order of 6 in the density of crazes in rubber filled composites, so it is therefore interesting to speculate on whether craze breakdown is the instrumental mechanism resulting in ultimate rupture of the material.

In 1982(a), Donald and Kramer demonstrated failure in HIPS to initiate at the equatorial rubber/matrix interface of solid rubber particles. The particles were observed to extend with the accompanying crazes. However the solid rubber particles contracted at the equator of the particle, along the direction perpendicular to the tensile axis, resulting in failure of the interface between the craze and the rubber particle. Donald and Kramer showed that in a heavily crazed specimen, of the solid rubber particles that initiated crazes, 25 % had initiated cracks while none of the occluded particles had initiated cracks. The occluded particles, because of the hard sub-inclusions and fibrillation of the shells surrounding the sub-inclusions, do not undergo significant lateral contraction, and hence can comfortably withstand considerable elongation without interfacial breakdown occurring. This was also reiterated by Sauer et al. (1989) who showed that good interfacial adhesion is necessary to optimise the toughness of Medium Impact Polystyrene (MIPS). Donald and Kramer (1982c) suggested for reasons of craze nucleation and rubber particle breakdown, all rubber particles in HIPS below the size that efficiently initiate crazes (~1 μm diameter), should be precluded from the material. Similar behaviour has been found in experiments on HIPS by Sauer et al. (1989) and Keskkula et al. (1986). Keskkula et al. also

showed void development at the interface between the rubber particles and the accompanying craze. They showed large voids formed in the rubber membranes in the particles and in the crazes, but could not conclude whether the voids in the crazes were incurred during microtoming or testing.

Hobbs (1986) used computer modelling to correlate particle size with impact strength of HIPS. The model made several assumptions regarding the deformation mechanisms in HIPS. The most important assumption which gave the fundamental explanation of the experimental results, was that large particles through craze pinning, are more effective at terminating crazes than small particles (<0.2 μm). This allowed the hypothesis that the material fails when the maximum craze length exceeds a critical value L, which is dependent on rubber particle size and volume fraction, and this would control the impact strength of the material. Chen and Sauer (1990) in studies of ABS deformed through crazing, matrix shear yielding and rubber cavitation, showed that under low tensile strain rate, specimen fracture was associated with a large cone shaped cavity, at the centre of which, lay a large imperfection of diameter approximately 70 μm. At higher rates, fracture tended to initiate from a source on the surface of the specimen. However the authors could not say if the source was craze breakdown, rubber breakdown, an imperfection or matrix failure.

Sjoerdsma and Boyens in 1994 investigated the fracture probability of HIPS, and related it to plastic strain and time under load. Sjoerdsma et al. argued that on the basis of evidence of good adhesion between rubber particles and the matrix, and evidence that rubber particles stabilise crazes, rubber particles do not act as crack-initiating heterogeneities. Instead, due to the high density of crazes present in HIPS, it was more likely that crack-initiation resulted when crazes impinged upon each other, breakdown resulting from the inevitable misalignment of the craze fibrils. Sjoerdsma and Boyens proposed a model which relates the

plastic strain on the composite to the probability of failure and examined its predictions with respect to different temperatures and applied stresses, for specimens deformed under un-notched uni-axial creep. The ground breaking achievement of this work is the identification of strain as the critical factor controlling failure. The predictions of Sjoerdsma and Boyens' model were examined extensively in this study, and a more in-depth analysis and discussion of its derivation is given later.

Maestrini et al. (1992) in experiments on two grades of HIPS, with small core shell particles in one, and multiple inclusion particles in the other, showed that small particles are not effective craze terminators as some workers have previously held. These workers observed considerable fibril breakdown as the growing craze encountered rubber particles in the core shell modified material. Assuming the rubber particle has not initiated the adjoining craze, the collision between rubber particle and craze could occur either through craze tip advance or craze thickening. As a result of the former mechanism, the particle is seen to be located on the midrib of the craze which, because of the high stress which the craze fibrils are known to encounter in forming the midrib, suggests that these particles experience a very large deformation. Some of the core shell particles entrapped within the craze, which the authors say have interacted with the craze in the manner mentioned above, have been very heavily deformed at the equator, and are indeed almost fractured. However while the particles are heavily damaged, the craze structure is still reasonably intact.

However, it should be considered that the particles may not have encountered the craze in this manner, but rather have initiated a craze which has grown in conjunction with crazes initiated at neighbouring particles, thus producing the one large craze exhibited by Maestrini et al. This is an important issue in sub-critical failure of rubber toughened polymers, but it is interesting to

note from this type of interaction of core shell particles and crazes that: (1) failure of the rubber particle can occur before failure of the craze and (2) extensive deformation of the particle does not necessarily mean immediate breakdown of the craze.

However interaction of the core-shell particles with crazes by the craze thickening mechanism seems to result in considerable damage to the craze structure. The one particle illustrated, which has been completely entrapped through the craze thickening process, appears to be intact, but extensive fibrillation of the interface has occurred at its poles.

In the material toughened with salami particles, the authors state that no broken particles were observed on the midrib, but it is not clear from the displayed micrograph whether the one particle in the craze has nucleated the craze, or has been encountered through collision with the craze tip. It is however interesting to note that as observed in the core-shell particles, extensive fibrillation of the particle has occurred at its poles but in this case the continuity of the craze is maintained. This implies that the particles are considerably loaded with a nominal stress comparable to that of the craze. In a later paper Maestrini (1996) developed the model derived by Yang et al. (1986), which describes the breakdown statistics of craze fibrils in PS. Maestrini et al. observed craze damage associated with small core shell particles and assumed the particles were acting as breakdown 'seeds', in the same manner as dust particles cause failure in PS and HIPS. These authors incorporated Weibull statistics to form a relationship between a Weibull parameter, which described the distribution of effectiveness of the breakdown 'seeds' i.e. rubber particles, and the Paris law for slow crack propagation.

It is also interesting to note, that Maestrini et al. (1992) observed large craze damage in materials containing particles of high rubber shear modulus, while little craze damage was seen in materials containing particles of low shear modulus. The authors attributed this phenomenon to the high probability that poorly cross-linked particles can maintain the craze structure when crossing the craze-bulk interface. There is the possibility that the craze fibril structure in the material toughened with low modulus rubber particles is maintained, through a mechanism where the rubber plastizies the craze fibrils, thereby decreasing the stress on them, as recently observed by Brown et al. (1989).

2.3 Effects of Irradiation and Sulfur on PB, PS and HIPS

2.3.1 Rubber

There are many interrelated material parameters in rubber toughened composites. Varying one almost invariably means changing some of the others, but the fundamental basis of a school science experiment is to change one variable and observe the effects on the other parameters. In this study, this is the objective behind irradiation and sulfur treatment of HIPS and ABS.

Sulfur vulcanisation of natural rubber was discovered by Charles Goodyear, and has since been an instrumental process in the car tyre industry. On its own sulfur is not very efficient in cross-linking, as an unnecessary large number of sulfur atoms can combine to create one cross-link (Brydson, 1978). However with the addition of certain metal oxides such as zinc oxide, fatty acids and compounds known collectively as 'accelerators', far superior cross-linking efficiency is possible. These cross-linked materials are known as vulcanisates and an extensive review of these is given in Brydson (1978).

The energy to induce chemical reactions in organic materials is of the order of 2 to 6 eV. Radioactive cobalt has been widely used as a gamma source. Its isotope cobalt 60 disintegrates to emit two gamma photons differing in energy, both of which are easily of sufficient energy to excite electrons in organic materials. The unit of energy absorption of radiation is the rad, and it is equivalent to an energy absorption of 100 ergs per gramme of the material irradiated. In organic materials, the effects of irradiation will depend on the ease which the material can create bonds or break bonds. Two cases may be considered: the first is where an increase in molecular weight results, and eventually the formation of a closed network system, this is termed cross-linking. The second is where the molecular weight is decreased, which can occur through main chain fracture, and is termed degradation. In both cases the process occurs by the creation of free radicals or ionised particles, which can then either react to form cross-links, or can stabilise end groups formed earlier.

As early as 1933, Newton patented the vulcanisation of rubber by short exposures to 250 kV cathode rays (in Brydson, 1978). From this emanated work in the 1940's, on the effects of radiation on rubber. The driving force was the wish to develop radiation resistant materials capable of use in nuclear reactors. The properties of polybutadiene are affected by relatively low levels of irradiation due to the facile reaction of the C=C bond to form cross-links. Charlesby (1960) described how he had observed a linear relationship between the solubility of irradiated rubber and the dosage applied to the material. He also showed that the molecular weight between cross-links and the elastic modulus both varied linearly with irradiation dosage. Charlesby and Von Arnim showed at high elongations, the rubber stress-strain relationship is no longer linear, and that with irradiation, the stress at a given elongation is increased (in Charlesby, 1960). Zhao et al. (1994) in studies of γ irradiation effects on hydrogenated Acrylonitrile Butadiene rubber (HNBR), found that the gelation dose, i.e. the irradiation dose

at which an insoluble network is formed, was 3.8 Mrad. These authors observed that the tensile strength of the rubber increased with irradiation, while the elongation at break decreased from 650 %, for rubber irradiated with 8 Mrad, to 380 % for rubber irradiated with 23 Mrad.

2.3.2 Polystyrene

In 1960 Charlesby stated that polystyrene is one of the most radiation resistant long chain polymers in existence. Soares (1994) in an extensive study on the effects of irradiation on HIPS, irradiated PS and HIPS under vacuum conditions with doses of up to 80 Mrad. Soares found through molecular weight analysis of PS irradiated with doses up to 20 Mrad, that irradiation had a mild effect on PS, mainly through a chain scission effect concentrated at the surface of the material. The cross-link density of the material was increased with increased irradiation dosage, to the extent that an increase of 25 % was observed in the weight average molecular weight at a dose of 80 Mrad. Soares also blended irradiated PS with HIPS, and as a control also blended non-irradiated PS with HIPS. It was found that creep rates and elongation at break were slightly affected by the irradiation of the PS. Soares correlated her results with Bowmer et al., and attributed their irradiation induced change in the tensile strength to the fact that these workers irradiated the PS under air, thereby increasing oxidation of the material (in Soares, 1994). Soares also found using infra-red analysis that following irradiation, no bands were detected in the absorption region of carbonyl or hydroxyl groups, which would be expected if free radicals were formed. It is clear from these studies that irradiation of PS under an inert gas such as nitrogen would further reduce the generation of free radicals.

2.3.3 HIPS

Soares (1994) investigated the changes in toughness induced through irradiation of HIPS. The mechanical changes observed from the materials were attributed

predominantly to changes in the rubber shear modulus, and not cross-linking or chain scission in the PS. This conclusion was supported by the results discussed above. Following infra-red analysis, the spectra of HIPS irradiated up to 80 Mrad were examined, and it was found that no new bands were detected, verifying the conclusion that the PS was only mildly affected by irradiation. Dynamical thermal analysis also showed that the T_g of the PS, was unchanged while the T_g of the rubber increased with increasing radiation dosage. Soares observed an increase in the Young's modulus, yield and flow stresses, but a decrease in the elongation at break, with increasing rubber cross-link density.

Birkinshaw et al. (1993) studied irradiation effects on HIPS and ABS with doses of 12.5 Mrad and 20 Mrad. They observed an increased strain at which crazing takes place, and attributed this to cross-linking in the rubber phase. Wagner and Robeson (1970) blended sulfur with HIPS of rubber content 6 % and rubber phase volume 22 %. Dynamical thermal analysis revealed a shift in the glass transition temperature T_g with increasing quantities of sulfur, and a broadening of the damping peak. They attributed the shift in the T_g to elastomer cross-linking, and observed that this had an extreme effect on the mechanical properties of the composite. For a sulfur content ranging from 0 to 2 %, the elongation at break decreased from 40 % to 2 %, and the impact strength and the swelling index also decreased. Also the T_g increased by 97 °C and the tensile modulus by 0.83 GPa. The authors explained the increasingly brittle behaviour of the material through citing work by Bucknall (1969). Bucknall pointed out that the stress concentration at the rubber particle/matrix interface is affected by the rubber modulus, and this in turn would have an effect on the craze formation mechanisms. If the rubber modulus is increased the stress concentration at the interface would decrease, thereby inhibiting the generation of crazes. The material would therefore tend to behave in a manner more indicative of the unfilled matrix, than a rubber filled composite. Wagner and Robeson also

proposed that some degree of rubber cross-linking must exist following the styrene polymerisation, otherwise it would combine with the matrix during processing, and the characteristic salami structure would not be maintained.

Perche (1995) observed similar behaviour to that of Wagner and Robeson (1970). Perche examined the effects of sulfur cross-linking on the toughening mechanisms of HIPS, and recorded increases in the yield stress, flow stress and the T_g of the rubber, while the elongation at break was seen to decrease. With the addition of 0.6 % sulfur, the shear modulus of the rubber phase was calculated using Gaussian statistical theory to increase by 2.8 MPa. However in making these calculations, Perche made several assumptions which under scrutiny, might be inappropriate to the system under investigation. Included in these is the correlation of cross-linking with change in T_g, for which he used a conversion factor calculated by Mason (1964). Mason, however used a different cross-linking agent, a factor which must be crucial to the generation of cross-links.

Cook, Plumtree and Rudin (1993) changed the cross-link density of poly(n-butyl acrylate) which was blended with PS. They found that the impact energy decreased with increasing cross-link density, and proposed that the comparatively much greater impact energies characteristic of HIPS, (polybutadiene particles) must be due to the much lower T_g of the polybutadiene. They also proposed that to achieve optimum composite toughness, the rubber phase must carry and support a load in order to play a part in slowing crack propagation. It is interesting to note from these cross-linking experiments, that the rubber cannot be too strong because for improved toughness, the crack must propagate through the rubber particles and not be deflected around them.

3. MATERIALS AND METHODS

3.1 Materials

The materials examined in this study are based on commercial grades of High Impact Polystyrene (denoted HIPS8), Acrylonitrile Butadiene Styrene (denoted ABS8), and Advanced Impact Modifier (denoted AIM). HIPS8 and ABS8 were blended with general purpose Polystyrene (G.P.P.S) and general purpose Styrene Acrylonitrile (G.P.S.A.N.) respectively, and all materials were also blended with sulfur. The rubber particle volume fraction of HIPS8 and ABS8 was measured as 35 %. Schematic diagrams outlining the materials investigated are shown in Figure 3-1 and Figure 3-2.

3.2 Material Compounding

Before compounding the materials were dried under vacuum at a temperature of 80 °C for 3 hours. To minimise moisture intake, they were allowed to cool down slowly to room temperature before removing the vacuum. Blends of HIPS8 with G.P.P.S., in differing ratios, were compounded in a double screw co-rotational extruder, model ZSK 30 with medium shear screw profile and a processing barrel temperature of 200 °C. The material became noticeably less opaque as the ratio of PS to HIPS8 was increased. Compounding of sulfur with blends of HIPS8 and G.P.P.S. was carried out under the same processing conditions. The material became distinctly more yellowish/brownish with increasing quantities of sulfur.

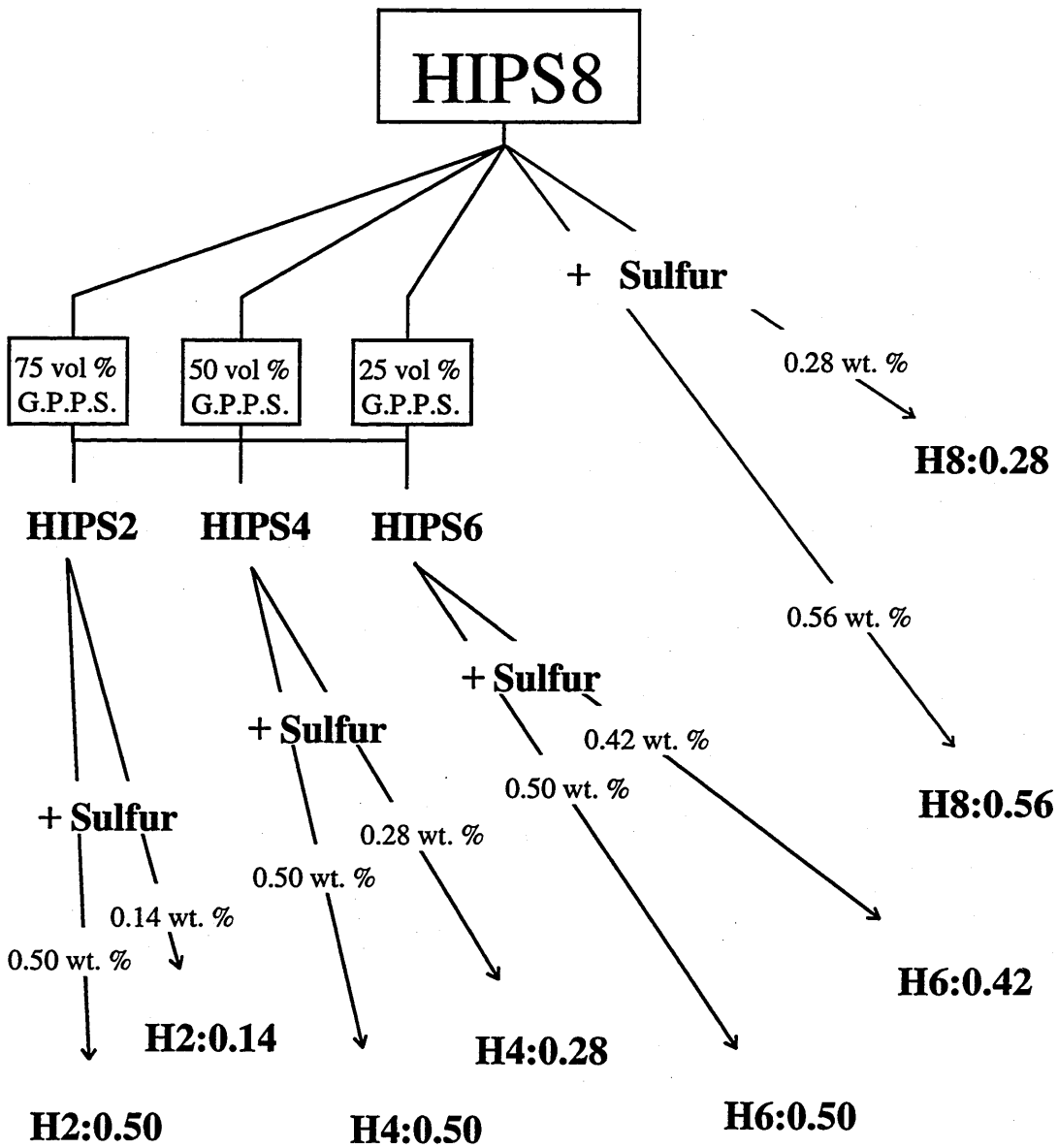

Figure 3-1 HIPS8 and its blends with general purpose polystyrene (G.P.P.S.) and sulfur.

Differing ratios of ABS8 to G.P.S.A.N were compounded in the aforementioned extruder with a processing barrel temperature of 190 °C. Again the material became less opaque as the ratio of SAN to ABS was increased. Compounding of sulfur with blends of ABS8 and G.P.S.A.N. was carried out under the same processing conditions. Blends of AIM with sulfur were also

compounded in the aforementioned extruder with a processing barrel temperature of 200 °C.

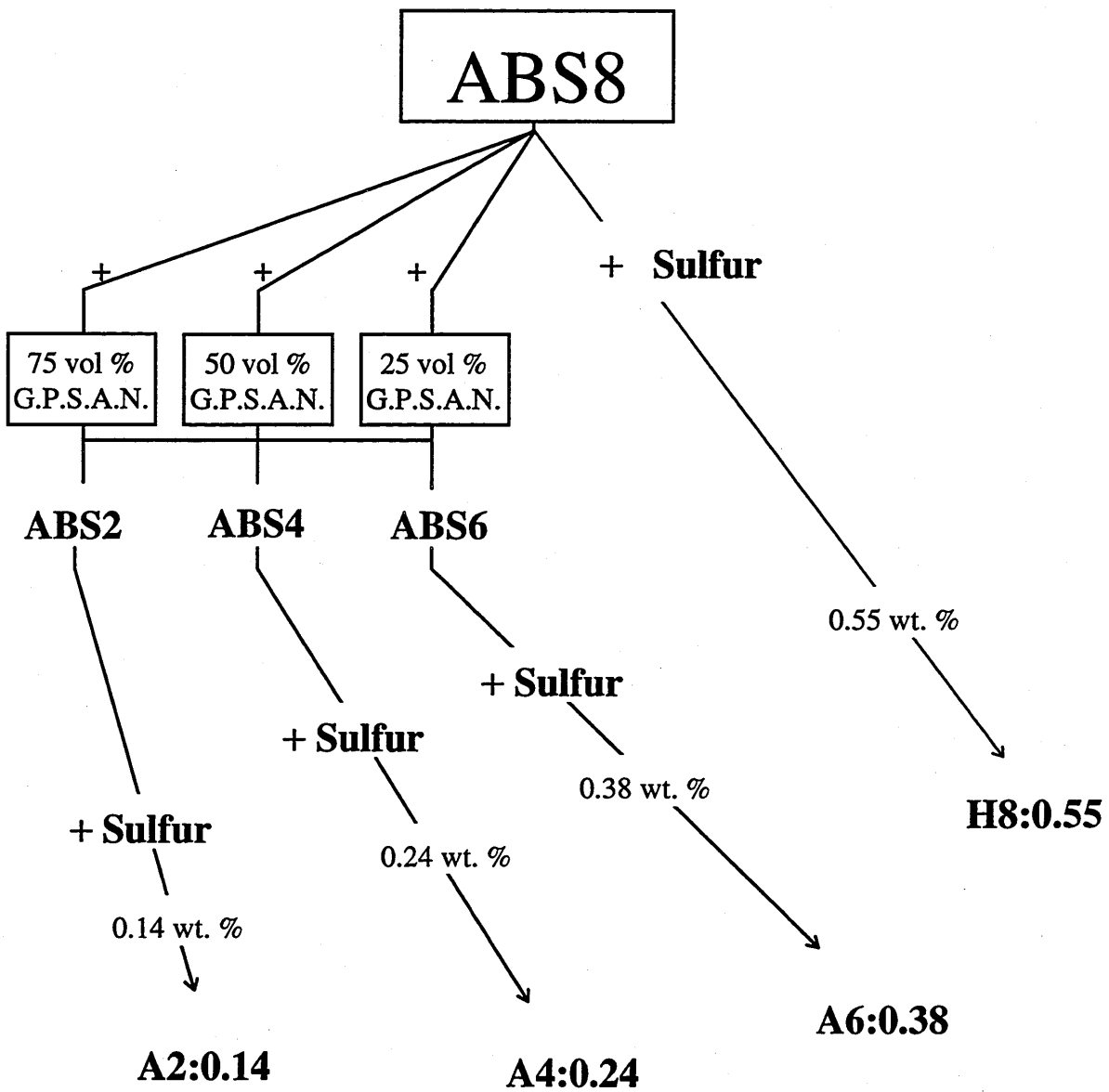

Figure 3-2. ABS8 blended with general purpose styrene acrylonitrile (G.P.S.A.N.) and sulfur.

3.3 Specimen Preparation

In order to avoid producing molecular orientation in the specimen, all materials were compression moulded. The compression moulding was completed according to the following procedure:

The material was first dried for 3 hours under vacuum, at a temperature of 80 °C. It was then allowed to cool slowly to room temperature before placing in a pre-heated press. For a plaque measuring 250 mm. x 250 mm. x 3.5 mm., 350 gms. of material was used. The material was heated for 10 minutes without pressure, and was then loaded to 7.5 MPa. This load was maintained until 'flash' was significantly reduced, (approximately 7 minutes), at which time the pressure was increased to 12 MPa. This load was again maintained until 'flash' was significantly reduced (approximately 7 minutes). The mould pressure was then increased to 25 MPa and left to cool slowly back to room temperature. Tensile test and DMTA specimens were prepared from these plaques.

3.3.1 Tensile Test Specimens

Tensile test specimens with gauge lengths measuring 29.5 x 5 x 3.5 mm. and 41.5 x 5.5 x 3.5 mm. were routed and then polished to remove surface flaws and scratches, with 1200 grade aluminium oxide paper. In a small number of experiments the specimens with gauge lengths measuring 41.5 x 5 x 3.5 mm. were used and these are indicated in Table 3.1 with #. All specimens were allowed to stress relax for at least three days before testing. The specimen gauge length cross sectional area was measured at three different positions, and when calculating the stress on the specimen, the smallest cross-sectional area was used.

Material	Constant stress (MPa)
HIPS8	14 #and 15#
HIPS6	18.5#, 16.2 and 13.7
HIPS4	22.5#, 19.6 and 16.2
HIPS2	26.5# and 25
H8:0.56	13.7#
H8:0.28	13.7
H6:0.42	23
H4:0.28	26.5
H2:0.14	31.5
H6:0.50	22.5 and 21
H4:0.50	33 and 28
H2:0.50	—
ABS8	26#
ABS6	31.5 and 24.5
ABS4	37.5 and 35
ABS2	47.5 and 39.5
A8:0.55	34
A6:0.38	37.5
A4:0.24	42
A2:0.12	57.5
AIM	15.7 and 16.7
AIM:0.55	20

Table 3-1. List of creep rupture tests performed in this study.

3.3.2 DMTA specimens

Specimens measuring 3.5 x 3.5 x 9.0 mm or 6.0 x 6.0 x 9.0 mm were cut from 3.5 mm. and 6 mm. thick plaques, and polished with 1200 grade aluminium oxide paper.

3.4 Test Methods

3.4.1 Instron

All tensile experiments were carried out on either an Instron screw machine, or a custom designed creep rig. Strain measurements on the Instron were made using a clip-on, 25 mm. gauge length and 20 gm. extensometer. In order to prevent the extensometer blades damaging the surface of the specimen, they were covered with double sided sticky tape. The tape was renewed for every specimen, thus ensuring that any damage inflicted by the blades will be constant. However fracture did not noticeably occur preferentially at the extensometer blades. Absolute strains were recorded to the fifth decimal place, and creep tests were carried out using a load control feedback loop.

Constant displacement rate tests were completed in the Instron at a cross head speed of 2 $mm.min^{-1}$. The yield stress was taken at the peak in the stress-strain curve and the flow stress was taken at the minimum stress after yield occurs.

3.4.2 Creep Rig

The statistical nature of this study meant that a large number of specimens had to be tested for any one result. As a result of this and the generally long term nature of creep tests, a creep rig was designed and built. Following testing on a prototype, the rig was built in the Cranfield University Engineering Workshop. The specimens are stressed by lowering weights from the bottom of the specimen, by means of a tensile testing lead screw driven by a geared motor,

thus allowing a wide range of loading speeds. The rig frame, as seen in Figure 3-3 and Figure 3-4, is made from very solid 40 mm. angle iron. The rig is mounted on rubber cushions and the specimen mounting jig, indicated in Figure 3-4, is separated from the rig frame by rubber washers. These three features help prevent cross-talk when specimens fracture. The extension of the specimen is 'channelled' through two guides, with friction minimised to a negligible degree by contacting ball-runners. The guides help prevent 'swing' and 'twist' of the specimen, two unwanted features observed in the prototype.

Extension of the specimen is measured using Solartron AC linear voltage displacement transducers and the data are logged in a custom written program on an IBM p.c. Unlike the extensometer, this system of strain measurement is non-contacting (see Figure 3.3) and records the full extension of the specimen. This necessitates the application of a correction factor to the creep rig results to allow for shoulder effects. It was found that the latter portion of the materials' creep curves, from approximately 0.3 x ε_{max} (ε_{max}=maximum fracture strain), the ratio of strain from extension to strain from extensometer was approximately 1.2.

3.4.3 Dynamic Mechanical Thermal Analysis

DMTA experiments were carried out using an Eplexor dynamic mechanical thermal spectrometer manufactured in Germany by Gabo Qualimeter GmbH. This machine can apply a maximum static load of 1500 N to the specimen in compression or tension, while simultaneously measuring dynamic mechanical properties at small load amplitudes.

For the experiments carried out in this study, specimens of cross-sectional area approximately 16 mm^2 or 36 mm^2 were tested in compression. A static load of 200 N with a superimposed dynamic load of 45 N was applied to the

specimen. The dynamic load was applied at a frequency of 1 Hz and the heating rate of the test was 1 $°C min^{-1}$.

3.4.4 Image Analysis

STEM micrographs were analysed in a Joyce-Loebl Image Analysis system using Genias software to determine rubber particle volume fractions. This involved clearly defining the particle/matrix interface with a black pen and calculating the total area within the borders. A rubber particle area fraction was then calculated from this measurement.

3.4.5 Transmission Electron Microscope

Electron microscopy was performed on ultrathin slices of the materials investigated using a Philips 200 KV CM20 microscope, with an accelerating voltage of 120 kV. Slices for transmission electron microscopy were prepared using the following procedure: Blocks measuring approximately 4 x 3.5 x 5 mm. were cut from the specimen's gauge length, trimmed to a pyramid, and subsequently stained with osmium tetroxide vapour in a sealed chamber. Slices measuring approximately 70 nm were then microtomed from the tip of the pyramid using a Reichert-Jung, Ultracut-E microtome, equipped with a 35° diamond knife, at room temperature. The ultrathin slices were floated onto a water bath, and subsequently picked up on a microscopy grid.

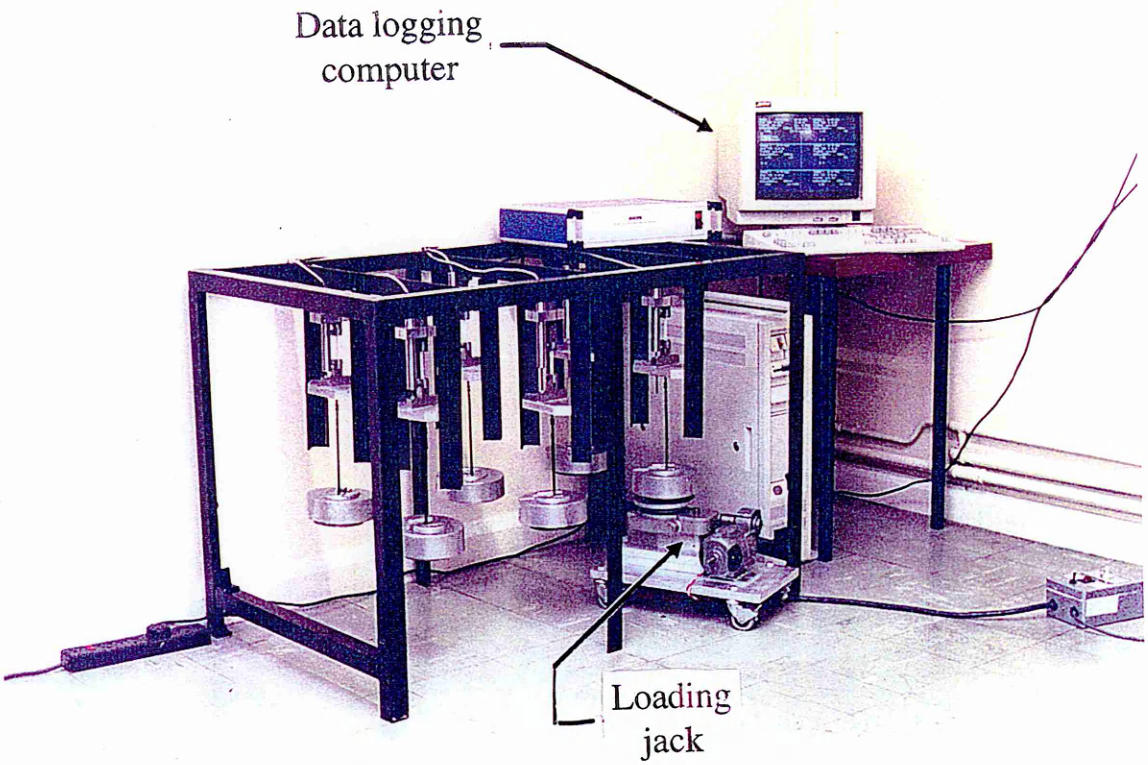

Figure 3-4. Creep rig testing station.

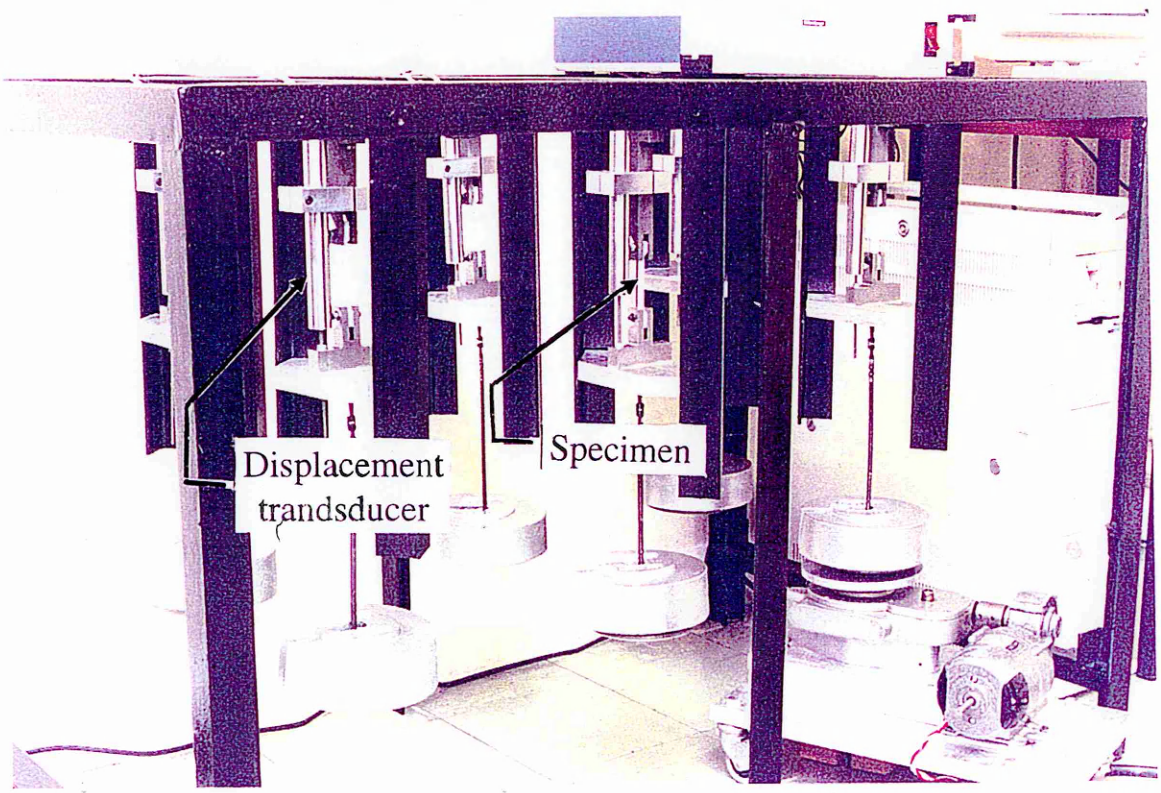

Figure 3-3. Creep rig testing station.

4. RESULTS. HIPS blended with general purpose polystyrene

4.1 Constant Displacement Rate

The following section characterises, with respect to material parameters such as yield stress, flow stress and fracture strain, the material HIPS8 and its blends with general purpose polystyrene. The majority of tests were carried out at a constant cross-head speed of 2 $mm.min^{-1}$ in an Instron testing station. Figure 4-1 shows stress/strain curves for HIPS blended with polystyrene. There was a noticeable reduction in stress whitening of the materials at fracture with decreasing rubber content. The Young's modulus of the material was measured between strains of 0.002 and 0.007 and was found to increase with increase in

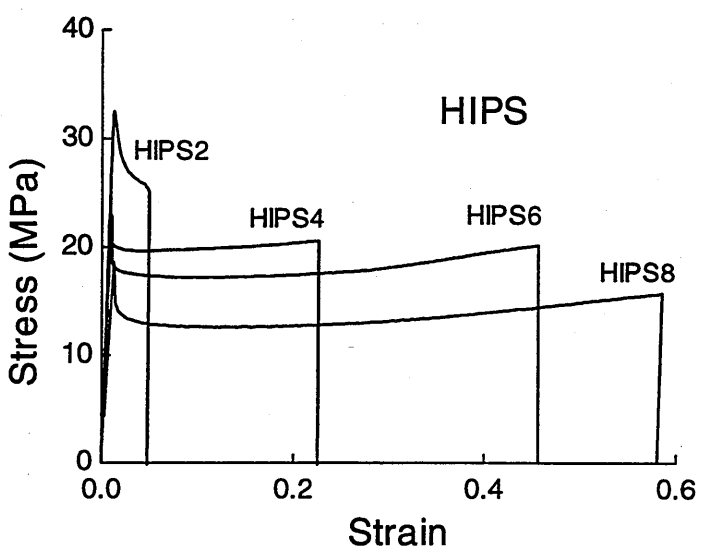

Figure 4-1. Stress/strain curves for HIPS8 blended with general purpose polystyrene

rubber particle volume fraction, from 1.69 GPa for HIPS8 to 3.1 GPa for HIPS2. Figure 4-2 shows the effect of rubber content on the yield, flow and breaking stresses of the material. The yield stress was taken as the peak in the stress/strain curve and the flow stress was taken as the minimum stress after yield occurs (plotted yield and flow results are each the average of three tests). The breaking stress obviously is the stress at specimen failure (the breaking stress data points in Figure 4-2 are each the maximum value of three tests). The breaking stress of PS is taken from Bucknall (1977). Consequently, from Figure 4-2 it can be seen that the flow and breaking stresses for HIPS2 coincide.

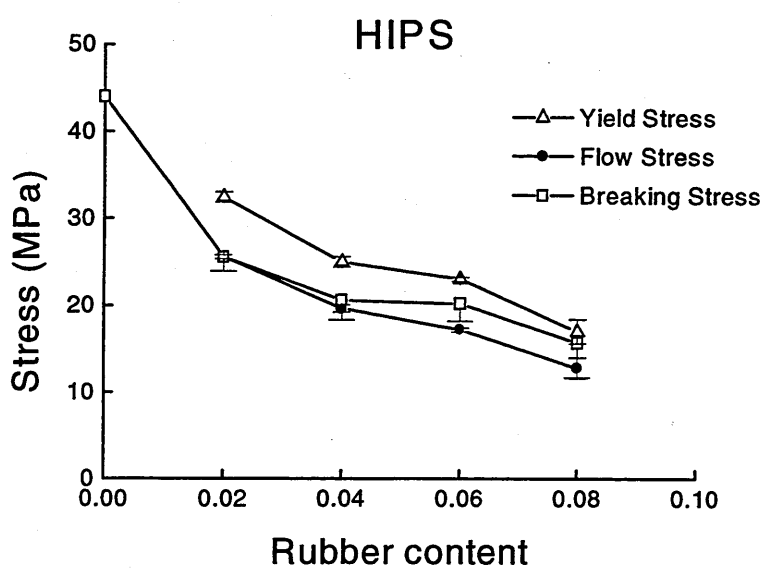

Figure 4-2. Change in material parameters with rubber content.

4.2 Creep

The HIPS materials were extended under constant load and the resulting deformation was recorded with respect to time. The effect of rubber content on the deformation of HIPS is apparent in Figure 4-3. HIPS6 and HIPS4 are extended to rupture under the same applied stress. The non-linear effect of stress

on strain rate parameters such as the induction period, previously illustrated by Bucknall et al. (1972), can be seen in Figure 4-3.

The induction time defined in Chapter 3 and shown in Figure 4-4, is considerably decreased with increase in rubber content, while the strain rate and the strain at failure increased with rubber content. Illustrated in Figure 4-4 is the

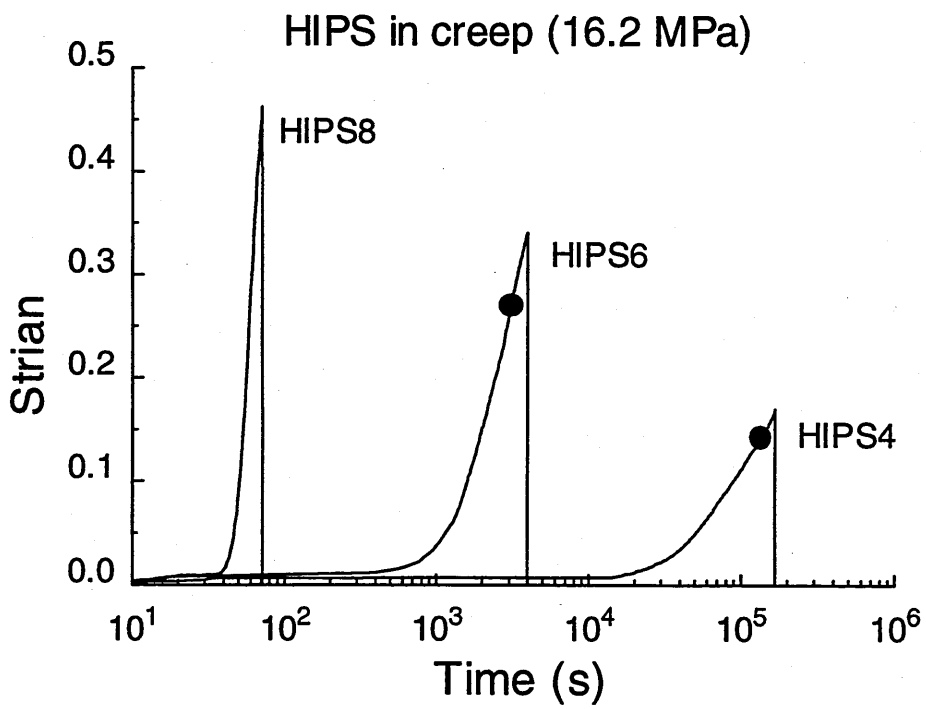

Figure 4-3. HIPS6 and HIPS4 deformed under the same constant nominal stress

determination of the induction time. The linear portion of the curve, at intermediate strain, is extrapolated back to the point at which the strain is equal to the instantaneous elastic strain. The definition of this parameter will become important later as it will be shown that it can be used as a lower limit of specimen failure, that is in medium to high impact polystyrene and ABS, no failures occur before the induction time.

Also plotted is the strain rate versus time curve for HIPS8 extended under an applied stress of 14 MPa. It can be seen that, following the induction period the strain rate increases, passes through a point of inflexion, and subsequently decreases. This non-linear behaviour demonstrates the difficulty in predicting failure for this material.

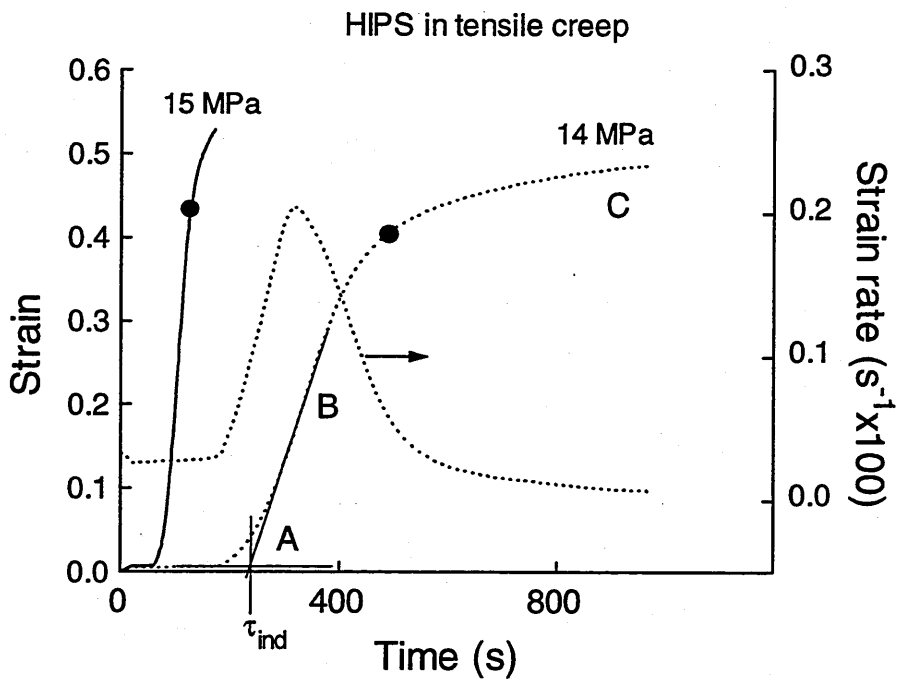

Figure 4-4. HIPS8 in creep under different applied stresses

4.3 Statistics and Cumulative Probabilities

Statistics is a field of study with two basic objectives: (1) to describe or summarise data and (2) to provide a valid method for making generalisations or inferences from a **sample** about a **population**. A sample is a sub collection of units from the population, usually greater than 20, which are selected to be a representative sample of the population and to infer and deduce characteristics of the population (Brockett and Levine, 1984).

There are three probability functions, which are generally used in interpreting the physical causes of component failure in terms of probability distributions. These functions are defined in the following text in terms of time but other variables are equally applicable. The experiment on the component under investigation, is started at time t =0, at which time the component is in a non-failure condition. The component then operates successfully until failure occurs at time t = T. The probability of failure of the component with respect to time can now be described using the following three distributions, (which are all interrelated) **probability density function**, **cumulative distribution** and **conditional failure rate.**

4.3.1 Probability density function

This is defined as the probability that the time to failure T, of the component under examination occurs in the time interval t_a to t_b, such that

$$\overline{P}(t_a \leq T \leq t_b) = \sum_{i=1}^{n} f(t_i).\Delta t \qquad (4\text{-}1)$$

and

$$\overline{P}(t_a \leq T \leq t_b) = \int_a^b f(t)dt \qquad (4\text{-}2)$$

where the interval t_a to t_b is divided into n equal subintervals of width Δt each containing the points t_1, t_2 ..... t_n. The probability that T will occur in the subinterval containing t_i can be given by $f(t_i).\Delta t$, where f(t) is the probability density function. This is simply the frequency which components fail between t_a and t_b, (Johnson, 1994).

For illustration purposes Figure 4-5 shows a probability density function f(x) for human mortality rates, taken from Chorafas (1960). If one assumed that this plot were describing the mortality probability of the entire human population then the graph in Figure 4-5 would be the **population distribution**. (The 'population' in this case refers to the underlying distribution which an experiment, through drawing a representative sample, is attempting to gain information about). However it is certain that this plot was recorded for a 'sample' of the population and one can see that for this sample, the highest probability of mortality occurs at an age corresponding to the peak in the plot. It is also clear that, for example, if there was a war or national disaster in the country of origin of the data, then the peak in the plot would occur at a lower age.

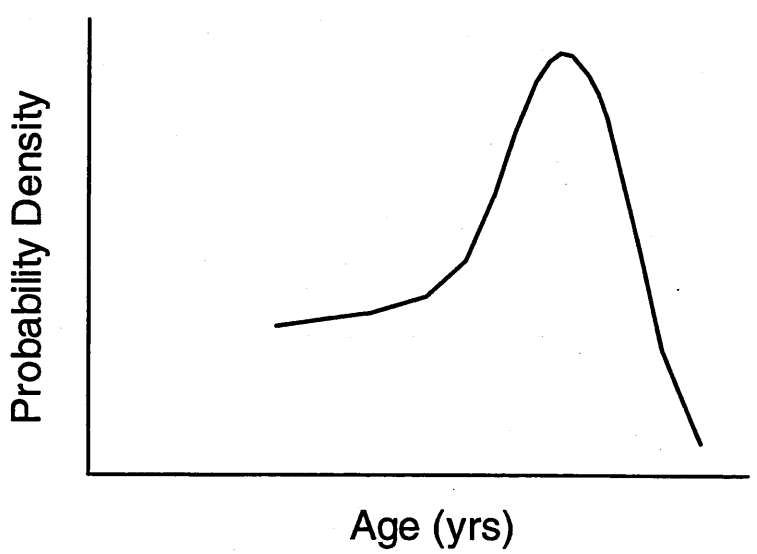

Figure 4-5. Mortality probability density distribution, Chorafas, (1960)

4.3.2 Cumulative probability

The cumulative probability of a sample failing in the time interval 0 to t is represented by $\overline{P}_f(t)$ for a cumulative failure distribution and $\overline{P}_{nf}(t)$ for a cumulative survival distribution. Thus $\overline{P}_f(t) = P(T \leq t)$ and is thus equal to a summation of f(t), the probability density function described above:

$$\overline{P}_f(T \leq t) = \int_0^t f(t).dt \qquad (4\text{-}3)$$

Figure 4-6 shows the cumulative distribution function $P_f(t)$ for the data plotted in Figure 4-5. Again if this plot were representative of the entire population, then it would be more specifically the **cumulative mortality population distribution.** The value of the cumulative distribution function at a

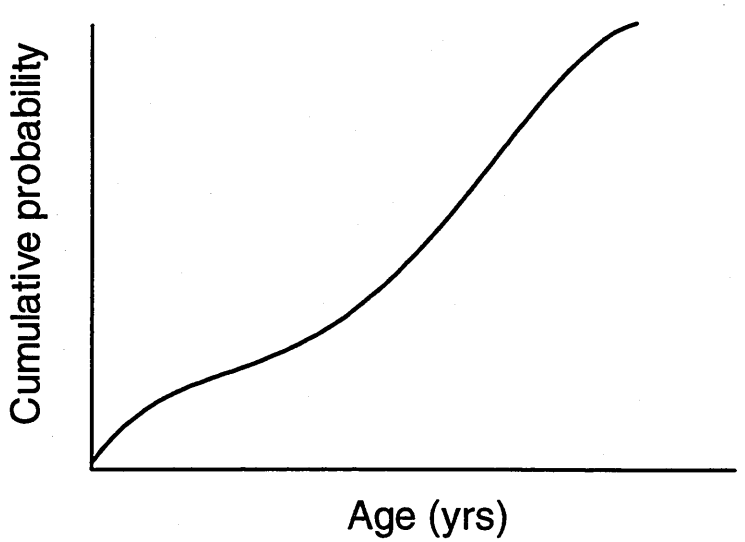

Figure 4-6. Cumulative distribution for human mortality, Chorafas, (1960)

given time, is obtained by summing the area under the curve of the probability distribution, up to and including that time. The converse of the cumulative mortality (or failure) population distribution is the cumulative survival population distribution, sometimes known as the cumulative reliability population distribution. These are related as follows:

$$\overline{P}_f(t) = \left(1 - \overline{P}_{nf}(t)\right) = \int_0^t f(t) \qquad \textbf{(4-4)}$$

where $\overline{P}_f$ is the cumulative failure population distribution, $\overline{P}_{nf}$ is the cumulative survival population distribution and f(t) is the population density function described earlier.

While this allows the calculation of the cumulative population distribution (CPD) from the population distribution, in real terms the nature of the population distribution may not be known. The CPD can then be estimated by the **cumulative survival sample distribution** P_{nf}, as follows:

A) Let $x_1, \ldots\ldots\ldots\ldots\ldots, x_n$ represent the sample consisting of n values arranged in increasing order.

B) The estimate $P_{nf}(x)$ of $\overline{P}_{nf}(x)$ is equal to $1-(n_x/(n+1))$, where n_x is the number of values in the sequence $x_1, x_2, x_3, \ldots\ldots\ldots\ldots x_n$ that are less than or equal to x; i.e. P_{nf} is the fraction of the sample that is less than or equal to x, Johnson, 1994, Chatfield, 1983 and Brockett and Levine, 1984).

Table 4-1 shows values taken from Lapin (1990) for the failure times of floppy diskettes. The cumulative population distribution can then be estimated

from this data set, which also allows the generation of the probability density distribution and the conditional failure rate.

Failure time (hrs.)	$P_{nf}(t)$, $1-(n_x/13)$
2.3	0.92
5.9	0.85
6.1	0.77
9.0	0.69
9.5	0.62
17.9	0.54
18.8	0.46
19.7	0.38
22.6	0.31
23	0.23
24.3	0.15
24.8	0.08

Table 4-1. Sample cumulative survival distribution for data taken from Lapin (1990).

4.3.3 Conditional failure rate

This function like the cumulative distribution is used extensively in reliability theory, which is the study of the performance of products over time. There are several names used to describe this function such as, "**the conditional density function**", "**the instantaneous failure rate**", "**the force of mortality**" or "**the intensity rate**", (Evans, 1992). The conditional failure rate at time t, is defined as the rate of change of probability of failure, given that the component has survived up to time t. This can be represented by

$$Z(t)\,dt = [Pt \le T \le t + dt] \qquad (4\text{-}5)$$

where $T \ge t$. This function can be related to the probability density function and the cumulative distribution in the following way:

$$Z(t) = \frac{f(t)}{P_{nf}(t)} = \frac{f(t)}{1 - P_f(t)} \qquad (4\text{-}6)$$

While the conditional failure rate and the probability density function appear similar, there are important differences between them. The quantity f(t).dt is the unconditional probability that the component will fail in the interval t to (t+dt), whereas the quantity Z(t).dt is the conditional probability that it will fail in the same interval, given that it has survived until time t. A useful analogy is;

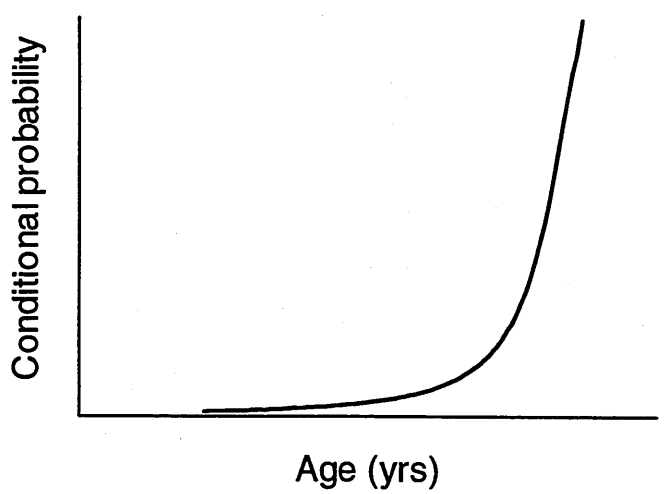

Figure 4-7. Conditional failure rate for human mortality, Chorafas, (1960)

the probability that a new-born child will die at an age between 99 and 100 is quite small because few of them will survive that long. However the probability of dying in that same period, provided that the child has survived until age 99, is much greater. This can be seen in Figure 4-7 and compared with Figure 4-5. The frequency (rate) of mortality for older people is low (Figure 4-5), while the conditional rate of mortality is ever increasing (Figure 4-7).

The work in this study, involved the investigation of the probability of failure of HIPS and ABS with respect to the rubber particle parameters. The statistical aspect of this study is based on work by Sjoerdsma and Boyens (1994), which will be reviewed later, who advanced a model based on the assumption that an underlying relationship exists between the cumulative distribution and the plastic strain in the material. Generally in the field of engineering, the most important probability function is the Reliability function, which is the engineering term for the cumulative survival distribution. Reliability, defined as the probability that a system performs its intended function satisfactorily (from the point of view of the customer) for its intended life, under specified environmental and operating conditions, is basically a design parameter, concerned with the life of the system from the success or failure point of view. For these reason the emphasis in the statistical analysis of the data in this study, is on the cumulative distribution

4.4 Sjoerdsma and Boyens' model for failure probability of High Impact Polystyrene.

Sjoerdsma and Boyens proposed a model based on the proposal that craze impingement causes failure of the material. The model is based on the hypothesis that lifetime predictions, which have been formulated for bulk polystyrene (Ritter et al., 1979) and for thin film polystyrene (Yang et al, 1986) using Weibull statistics, could be formulated for HIPS. Sjoerdsma and Boyens

argued that the rubber particles may act as crack initiating heterogeneities, but the authors discounted this on the evidence that grafted rubber particles stabilise crazes rather than cause craze breakdown. It was proposed that because in a typical HIPS there exists a very high density of crazes, it is inevitable that crazes will impinge resulting in craze breakdown and crack initiation. Due to the high density of crazes at large deformations in HIPS, craze impingement is likely but the fundamental basis of this model is that crack initiation occurs when two crazes impinge. While Sjoerdsma and Boyens acknowledged that they did not directly prove the proposition that craze impingement causes failure, they nevertheless identified the relationship between the strain on the composite and the likelihood of failure.

The model which Sjoerdsma and Boyens advanced is based on the principle of the weakest link. This assumes that a chain with N links is only as strong as its weakest link. Based on fracture occurring through the craze impingement mechanism outlined above, it is proposed that fracture must occur

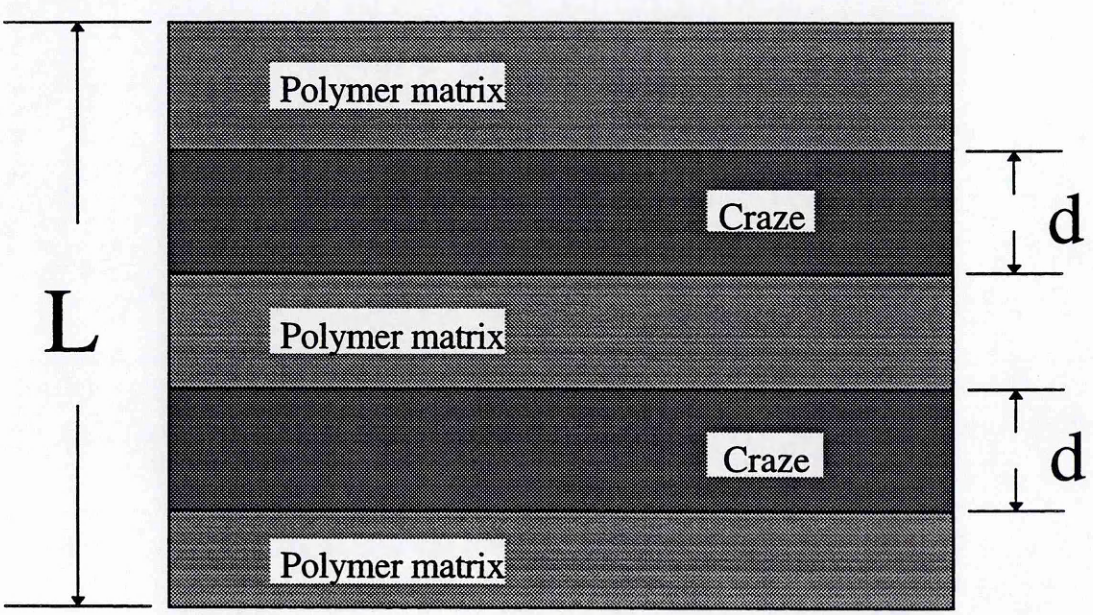

Figure 4-8. Strip of polymer containing N (=2) parallel crazes of thickness d.

at the site with the smallest intercraze distance. Neglecting the time needed for a crack to grow to a fatal size, the probability of non-fracture equals the probability that all intercraze (centre to centre) distances are larger than the craze thickness. In order to determine this probability, a strip of polymer was considered, of length L and containing N randomly placed but parallel crazes of thickness d.

The cumulative probability of non-fracture P_{nf}, that all intercraze distances exceed a value d is given by:

$$P_{nf} = \left(1 - \frac{(N+1)d}{L}\right)^{N} \qquad (4\text{-}7)$$

If the plastic strain due to crazing is given by:

$$\varepsilon_{cr} = \frac{Nd}{L}, \qquad (4\text{-}8)$$

and assuming N is large, through combining with equation (4-7), the non fracture probability P_{nf} can be represented as a function of the plastic strain:

$$P_{nf} = (1 - \varepsilon_{cr})^{\frac{\varepsilon_{\alpha} L}{d}} \qquad (4\text{-}9)$$

Assuming ε_{cr} is small, equation (4-9) can be approximated by:

$$P_{nf} = \exp\left(-\frac{L}{d}\varepsilon_{cr}^{2}\right) \qquad (4\text{-}10)$$

which describes the probability of survival for the strip of polymer with crazes extending along the full length of the slab of material. However Sjoerdsma and Boyens suggested that for the more realistic situation where crazes do not extend across the entire cross-section of the specimen, a better representation of the physical situation would be to divide the specimen volume into parallel columns, with cross-sectional areas equal to that of the crazes. This requires the incorporation into the model of the parameters A and A_c, the cross-sectional area of the specimen and the craze respectively:

$$P_{nf} = \left\{\exp\left(-\frac{L}{d}\varepsilon_{cr}^{2}\right)\right\}^{\frac{A}{A_{cr}}} \qquad (4\text{-}11)$$

or

$$P_{nf} = \exp\left(-\frac{V}{V_{cr}}\varepsilon_{cr}^{2}\right) \qquad (4\text{-}12)$$

where V and V_{cr} are the volume of the specimen and the volume of a craze, respectively. To allow for heterogeneities such as surface scratches, where crazes might initiate preferentially resulting in higher density of crazes, Sjoerdsma et al. generalised the equation to produce equation (4-13) such that k is a parameter that depends on the specimen geometry and the craze geometry. It can be seen from equation (4-13) that by plotting the logarithm of P_{nf} against $(\varepsilon_{cr})^2$ a straight line should result.

$$P_{nf} = \exp\left(-k\,\varepsilon_{cr}^{2}\right) \qquad (4\text{-}13)$$

Sjoerdsma and Boyens extended the model to describe the cumulative survival distribution as a function of the time to failure of the specimen. This was based on the premise that following craze initiation, the creep strain increases linearly with time, i.e. the strain rate to failure is constant. This is given by:

$$\varepsilon_{cr} = \dot{\varepsilon}\,(t - t_i) \qquad (4\text{-}14)$$

where $\dot{\varepsilon}$ is the creep rate, assumed constant, and t_i is the craze initiation time. Substituting for ε_{cr} into equation (4-13) gives the cumulative survival probability of the material with respect to the plastic strain, ε_{cr}:

$$P_{nf} = \exp\left(-k\dot{\varepsilon}^{2}(t - t_i)^{2}\right) \qquad (4\text{-}15)$$

which reduces to

$$P_{nf} = \exp\left[-k\,\dot{\varepsilon}^{2}t^{2}\right] \qquad (4\text{-}16)$$

if the craze initiation time is small compared with the fracture time. Again it can be seen from equation (4-16) that a straight line is expected from plotting the logarithm of P_{nf} against the fracture time squared.

4.5 The Sjoerdsma and Boyens Model applied to fracture strains of HIPS8 blended with PS

The fracture strain data for HIPS blended with polystyrene are plotted in Figure 4-9 against the cumulative survival probability. This plot is seen to exhibit the inverted S shape typical of cumulative distribution plots. The wide distribution of fracture strains, ranging from 0.09 to 0.43 for HIPS6, demonstrates the difficulty and importance in predicting failure of the material. This range of 0.34 corresponds to 80 % of the maximum strain possible for this material. Taking

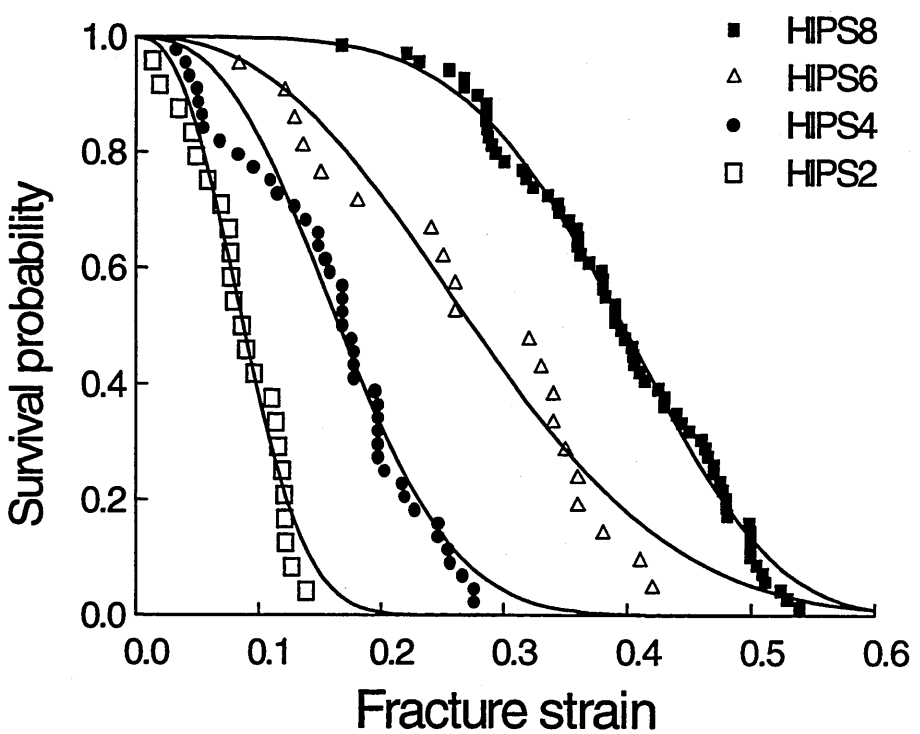

Figure 4-9. Cumulative survival probability for HIPS tested at a constant stress. HIPS8: 14 MPa ; HIPS6: 18.5 MPa ; HIPS4: 22.5 MPa ; HIPS2: 26.5 MPa. The solid lines are fitted according to the Weibull equation introduced later.

into account the finite number of specimens tested for any one experiment it is reasonable to expect some bunching of the data as seen in Figure 4-9, HIPS6.

Figure 4-10 shows the results of a computer based experiment, similar to that of Glandus et al. (1984), in which the survival probability of a perfect Weibull distribution was sampled randomly thirty times. The solid line in Figure 4-10 represents the **cumulative survival population distribution** of failure strains (see Section 4.3.2). The survival probability of this distribution is sampled through generating a random sequence of 30 numbers from the range 0 $< P_{nf} <$ 1. The 'failure strains' corresponding to these survival probabilities, which can directly read off the population distribution, are arranged in descending order and the **cumulative survival sample distribution** is generated in the manner described in Section 4.3.2. The population distribution chosen was similar in breadth and "failure strains" to the failure strain values of HIPS8. The

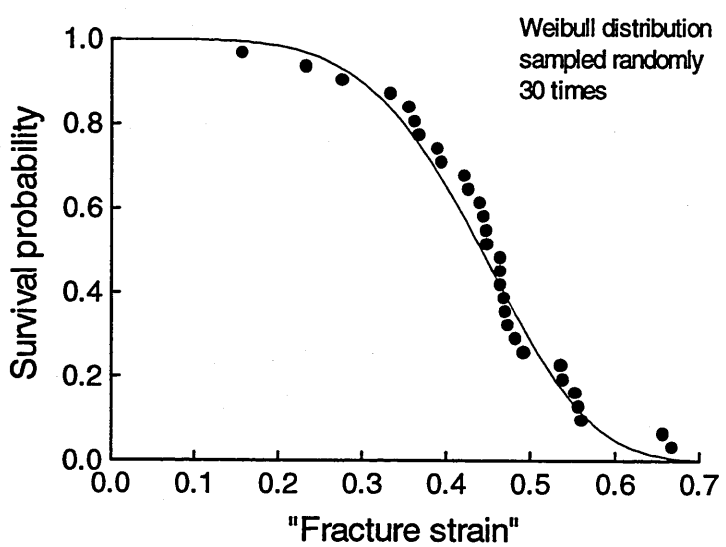

Figure 4-10 Experiment demonstrating the difficulty in sampling the parent distribution by using a finite number of data points. The solid line is the population or parent distribution, and the solid circles are data estimating the population distribution.

sample distribution values were plotted in Figure 4-10. It can be seen that the data bunch around specific strain values, in a similar fashion to that observed for the failure strain distribution of HIPS.

This problem can be alleviated by increasing the number of specimens tested for any one sample, as seen in Figure 4-9, HIPS8. In this sample 68 specimens were tested (as opposed to 20 for HIPS6), and hence the plot is much smoother. However this number of specimens would translate to unreasonably long experimental times. For this reason, the number of specimens ruptured in any one sample averaged 30. In these plots it is important to focus on the overall trend of the data points. Also plotted in Figure 4-9 are curves fitted according to Weibull statistics. These will be referred to in later text.

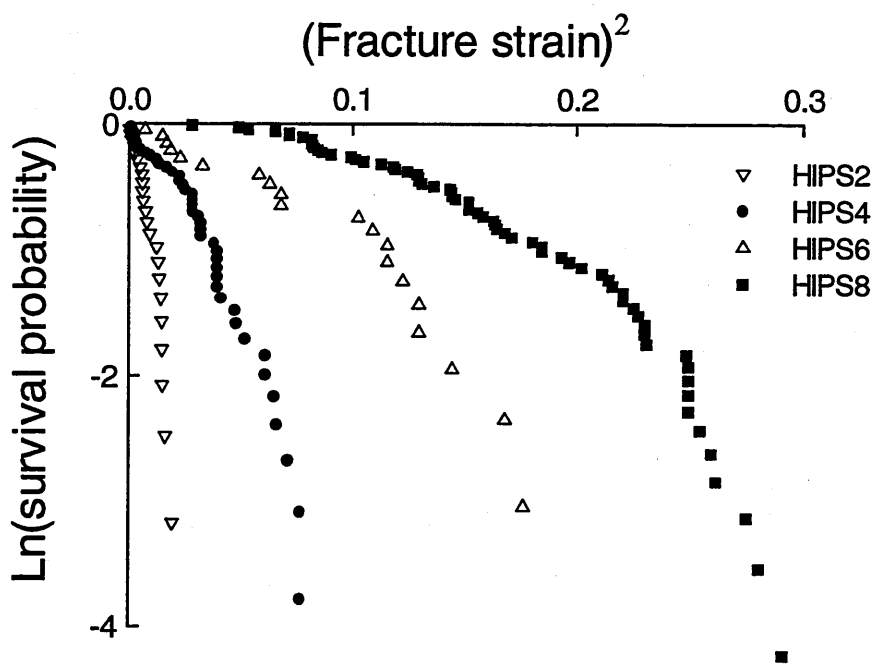

Figure 4-11. Fracture strain results for data shown in Figure 4-9, plotted according to the method described by Sjoerdsma and Boyens (1994).

Sjoerdsma and Boyens defined the craze strain to be the post yield plastic strain, but in the light of recent results due to Buckley (1991) it appears that this is not the case in HIPS and ABS. Buckley in experiments on HIPS using Small Angle X-ray Scattering, found that the fractional contribution of the crazes to the total dilatation, is much smaller than was previously thought. This worker found that the contribution of crazes was at most 50 % for HIPS and even less for ABS. For this reason it is deemed inappropriate to use the term craze strain as defined by Sjoerdsma and Boyens to describe the plastic strain. In the following text the post yield dilatational strain or plastic strain at fracture, calculated as the total strain at failure minus the initial elastic strain (σ_{app} /E), will be simply termed "fracture strain" or ε_{fr}.

The data shown in Figure 4-9, were plotted in Figure 4-11 according to the Sjoerdsma and Boyens method. This shows the natural logarithm of the cumulative survival probability $\ln(P_{nf})$, plotted vs. the fracture strain squared $(\varepsilon_{fr})^2$. Although the Sjoerdsma and Boyens model predicted a linear relationship for this plot, what is observed could not be termed linear. In HIPS6 for example, it could be argued that there is initial linearity up to 0.1, then a change in the slope of the relationship occurs, and a linear relationship again transpires up to a value of 0.16. The HIPS2 plot appears to be linear and indeed it is more linear than HIPS8, but if the scale is increased it can be seen that the plot does in fact display non-linearity, all of which points to the conclusion that the model advanced by Sjoerdsma and Boyens does not correlate the fracture strain data for this material.

4.6 An alternative approach: Weibull equation

The Swedish scientist Walodi Weibull, through analysis of the dynamic breaking strengths of steels, formulated a distribution which today bears his name. The

Weibull distribution is widely used in the fields of reliability, statistics, fatigue and fracture, but its application to material failure is most pertinent to this study. Identical components under identical conditions will fail at different and unpredictable times. The 'weakest link' or 'largest flaw' theory advanced by Griffith, proposed that the reduced strengths of materials is a result of discontinuities, flaws or defects spread at random throughout the specimen. Weibull applied statistics to this principle and formulated an expression, which gives the probability of survival as having a dependence, though statistical in nature, on the size of the specimen.

Using the analogy of a chain made up of n links, Weibull proposed that the chain must fail should any one of its segments fail. Thus if the probability of failure of one its links is P, then the probability of non-failure is (1-P). For a chain with n links, the probability of failure of the chain is P_n, and accordingly the probability of non-failure is $(1-P_n)$, which must equal the combined non-fracture probability of all the links i.e. $(1-P)^n$. If the cumulative distribution can be expressed as:

$$P(X \leq x) = F(x) \qquad \textbf{(4-17)}$$

or $$F(x) = 1 - \exp(-\lambda(x)) \qquad \textbf{(4-18)}$$

and $$(1-P)^n = \exp(-n\lambda(x)) \qquad \textbf{(4-19)}$$

then the cumulative distribution function for a chain of n links takes the form:

$$P_n = \exp(-n\lambda(x)) \qquad \textbf{(4-20)}$$

Weibull defined the function $\lambda(x)$ as a positive non-decreasing function and the simplest function satisfying this condition is

$$\alpha(x-\gamma)^{\beta} \text{ which gives } F(x)=1-\exp\left(-\alpha(x-\gamma)^{\beta}\right) \qquad \textbf{(4-21)}$$

This is known as the three parameter Weibull distribution. Also popular in reliability theory is the two parameter Weibull distribution which is a slightly simplified version of the three parameter distribution. This can be represented by:

$$F(x)=1-\exp\left(-\alpha x^{\beta}\right) \qquad \textbf{(4-22)}$$

and the probability density function is given by

$$f(x)=\frac{dF(x)}{dx}=\alpha\beta(x)^{\beta-1}\exp\left(-\alpha(x)^{\beta}\right) \qquad \textbf{(4-23)}$$

Weibull noted that this method of reasoning could be applied to a large group of problems, *"where the occurrence of an event in any part of an object, may be said to have occurred in the object as a whole"*, and proceeded to demonstrate how this equation could be applied to a wide range of distributions such as yield strength of steel, size distribution of fly ash, fiber strength of cotton and others (Weibull, 1951). In material science and engineering, the Weibull

distribution has been used by many workers such as Yang et al. (1986) who investigated the probability of craze breakdown, and Fedors and Landel (1965), who noted that the Weibull distribution described the variation in the stress and strain at break of SBR-sulfur gum vulcanizates of varying cross-link densities.

Curve fitting was used to correlate the Weibull distribution equation (4-22) with the failure strain data sets. This was carried out using a software package which used the parameters α and β to fit the Weibull distribution to the relevant data sets. The estimated Weibull distributions for samples of HIPS8, HIPS6, HIPS4 and HIPS2 are shown in Figure 4-9.

HIPS6 was tested to rupture in the creep testing station described earlier

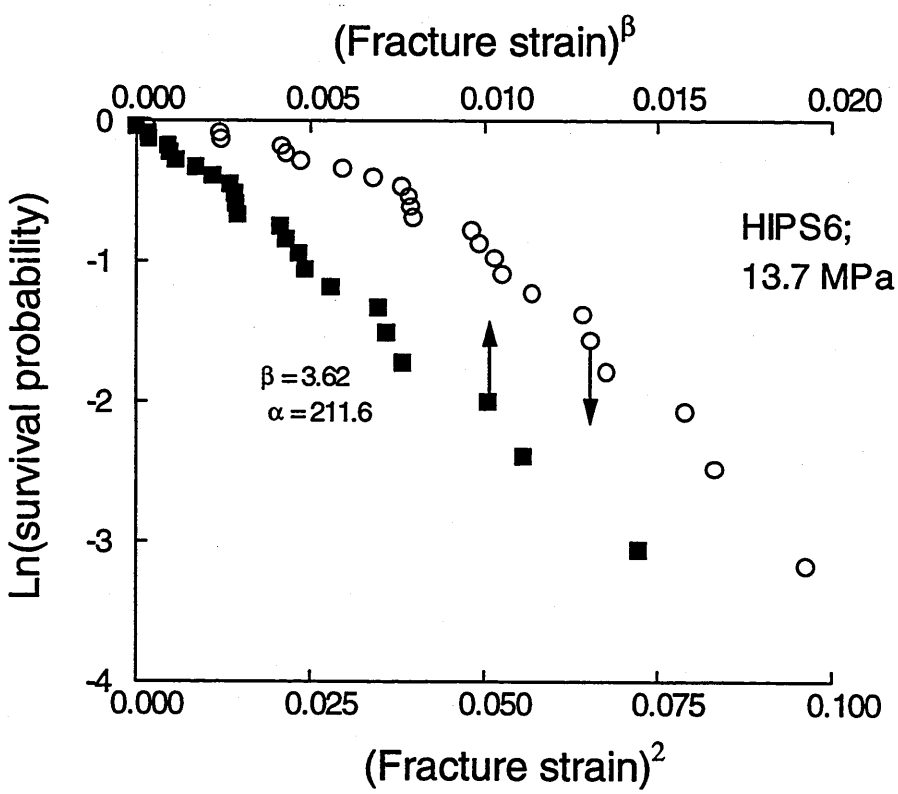

Figure 4-12. Fracture strain data for sample of HIPS6 tested at a constant stress of 16.2 MPa. The data are plotted according to the method due to Sjoerdsma and Boyens (1994) and according to Weibull statistics, equation (4-22).

in Chapter 3, under a constant stress of 13.7 MPa. It is also apparent from equation (4-22) that plotting Ln(survival probability) vs. (fracture strain)$^{\beta}$, should yield a straight line. This can be seen for HIPS6 in Figure 4-12, also as in Figure 4-11, the data are plotted according to Sjoerdsma and Boyens i.e. Ln(survival probability) vs. (fracture strain)^2. Comparison of these methods in Figure 4-12, reveals that the Sjoerdsma and Boyens model does not yield a straight line, indicating again that this model is inappropriate for the HIPS investigated in this study. The Weibull equation appears to be more congruous with the distribution of fracture strains of HIPS6 than the Sjoerdsma and Boyens model does. This will be discussed further later where it will be explained why the Sjoerdsma et al. model is inappropriate for these data.

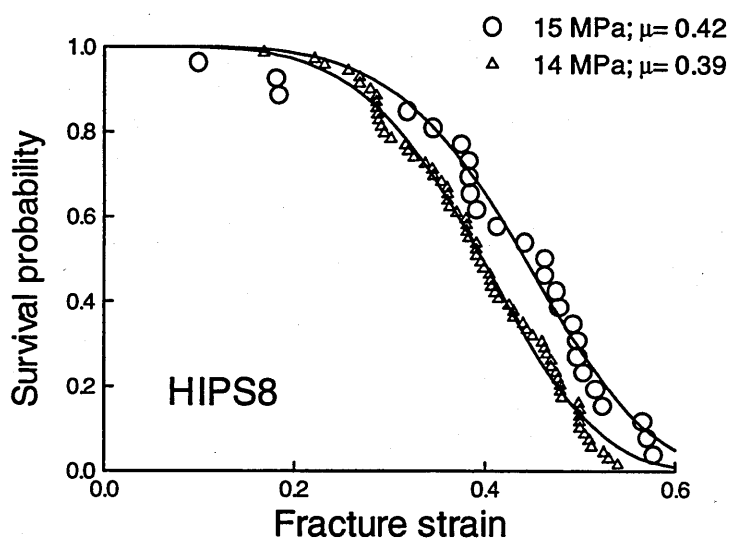

Figure 4-13. HIPS8 cumulative probability of survival assuming subsets of different populations. μ: arithmetic mean fracture strain for sample. The full lines are curves fitted according to equation **(4-22)**, with parameters: Δ: $\alpha = 48.5$; $\beta = 4.6$; O:$\alpha = 34.9$; $\beta = 4.8$.

HIPS8 was extended in tensile creep conditions at two applied stresses. 68 specimens were deformed under an applied stress of 14 MPa, and 25 specimens were deformed under an applied stress of 15 MPa. The cumulative

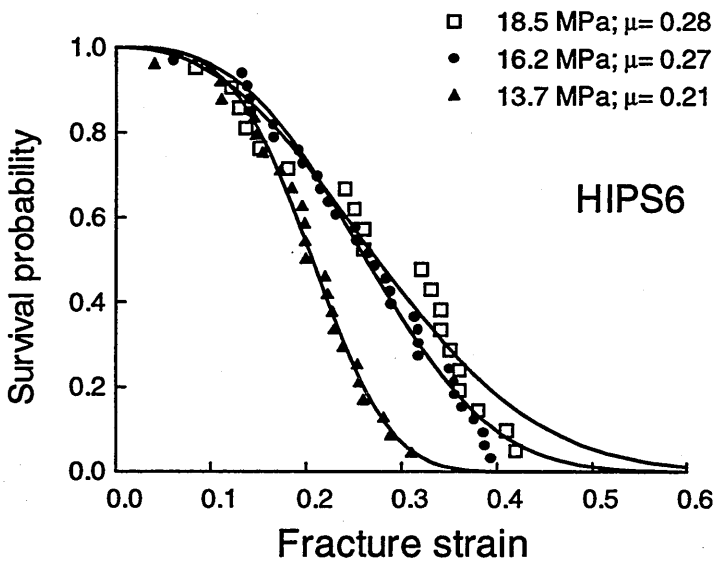

Figure 4-14. Cumulative probability of survival for HIPS6 extended under constant stress. The additional lines are curves fitted according to the Weibull equation with parameters: 18.5 MPa: β= 2.4; α= 15.7; 16.2 MPa: β= 2.9; α= 34.2; 13.7 MPa: β= 3.6; α= 211.6.

probability of survival with respect to strain is shown in Figure 4-13. Also shown is the Weibull distribution fitted to the data. The mean fracture strain of the data is also indicated in the graph. The data in Figure 4-13 are plotted with the assumption that the two data sets are subsets of different populations. This implies that when this material is extended under different applied stresses the probability of failure at a given strain is not necessarily the same.

Three samples of HIPS6, numbering 20, 33 and 23 specimens, were extended to rupture under a constant stress, and the survival probability is plotted in Figure 4-14. Again the Weibull equation is used to correlate the data. Figure 4-13 and Figure 4-14 demonstrate well the effect of applied stress on the probability of failure.

4.7 Histograms of HIPS blended with polystyrene

The fracture strain data for HIPS8 and HIPS blended with polystyrene was analysed to generate histograms. Histograms give an indication of the shape of the probability density function, which was mentioned earlier in Section 4.3.1. The histograms representing the failure strains for the materials HIPS8 and HIPS4, are shown in Figure 4-15 and Figure 4-16. Also plotted in these graphs are Weibull density distributions, generated from fitting the Weibull equation to the cumulative distributions. These are plotted using the Weibull parameters for each sample, (some of which are given in the captions of Figure 4-9 and Figure 4-14) in conjunction with equation (4-23).

Figure 4-17 shows the variation in the failure strain distribution, according to the fitted Weibull distributions, when the rubber content of High Impact Polystyrene is modified. Both the width and the mean of the distributions are seen to increase with rubber content (β increased and α decreased), and the mean is also observed to increase slightly with applied stress.

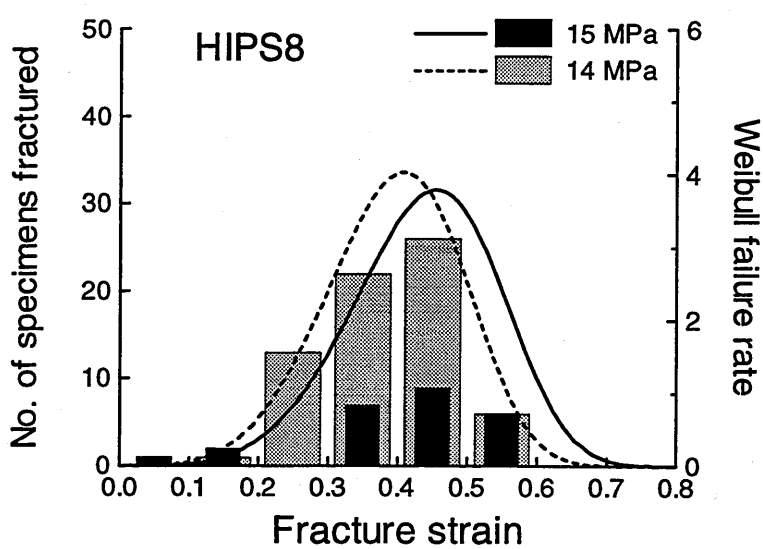

Figure 4-15. Histogram of HIPS8 samples and fitted Weibull distribution

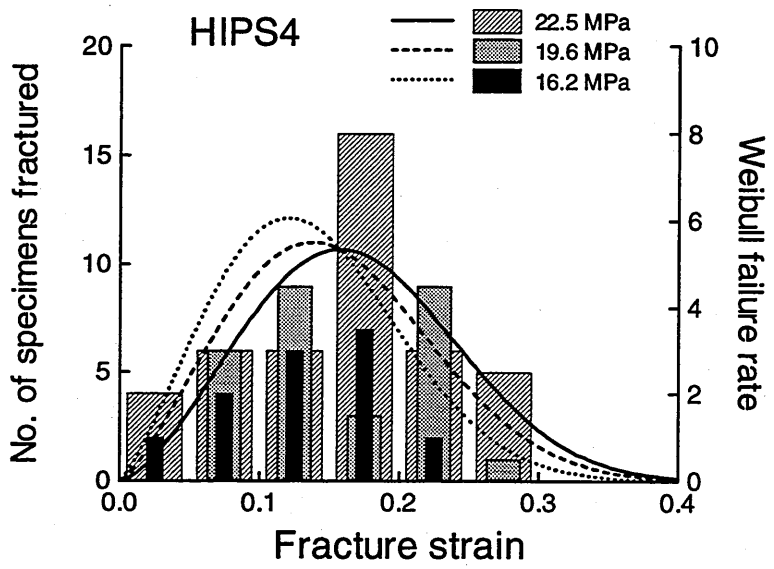

Figure 4-16. Histogram of HIPS6 samples and fitted Weibull distribution

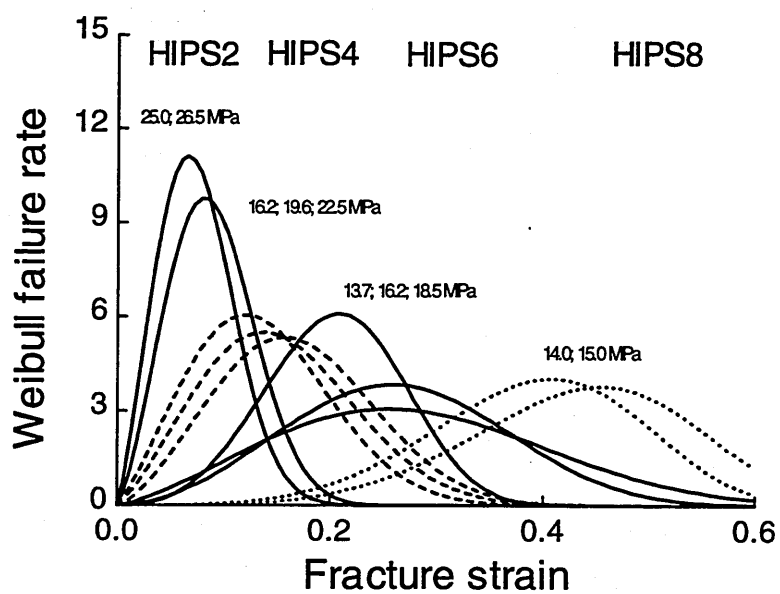

Figure 4-17. Comparison of Weibull density distribution fitted to HIPS8, 6, 4, and 2.

5. RESULTS. HIPS blended with Polystyrene and Sulfur

5.1 Rubber T_g and Constant Displacement Rate

The volume fraction of rubber in HIPS8 was modified, and the effects on the mechanical behaviour characterised in Section 4-1. It is well known that adding sulfur to rubber causes increased cross-linking, and it has been shown that changes in the cross-link density of the rubber has significant effects on the mechanical behaviour of HIPS (Soares, 1994 and Wagner and Robeson, 1970). In this study, the effects of the rubber cross-link density on the mechanical behaviour of HIPS were investigated with respect to failure probability.

HIPS8 was blended with polystyrene to produce HIPS6, HIPS4 and HIPS2, High Impact Polystyrenes with decreasing quantities of rubber. These materials were then blended with sulfur to increase the cross-link density of the rubber. In one experiment, the ratio of sulfur to rubber was kept constant, while in the other the ratio of sulfur to HIPS was kept constant. Increasing quantities of sulfur increases the number of cross-links formed. This is limited by a saturation point where the polybutadiene molecules available for cross-linking are exhausted. In order to keep the same degree of cross-linking in all blends, the concentration of sulfur to rubber phase, designated η, was held approximately constant. Due to the small quantities of sulfur involved, it was very difficult to ensure η was kept constant. For example, a 1.5 kg batch of HIPS2, required a sulfur content of 2.1 gms. Blending this with the HIPS invariably resulted in some sulfur remaining attached to the mixing bag, a feature which to some extent, can be allowed for. Table 5-1 shows the compound names and the constituents of the blends.

Blend name	Ratio of HIPS8 to PS	wt. % Sulfur added
H8:0.28	100:0	0.28
H8:0.56	100:0	0.56
H6:0.42	75:25	0.42
H4:0.28	50:50	0.28
H2:0.14	25:75	0.14

Table 5-1. HIPS8 blended with polystyrene and sulfur. η is kept approximately constant for the latter four blends.

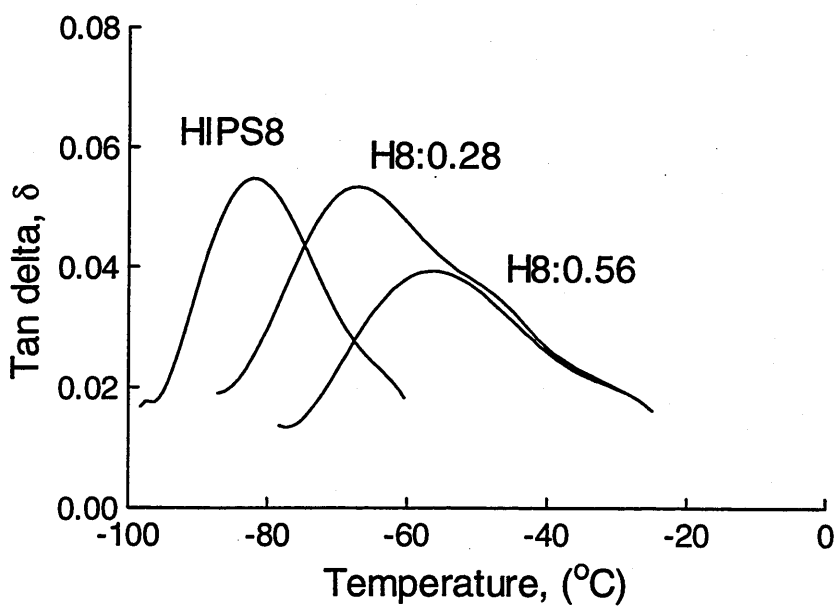

Figure 5-1. Effect of sulfur on the Tan delta peak of HIPS8.

The effect of sulfur on the relaxation spectrum for the rubber part of HIPS is shown in Figure 5-1. The position of this peak gives an indication of the glass transition temperature and therefore, the cross-link density of the rubber. It can be seen that increasing the concentration of sulfur increases the T_g of the rubber, and this relationship has previously been seen to be linear (Perche, 1995).

The polybutadiene tan delta peaks for the blends with constant η, are shown in Figure 5-2. Neat HIPS8 has a glass transition temperature of – 82 °C, while the HIPS blended with sulfur have an average glass transition temperature of – 55 °C. This translates to an increase of 27 degrees. While this is a

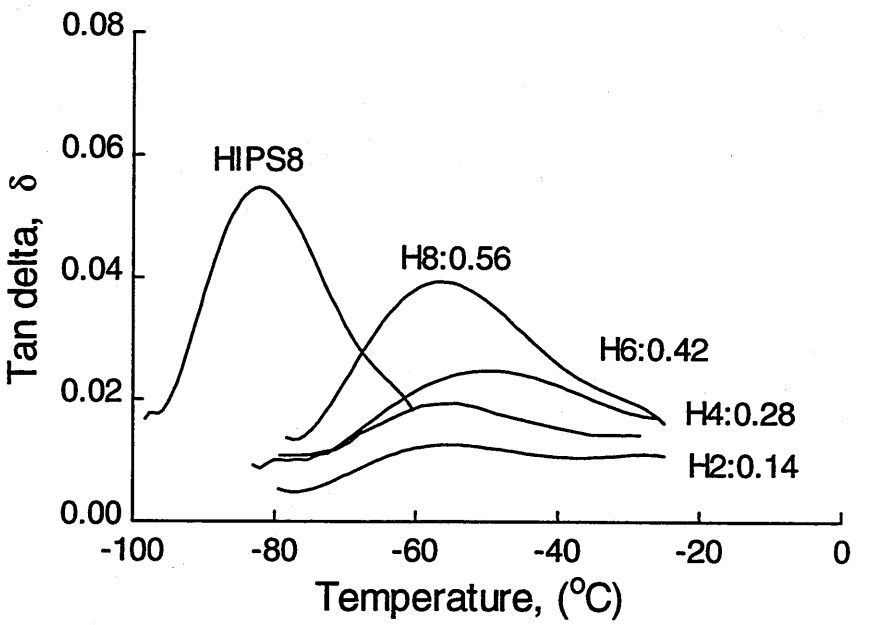

Figure 5-2. Effect of sulfur on the relaxation spectrum of polybutadiene

significant increase, the glass transition temperature is still considerably below the testing temperature and as such the rubber can still be considered rubbery. Previous workers have demonstrated mechanical changes in HIPS due to the addition of sulfur (Wagner and Robeson, 1970; Perche, 1995 and Lin, 1997). Perche (1995) investigated the effects of sulfur on the toughening mechanisms of HIPS, and found a similar shift in the polybutadiene T_g as observed in this study. This worker did not observe any change to the position of the peak corresponding to the glass transition of polystyrene, and concluded that the addition of sulfur did not effect the matrix. In a more recent and detailed study Lin (1997), also in an examination of the effects of sulfur on the toughening

mechanisms of HIPS, found that the rubber T_g increased with the addition of sulfur, and indeed following the addition of 2.4 wt. % sulfur, observed the rubber T_g to shift from – 81 °C to 10 °C. Lin also found that the rubber molecular weight increased, while the matrix molecular weight remained relatively unchanged. With this in mind, it is concluded that any changes detected in the mechanical behaviour of the material following the addition of sulfur, are a direct consequence of the increased rubber cross-link density.

The stress vs. strain curves for the vulcanisates with constant η are shown in Figure 5-3. The material parameters pertaining to the HIPS/PS/sulfur blends can be compared with the material parameters pertaining to HIPS/PS blends, so that variations induced by increased rubber cross-link density can be detected. The elastic modulus was observed to increase from 1.69 GPa for HIPS8 to 1.88 GPa for H8:0.56, and the fracture strain was seen to decrease. Further changes are more apparent from Figure 5-4, where it can also be seen that following the

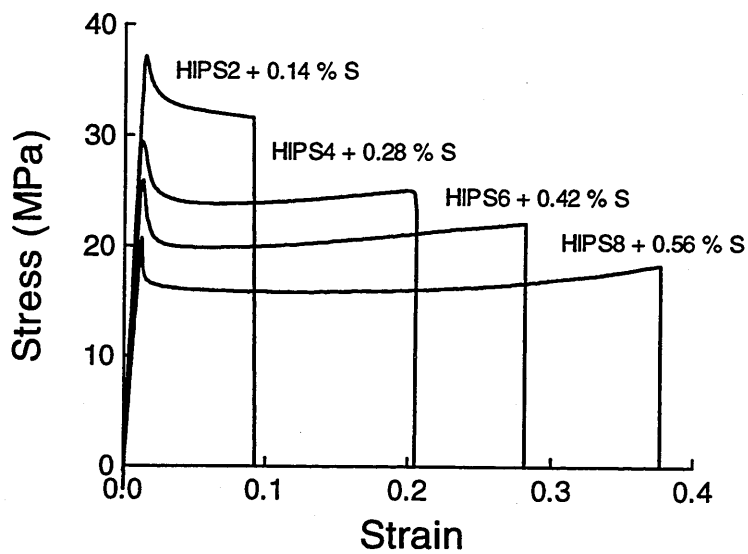

Figure 5-3. Stress/strain curves for HIPS blended with general purpose polystyrene and sulfur.

addition of sulfur, the yield, flow and breaking stresses all increase.

HIPS with decreasing volume fraction of rubber, was also blended with a constant HIPS/sulfur ratio, i.e. η varying. It is clear that if a constant weight percentage of sulfur is added to materials containing a decreasing rubber content, then the ratio of sulfur to rubber increases. Table 5-2 shows the blend names and the constituents of these materials.

Blend name	Ratio of HIPS8 to PS	wt. % Sulfur added
H6:0.50	75:25	0.50
H4:0.50	50:50	0.50
H2:0.50	25:75	0.50

Table 5-2. HIPS8 blended with polystyrene and sulfur. η is increasing with decreasing rubber content.

The effect of this is seen in Figure 5-5 where the traits observed in Figure 5-3 are heightened. H2:0.50 has the lowest volume fraction of rubber and thus will have the highest value of η. As a result, it exhibits behaviour which is not unlike that of unfilled polystyrene. Bucknall (1977) shows polystyrene undergoing brittle failure at a fracture stress of circa. 44 MPa. It appears that increasing the modulus of the rubber until it is comparative with the modulus of the matrix, produces a level of deformation in the composite, which is more characteristic of the unfilled material.

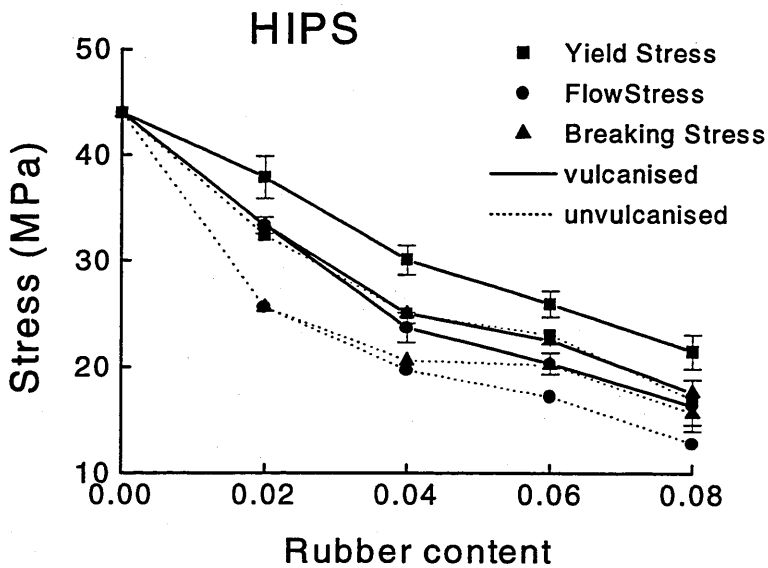

Figure 5-4. Effect of rubber cross-link density (constant η) on the yield, flow and breaking stress of HIPS.

A more non-linear perturbation to the tensile parameters is noticed for the materials with η varying. This non-linear trend is compounded by the fact that HIPS8 was blended with 0.56 wt % sulfur in comparison with 0.50 wt. % sulfur for the other three materials. In other words while we are assuming that the weight percentage of sulfur in the blends is constant, HIPS8 has a sulfur content which is slightly higher than the others. Figure 5-6 illustrates this non-linearity through comparing the yield, flow and breaking stresses. Each plotted yield or flow stress value is the average of three tests. Each breaking stress value is the maximum of three tests. As previously mentioned, because of a slight difference in the actual quantities of sulfur blended, H8:0.56 exhibits slightly higher values than extrapolation of the results from the other materials would suggest.

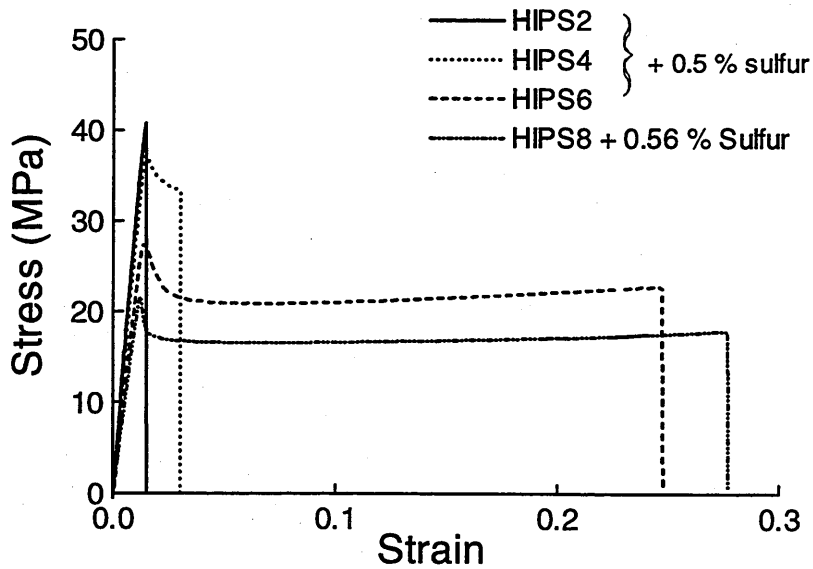

Figure 5-5. Effect of rubber cross-link density (varying η) on the constant displacement rate behaviour of HIPS.

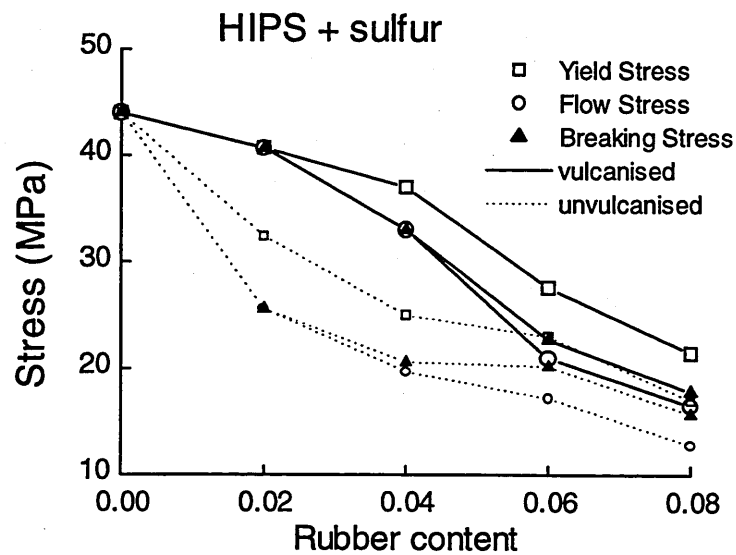

Figure 5-6. Effect of increasing η with decreasing rubber particle volume fraction, on the yield, flow and breaking stress of HIPS.

As seen in Figure 5-4, Figure 5-6 shows that the slope of the vulcanised materials relationship decreases at lower rubber particle volume fraction, due presumably, to saturation of the rubber phase with sulfur, and shows that the

composite behaviour approaches that of the unfilled matrix. The breaking stress for unvulcanised polystyrene indicated in Figure 5-6 is taken from Bucknall (1977), and as sulfur should have little effect on polystyrene, the same value is assumed for polystyrene blended with sulfur.

5.2 HIPS blended with PS and Sulfur extended in creep

The rubber cross-link density clearly has a significant effect on the deformation behaviour of HIPS extended at a constant displacement rate. These materials were also investigated under creep conditions and the results are shown below. HIPS8, H8:0.28 and H8:0.56 were extended under a constant stress of

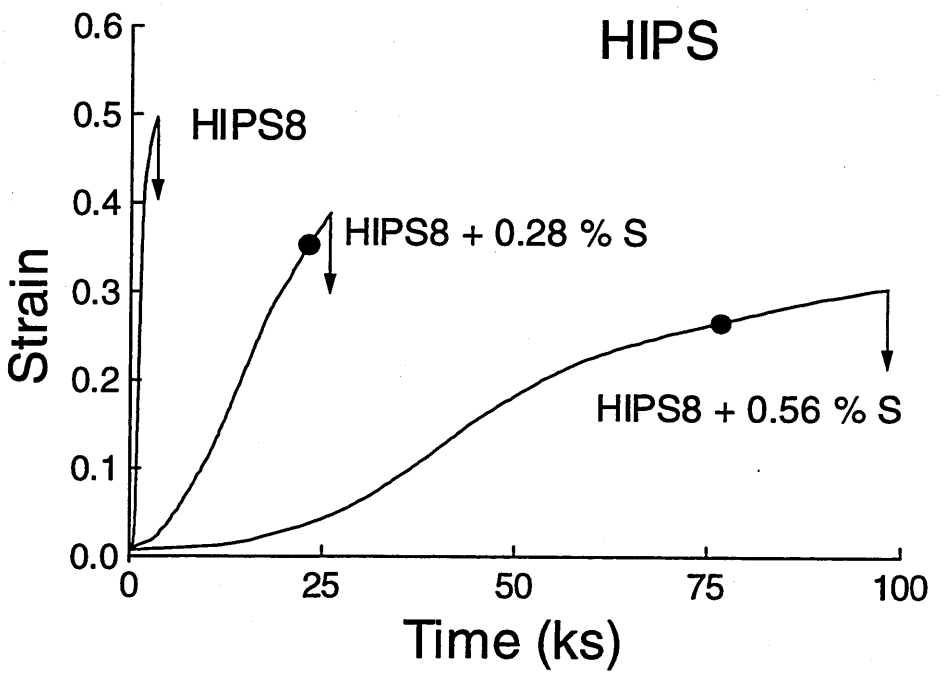

Figure 5-7. Effect of rubber cross-link density on the creep behaviour of HIPS. The specimens were deformed at an applied stress of 13.7 MPa.

13.7 MPa and the strain was monitored with respect to time. The results shown in Figure 5-7, demonstrates the considerable effect rubber cross-link density has on the creep behaviour of HIPS. (Note: the unit of time in the x axis is kiloseconds). The induction time is considerably increased following the

addition of sulfur, which indicates that the kinetic process controlling the initiation of crazes, is somehow influenced by the cross-link density of the rubber phase. It is also clear from Figure 5-7 that the strain rate of the material is considerably reduced with the addition of sulfur. The maximum rate of strain of the materials decreased from 4.6×10^{-2} s^{-1} for HIPS8 to 6.5×10^{-4} s^{-1} for H8:0.56. The strain at failure of HIPS is also seen to be considerably affected by the cross-link density of the rubber. 25 specimens of HIPS8 were extended under an applied stress of 15 MPa, and the highest recorded value of strain at failure was 0.583. For 21 specimens of H8:0.28 and 20 specimens of H8:0.56 extended under an applied stress of 13.7 MPa, the highest recorded values for the strain at failure were 0.47 and 0.33 respectively.

Therefore, the cross-link density of the rubber phase affects the kinetic processes controlling the rate of extension, namely craze initiation and dilatation, and also affects the mechanism controlling the final rupture of the material.

5.2.1 The Weibull model applied to the creep rupture data of HIPS blended with PS and sulfur.

The probability of survival of HIPS blended with polystyrene and sulfur, deformed under creep conditions was examined, and Weibull statistics were used to correlate the results. Figure 5-8 shows the cumulative probability of survival of the materials. Comparison of Figure 5-8 with Figure 4-9 reveals that the addition of sulfur causes a shift to lower failure strains. This indicates that the probability of survival at a given strain, decreases with increasing rubber cross-link density. This seems to suggest that the rubber cross-link density should be minimised to maximise the fracture strain. However as can be seen from Figure 5-3, decrease in rubber cross-link density results in a decrease in the flow stress, which counteracts favourable increases in the strain at break. Also Wagner and Robeson (1970) proposed that some cross-linking is necessary, in order to

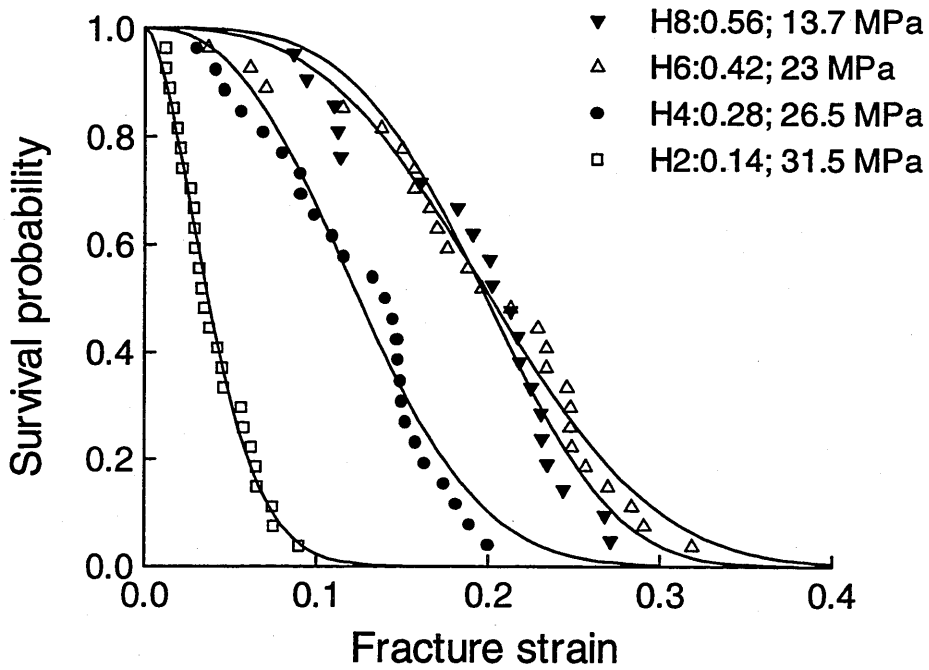

Figure 5-8. Cumulative probability of survival of HIPS blended with PS and sulfur. η, the ratio of sulfur to rubber, is held constant in the blend recipes. The solid lines are Weibull distributions fitted to the data using the following parameters. H8:0.56: α = 307; β = 3.7; H6:0.42: α = 86; β = 3.0; H4:0.28: α = 128 β = 2.5; H2:0.14: α = 183; β = 1.7;

maintain the structure of the rubber particles during melt processing.

It is noticeable from extrapolation of the mean failure strain for the other materials in Figure 5-8, that the average failure strain for H8:0.56 is lower than expected. This will explained later to be a consequence of the level of applied stress, because reference to Figure 4.13 and Figure 4.14, demonstrates a stress dependent probability of failure for HIPS. As the applied stress is increased, the probability of failure at a given strain increases. This effect is discussed in more detail in Chapter 11.

Figure 5-9 shows the cumulative probability of survival for HIP6 compared with H6:0.42. Again, as discussed earlier, the probability of failure of the material at a given strain increases with increase in cross-link density of the rubber phase. Samples of H6:0.5 and H4:0.5 were also tested in creep and,

owing to the higher values for η, the changes to the creep behaviour of the material were even greater.

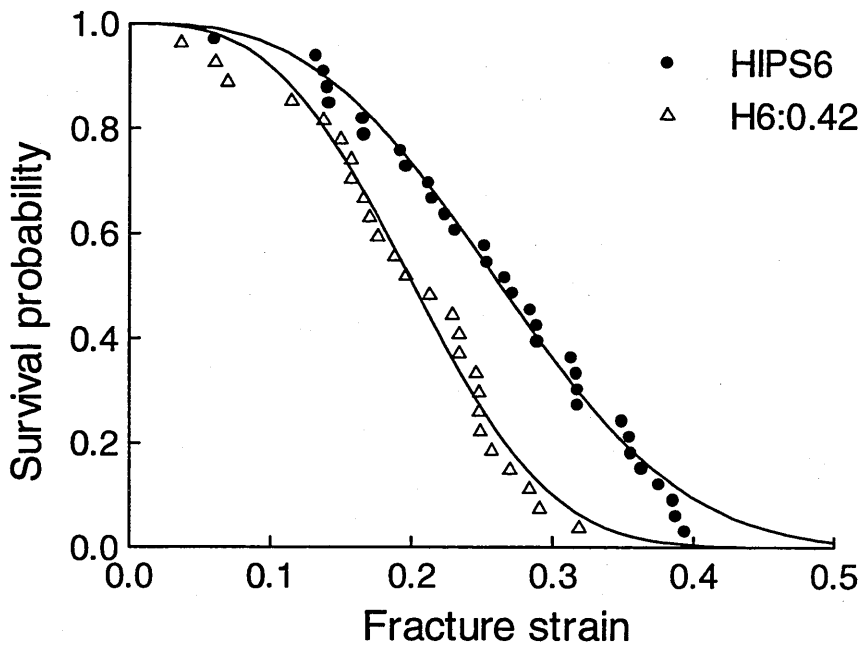

Figure 5-9. The effect of varying the rubber cross-link density on the cumulative probability of survival of HIPS6. Unvulcanised σ_{app}= 18.5 MPa; vulcanised σ_{app}= 23 MPa.

6. RESULTS. Effect of stress and irradiation on HIPS

6.1 Effect of creep stress and pre-stressing on flow rates of HIPS

The period before rapid dilatation, denoted the induction period by Bucknall and Clayton (1972), serves as a useful lower limit of the failure time of HIPS and ABS. That is to say, the vast majority of specimens do not fail before the induction time has elapsed. This is a useful material parameter in renewal theory and engineering design, because one can say with conviction, that the probability of failure under uni-axial stress before the induction time is reached, is almost negligible. For a given material the induction time varies considerably with applied stress and temperature. Other factors can also produce significant changes such as rubber content (Bucknall et al., 1986b), and rubber cross-link density (O' Connor and Bucknall, 1997). Bucknall et al (1986b) showed that the

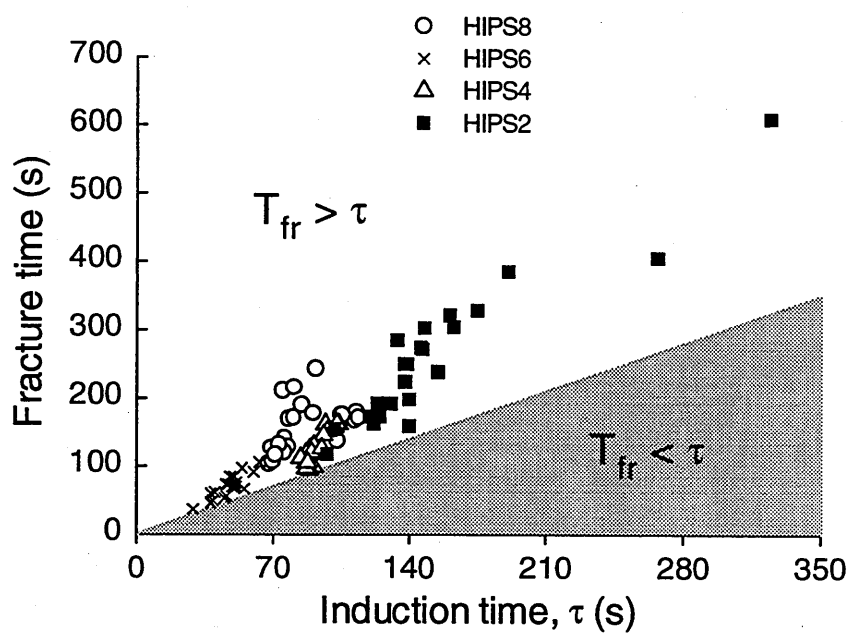

Figure 6-1. Plot showing failure of HIPS occurring predominantly after the induction time τ was reached.

Eyring rate equation could be used to describe the relationship between stress and induction time, and stress and maximum strain rate.

6.1.1 Eyring Flow Model

It is now generally accepted that Eyring rate theory can be used to describe stress and temperature activated flow processes in materials. Eyring rate treatment is an extension of the Arrhenius analysis of chemical rate processes, which states that the reactant molecules must jump over an energy barrier in order to convert to product molecules. In describing flow of polymers, the fundamental idea is that a

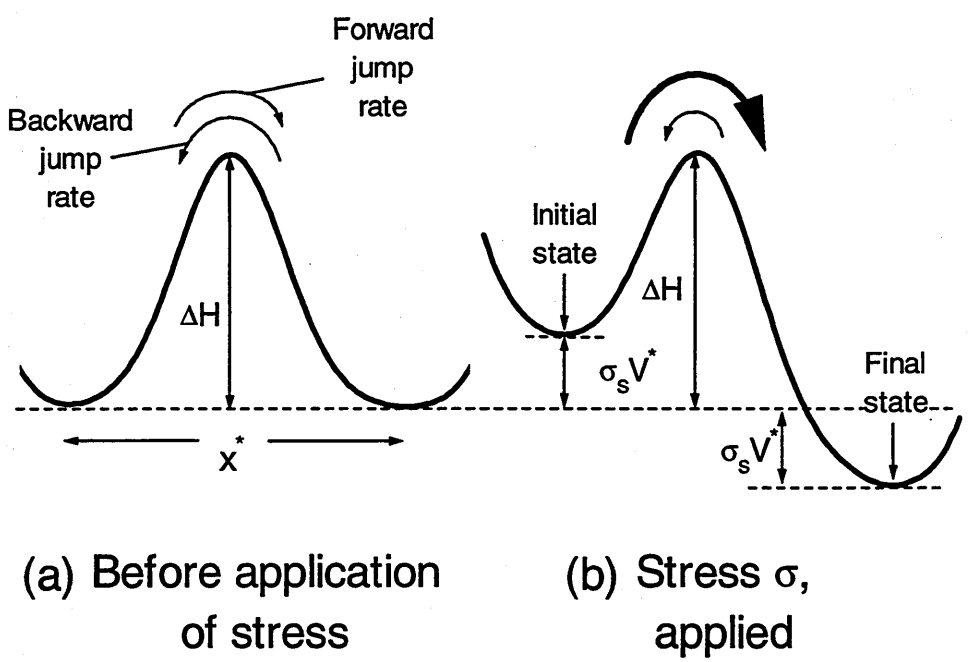

Figure 6-2. Eyring model for flow of polymers. (a) at zero applied stress the molecules exist in potential wells, separated from neighbouring potential wells by an enthalpy barrier ΔH and a distance x^*. The molecules pass over this barrier infrequently and in a random direction; (b) on application of shear stress the height of the enthalpy barrier is changed: (1) in the forward direction to $\Delta H - \sigma x^*$, thereby making it easier to jump to a neighbouring position, (2) and the backward direction to $\Delta H + \sigma x^*$, thus making it more difficult to jump backwards to a neighbouring position (McCrum et al., 1988).

section of a macromolecule must overcome an energy barrier to move from one position to another in the solid. In the unloaded material, the segments seldom have enough energy to pass over this barrier and the direction is random (McCrum et al., 1988). This rate of jump can be given by

$$\text{jump rate} = Q\exp\left(-\frac{\Delta H}{RT}\right) \qquad \textbf{(6-1)}$$

where ΔH is the enthalpy required to take a mole of the macromolecule from the potential well to the top of the barrier, see Figure 6-2, T is the temperature and Q is a constant. With the application of a shear stress, the enthalpy barrier is modified so that the probability of segments having enough energy to pass over the barrier in the forward direction, is now much greater. The converse is true for the backward direction, because the enthalpy barrier is now greater in this direction. The rate of jump in the direction of the applied stress is represented by:

$$\text{forward jump rate} = Q\exp\left(-\frac{\Delta H - \sigma_s V^*}{RT}\right) \qquad \textbf{(6-2)}$$

where V^* is the activation volume, defined as the area of the polymer segment A^*, times the distance between equilibrium positions, shown in Figure 6-2 as x^*. The ratio of forward to backward jumps can now increase to such an extent as to produce a measurable change in the strain (McCrum et al., 1988).

The net jump rate can be given by:

$$\text{net jump rate} = Q\left\{\exp\left(-\frac{\Delta H - \sigma_s V^*}{RT}\right) - \exp\left(-\frac{\Delta H + \sigma_s V^*}{RT}\right)\right\} \qquad \textbf{(6-3)}$$

which reduces further, because the rate of backward jumps is even lower than before the stress was applied, and can therefore be assumed negligible. The final form of the Eyring equation used to describe rate effects under creep conditions is given by:

$$\text{rate} = A \exp\left(-\frac{\Delta H - \gamma V^* \sigma_{app}}{RT} \right) \qquad (6\text{-}4)$$

where γ is a stress concentration factor to allow for increased local stresses on the flow segment (Bucknall, 1986b) and σ_{app} is the creep stress.

Bucknall and Clayton (1972) plotted rate of dilatation and reciprocal induction time τ against applied stress. In later work Bucknall et al (1986b) examined the effects of rubber content on the yield behaviour of HIPS, and again used the Eyring equation to describe the relationship between the rate of dilatation and the applied stress, and the relationship between the reciprocal induction time and the applied stress. However, unlike pure shear yielding in materials such as polycarbonate, which display a constant slope of the relationship between the logarithm of flow rate and stress/T (McCrum et al. 1988), the rate/stress relationship for HIPS was seen to be more complex. Bucknall et al. (1986b) demonstrated that the slope of the plot: logarithm of flow rate vs. stress, increased with increase in rubber content. Bucknall and co-workers concluded that the differences in the slopes of the Eyring plots for HIPS of different rubber particle volume fractions were due to different stress concentration factors affecting the rate controlling step. Assuming a value of 1.4 nm^3 for the activation volume V* of polystyrene, and using the slope of the Eyring plot for reciprocal induction time, these workers showed that the stress concentration factor increased from 2.6 for a HIPS blend with 10.5 % rubber particle volume fraction, to 6.5 for a HIPS blend with 35 % rubber volume

particle fraction. They also demonstrated higher slopes for the Eyring plots of maximum strain rate vs. stress, which using 1.4 nm^3 for V*, translates to higher stress concentration factors.

6.1 Effect of creep stress and pre-stressing on flow rates of HIPS (Cont'd)

The flow rates of HIPS8 and its blends with G.P.P.S. were also seen to follow the Eyring rate equation. Figure 6-3 and Figure 6-4 show the Eyring plots: log(induction time) vs. applied stress, and log(maximum strain rate) vs. applied stress respectively.

In order to observe changes to the flow rates and failure probabilities of HIPS8, the material was loaded to a high stress for a short period, and subsequently extended to rupture under a lower constant stress. The stress was

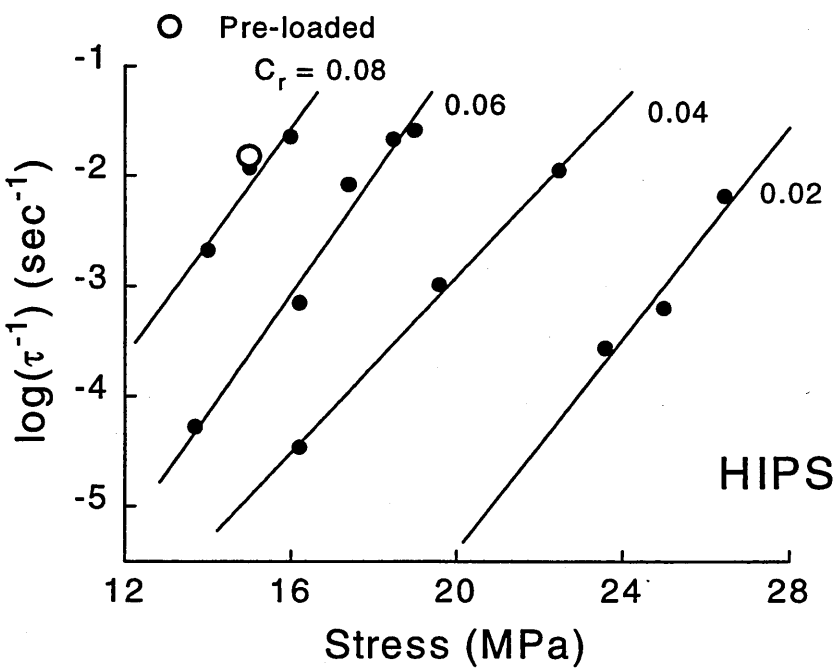

Figure 6-3. Eyring plot of log(induction time, τ) vs. creep stress. Also indicated is the induction time for a specimen which was pre-stressed under 16 MPa for 10 seconds, followed by extension to failure at 15 MPa.

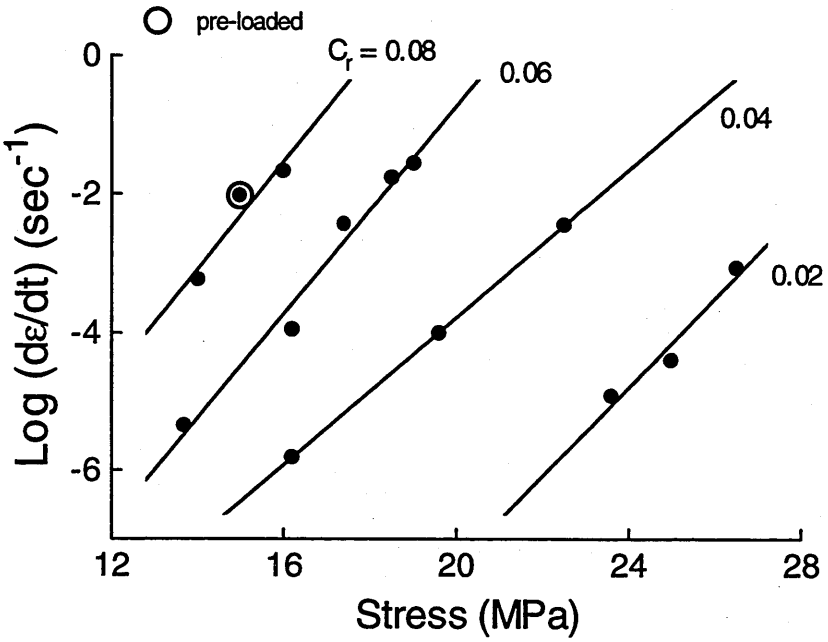

Figure 6-4. Eyring plot of log (maximum strain rate) vs. creep stress. Also indicated is the maximum strain rate for a specimen which was pre-stressed under 16 MPa for 10 seconds, followed by extension to failure at 15 MPa.

initially increased to 16 MPa, before any widespread craze formation should have taken place, and then decreased to 15 MPa, which was held constant until failure resulted. The stress/time plot is shown in Figure 6-5, where it is observed that application of the pre-load decreased the induction time by a factor of 2, (this can also be seen in Figure 6-3. This is underlined by the fact that the material was under the high stress for only what would have been 10 % of the induction time. This again suggests that the initiation rate determining step in deformation of HIPS is an activated process, and it is highly dependent upon stress. However pre-loading appears to have little effect on the maximum strain rate. Figure 6-4 demonstrates that the maximum strain rate is unchanged by the applied pre-load, and depends only on the level of applied stress during widespread deformation.

6.2 Effect of pre-stress on the failure strain and the failure time of HIPS

The effect of pre-loading on the failure probability of HIPS, can be seen in Figure

6-6. Pre-loading appears to have a slight effect, as it was found that the mean failure strain for the 15 MPa batch is 0.423, compared with 0.432 for the pre-loaded batch. Also the maximum failure strain for the 15 MPa sample is 0.581 compared with 0.591 for the pre-loaded batch. Of course these shifts may be an aberration of scatter of the data.

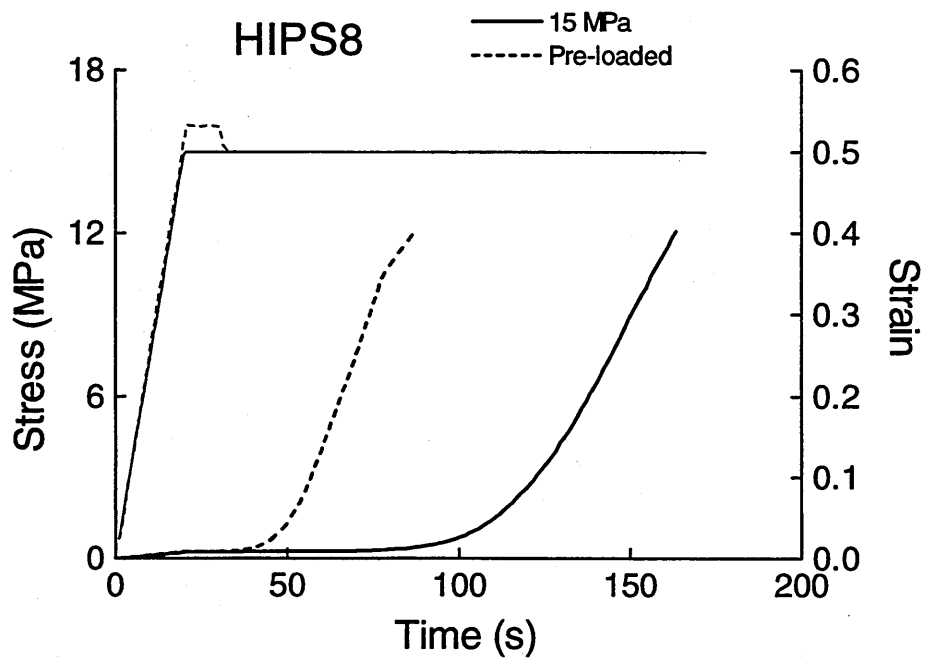

Figure 6-5. Plot showing stress/strain curves and creep curves for HIPS8, which was pre-stressed under 16 MPa for 10 seconds, followed by extension to failure at 15 MPa

The probability of failure with respect to time was considerably affected by the pre-loading, see Figure 6-7. The mean failure time for the 15 MPa sample is 150 seconds, compared with 124 seconds for the pre-loaded sample. This in fact, is a deceiving comparison because two of the pre-loaded specimens extended for much longer times than the others, which increases the mean failure time for the batch. The shape of the distribution of failure times of the pre-loaded sample is seen to be quite different than the no pre-load sample. For the initial 50 % of specimens, the application of the pre-load appears to just shift the no pre-

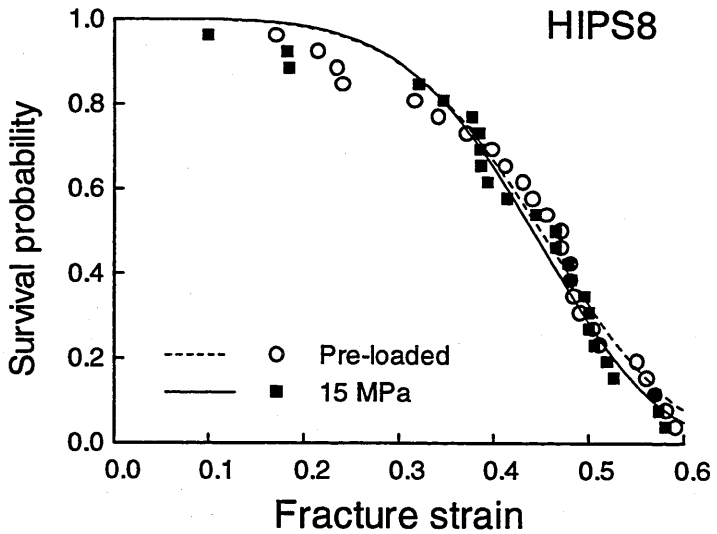

Figure 6-6. Effect of pre-loading on cumulative probability of HIPS8 with respect to strain. Full lines are distributions fitted according to Weibull statistics.

load distribution to lower times, i.e. the rate of specimen failure at 50 seconds for the **pre-loaded** batch is similar to the **no pre-load** batch rate of specimen failure at 120 seconds.

However the latter 50 % of the pre-loaded specimens, appear to be able to stabilise better than the no pre-load specimens, and indeed as mentioned, two pre-loaded specimens extended much longer than any of the no pre-load specimens.

6.3 HIPS modified with Gamma irradiation

It was previously shown in Chapter 5 how the addition of sulfur to HIPS, through increasing the cross-link density of the rubber phase, significantly changes the deformation behaviour of the composite. Blending with sulfur caused a marked increase in yield, flow and breaking stresses, and the strain at failure was seen to significantly decrease. However the drawback of this, is that the composite has to

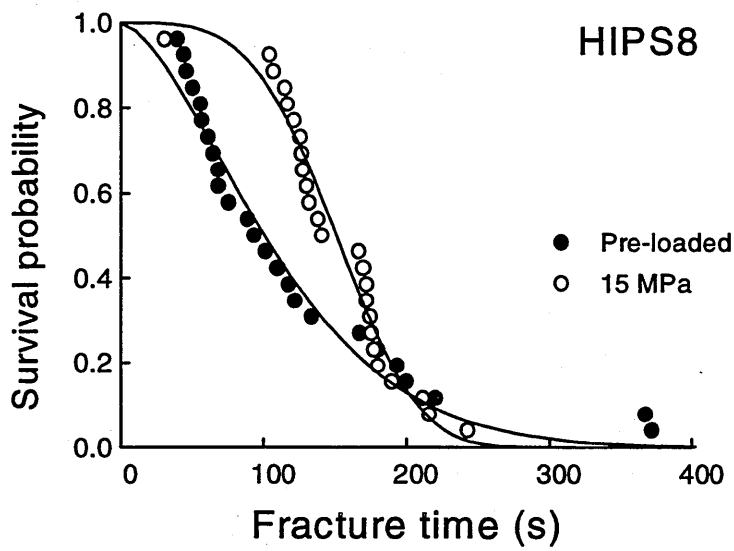

Figure 6-7. Effect of pre-loading on cumulative probability of HIPS8 with respect to time. Full lines are distributions fitted according to Weibull statistics.

be melt blended with the sulfur in order that the cross-linking reaction can take place.

An inherent problem with characterising changes in material properties, which result from modification of the rubber cross-link density, is normalisation of the number of crazes with respect to strain. At a given strain, a composite with a low rubber shear modulus may have a different number of crazes than a composite with a high rubber shear modulus. Moreover, the number of crazes dictates the following:

- the rate of displacement of the craze/bulk interface (thus the stress on the active zone) and
- the extension to which the accompanying rubber particle fibrils will be stretched to accommodate craze thickening.

Irradiation allows mechanical testing of the material in conjunction with

intermediate rubber cross-linking. Thus the material can be damaged, creating approximately the same number of crazes, followed by an increase in the rubber shear modulus. Using this principle, the effects of rubber cross-link density on the high strain deformation of HIPS8 was probed.

A batch of HIPS8 was pre-strained to 20 % under a constant stress of 14 MPa. Half of the specimens in the batch, were subsequently irradiated under nitrogen with 20 Mrad gamma irradiation, while the other half were stored at room temperature. The load was then reapplied to both batches and the specimen's response monitored with respect to time. Figure 6-8 shows the initial loading, followed by this material's non-linear (with respect to time) extension.

It can be seen that the strain rate is significantly affected by the rubber shear modulus. The non-irradiated HIPS continued as if uninterrupted, indeed the strain rate is typical of HIPS8 at a constant stress of 14 MPa. However the strain

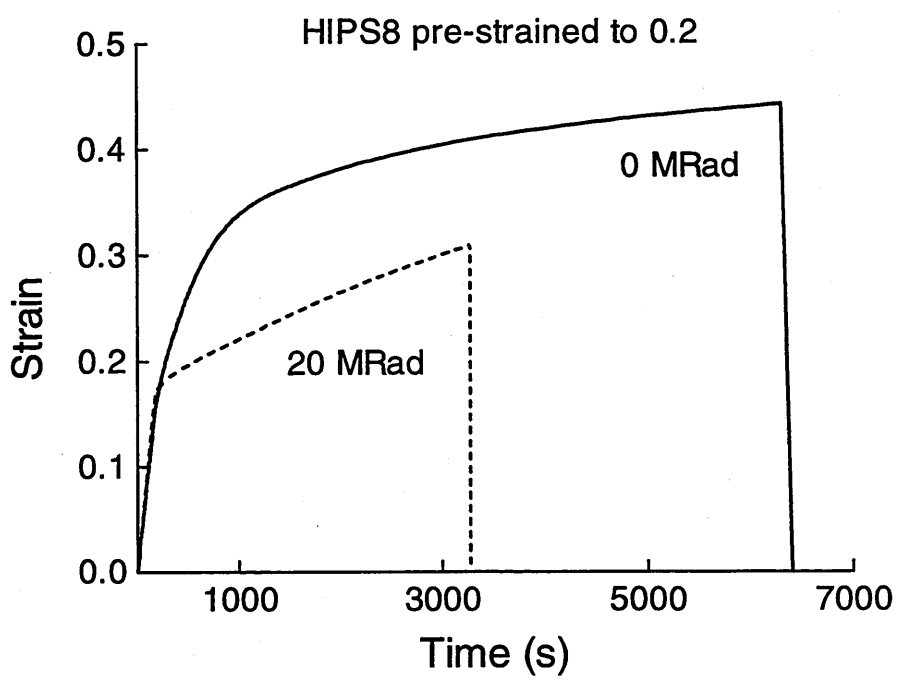

Figure 6-8. HIPS8 pre-strained to 0.2, irradiated, followed by creep at 14 MPa.

rate of the irradiated HIPS decreases significantly, and the mean strain at failure is also depressed. Indeed it was observed that 5 out of the 10 specimens irradiated, failed at strains < 0.16, i.e. these specimens failed before they reached the pre-strain level to which they were previously subjected. The effects on the strain rate are shown in Figure 6-9.

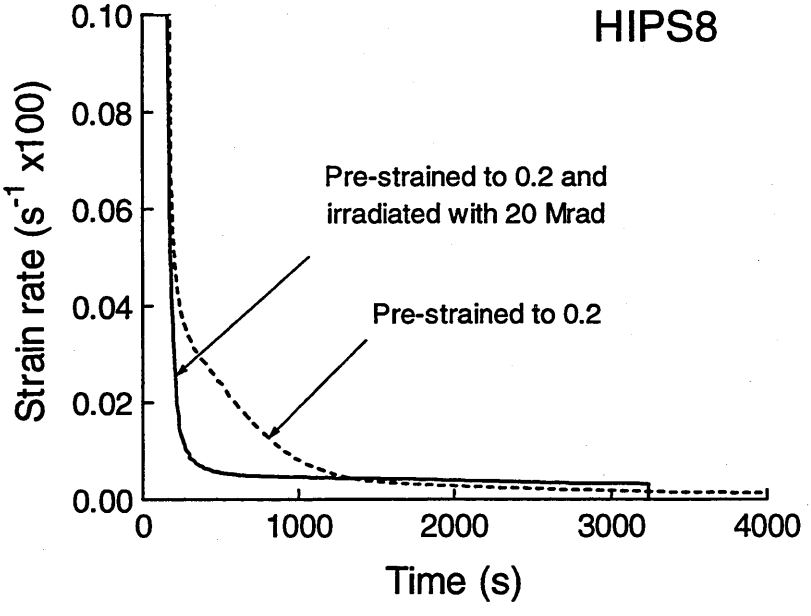

Figure 6-9. Effects of rubber shear modulus on strain rate of HIPS8 under an applied stress of 14 MPa.

7. RESULTS. ABS blended with general purpose SAN

7.1 Constant displacement rate

The following section characterises ABS8 and its blends with styrene-acrylonitrile, with respect to material parameters such as yield, flow and breaking stresses. All constant displacement rate tests were carried out in an Instron screw machine at a rate of 2 $mm.min^{-1}$. As with HIPS, there was a noticeable reduction in stress whitening of the materials at failure, with decreasing rubber content. Stress is plotted against strain in Figure 7-1, and the expected decrease in the strain at failure is apparent. Through calculation of the area under the stress/strain curve for each blend, it was found that ABS6 absorbs more energy than ABS8, which gives an indication of the critical rubber content for optimum toughness of this material

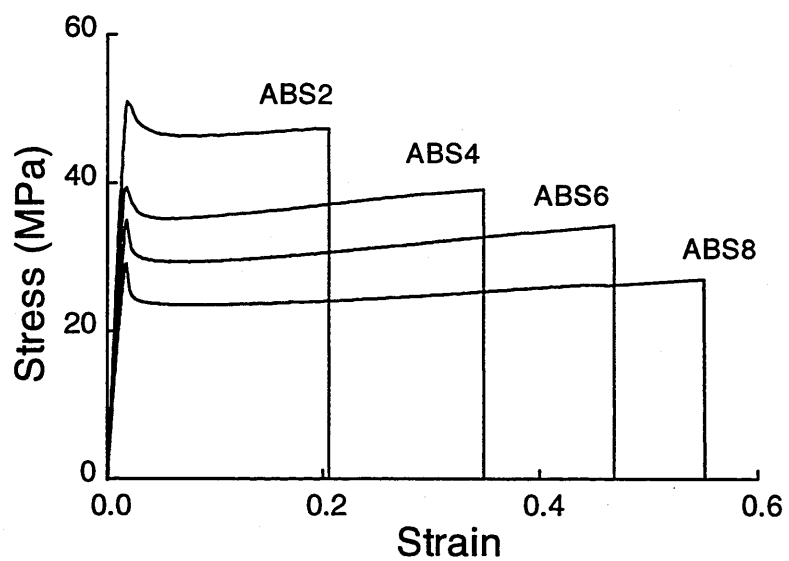

Figure 7-1. Stress/Strain curves for ABS8 blended with general purpose poly(styrene-acrylonitrile).

Figure 7-2 displays the effect of rubber content on the stress on the material at yield, at flow and at break. Each plotted yield or flow stress value is the average of three tests. Each breaking stress value is the maximum of three tests. The yield stress of SAN is taken from Lavengood et al. (1973). As with HIPS, the breaking stress is always greater than the flow stress, by an amount which gives an indication of the load carried by the rubber at high strain.

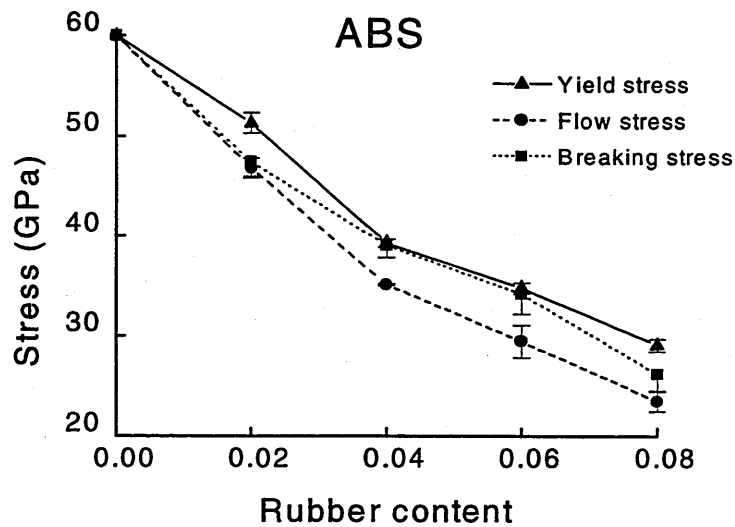

Figure 7-2. Change in material parameters with rubber content.

7.2 Creep of ABS

ABS was extended under different applied loads and its deformation was observed with respect to time. The effect of rubber content on its creep behaviour can be observed in Figure 7-3. Although the material with the lower rubber content, is deformed under a stress which is almost double that of the material with the higher content, the rate of extension is much lower and the strain at failure is also lower. The blends ABS4 and ABS6 behave in a similar manner to that shown in Figure 7-3.

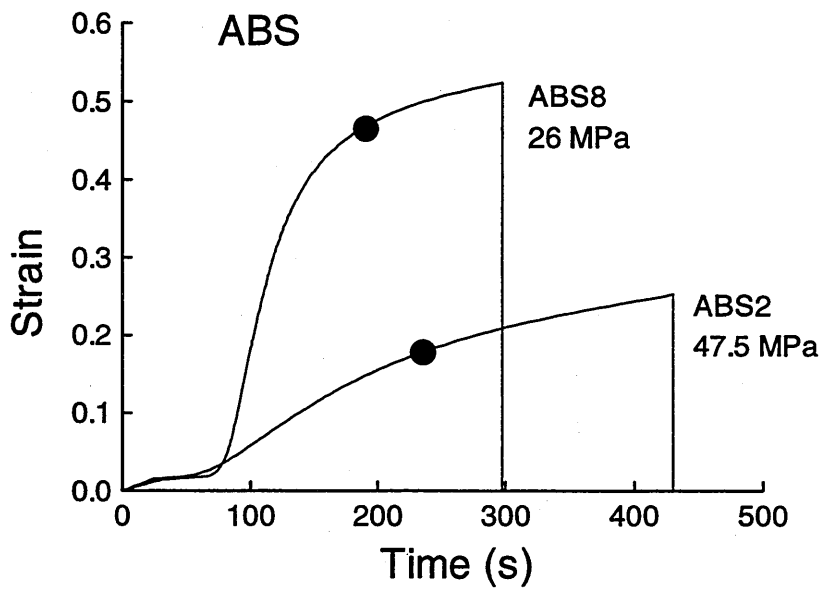

Figure 7-3. ABS8 and ABS2 extended under different applied stresses. Full circles indicate mean failure strain for batch of specimens.

7.3 Sjoerdsma and Boyens model applied to fracture strains of ABS8 blended with general purpose SAN.

The plastic strain at failure, calculated as the total strain at failure minus the initial elastic strain (σ_{app}/E), is plotted against the cumulative probability of survival, ($1-P_f$). There is a noticeable shift to lower strains with reduction in rubber content and although some 'bunching' of the data occurs, the data sets are generally well distributed. The problem of data 'bunching' was addressed in Chapter 4. It was proposed that the tendency of data to cluster, is a consequence of the sample size. Through comparing ABS with HIPS, it can be seen that the ABS distributions are prevalently more uniformly distributed, i.e. they do not bunch to the same extent as the HIPS distributions. This may be a consequence of the width of the distributions, because from comparison of HIPS8 and ABS8, which have similar maximum fracture strains, it can be seen that HIPS8 has a

range of 0.37 (= ε_{max}–ε_{min}), while ABS8 has a range of 0.23. Thus for a given number of specimens, the mean interval between two data points will be smaller for an ABS distribution.

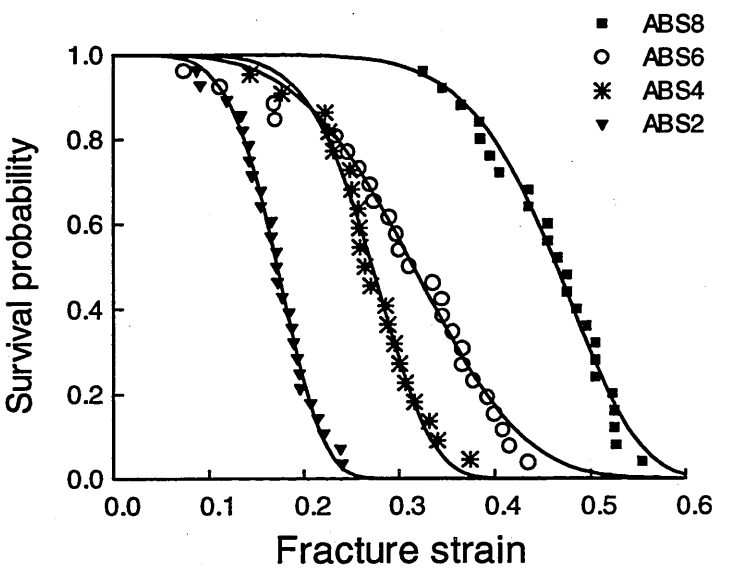

Figure 7-4. Cumulative probability for ABS tested in creep. ABS8: 26 MPa; ABS6: 24.5 MPa; ABS4: 37.5 MPa; ABS2: 47.5 MPa

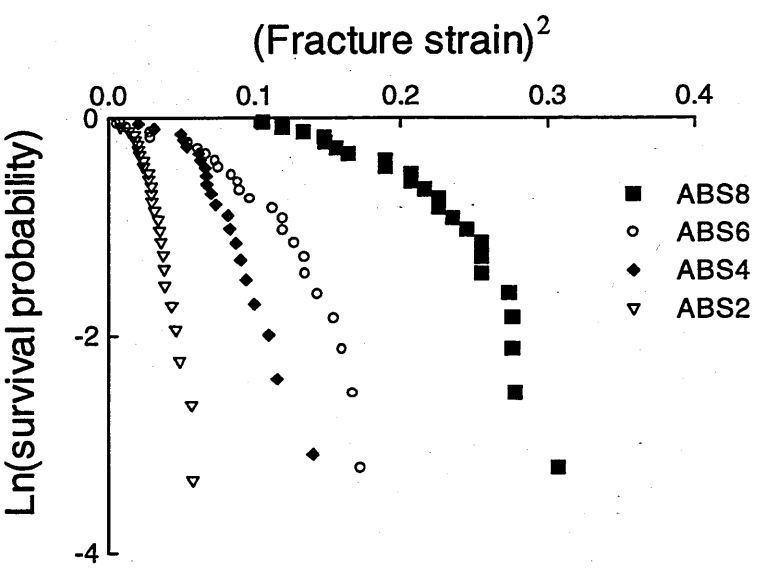

Figure 7-5. Fracture strain data for ABS plotted according to the method described by Sjoerdsma and Boyens (1994).

Figure 7-5 shows the data from Figure 7-4 plotted according to the Sjoerdsma and Boyens model, which predicts a linear relationship between the logarithm of the survival probability and the square of the plastic strain. Again, as with HIPS, this model is seen to be incongruous with the fracture strain data for these materials.

7.4 Weibull statistics applied to fracture strains of ABS8 blended with SAN

Some examples of the Weibull equation applied to the fracture strain data of ABS are shown in Figure 7-4. The fitting parameters for ABS4, the shape parameter β and scale parameter α, were found to be: $\beta = 7.85$ and $\alpha = 16080$. This allows replotting of the data as in Figure 7-6, to check the validity of using the Weibull distribution to describe the failure strain data of this material. In this plot the

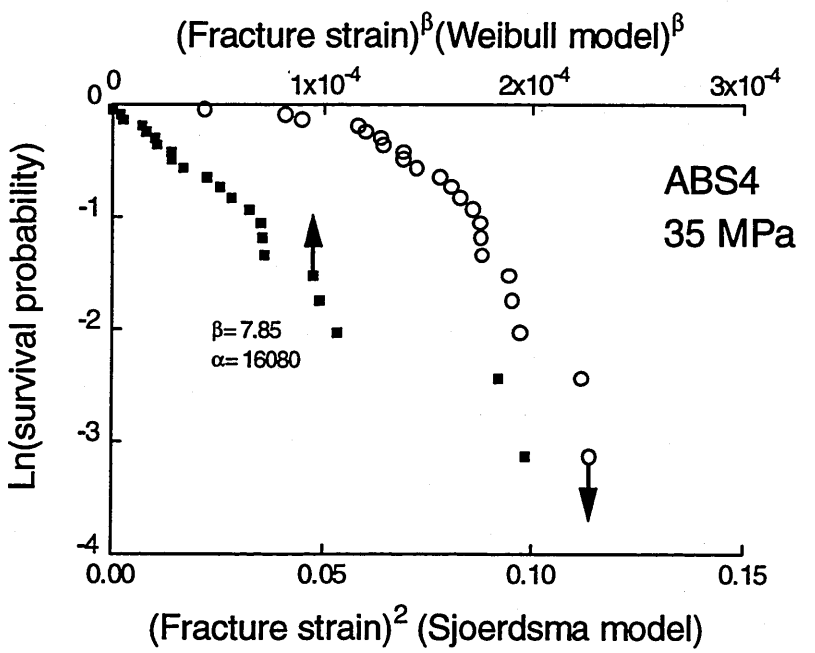

Figure 7-6. Fracture strain results for ABS4 plotted according to Sjoerdmsa model and Weibull function.

logarithm of the survival probability is plotted against (fracture strain)$^{\beta}$. The good linearity observed, suggests that the probability of failure of ABS4 can be well represented by a Weibull distribution. Also shown in Figure 7-6, is the same data plotted according to the Sjoerdsma and Boyens model, which when compared with the good fit of the Weibull plot, attests to the argument that the Weibull function is more congruous with the failure strain data of these materials.

Two samples of ABS2, numbering 27 and 22 specimens, were extended under a constant applied tensile stress until failure occurred. The failure strain data are plotted against the cumulative probability of survival and the results are shown in Figure 7-7. There is a discernible shift to lower strains with decrease in applied stress, which is consistent with other ABS and HIPS materials. Weibull statistics are applied to the data, and the correlated distributions are the continuous lines shown in the plot.

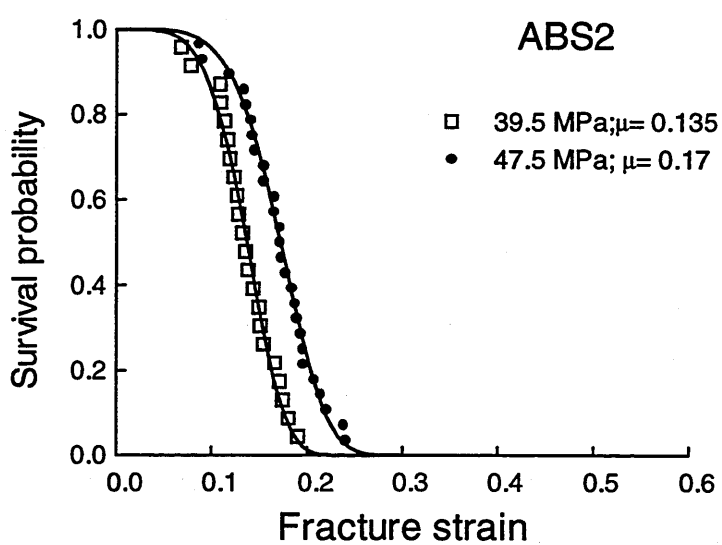

Figure 7-7. Cumulative probability of survival with respect to strain for ABS2. Also shown are fitted Weibull distributions with parameters; (●): $\beta = 4.9$, $\alpha = 4240$ and (□): $\beta = 4.7$, $\alpha = 9210$.

Two samples of ABS6, numbering 22 and 24, were extended under stresses of 31.5 MPa and 24.5 MPa, respectively. The specimen rupture strains are plotted in Figure 7-8. Weibull statistics were applied to the data and the correlated distributions are also plotted.

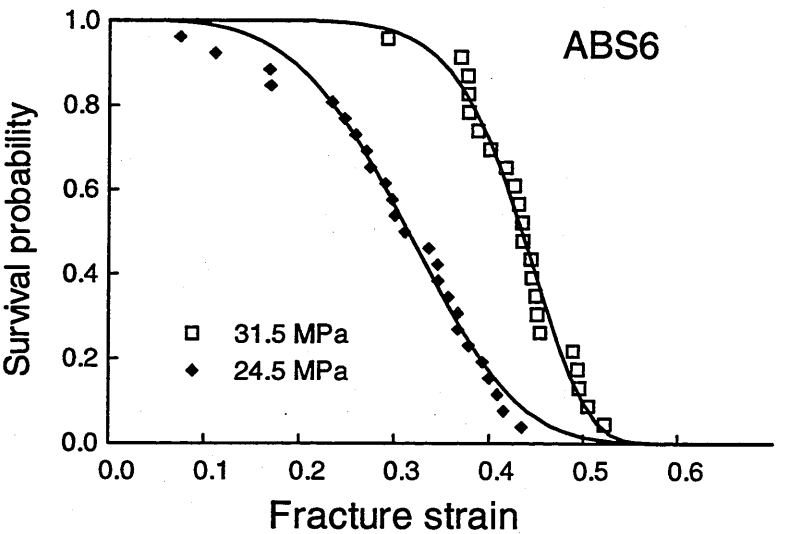

Figure 7-8. Cumulative probability of survival with respect to strain, for ABS6. The additional lines are curves plotted according to Weibull statistics with parameters;(□): $\beta = 8.7$, $\alpha = 1017$ and (◆): $\beta = 3.9$ and $\alpha = 62.4$.

7.5 Histograms of ABS blended with Styrene-Acrylonitrile

Histograms representing the probability density function give a clear visual signal of the variance of data, or in this case the failure strains. Also, histograms indicate clearly the mode failure strain, which is defined as the strain corresponding to the highest rate of failure, and the mean failure strain is also discernible. The effect of stress on the failure strain probability density function of ABS2 is apparent from Figure 7-9. The difference between the level of stress applied to the two samples of ABS2 is 8 MPa. As mentioned earlier, there is a noticeable shift to lower failure strains, when a lower stress is applied to the

material. This observation is underlined in Figure 7-10, which shows a histogram of two samples of ABS4. The difference in applied stresses between these samples is 2.5 MPa, hence the shift in the mean failure strain is lower than for ABS2.

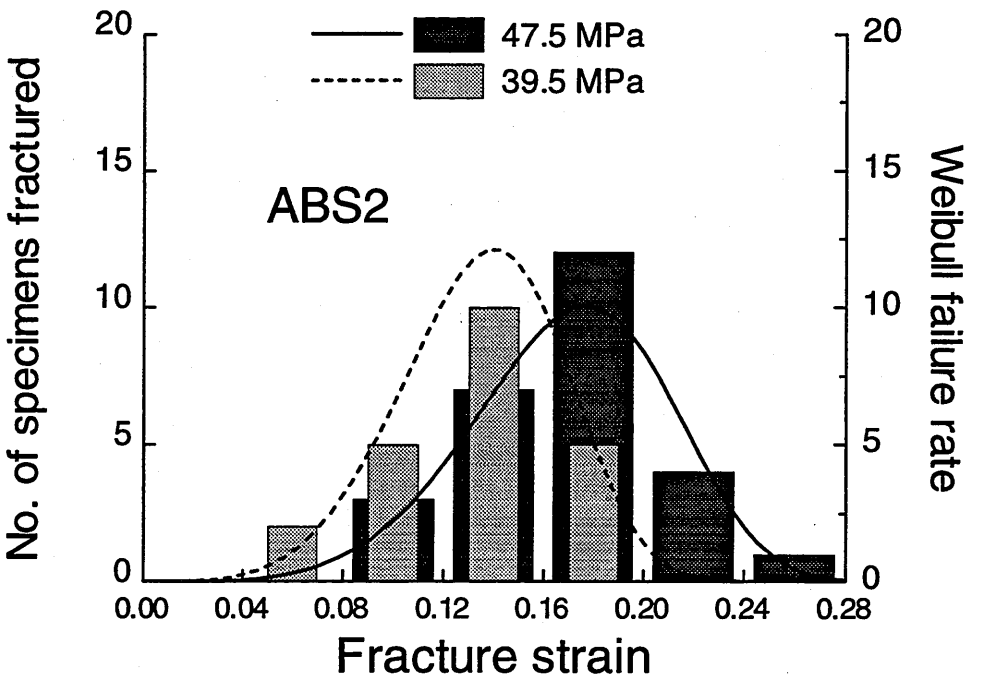

Figure 7-9. Histogram of ABS2 samples and fitted Weibull distribution.

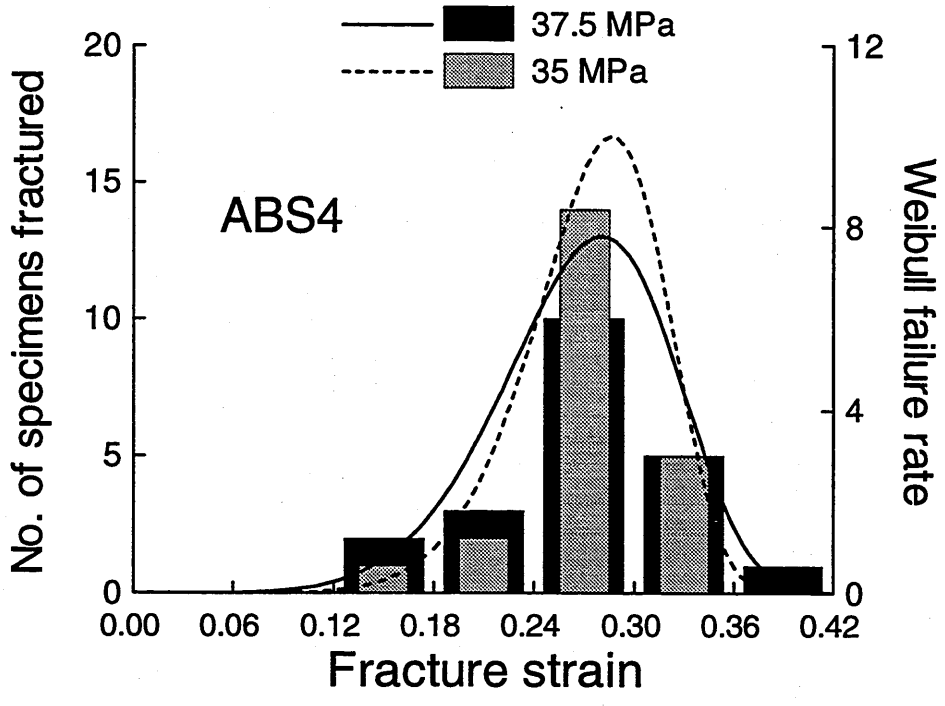

Figure 7-10. Histogram of ABS4 samples and fitted Weibull distribution

8. RESULTS. ABS blended with SAN and Sulfur

8.1 Constant displacement rate

ABS was blended with poly(styrene-acrylonitrile) and the resulting mechanical properties are characterised in Chapter 7. It has also been shown that blending sulfur with HIPS, results in a shift in the T_g of the rubber part of the composite, which indicates an increase in the cross-link density of the rubber phase. It was illustrated how the increase in the rubber shear modulus has a discernible effect on the mechanical properties of HIPS. In this section it will be shown that blending ABS with sulfur also causes an increase in the T_g of the rubber phase, and the effects of this will be characterised with standard tensile tests and creep tests, and the effects on the probability of failure will also be demonstrated. The ABS materials with different rubber contents were vulcanised with η held constant, i.e. the same ratio of sulfur to rubber. Again, as with HIPS, because the ratio of sulfur to ABS is very small, it is difficult to ensure the full quantity of sulfur enters the blend.

Blend name	Ratio of ABS8 to SAN	wt. % Sulfur added
A8:0.55	100:0	0.55
A6:0.38	75:25	0.38
A4:0.24	50:50	0.24
A2:0.12	15:75	0.12

Table 8-1. shows the blend name and weight percentage of sulfur added to the material.

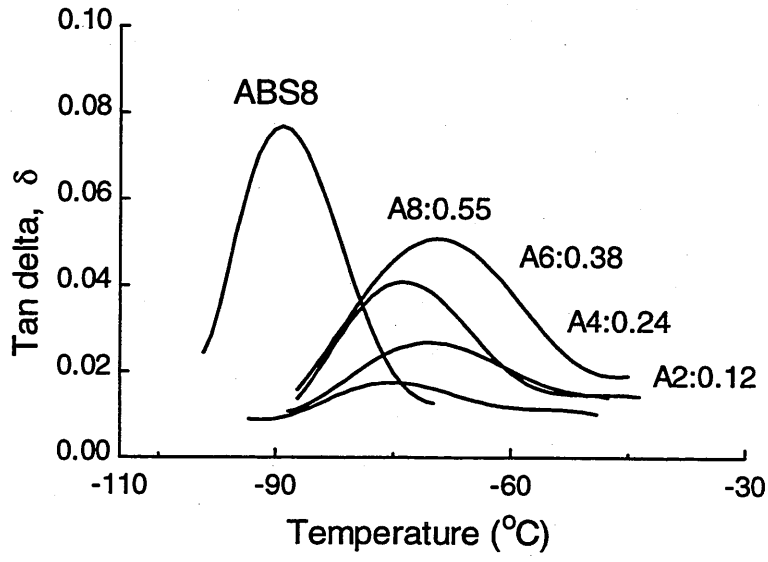

Figure 8-1. Relaxation spectrum of the rubber part of ABS blended with SAN and sulfur (η constant).

However as Figure 8-1 shows, the shift in the peak of the relaxation spectra to higher temperatures, for ABS of varying rubber content, is reasonably consistent. The neat ABS has a T_g of -89 °C while the vulcanised ABS have an average T_g of –72 °C, which is an increase of 17 °C. Ikawa et al. (1997) recently reported a variation in impact strength of ABS, when the gel content of the toughening rubber particles is varied. Figure 8-2 shows the stress/strain curves for ABS8 blended with SAN and sulfur, and it can be seen that a significant change to the tensile behaviour has resulted from vulcanisation. As with HIPS, the Young's modulus and the yield, flow and breaking stresses have increased, while the failure strains have decreased. Young's modulus was measured between strains of 0.002 and 0.01, and was observed to increase from 1.79 GPa for ABS8 to 1.84 GPa for A8:0.55. The tensile stress parameters for the unvulcanised materials, are compared in Figure 8-3 with those for the vulcanised.

Each plotted yield or flow stress value is the average of three tests. Each breaking stress value is the maximum of three tests. From comparison of Figure 8-3 with Figure 4-1, it is observed that the breaking stress of ABS can exceed the material's yield stress, but in HIPS however, this rarely occurs. This indicates that before failure occurs, ABS can strain-harden more effectively than HIPS, which implies a more efficient deformation stabilisation system.

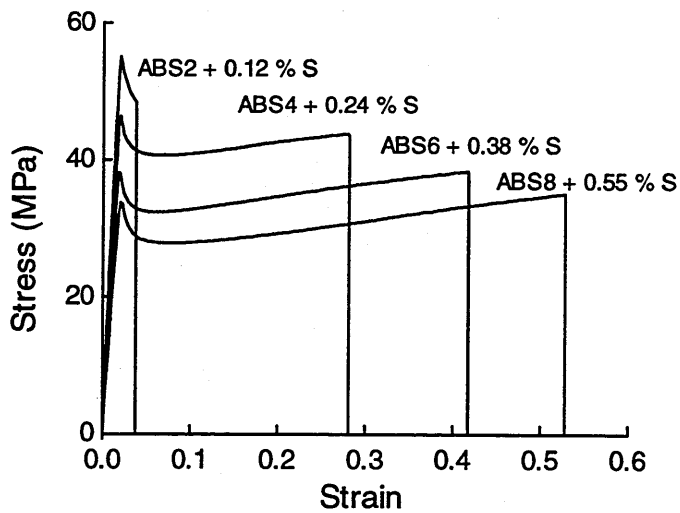

Figure 8-2. ABS8 blended with SAN and sulfur in tension at a constant displacement rate.

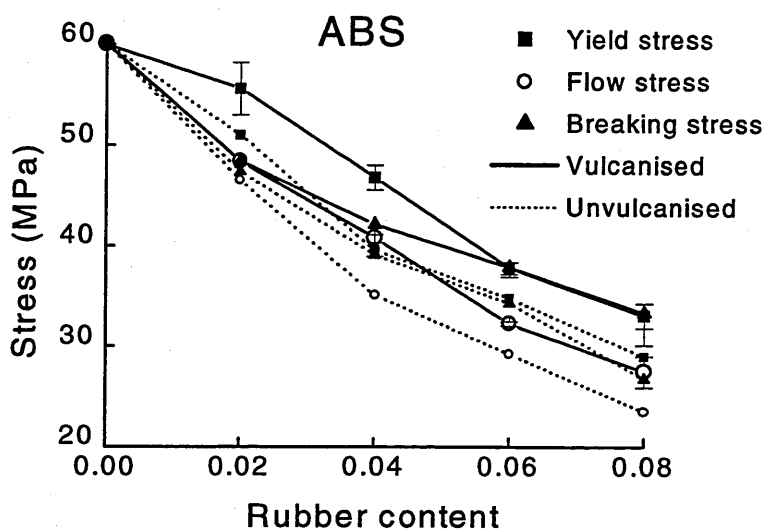

Figure 8-3. Yield, flow and breaking stresses for vulcanised and unvulcanised ABS extended at a constant displacement rate.

8.2 Creep of ABS blended with sulfur, and Weibull statistics

While it is clear that blending ABS with sulfur has a significant effect on the mechanical properties of the material, the effects of the rubber shear modulus on the probability of failure of the material also need to be addressed. The influence of increasing the rubber cross-link density on the creep behaviour of ABS is shown in Figure 8-4. In a similar manner to HIPS, the induction time is seen to increase and the strain rate is seen to decrease, following the addition of sulfur. It is apparent that the kinetic processes controlling initiation and/or propagation of deformation are seen to be significantly impaired.

Batches, numbering not less that twenty, of these materials were extended under constant applied stress, until rupture occurred. The results of these tests are shown in Figure 8-5. As with HIPS, at a given strain the probability of survival of vulcanised ABS, increases with rubber content, but decreases following the addition of sulfur. Weibull distributions are correlated with the data according to equation 4.22. It can be seen that the data are well described by the Weibull equation. If A8:0.55 in Figure 8-5 is compared with ABS8 in Figure 7.4, it can be seen that the maximum recorded failure strain is larger for A8:0.55 ($0.69 > 0.56$). This is possibly, a result of the level of applied stress utilised in the experiment. The creep stress applied to ABS8 was 26 MPa, which corresponds to 89 % of the yield stress, whereas the creep stress applied to A8:0.55 was 34 MPa and this corresponds to 100 % of the yield stress. It was previously mentioned that there is a definite effect of creep stress on the probability of failure, as illustrated in Figure 4.13 for HIPS and Figure 7.7 for ABS. This reiterates the point that an increase in applied stress affects not only the kinetics of deformation initiation and propagation, but also the mechanisms controlling failure.

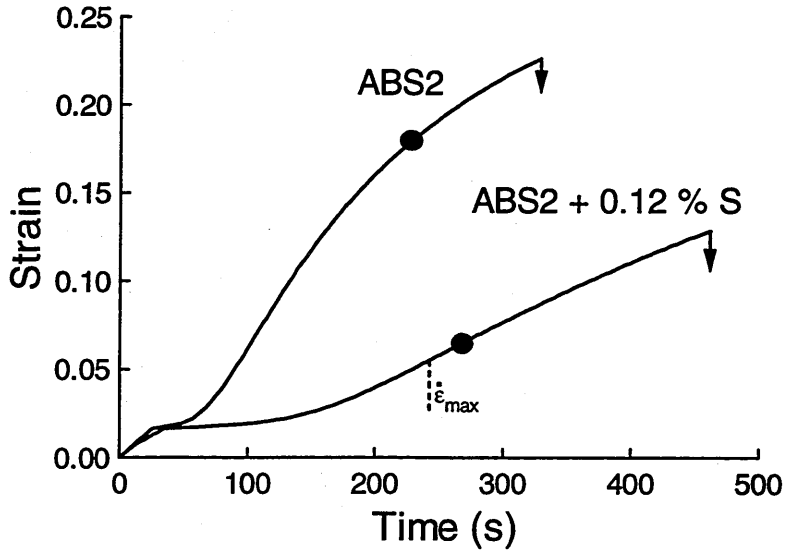

Figure 8-4. Creep behaviour of ABS blended with sulfur extended under an applied stress of 47.5 MPa.

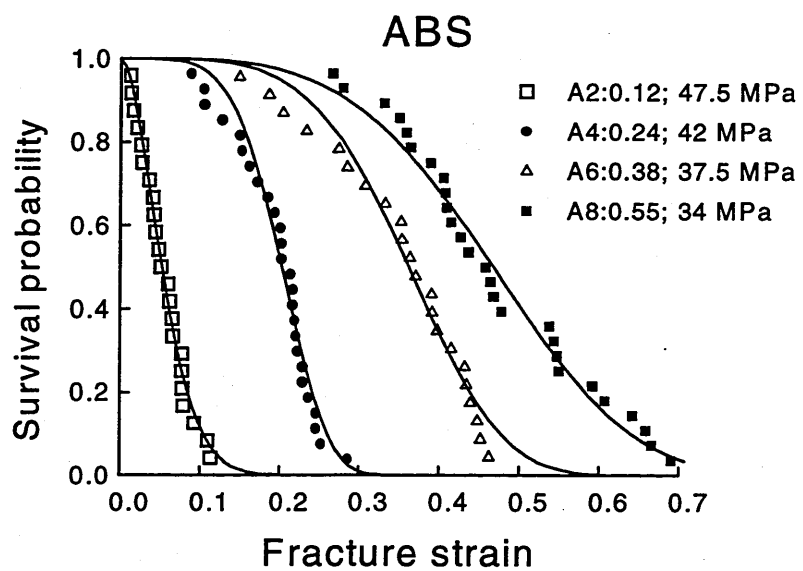

Figure 8-5. Cumulative probability of survival of ABS blended with SAN and sulfur. η, the ratio of sulfur to rubber, is held constant in the blend recipes. The solid lines are Weibull distributions fitted to the data using the following parameters: **A8:0.55:** $\alpha = 12.7$; $\beta = 3.8$, **A6:0.38:** $\alpha = 58.3$; $\beta = 4.3$, **A4:0.24:** $\alpha = 1510$; $\beta = 4.8$, **A2:0.12:** $\alpha = 114$; $\beta = 1.7$.

9. RESULTS Advanced Impact Modifier (blended with sulfur)

9.1 Constant Displacement Rate

AIM is a polymer of polystyrene matrix, toughened with core shell rubber particles. The rubber morphology is of the type known as 'labyrinth' or 'can of worms' morphology which consists of rod-like or thread-like rubbery elements localised in a glassy polymer domain (Bucknall, 1997). Characterisation of this material revealed that the deformation behaviour is dissimilar from that of HIPS and ABS, in several fundamental ways. Constant displacement rate tests were carried out on this material at a number of control speeds. AIM extended at a cross-head displacement speed of 2 $mm.min^{-1}$ is shown in Figure 9-1. If this is compared with plots of HIPS8 and ABS8, it can be seen that at low strains the yield behaviour is quite similar. However, in HIPS and ABS as the strain increases, the stress required to maintain the test speed also **increases**, i.e. the

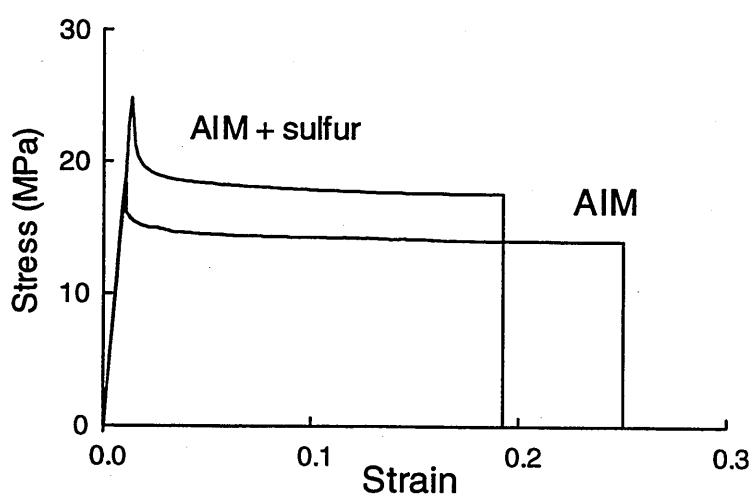

Figure 9-1. AIM and AIM:0.55 extended at a constant displacement rate.

flow stress increases, whereas in AIM the flow stress continues to **decrease.** This signifies macroscopic strain-softening up to the point of failure. Visually, the specimen deformation is similar to HIPS and ABS. It is noticeable that the specimen cross-sectional area does not change noticeably with extension and thin white bands form at low strains which, as the strain increases, appear to grow into each other. The Young's modulus of the material, measured between strains of 0.002 and 0.007, was found to be 1.76 GPa. The yield, flow and breaking stresses were measured as 16.7, 14 and 14 MPa respectively. Because the 'flow stress' is defined as the minimum stress after yield, and because the flow stress in this material progressively decreases, the recorded flow stress will always be equal to the breaking stress.

It was illustrated earlier how, in order to increase the rubber cross-link density, HIPS and ABS were blended with sulfur. This process was repeated for AIM, through compounding with 0.55 wt. % sulfur. The relaxation spectrum of

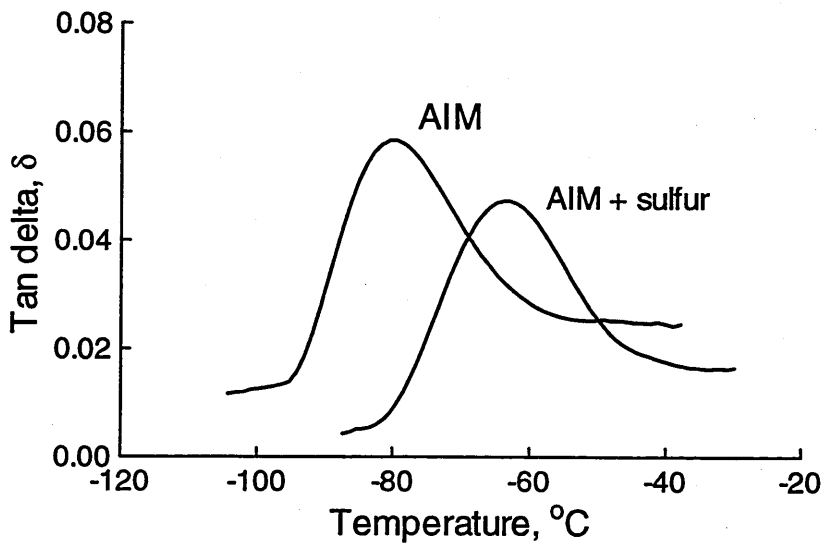

Figure 9-2. Relaxation spectrum of AIM and AIM blended with sulfur.

the second phase of AIM is shown in Figure 9-2. It can be seen that the T_g of the rubber phase, indicated by the peak tan delta value, shifts to higher temperatures by almost 17 °C. Wagner et al.(1970), Perche (1995) and Lin (1997) showed negligible perturbation to the matrix T_g when HIPS was blended with sulfur, and as the matrix polymer in AIM is also polystyrene, it is assumed that sulfur will selectively affect the rubber particles.

The effects of increasing rubber cross-link density on the mechanical behaviour of the material extended at a constant displacement rate, is shown in Figure 9-1. It can be seen that the Young's modulus of the material increases, as does the yield, flow and breaking stress. The failure strain was seen to decrease, but the strain-hardening phenomenon observed in HIPS and ABS, is not apparent up to the point of failure. In general, the mechanical changes observed when vulcanised AIM is extended at a constant displacement rate, are synonymous with changes observed in both vulcanised High Impact Polystyrene, and vulcanised Acrylonitrile Butadiene Styrene.

9.2 AIM in creep rupture

AIM was extended at a constant stress until rupture occurred. Typical creep behaviour of this material is shown in Figure 9-3 and Figure 9-4. There are several features of these plots which are similar to the creep behaviour of HIPS and ABS. Following the initial elastic response, a period of low strain rate follows (i.e. the induction period), succeeded by an increasing rate of dilatation. It is interesting to note, that comparison of the strain rate/time relationship of AIM with that of HIPS, reveals that the rate of dilatation in AIM is ever-increasing (see Figure 9-4), while in HIPS (and ABS), the strain rate decreases at high strain. This feature is more defined in HIPS8 and ABS8 for which, at high strains the strain rate can reduce to comparatively negligible amounts.

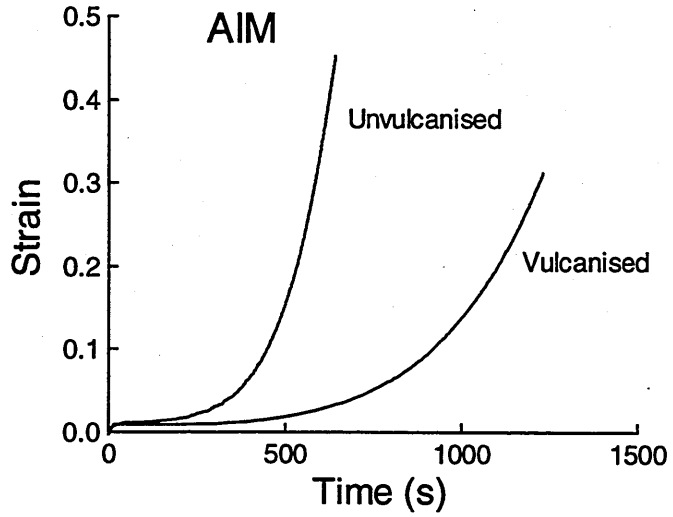

Figure 9-3. Mechanical behaviour of AIM extended under a constant stress of 16.7 MPa.

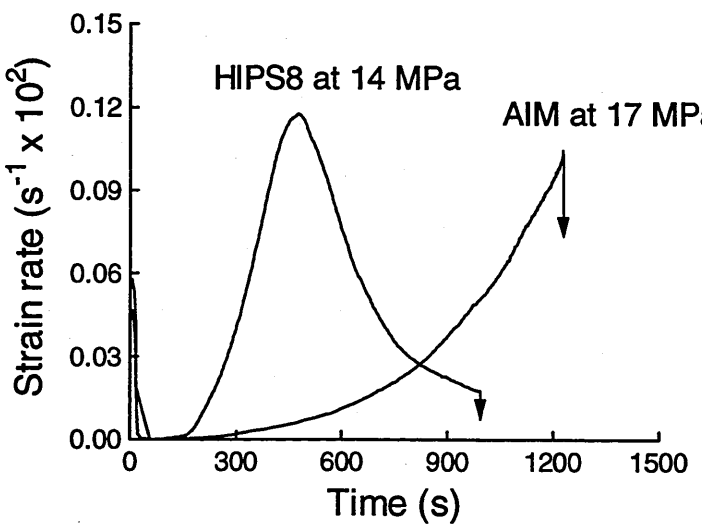

Figure 9-4. Comparison between strain rate behaviour of HIPS and AIM. Note AIM does not macroscopically strain-harden before failure

9.3 Statistics of failure applied to AIM

AIM was extended under applied stresses of 15.7 and 16.7 MPa, and the failure strain data are plotted against the cumulative probability of survival in Figure 9-5. AIM blended with sulfur was also extended under a creep stress of 20 MPa, and these data are also shown. There are several points worth noting. Generally the data are seen to be well described by a Weibull distribution, and while it was

observed that the Weibull distribution overestimated the probability of survival of HIPS at high strain, this effect was not apparent for unvulcanised AIM. The data average about the fitted Weibull distribution along the full scale of strain. As was seen with HIPS, bunching of the data at different strains for each material, is again observed.

If the failure strain distribution of AIM tested at 15.7 MPa is compared with that of AIM tested at 16.7 MPa, it can be seen that a definite difference exists between the two failure distributions. At a given strain the probability of failure increases if the applied stress is increased. This is contrary to observations of HIPS and ABS for which, at a given strain, the probability of failure decreases if the applied stress is increased.

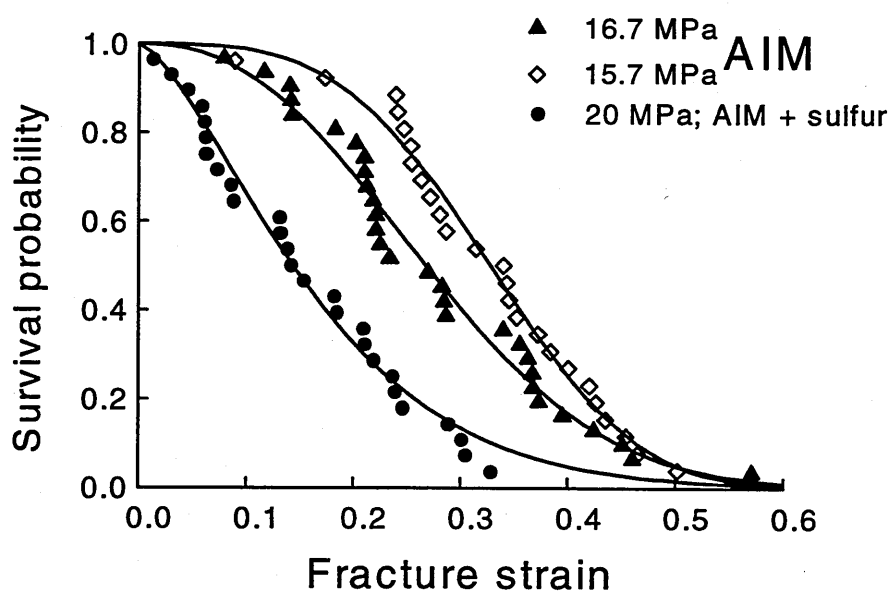

Figure 9-5. Probability of survival of AIM and the probability of survival of AIM blended with sulfur, both extended under constant applied stress.

The probability of survival of AIM is plotted according to the Sjoerdsma and Boyens method in Figure 9-6. It can be seen that this model describes reasonably well the failure strain distribution of AIM.

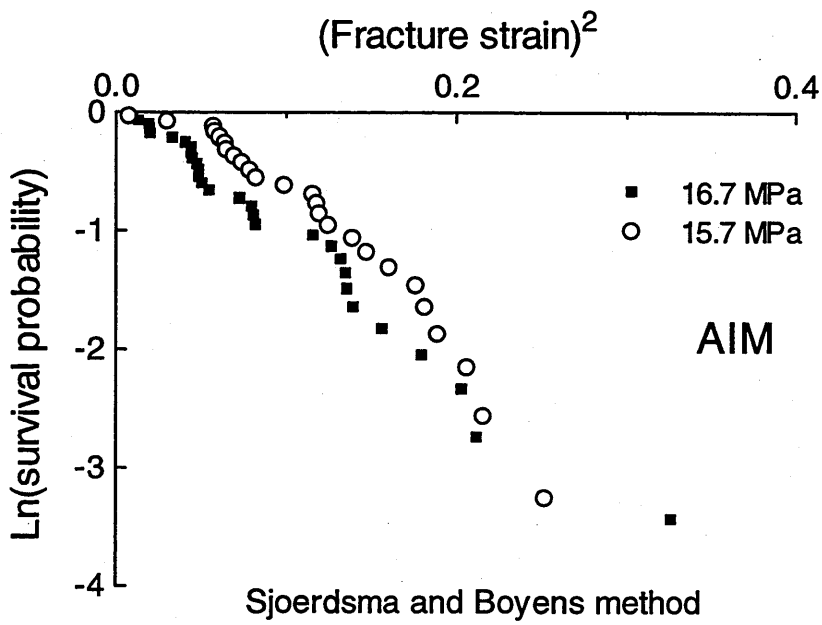

Figure 9-6. Survival probability of AIM plotted according to the method described by Sjoerdsma and Boyens (1994)

10. DISCUSSION. Initiation and percolation of deformation in HIPS and ABS

The mechanisms through which rubber particles greatly enhance the ability of glassy polymers to absorb and dissipate energy, are still not completely understood. As a result, identifying the dominant failure mechanism is difficult and in a way, it is analogous to identifying the cause of failure in polystyrene, (successfully addressed by Yang et al., 1986 and Kramer and Berger, 1990), because that issue could not have been resolved without understanding how the crazes extend and thicken (Argon and Salama, 1977 and Lauterwasser and Kramer, 1979). In the same manner, identifying the mechanism which controls failure in HIPS and ABS is impossible, without understanding how deformation percolates through the material. Hence a discussion of these processes is given in this chapter.

The problem is outlined as follows. In air at room temperature, polystyrene and poly(styrene-acrylonitrile) form only 10's of crazes before fracturing at low strain. If the number of stress concentrations is increased through introducing large numbers of rubber particles, the number of crazes also increases by a factor of 10^6. Unless widespread shear yielding takes place simultaneously, the specimen cross-sectional area remains relatively unchanged. The cross-sectional area of HIPS can remain unchanged because necking takes place internally, through matrix and rubber fibrillation. However there is evidence to support the argument that the rubber particles are not just craze nucleation sites but also control the thickness of the crazes, and thus force the deformation to percolate through the material. For example, the addition of glass

beads (Lavengood et al., 1973) or chalk (Braun et al., 1996) to glassy polymers can initiate dilatation, but good particle/matrix interfacial adhesion is necessary to delay fracture until high strain.

While a considerable amount of literature discusses the effects of rubber content on the yield behaviour of HIPS, there are still many unanswered questions. Many workers have identified a correlation between the concentration of rubber in the composite and its impact strength (Wagner and Robeson, 1970; Keskkula et al., 1971 and Bucknall et al. 1986a). When the rubber content of a toughened composite is decreased, one of the most noticeable changes to the mechanical behaviour is a reduction in the failure strain. While the yield, flow and breaking stresses can increase by a factor of 2 to 3, the failure strain will reduce by a factor of 20-30. The Young's modulus is also affected by the rubber content. Increase in the shear modulus of the rubber phase produces similar effects i.e. increased yield, flow and breaking stresses and decreased failure strain. These effects result even if the rubber T_g has only increased from –90 °C to –80 °C (Soares, 1994), which means the rubber is still in its rubbery state. In this study, HIPS and ABS were blended with different quantities of sulfur, which produced an increase in the T_g of at most, 26 °C (see Figures 5.1, 5.2 and 8.1). The results found, give an indication of the important role the rubber shear modulus plays in deformation of HIPS and ABS. This is discussed further below.

While the bulk of the experiments carried out in this study were creep tests, the materials were also characterised using standard tensile tests. In this way any perturbations to the deformation behaviour of the material, for example following the addition of sulfur, are easily discernible through the parameters yield, flow and breaking stresses, Young's modulus, strain at break etc. It was thought simpler to introduce and discuss the composites' yield and flow

behaviour in terms of these well known parameters. Therefore the following section introduces and discusses how deformation might initiate thus producing composite yield, and section 10.2 introduces and discusses how deformation might percolate through the material. These concepts are discussed with respect to rubber content and rubber shear modulus. While the mechanisms controlling initiation may not directly produce catastrophic rupture in the material, they are important, because initiation and percolation occurs throughout the lifetime of the specimen, and therefore must have a bearing on the statistics of failure. The issue of dilatation initiation in rubber toughened polymers is a complicated and controversial one, and while the discussion advanced in the next section conveniently explains some of the results described in Chapter 11, it seems unlikely that the exact processes through which deformation nucleates, has a direct bearing on ultimate failure of the material.

10.1 Effect of rubber content and rubber cross-link density on the yield stress of HIPS and ABS.

10.1.1 Rubber content

Loosely speaking, the yield stress of a material is the stress at which widespread plastic flow occurs, i.e. it is the peak stress prior to plastic flow of the material. It is now clear that in many rubber toughened polymers, the yield stress does not necessarily mark the onset of plastic dilatation, as this may also occur in the pre-yield region. In rubber toughened materials such as high impact polystyrene and acrylonitrile butadiene styrene, viscoelastic flow occurs in the form of rubber cavitation and/or crazing and/or shear yielding. The nucleation of crazes and shear bands can take place at flaws, scratches or other stress concentrating defects, but rubber particles are also known to be good initiators of these mechanisms. Various explanations have been given for this propensity of rubber particles to initiate damage. In the case of crazing, many workers believe that the overlapping of stress fields, which result from the low modulus rubber particles,

provides the stress intensity required for craze nucleation. This would place the craze initiation site some distance from the particle. Other theories hold that the applied stress is magnified at the equator of the particles to the extent that craze initiation takes place at this point. This is supported by extensive microscopic evidence of crazes extending predominantly from the equators of (well bonded) rubber particles.(See Figure 10-1).

A recent development in rubber toughened polymers, is the recognition of the importance of rubber cavitation in composite yielding (Bubeck et al., 1990 and Buckley, 1991). Indeed some workers believe that it could be the rate determining step (Bucknall and Lazzeri, 1993 and Bucknall, 1997). Crazes are

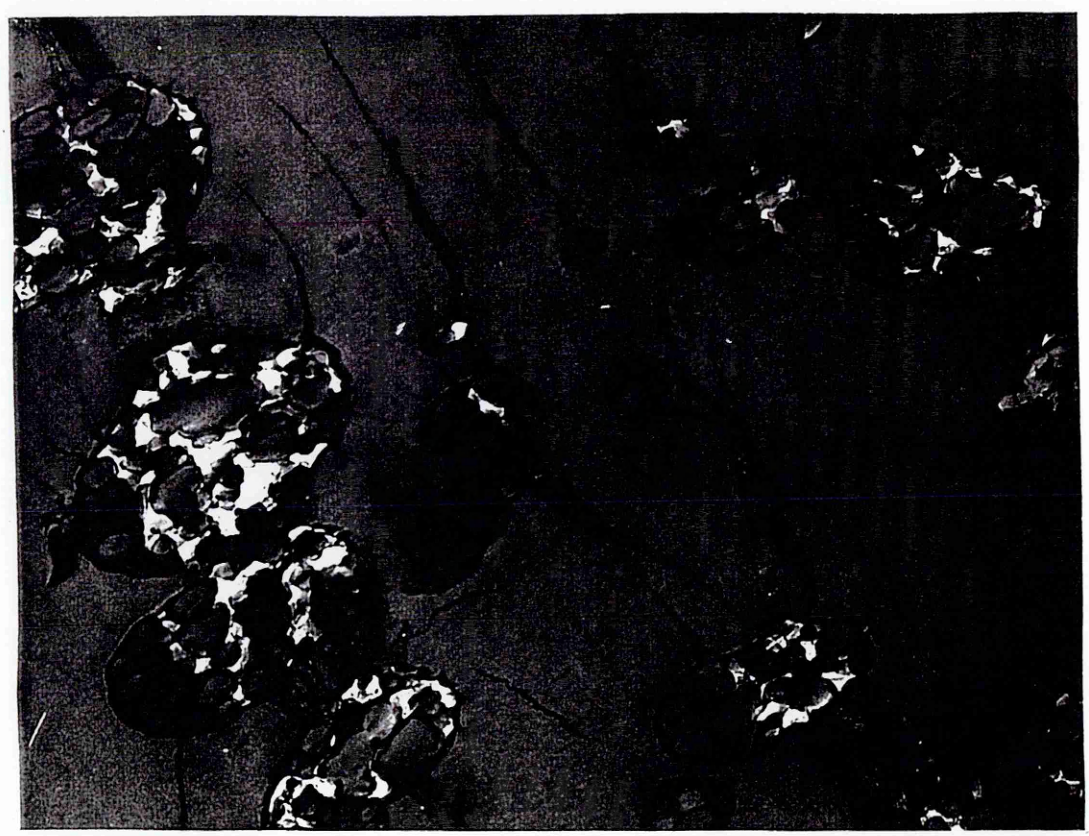

Figure 10-1. ABS deformed in creep. Note the crazes extending from the equators of the particles.(1 μm ———)

known to initiate at free surfaces rather than in the bulk (Argon and Hannoosh, 1977), and are also known to initiate at or near the surface of rubber particles. It is therefore possible that rubber cavitation; (1) precedes craze initiation and (2) is a necessary precursor to craze initiation (Bucknall, 1997). Yang et al. recently presented work showing that rubber cavitation does indeed precede crazing in HIPS (Yang and Bucknall, 1996 and Yang, 1997). In these studies, specimens were subjected to tensile pre-strains of between 0.001 and 0.30, unloaded and annealed above the matrix T_g, and retested. Following annealing, the crazes in the matrix are repaired, but because rubber cavitation involves rupture of primary bonds, the rubber phase is unchanged by the annealing process. Two factors in support of the premise that the matrix was repaired are (1) the flow stress is unchanged regardless of the prestrain level and, while polystyrene chain scission cannot be repaired by the annealing process, this indicates that the matrix entanglement network has recovered, to the extent that the same flow stress is required to maintain the drawing rate; (2) TEM evidence shows that following annealing, crazes do not preferentially nucleate from the same location, indicating that the matrix is not weaker at the site of craze repair.

Prestrains of between 0.0025 and 0.05 produced a continuous decrease in the yield stress, but no change to the flow stress was noted. Considering that the level of prestress which produced irreversible damage in the material is only 3 – 4 MPa, Yang concluded that it is unlikely that this is a sufficient stress to produce cavitation in the rubber. However, following melt processing, upon cooling ,the different thermal coefficients of expansion of the rubber and matrix, produce significant dilatation stresses which, combined with a low tensile stress, might be enough to cavitate large particles (Bucknall, 1997, Lin et al., 1997 and Yang, 1997).

A model proposed by Bucknall and Lazzeri (1993), and developed recently by Bucknall, Karpodinis and Zhang (1994), describes the energy balance relationship of a cavitated rubber particle, and this explains some observed effects in rubber toughened composites. In modelling the thermodynamics required to grow a void within the particle, the authors described the relationship between the stored energy in the particle and the cavity size. For a rubber particle of radius R and bulk modulus K_r, at volume strain Δ_v, the volumetric stored energy $U_v(0)$ is:

$$U_v(0)=\frac{2}{3}\pi R^3 K_r \Delta_v^2 \qquad \textbf{(10-1)}$$

and the energy of the cavitated particle with void radius r is:

$$U_v(r)=\frac{2}{3}\pi R^3 K_r \left(\Delta_v^2-\frac{r^3}{R^3}\right)^2+4\pi r^2\Gamma+2\pi r^3 G_r F(\lambda_f) \qquad \textbf{(10-2)}$$

Following cavitation, the volumetric strain energy is reduced through the formation of a void. The growth of the void required stretching of the surrounding rubber of shear modulus G_r, to form a new surface of specific surface energy Γ. $F(\lambda_f)$ is a function relating to the work done in stretching the rubber surrounding the void. This model revealed that with a constant volume strain on the particle, cavity growth will only occur in rubber particles of diameter greater than a critical value. Using this thermodynamic approach, it was possible to define if it was feasible that cavitation could take place.

Some of the effects of variables such as particle size, rubber modulus and temperature, on the yielding behaviour of rubber toughened materials, can be explained through proposing rubber cavitation as the rate determining step. The

reduction in yield stress with increasing rubber content, will be a consequence of the increased stress on the matrix, and the increase in the number of craze nucleation sites. The increase in the matrix stress, which is a consequence of the greater area of low modulus particles in any cross-section of the composite, can be analysed quantitatively using the Ishai-Cohen model. This model, proposed by Ori Ishai and Leslie Cohen in 1968, gave the stress concentration in a cubical element resulting from a spherical soft inclusion or void, under uniaxial tension, see Figure 10-2.

$$\gamma = \left((1 - 1.21(\varphi)^{2/3}\right)^{-1} \qquad \textbf{(10-3)}$$

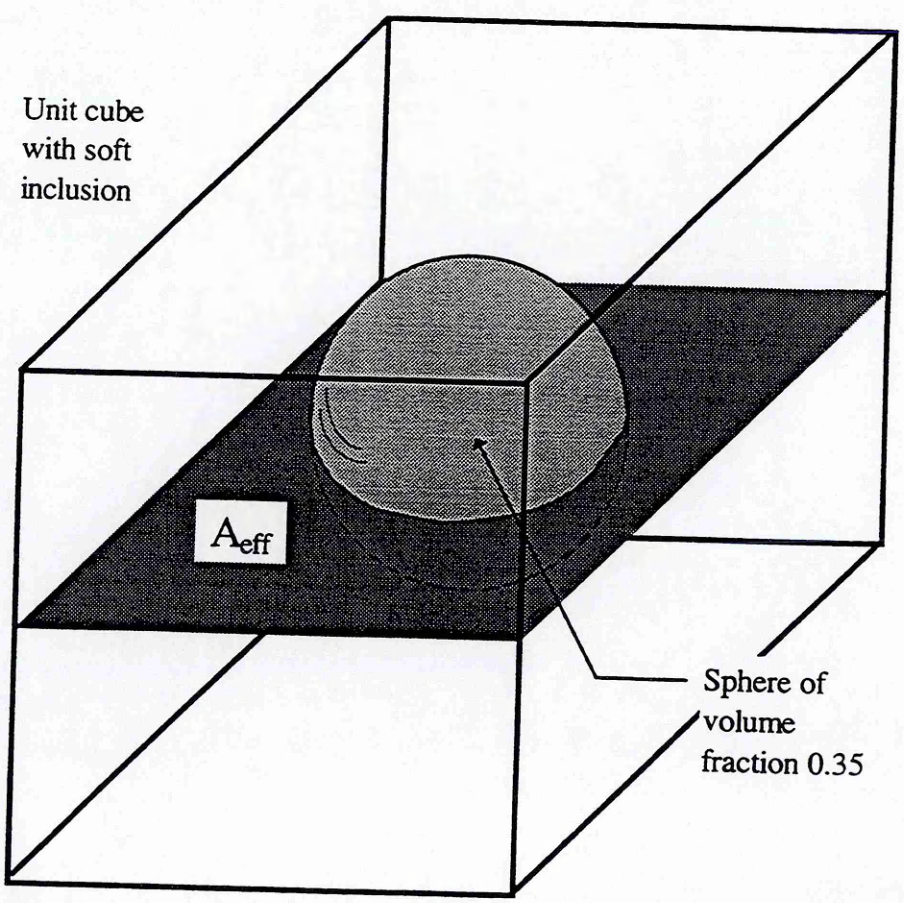

Figure 10-2. Unit cube containing soft inclusion of volume fraction =0.35 (as in HIPS8). The stress concentration on the dark shaded area is given by equation (10-3).

If a nominal stress of 15 MPa is applied to HIPS8, which has a rubber particle volume fraction of 0.35, then from equation (10-3), the average stress on the matrix would be 37.5 MPa. Under the same macroscopic stress, the average matrix stress of HIPS4 would be 24 MPa. The effect of increased matrix stress on the yield behaviour of HIPS is two fold: (1) it will produce a greater volume strain on the rubber particle thus promoting rubber cavitation. Rubber voiding enhances the free surface necessary for craze formation (Argon and Hannoosh, 1977); (2) The increased stress heightens the rate of propagation of damage through the material, through increasing craze extension rates.

Therefore the increased yield stress with decreasing rubber content, results mainly from a depressing of the stress on the matrix, which in turn affects rubber cavitation and matrix yielding (crazing), and from an increase in the number of convenient craze nucleation sites.

10.1.2 Rubber shear modulus

Rubber shear modulus significantly affects the yield behaviour in two ways: **(1)** The importance of rubber cavitation in yielding of rubber toughened polymers was discussed in the preceding section. If the rubber shear modulus is increased the critical volume strain to cavitate the rubber particles (from equation (10-2)) also increases, thereby increasing the stress to produce yielding in the material. This is apparent in equation (10-3) as the dependence of the energy of the cavitated rubber particle on G_r and K_r. **(2)** With the reasonable assumption that for yielding to occur, a sufficient number of crazes have to be formed and propagated, it follows logically that the stress on the craze will be critical to the yield behaviour. If the mean stress on the crazes is reduced, then to produce the required macroscopic rate, either the number of crazes increases, and/or the macroscopic stress increases. The stress on the craze can decrease as a

consequence of the load balance relationship between the rubber particles and the matrix.

The Takayanagi model has been used to analyse quantitatively various material parameters, but in this case it is used to describe the load bearing balance between the rubber phase and the matrix. The load balance between rubber particles and matrix can be represented by:

$$\sigma_r V_r + \sigma_m V_m = \sigma_{app} V_t \qquad \textbf{(10-4)}$$

where σ_r and σ_m is the stress on the rubber and matrix respectively, and V_r and V_m is the volume of rubber and matrix respectively. Rearranging gives:

$$\sigma_r \phi_r + \sigma_m (1 - \phi_r) = \sigma_{app}$$

where $\phi_r = V_r/V_t = 1-(V_m/V_T)$. Considering a unit cube of material, with a soft inclusion of volume fraction 0.35 (i.e. as in HIPS8), it is reasonable to assume that the damage will propagate through the path of least resistance, i.e. at the equator of the rubber particle, see Figure 10-2. The matrix area fraction at the equator of the particle can be determined using the Ishai-Cohen equation (10-3):

$$\sigma_r (1 - A_{eff}) + \sigma_m (A_{eff}) = \sigma_{app}$$

and $$\sigma_r \left(1.21(\phi_r)^{2/3}\right) + \sigma_m \left(1 - 1.21(\phi_r)^{2/3}\right) = \sigma_{app} \qquad \textbf{(10-5)}$$

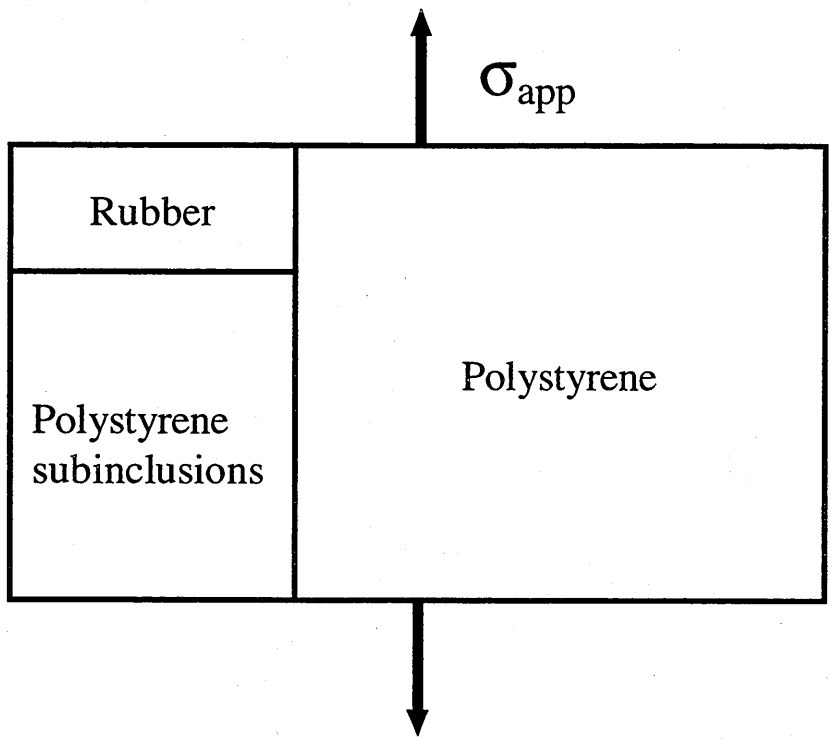

Figure 10-3. The Takayanagi model representing two phase polymers. The matrix bulk extends in parallel with the rubber particles. Within the rubber particles, the rubber is in series with the subinclusions.

For HIPS8, the effective matrix area fraction A_{eff} is 0.4 which, under an applied stress of 15 MPa, gives σ_m = 37.5 MPa. However, this assumes that the soft inclusion supports zero load which, as experiments on the importance of good particle/matrix interfacial adhesion have shown, is unlikely (Kinloch and Young, 1983). Assuming the mean stress on the surface of the craze is ~ 26 MPa (Donald and Kramer, 1982c, Bevan, 1983), then according to equation (10-5), the stress on the rubber is 7.6 MPa, which is a reasonable value. An increase in the shear modulus of the rubber, will increase the stress supported by the second phase, thus decreasing σ_m, for example an increase in σ_r of 1 MPa depresses the stress on the craze to 24.6 MPa. Moreover, it is well known that craze kinetics can be described using the Eyring equation (Bucknall and Clayton, 1972 and Bucknall, 1977). It follows therefore that a small decrease in the stress on the craze, will produce a considerable decrease in the rate of craze dilatation.

In summary, in a standard tensile test, an increase in the rubber shear modulus will necessitate an increase in the macroscopic stress to produce yielding because; (1) in order to cavitate the stiffer rubber, the stress on the particle has to increase to generate the necessary volume strain and (2) the applied stress has to compensate for the load drop on the crazes, due to the increased load bearing capacity of the stronger rubber particles.

10.2 Effect of rubber content and cross-link density on the flow stress of a rubber toughened composite.

In a tensile test, prior to yield, the applied stress continues to rise until the necessary conditions for yielding and strain softening of the material are achieved. It is as a result of widespread crazing, shear yielding and rubber cavitation/fibrillation that HIPS and ABS perform excellently in impact. Following yield, the stress will drop as a result of the softening of the matrix through crazing, and owing to the low stress carried by the rubber at small extensions.

Yang et al. (1996) observed a progressive decrease in the post yield drop, when HIPS and ABS were prestrained to increasing levels. Following prestrain, the material was annealed above the T_g of the matrix, to repair damage from crazing. Yang et al. proposed that cavitation of the rubber phase, which cannot be repaired by the annealing process, could produce the decrease in the post yield drop in the following way. Voids in the rubber phase provide the free surface necessary for craze formation, therefore predamaging the rubber decreases the stress required to generate sufficient voids and crazes for viscoelastic flow.

While the material yields at the stress required to initiate and propagate a sufficient amount of deformation to support the cross head displacement, the material flows at the equilibrium stress required to continue the viscoelastic deformation at the same strain rate. Thus the flow stress of a rubber toughened polymer is defined as the minimum stress after yield. It should be noted that the strict definition of "flow stress" is given as the minimum stress following yield, and while quoted values of flow stress refer to this definition, the term is also used in the text to refer to the stress on the material **at any strain following yield**. The yield and flow stress give an indication of the strength of the material (strength points to the material's ability to resist high stresses), but the product of flow stress and failure strain denotes the toughness of the material. (Good toughness is characteristic of rubber toughened polymers, and defines their ability to delay fracture through absorbing and dispersing energy, Donald, 1994).

At low extensions the rubber load bearing capacity is very low, and therefore consigns the majority of stress to the crazes. It was discussed in section 10.1.2, how the distribution of load between the crazes and the adjoining rubber particles can change, when the cross-link density of the rubber is varied. In natural rubber at high strain, crystallisation and the finite extensibility of the rubber network causes a sharp increase in the stress required to extend the material, while in synthetic rubbers such as polybutadiene (PB) and styrene butadiene rubber (SBR), the former mechanism does not occur to any large extent. Before the effects of rubber content and shear modulus on the flow stress of HIPS and ABS are discussed, a brief description of current theories and models which describe the process of rubber strain hardening is given below.

10.2.1 Rubber strain hardening

In many polymers, the strain softened region of the stress/strain curve is followed by a strain hardening region. This is visible as an increase in the stress

required to increase the strain. In unfilled polymers such as polyethylene terephthalate (PET), a neck forms at a geometric weakness or variation in the cross-sectional area of the parallel gauge portion of the specimen. Should the material deform in the neck, to the extent that the chain axes are rotated towards the direction of maximum extension, then the chains will support more load. This can be represented simply as in Figure 10-4, where a schematic drawing of just one section of a chain fixed by two entanglements or cross-linking points, is shown. When a stress is applied, the two entanglement points will move apart, thereby elongating the chain. As the chain is further stretched, the critical extension ratio at which strain hardening or "orientation hardening" begins to take place, is given by:

$$\lambda = \frac{I_e}{d} \qquad \text{where} \qquad I_e = I_0 \frac{M_e}{M_0} \qquad \textbf{(10-6)}$$

where d is the r.m.s. end to end distance between fixed points, and I_e is the chain contour length between fixed points and, as shown, this can be determined through knowledge of the entanglement molecular weight M_e, and the molecular weight M_0 of the average projected length I_o of a stiff unit along the chain (Kramer and Berger, 1990). The parameter d, can be calculated using the following expression:

$$d = k\,(M_e)^{0.5}$$

where k is a constant that can be determined from neutron scattering measurements of the radius of gyration of molecular coils in the polymer glass. It is clear from equation (10-6) that increase in the chain contour length between entanglements, increases the strain hardening chain extension (Kramer and Berger, 1990).

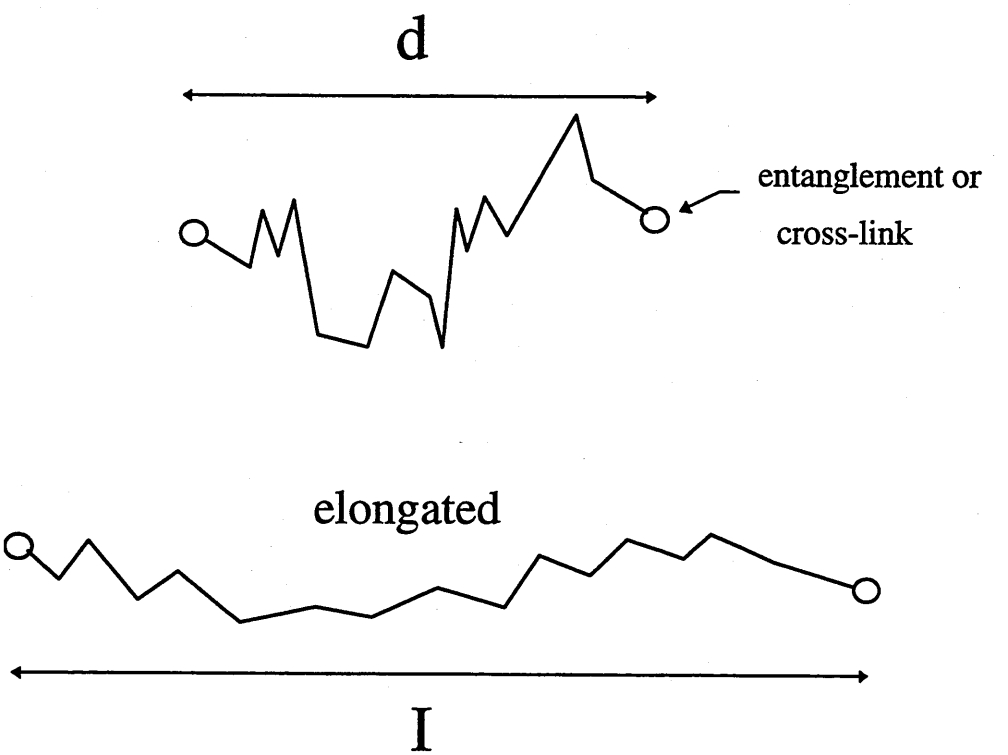

Figure 10-4. The effect of elongating a chain

A typical stress/strain curve for natural rubber is shown in Figure 10-5. The significant strain hardening, noticeable at high extensions, demonstrates the finite extensibility of the chains and of the network. Several theories/equations have been proposed to predict the stress/strain behaviour of rubber including: the Gaussian statistical theory (eqn. (10-7)) (in McCrum et al., 1988), the semi-empirical Mooney-Rivlin equation (eqn. (10-8)) (in Ferry, 1970), the Langevin equation (in Treloar, 1975) and the empirical Martin, Roth and Stiehler equation (eqn. (10-9)) (in Ferry, 1970).

$$f = A_i G\left[\lambda - \frac{1}{\lambda^2}\right] \qquad \textbf{(10-7)}$$

$$f = 2A_i\left(\lambda - \frac{1}{\lambda^2}\right)\left(C_1 + \frac{C_2}{\lambda}\right) \qquad \textbf{(10-8)}$$

$$f = 3G\left[1 - \frac{1}{\lambda^2}\right] \exp\left[k\left(\lambda - \frac{1}{\lambda^2}\right)\right] \qquad \textbf{(10-9)}$$

Plotting the reduced force $f^*(=f / [\lambda - 1/\lambda^2])$ against λ^{-1} is known as a Mooney plot, which yields a straight line of slope C_2 and intercept C_1. C_1 is a term consisting of the cross-links' contribution to the rubber modulus, but also incorporates part of the topological contribution. The Mooney-Rivlin equation is described as semi-empirical because the origin of the C_2 term is uncertain. Unlike C_1, the value of C_2 is found to be independent of the nature of the rubber, and of the degree of vulcanization (Wagner, 1994). Recently Wagner (1994) proposed that the C_2 term originates from the non-affine deformation of the entanglement network. The non-affine deformation is caused by an increasing lateral restriction due to neighbouring chains, which explains the familiar disappearance of the C_2 term when the rubber is highly swollen.

While all of these theories describe well, the behaviour of the material at low to intermediate strain, agreement between theory and experiment at high strain is rather poor. In an elegant piece of work, Edwards and Vilgis (1986) developed a model advanced by Ball et al. (1981), which described the full stress/strain curve for rubber in terms of 4 parameters: N_c is the number of cross-links, N_s is the number of slip links, η is a measure of the slip link freedom as compared with that of a cross-link, and α $(=\lambda_{max}^{-1})$ is the limited extensibility of the network, owing to the entanglements.

The authors argued that predicting the maximum extension ratio based on fully extended polymer chains between cross-links, gives extensions which are

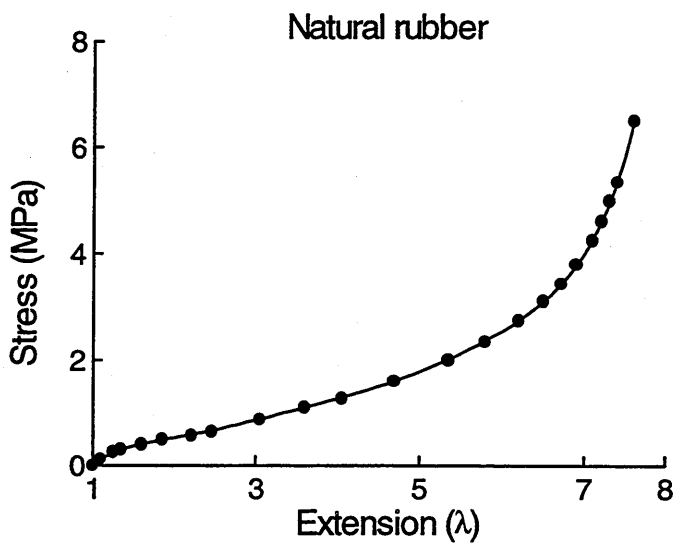

Figure 10-5. Natural rubber in simple extension; G = 0.39 MPa. Taken from Treloar (1975).

much greater than experimentally observed. Instead, it was proposed that network strain hardening results from constraints imposed by the topological entanglements. Thus the finite extensibility of the network results from complete stretching of the polymer between entanglements, rather than between cross-links, and so the maximum extension ratio was calculated accordingly. The Edwards-Vilgis model was found to describe excellently, the complete stress/strain curve for rubber.

In summation, while the classical statistical Gaussian chain theory has a firm molecular basis and predicts strain in compression well, it does not describe well the stress/strain relationship above extensions of ~ 1.2 (Ferry, 1970). The Mooney-Rivlin equation, while being semi-empirical and poorly describes strain in compression, is extensively used in rubber technology to describe intermediate extensions (2 – 3). It fails to accurately predict extensions greater than this (Fukahori et al., 1992). In the classical theory, the expression for the free energy fails to incorporate the additional free energy contributed by the topological constraints, i.e. entanglements, which provide additional elastic

energy through making a sliding contact with the chain (Ball et al., 1981). This was incorporated into the classical theory by Ball et al. (1981), and developed by Edwards and Vilgis (1986). These latter authors proposed that, contrary to popular belief, the network finite extensibility was not due to the single chain limit, i.e. complete extension of the polymer chain between cross-links, but instead was due to extension of the polymer chain between entanglements.

Thus three reasons have been given to explain how the rubber's load bearing capacity can increase: increase in the rubber cross-link density, rubber strain-hardening and in natural rubber: crystallisation. In the case of 'salami' rubber particles, a fourth reason is the presence of matrix inclusions. These hard glassy inclusions serve to stabilise and prevent lateral contraction of the particles, through promoting fibrillation of the rubber, a favourable feature of salami particles, because fibrillation produces internal necking of the rubber. This is elucidated through comparing with a solid rubber particle which does not fibrillate. In this case, the rubber cannot extend without considerable lateral contraction at the equator of the particle. It has been shown that craze breakdown can result from this feature at the particle interface (Donald and Kramer, 1982a).

10.2 Effect of rubber content and cross-link density on the flow stress of a rubber toughened composite. (contd)

10.2.2 Craze percolation

Generally in HIPS and ABS, following the post yield load drop, the material strain-softens and flows at a constant stress. The stress then begins to progressively rise until the specimen breaks. It is a common presumption, that the rise in flow stress is a result of the progressive decrease in the number of craze initiation sites as the material is extended. However it should be remembered that crazes extend by the meniscus instability mechanism and thicken by surface drawing, implying that theoretically the specimen could

become completely fibrillated. This would result in an ever-decreasing specimen modulus, and corresponding ever-decreasing flow stress, with increase in strain.

The explanation for the increasing flow stress seen in Figures 4.1, 5.3, 5.5 and 6.1 etc. could lie in an amalgamation of both features. As the rubber particles cavitate and fibrillate, the number of sites for craze initiation decreases. However instead of complete crazing of the matrix, the crazes are unloaded and prevented from unlimited thickening by the strain-hardening action of the rubber fibrils (Soares, 1994). Even at low extensions, thin stress whitened bands are observed in HIPS and ABS. This indicates that considerable dilatation and high strain can exist locally, while the majority of the specimen is at modest strains. This suggests two questions which are critical to the understanding of the deformation and failure of HIPS and ABS:

i. if at low macroscopic strains, anomalously high dilatation and strain exists locally, why does the material rarely rupture at low strains ? i.e. what mechanisms operate in rubber toughened polymers that do not in unfilled glassy polymers ?
ii. How does the deformation percolate through the material ?

The same explanation could apply to both questions. While the strain can be very high in local pockets of the material, for a crack to initiate, one of several events must occur:

(1) a craze must encounter a dust particle of sufficient size to produce craze breakdown (Yang et al., 1986; Kramer and Berger, 1990 and Berger, 1991). At small strains this is possible, but considered unlikely because of the low probability of the small number of crazes formed, encountering one of the few dust particles present.

(2) According to a model proposed by Yang et al. (1986), and developed by Kramer and Berger (1990), the probability of craze fibril disentanglement in polystyrene, increases with increasing stress on the craze. However, in HIPS, the much larger quantity of crazes ensures that, to produce the same displacement rate, the mean stress on the crazes is much lower than in unfilled polymers. The result will be less disentanglement of the molecules in forming the craze fibrils, producing more stable crazes which are less likely to breakdown.

(3) The crazes must thicken and draw the adjoining particles until rupture of the rubber occurs. The load sharing balance between the system of fibrillated rubber particles in parallel with crazes, was discussed in section 10.2. It was discussed how the rate of craze thickening, which is known to follow Eyring kinetics, can be significantly affected by the stress on the adjoining rubber particles. Therefore as the rubber strain-hardens, it carries more of the applied stress, thereby unloading and slowing the rate of extension of the adjoining craze. As the stress increases on a fibrillated rubber layer, there are three options (a) the rubber is pulled apart by the thickening craze(s); (b) the stress is insufficient to rupture the rubber but is still high enough to continue thickening the craze, thus enveloping the entire particle or (c) the stress on the craze and stretched rubber is relieved, through 'fresh' dilatation nucleating in their vicinity. Hence an energy balance exists in the material between the propagation of existing deformation, and the nucleation of 'new' deformation. Nucleation can occur as a result of secondary rubber cavitation, when bifurcating crazes collide with unfibrillated particles, and also through primary rubber cavitation. Primary cavitation can occur in a spatially random manner, as particles overcome the cavitation energy barrier, but the conditions for cavitation can be enhanced if the stress on the particle increases. Thus, as the fibrillated and stretched rubber layer strain-hardens, the stress is transferred to other parts of the same rubber particle,

and to neighbouring rubber particles. If the energy required to extend an existing rubber particle and craze, is greater than the energy required to initiate and propagate a new craze, then fresh craze formation will result. This is the fundamental basis of the **initiation/propagation** energy balance relationship and this explains how deformation in the specimen is initially confined to thin white bands, but eventually percolates throughout the entire specimen. This is discussed further as follows.

The energy potential U_D between mechanisms is given by:

$$U_D = U_I - U_P \qquad (10\text{-}10)$$

$$\begin{cases} \text{if } U_D \text{ is positive then craze propagation occurs} \\ \text{if } U_D \text{ is negative then craze initiation occurs} \end{cases}$$

where U_P is the energy to thicken an existing craze and U_I is the energy to nucleate a new craze. Figure 10-6 shows the deformation of a thin film of HIPS8 strained in the TEM (Laatsch, 1997). It is clearly visible that the dilatation is originally confined to thin white bands, but percolates through the material in the direction of the uni-axial tensile stress.

It appears that the only reasonable way in which failure can occur at low strain, is through case (3) above, but in HIPS and ABS with rubber volume particle fractions typically of 20 to 30 %, failure should not occur at low strains, because the volume fraction of unfibrillated rubber and uncrazed matrix is very high. At small strains in materials of these rubber contents, when the advanced fibrillated rubber layers extend and strain-harden, it is energetically more economical to dilatate some of the neighbouring abundance of unfibrillated material, than extend the existing rubber layer and crazes. This immediately implies two effects: the effect of rubber content and rubber shear modulus on the propagation/initiation energy balance and stability of the material. The

complicated nature of these combined effects on the percolation of deformation through HIPS and ABS dictates that they are discussed separately.

10.2.2.1 Rubber content and its effect on deformation percolation and material stability

It is well known that decreasing the rubber content of toughened polymers reduces the density of crazes formed under stress. As was discussed in section 10.1, this is due to a reduction in the number of stress concentration sites and a depressing of the stress on the matrix. If the rubber content is reduced, the modulus of the composite surrounding the rubber/craze system is increased. Closure forces acting on the craze tip are higher (compounding the lower stress on the matrix), thus producing lower rates of craze extension and thickening. Thus the flow stress increases with decreasing rubber content to counteract these effects.

In varying the rubber content of HIPS and ABS, the initiation/propagation energy balance is also affected. When the material flows, new sites of dilatation form if the stress transferred through existing rubber/craze systems is such, that craze nucleation takes place in unfibrillated material. Decreasing the volume of rubber decreases the number of craze nucleation sites and critically, also decreases the number of large particles in the material. Some particle size effects, as discussed earlier, can be explained through rubber cavitation models (Bucknall, 1997), which reveal that the critical stress to cavitate a particle increases with decreasing particle diameter. Hence the critical stress to produce cavitation and new sites of crazing in a volume of material toughened with small particles, will be higher than if the volume were toughened with an equal volume of large particles. Thus crucially, this stress is transferred through existing stressed rubber/craze systems, decreasing the stability of the material.

Increase in the critical stress to cause deformation percolation, denoted the **percolation stress**, raises the flow stress of the composite and increases the extension of the fibrillated rubber layers. The former is favourable because through raising the stress required to produce macroscopic flow, the material strength also increases. With the rubber layers already at high extension, the latter is an undesirable characteristic, because there is the possibility that the highly stressed rubber fibrils could rupture. This seems to imply that rubber fibrillation, through introducing potential defects, is deleterious to composite toughness. Widespread craze formation, extension and thickening, which are promoted by rubber cavitation (Bucknall, 1997), are advantageous toughening mechanisms which optimise the volume of material involved in the deformation.

Figure 10-6. 1 μm thick film of HIPS8 extended in-situ(Laatsch, 1997). Crazes extend in the direction perpendicular to the applied stress, thus deformation percolates through the material in the direction parallel to the applied stress (as indicated). (2μm ▬▬)

For example for a volume strain V, 100 crazes will have to break many more bonds and create a much more free surface, than that of 1 craze producing the same volume strain. Energy absorption is higher due to this surface to volume ratio. There is also the possibility of craze fibril creep in very thick crazes (Trassert and Schirrer, 1983 and Verhuelpen-Heymans, 1984), although this was discounted by Kramer and Berger (1990).

10.2.2.2 Rubber shear modulus and its effect on deformation percolation and material stability

Increasing the cross-link density of rubber significantly affects the mechanical behaviour of HIPS and ABS. Equation 10.2 shows the energy to cavitate a rubber particle scales with the shear modulus. Assuming that rubber cavitation promotes crazing, perturbation of the energy to cavitate the rubber, should have significant effects on the macroscopic flow of these materials. This indeed was observed for HIPS, ABS and AIM. Increase in the mean critical stress to cavitate the rubber particles, dictates that the percolation stress also increases. The result is similar to that observed when the rubber content is reduced, because if the stress to produce new sites of dilatation is increased, then the stress transferred through existing rubber/craze systems is also increased.

Increasing the rubber cross-link density, decreases the extension at which strain-hardening appears, and the extension at break. As the crazes thicken, strain-hardening produces a sharp increase in stress on the rubber, resulting in unloading of the adjoining crazes. Thus the two effects should combine to produce thinner crazes, which translates to less matrix dilatation per rubber particle and lower overall strains.

10.3 Strain at break (constant displacement rate)

The stability of rubber toughened polymers are clearly affected by the rubber content and shear modulus, but the precise mechanisms controlling failure in HIPS and ABS are not well understood. The majority of information comes from constant displacement rate tensile tests, but it is not clear from these tests whether stress or strain is the limiting factor. This question was resolved by Sjoerdsma and Boyens (1994), who found the probability of failure of HIPS at constant stress, scaled with the plastic strain. This work (outlined in section 4.4) clearly identifies strain as the critical factor controlling failure, but it was also found in this study that the level of applied stress also affects the mean possible strain. It was observed that specimens tested at a constant displacement rate, generally deform to consistently high strains, whereas the standard deviation of failure strains for creep tests is much larger. One possible explanation is that during a standard tensile test, the applied stress reaches a peak level which is much higher than generally applied in creep experiments. Under the application of this high stress, a significant proportion of rubber particles will cavitate, resulting in free surfaces readily available for craze nucleation throughout the material. The high proportion of convenient sites of craze nucleation reduces the mean percolation stress, resulting in lower stresses on existing rubber/craze systems. This translates to a narrower distribution of rubber extensions and craze thicknesses than in creep tests, i.e. the deformation is more homogeneously distributed throughout the specimen. The result of this, is less fibrillated material becomes highly strained at low macroscopic strain, decreasing the likelihood of failure.

11. DISCUSSION. Failure Statistics of HIPS, ABS and AIM under creep conditions.

For a long time it was not clear whether stress or strain is the limiting factor in failure of rubber toughened materials. This problem was resolved by Sjoerdsma and Boyens (1994) who showed that the probability of failure of HIPS is directly dependent on the plastic strain of the specimen. This dependence was investigated for the aforementioned materials and in agreement with the aforementioned authors, the probability of failure was again found to increase with plastic strain on the material. But in order to gain a meaningful understanding of how the probability of failure might scale with plastic strain, the deformation kinetics of HIPS and ABS under a constant applied stress, are discussed first.

The effect of rubber content on the deformation kinetics of HIPS is shown in Figure 4.3. It can be seen that reducing the rubber content produces a non-linear increase in the induction time of HIPS. Using the Ishai-Cohen model (equation (10.3)), the mean stress on the matrix can be determined for the three grades of HIPS plotted in Figure 4.3. For an applied stress of 16.2 MPa, the stress on the matrix of HIPS8 (ϕ_r=35 vol.%) is 40.6 MPa, in HIPS6 (ϕ_r=26 vol. %) it is 32 MPa and in HIPS4 (ϕ_r=17 vol. %) it is 26 MPa, thus demonstrating a decreasing matrix stress with decrease in rubber content. The induction time, i.e. the period preceding rapid dilatation (indicated in Figure 4.4, point A), gives an indication of the rate of deformation initiation. Rapid dilatation of HIPS and ABS in creep, takes place for the same reasons as the post yield stress drop is observed in a standard tensile test. Before rapid dilatation can take place,

sufficient fibrillation of the matrix and rubber must have occurred. In low rate creep of HIPS and ABS, long thin crazes form during the induction period, and extend across the specimen. When crazes overcome the closure force at the craze tip, the rate of craze thickening in the layer can increase significantly. Fibrillated layers in the form of thin stress-whitened bands perpendicular to the applied stress, can be seen on the surface of the specimen. These are observed to form at low strains (< 3 %), which coincide with an increase in the overall creep rate.

The existence of an induction period in creep of HIPS and ABS, seems to indicate that the mechanism controlling deformation initiation is an activated process. Bucknall (1997) has shown that for a particle to cavitate, the stored energy of the particle must overcome a small energy barrier. If this is the case, then the induction period will be heavily dependent on the time to cavitate the rubber particles. It is difficult to determine the effects of stress, rubber content and rubber cross-link density on the rates of deformation initiation using kinetic parameters such as the induction time, because there are many interdependent mechanisms at work. Thus while a variation in the induction period of HIPS and ABS, gives an indication of a change in the rate of deformation initiation, it is not a direct measure.

Following the induction period, the strain rate increases significantly. The number of crazes multiply because an increasing number of rubber particles have overcome the cavitation energy barrier, and secondary particle cavitation occurs as a result of particles colliding with extending crazes. As can be seen from Figure 6.1, during the induction period, the probability of failure is negligible. Hence with respect to identifying the mechanism controlling failure, it appears that understanding how the deformation percolates through the material is of crucial importance. The principle of deformation percolation was discussed in

section 10.2 and the fundamental principle is, that the strain on a craze, thickening in parallel with adjoining rubber particles, is limited by strain hardening of the rubber particles. The increased load carried by the rubber is transferred to the surrounding material, thus generating new crazes and rubber fibrillation, see Figure 11-1. Crazes can also nucleate as a result of secondary cavitation, i.e. percolation also results when crazes bifurcate through the specimen. The rate of deformation percolation (and so strain rate) continues to increase, so long as there is a plentiful supply of unfibrillated rubber available to promote profuse crazing. The rate of dilatation reaches a maximum coinciding with the maximum rate of craze thickening, (indicated in Figure 4.4, point B). As the volume of unfibrillated rubber decreases, the rate of craze growth and rubber voiding also decreases, producing an overall decrease in the dilatational rate of the material. This coincides with a strain of approximately 0.2 for HIPS8 (which is a similar value to that observed by Soares (1994)), decreasing to 0.07 for HIPS2. The macroscopic strain at which ABS8 strain hardens, is approximately 0.15, and this decreases to 0.05 for ABS2.

In some creep tests on HIPS8 and ABS8 the rate of dilatation decreases until the rate is almost zero. This can occur if the rate of craze thickening can be significantly reduced. This phenomenon is not seen in intermediate creep rate tests on materials with lower rubber contents, such as HIPS6, 4, 2 or ABS6 etc. This indicates that the degree to which the rate is reduced, is dependent on the volume of rubber in the material and obviously the stress on the specimen. This can be illustrated using a simple model consisting of: one craze with initial stress S on the craze surface, thickening in parallel with a number of particles N. If N is very high then the load carried by the rubber is such that the resulting rate can be decreased significantly, as in HIPS8 and ABS8. As N is reduced the total load carried by the rubber decreases, allowing the craze to continue thickening. This means that in a material with N embedded rubber particles, the mean stress on

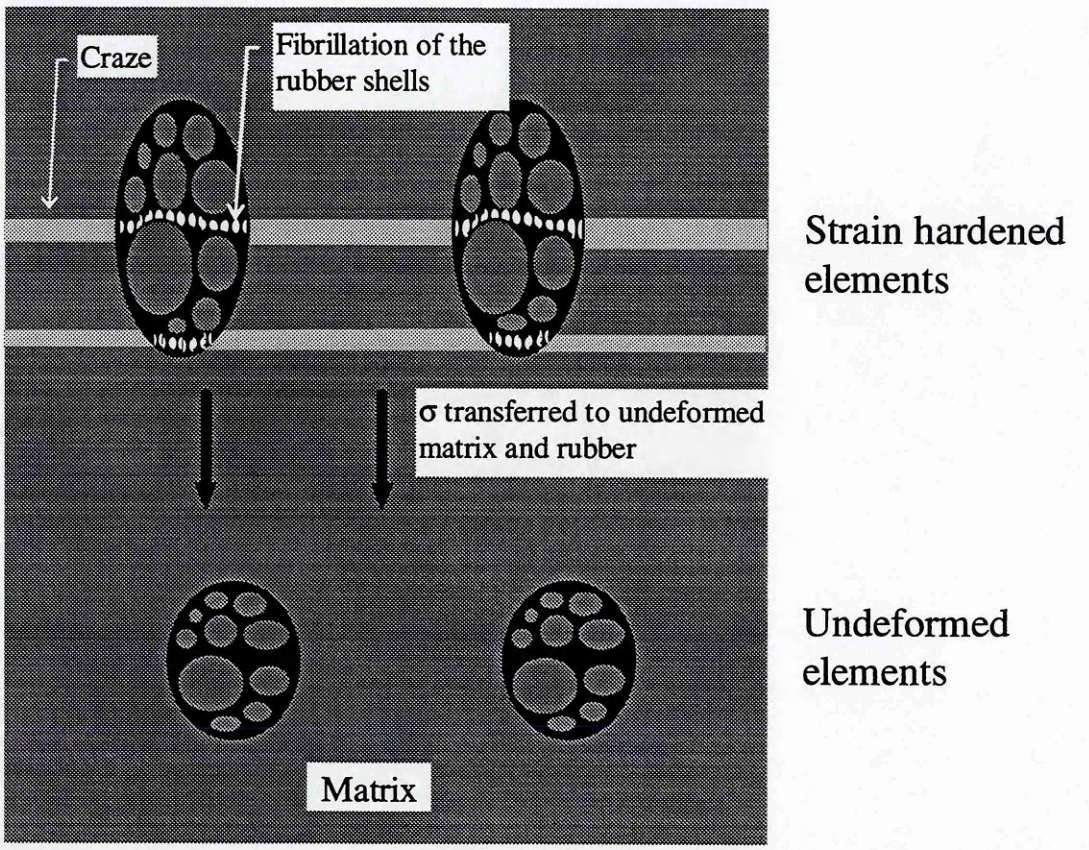

Figure 11-1. Schematic drawing of the effect of rubber strain hardening on deformation percolation

the rubber fibrils is enough to reduce the strain rate to ~ zero, whereas in a material with, for example < 0.75xN, the same mean stress may not reduce the strain rate to the same extent. However, it is likely that if the craze continues to draw the rubber fibrils, the stress on the rubber will eventually increase until the rate of craze thickening is significantly decreased. Nevertheless it is also likely that in such materials, catastrophic failure will occur before this craze stress has been attained. It can therefore be surmised that the strain hardening phenomenon is optimised, when sufficient particles are present in the direction perpendicular to the applied stress, whereas the amount of dilatation before failure, is optimised when sufficient particles are present in the direction parallel to the applied stress.

Increasing the shear modulus of the rubber phase depresses the number of crazes formed, and reduces the strain at which macroscopic strain hardening takes place, denoted the **inflexion strain**. The mean strain at failure also decreases with increase in the rubber shear modulus. HIPS2 was blended with 0.5 wt.% sulfur, which is a similar sulfur/rubber ratio as HIPS8 blended with 2 wt.% sulfur. This is a very high sulfur content, which produces a shift in the T_g of approximately 90 °C (Lin, 1997). Figure 5.5 shows that if the rubber content is sufficiently cross-linked, HIPS undergoes brittle failure at strains of approximately 0.02. Owing to the higher shear modulus, the extension at which rubber strain hardening takes place is lower. This could mean that the crazes are unloaded at smaller strains resulting in a lower inflexion strain. The inflexion strain reduced from 0.2 for HIPS8 to 0.13 for HIPS8 blended with 0.56 wt.% sulfur, (see Figure 5.7).

In polystyrene a critical molecular weight is necessary to produce stable crazes (Kramer and Berger, 1990), and although final rupture due to craze breakdown is not ruled out, the molecular weight of the matrix in HIPS is sufficient to produce stable crazes.

While the possibility of microscopic shear of interparticle ligaments has recently been proposed as an energy absorbing mechanism in HIPS (Bubeck et al., 1990 and Buckley, 1991), shear yielding was not observed in TEM examination of HIPS or ABS. The mechanism initiating ultimate rupture can hence be reduced to either craze breakdown or rubber rupture. Based on evidence by Yang et al. (1986) and Kramer and Berger (1990), who showed that thin film polystyrene fails by craze breakdown, it would not be surprising to find that HIPS fails in a similar manner. There is however, increasing evidence to suggest that the mechanism which initiates rupture in HIPS, is breakdown of the rubber particles.

What *is* clear, is the mean failure strain of HIPS and ABS is proportional to the rubber content and the rubber shear modulus. The observed dependence on rubber content is not surprising and is well documented, but how final failure occurs is not clear.

11.1 Statistics of failure of HIPS and ABS

According to the procedure described by Sjoerdsma and Boyens, the probability of failure of HIPS, ABS and AIM was investigated with respect to creep stress, and was also investigated with respect to rubber content and rubber shear modulus. The non-linearity of the extension rate of this material complicates any attempt to predict its lifetime. The induction time is plotted against the fracture time in Figure 6.1 and this reveals that failure almost never occurs before the induction time was reached. This indicates two important points:

- in order for failure to occur, some dilatation is necessary, presumably in the form of crazing and/or rubber cavitation;
- the induction period conveniently defines a lower time limit for failure of HIPS, because before this time the probability of failure is negligible.

Nevertheless, materials such as HIPS8 are designed to absorb large amounts of energy in impact and creep, well in excess of that absorbed during the induction period. Therefore for most design situations, an understanding of the statistics governing final rupture of the material would be of far more practical value than identifying a lower time limit for fracture, and would serve a real purpose in component design.

Samples of the aforementioned materials, numbering not less than 20, were tested and the failure strain results statistically analysed. The cumulative probability of failure is shown in Figure 4.9 for HIPS blended with polystyrene, and is shown in Figure 7.4 for ABS blended with styrene acrylonitrile. In both HIPS and ABS the mean failure strain is observed to increase with increase in rubber content. Also, in accord with the findings of Sjoerdsma and Boyens, the probability of survival (1–probability of failure) decreases with the plastic strain on the material.

The work by Sjoerdsma and Boyens provides the essential keys to reveal the dominant mechanism controlling final failure in HIPS. They identified that a correlation exists between the plastic strain and the likelihood that the material will fail. The equation which describes the probability of failure is:

$$P_{nf} = \exp\left(-k\,\varepsilon_{cr}^{2}\right).$$

The failure strain data of HIPS, ABS and AIM were used to test this model, see Figures 4.11, 7.5 and 9.6. If this model correlated with the failure strain data, plotting ln(survival probability) vs. ε_{cr}^{2} should yield a straight line. It is apparent from these plots that with exceptions HIPS2 and AIM (16.7 MPa), this model does not correlate with the data. Later it will be explained why the model fits these samples only. The model advanced by Sjoerdsma and Boyens, holds that the final rupture of the material occurs when two crazes impinge upon each other. While it is plausible that the probability of failure of a polymer would increase with the number of crazes formed, this hypothesis suggests that a more failure resistant material results, if the number of crazes is reduced, through for example, reducing the rubber content. This is not the case for HIPS and ABS, as can be seen from Figures 4.9 and 7.4. TEM evidence does show

that craze breakdown can occur when two crazes impinge, but for reasons mentioned earlier and reasons which will be discussed now, this mechanism is deemed unlikely as the dominant cause of final failure.

As mentioned, Figure 6.1 shows that failure in HIPS is unlikely to occur before the material dilatates and deforms. The material dilatates through mainly craze extension and thickening, and rubber cavitation and fibrillation, (Buckley, 1991). The relationship between the plastic strain of the specimen and the likelihood of failure P_f, implies one or all of three things: (a) the possibility of a craze encountering a defect (dust particle etc.), or the possibility of a fibril forming which has few entanglements, increases with the number and size of crazes; (b) the number of crazes in the material is growing, thus increasing the chance of several crazes impinging; (c) the number of defects in the material is growing, thereby increasing the probability of one forming which causes ultimate specimen failure.

It was discussed in section 10.1.2 how the load balance between the rubber phase and the matrix, changes as the specimen extends. This is also true in constant stress conditions, because although the stress on the cross-sectional area of the specimen is constant, stress inhomogeneites will exist throughout the specimen, because of strain softened regions such as crazes and rubber particles. Moreover, owing to the increasing load bearing capacity of the rubber phase, the stress on the crazes will decrease as the specimen is extended.

Because the crazes are more load bearing and therefore the crazes control the rate of dilatation of the material, it is reasonable to assume that the mean stress on the crazed material is highest, when the creep rate reaches its maximum. Kramer and Berger (1990) have shown that for thin film polystyrene, the probability of craze breakdown due to fibril disentanglement, scales with the

stress on the craze. This implies that if craze breakdown due to fibril disentanglement, is the dominant mechanism controlling failure in HIPS, the mean failure strain should coincide with the maximum creep rate.

It is apparent from Figures 4-3, 4-4, 5-7, 7-3 and 8-4 that the arithmetic mean failure strain occurs consistently at higher strains than that strain corresponding to the maximum strain rate, denoted **the inflexion strain**. This was observed for all blends of HIPS and ABS, both vulcanised and unvulcanised. Above the inflexion strain, the mean stress on the crazes decreases thus decreasing the probability of craze failure. Thus, because the conditional probability of ultimate failure increases as the material stain hardens, it can be logically deduced that unlike polystyrene, the dominant failure mechanism in HIPS and ABS is not craze fibril disentanglement. (The conditional probability is the probability at strain ε, that a surviving specimen will fail in the interval $\varepsilon + \Delta\varepsilon$). Moreover, the density of crazes in rubber filled polymers is greater than that in unfilled polymers by a factor of $\sim 10^6$. Therefore the stress on the crazes in unfilled glassy polymers such as polystyrene and SAN will be much greater than those in HIPS and ABS, hence producing more fibril disentanglement.

As with craze impingement, the possibility of failure resulting from defects such as dust particles can almost never be ruled out, but the vulcanisation experiments show that if the density of crazes is reduced for the same rubber content, the material becomes unstable at lower strains. This is contrary to what would be expected if craze breakdown occurred through encountering other objects (dust particles, crazes). It is therefore also deduced that neither dust particles nor craze impingement is the dominant failure initiating mechanism in HIPS and ABS.

The third option which the relationship between plastic strain and P_f suggests, is that the number of defects increases with strain. With craze breakdown ruled out, the other dilatational mechanism which might produce a defect in the material is rubber particle fibrillation. If each rubber fibril is construed as a potential defect, then the number of defects will increase with plastic strain on the composite. Rubber particle fibrillation can culminate in defects in the material, through for example a layer of rubber fibrils stretched past their extension at break. The rubber fibrils extend in parallel with crazes, consequently if the stress on the craze is sufficient to continue drawing the layer of rubber fibrils past their extension at break, then the rubber fibrils will rupture, see Figure 11-2. This has previously been suggested by Soares (1994). If one rubber fibril fails, it is unlikely that catastrophic failure will immediately result, but the stress is then concentrated on the remaining fibrils thus further increasing their strain. It is even unlikely that failure of one rubber particle will result in immediate failure of the composite, however if a sufficient number of particles

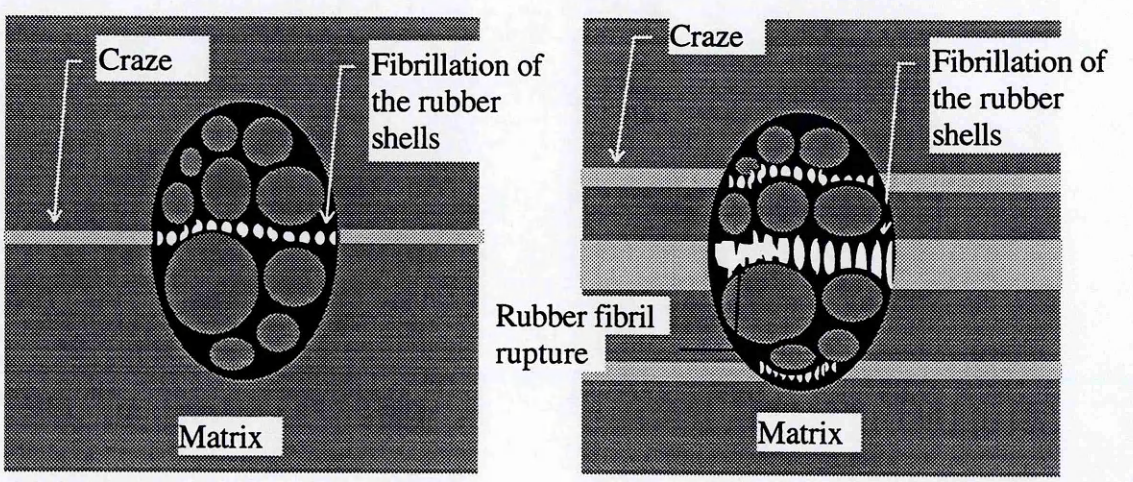

Figure 11-2. Deformation of HIPS and ABS. The craze thickening rate is decreased through rubber fibril strain-hardening. However if the craze strain rate is not decreased to zero, the crazes will draw the rubber particles, until the rubber fibrils rupture.

fail, or a particle of sufficient size fails, this would constitute crack initiation, culminating in failure of the specimen. Assuming therefore that rubber particle rupture is the dominant process controlling failure in HIPS and ABS, it would be expected that the conditional probability of failure would increase sharply as the mean stress on the rubber phase increases (i.e. as the composite strain hardens). This indeed is observed in Figures 4-3, 4-4, 5-7, 7-3 and 8-4, where the mean failure strain occurs after the material has strain hardened.

This proposal can be tested with many questions which to date have been unsatisfactorily answered. Some of these are addressed as follows.

11.1.1 Rubber matrix interfacial adhesion

It has been shown that some degree of toughness is achieved through the addition of glass beads or chalk to a glassy polymer matrix, but it is still substantially lower than that of rubber filled materials (Lavengood, 1973 and Braun, 1996). While it is generally accepted that good interfacial adhesion is necessary to absorb energy ahead of the craze tip and behind the crack tip, it is possible that the level of deformation attained in glass filled polymers, results from craze nucleation occurring at sites of particle debonding at the poles of the high modulus glassy inclusions. Nevertheless the fundamental difference in mechanical behaviour between HIPS and hard inclusion filled polymers, is that the failure strain is much lower in the glass filled composite, which is likely to result from the absence of craze stabilisation and deformation percolation, and also the presence of the initial void formed if the particle debonds. Failure is delayed in HIPS and ABS through stabilising crazes thus forcing the dilatation to percolate through the material.

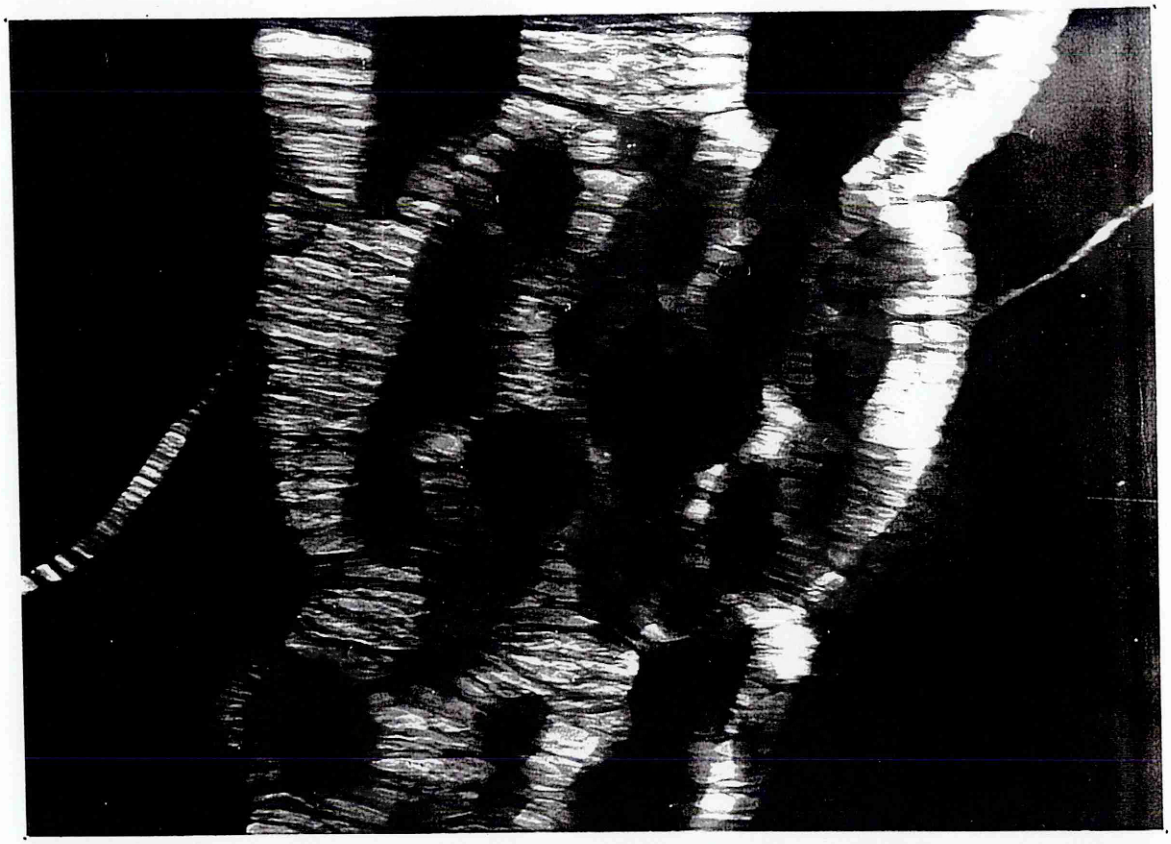

Figure 11-3. 1 μm thick film of HIPS8 extended in situ. Note extensive fibrillation of the rubber surrounding the hard sub-inclusions. (0.5μm ▬▬▬▬)(Laatsch, 1997)

11.1.2 Rubber particle morphology

The importance of particle morphology was underlined by Donald and Kramer (1982a), who observed failure of the rubber/craze interface at solid rubber particles (of diameter <1μm) in HIPS. This was attributed to contraction at the particle equator, a feature not observed with multiple inclusion particles. In HIPS8 all but the smallest particles are multiple inclusion, and it is possible that failure can result from breakdown of the interface of the smallest rubber particles. Also, as with interfacial adhesion, the particle morphology is of critical importance in stabilising crazes and delaying crack initiation. Solid particles will contract at the waist, hence forming voids and allowing uncontrolled craze

growth. The rubber shells in multiple inclusion particles fibrillate, (thus absorbing extra energy), strain harden, (thus controlling the craze thickening, and inducing percolation) and ensure efficient use of all the rubber through promoting percolation. Donald and Kramer concluded that the optimum salami particle morphology is a large number of small inclusions, rather than a small number of large inclusions. They suggested that this optimised structure results from minimisation of the size of the void which results when the rubber shells fibrillate.

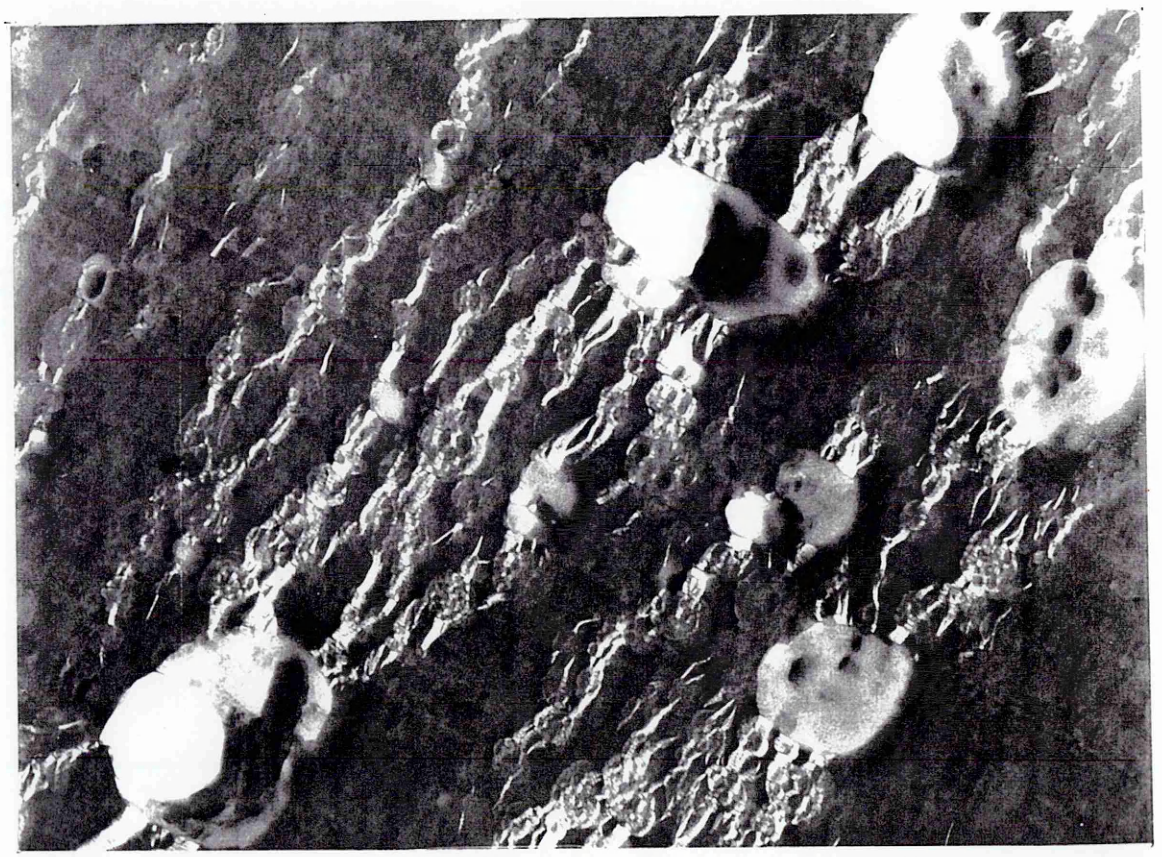

Figure 11-4. 1 μm thick film of HIPS8 extended in situ. Note extensive voiding of large anamolous particles. (5μm ▬▬▬▬). (Laatsch, 1997)

The volume of fibrils in a rubber layer adjoining a craze will determine the craze thickness, for example consider a craze fully unloaded by a rubber layer of primordial thickness 50 nm and extension 4. This produces a craze 200 nm thick, but if the primordial thickness of the rubber layer is 80 nm thick the thickness of the mature craze can now be 320 nm. This increased craze thickness is not necessarily an advantageous feature because as discussed earlier, creating crazes necessitates creating new surfaces, thus although shorter strain-hardened rubber fibrils will produce thinner crazes, they ensure that the number of initiation sites associated with a rubber particle is increased by preventing large thick crazes.

Some doubt however, has been cast on Donald and Kramer's proposal that the optimum salami particle morphology is a large number of small inclusions. It was observed in this study, and in recent work on the same grade of HIPS by Laatsch (1997), that anomalously large particles exist in HIPS with a morphology of large numbers of small inclusions surrounded by a relatively thick shell of rubber. These particles are invariably seen to form large voids, which can only be deleterious to the fracture resistance of the composite. Figure 11-4 shows large voids formed at particles of this type in a thin microtomed film of HIPS8 strained in-situ (Laatsch, 1997). This micrograph underlines the suggestion that the generation of these particles during material manufacture, should be kept to a minimum.

11.1.3 Rubber content

One of the fundamental questions this study set out to answer, is how does the volume fraction of rubber particles control the strain at failure of HIPS and ABS ? Essentially this relationship is a product of the amount of rubber available to initiate crazes, and the ratio of rubber to adjoining craze. In part, the stability of the system is determined by the volume of unfibrillated rubber available to initiate fresh deformation and dilatation. As long as there is an abundance of

unfibrillated rubber, the probability of failure should be minimal. Of course generally speaking, the probability of failure can be reduced through simply increasing the rubber content, however the toughness of the composite is then compromised, because of the resultant reduction in the flow stress of the material.

Theoretically, the material can extend until every molecule of rubber has extended and strain-hardened. At already high strain, further extension of the material, requires generation of fresh dilatation and/or continued extension of the existing fibrils. The maximum extension possible for the composite ε_{max}, is the extension at which all the rubber in the material has fibrillated and extended to just before its extension at break. There are two factors which interrelate and combine, to reduce the probability of the composite reaching its maximum possible strain; (a) there is a statistical probability of a layer of rubber fibrils becoming overloaded, based on, among other things, the spatial distribution of particles and (b) at a given strain, the number of unfibrillated particles decreases with increasing applied stress.

One facet of the statistical probability of survival, is the probability that the rubber fibrils slow the rate of craze thickening to the extent that the rubber fibrils are static. Bearing in mind that layers of rubber fibrils can be highly stretched at low macroscopic strains, and also the considerable numbers of crazes and rubber particles, it is not surprising that the standard deviation of the failure strain distributions is so high for HIPS and ABS. HIPS8 and ABS8 have a similar maximum failure strain, but the standard deviation of the failure strain distribution in HIPS, is much higher. For example $\varepsilon_{min}/\varepsilon_{max} = 0.3$ for HIPS8 while $\varepsilon_{min}/\varepsilon_{max} = 0.6$ for ABS8. Donald and Kramer (1982d) observed large voids in particles in ABS, but nevertheless did not find associative craze breakdown resulting from these voids. The authors attributed this to the lower true stress on

SAN craze fibrils as opposed to PS fibrils, indicating that a rubber particle rupturing in ABS, is not as critical as a particle of similar diameter rupturing in HIPS. Evidently the critical volume of ruptured rubber fibrils, necessary to cause craze breakdown and crack growth, is higher in ABS than in HIPS.

The stability of the composite will be affected by the volume of rubber adjoining the crazes. The effect of rubber content on the percolation mechanism was mentioned earlier in section 10.2, but, assuming rubber rupture causes ultimate failure, the statistical arrangement of particles will determine the actual failure site, and will play a significant role in producing a wide distribution of failure strains. From examination of the statistical process, it appears the actual failure point will depend on several features. Critical to this, is the principle that a strain-hardening rubber fibril is a potential defect, and the likelihood of it becoming a defect increases with extension. In order that a rubber particle becomes completely secure from failure, it must slow the strain rate of the adjoining craze to zero. Also the minimum tenable fracture strain for the composite, is that which corresponds to one fully stretched fibrillated layer of rubber. From arguments presented earlier (section 10.1), it can be imagined that the first rubber particles to undergo strain-hardening and so be at 'risk', are the large particles. However, in high rubber content materials, these 'pilgrim' strain-hardened particles are relieved through dilatation of the surrounding material. In sections of lower rubber content materials such as HIPS2, this may not be the case, thus resulting in failure at low strains ($\varepsilon_{min} = 0.02$).

In the higher rubber content materials, an anomalously high concentration of large particles, will produce a dense concentration of deformation at low macroscopic strains. Even if these particles can control locally the large number of crazes initiated, these crazes will bifurcate across the full plane of the specimen. Consequently if a low density of particles is present at some point in

the same plane as the high concentration of large particles, these isolated particles could be overcome by the ever-thickening crazes, see Figure 11-5. However, because it takes a finite time for the crazes to extend across the specimen, the rest of the specimen readily dilatates. Hence the lowest failure

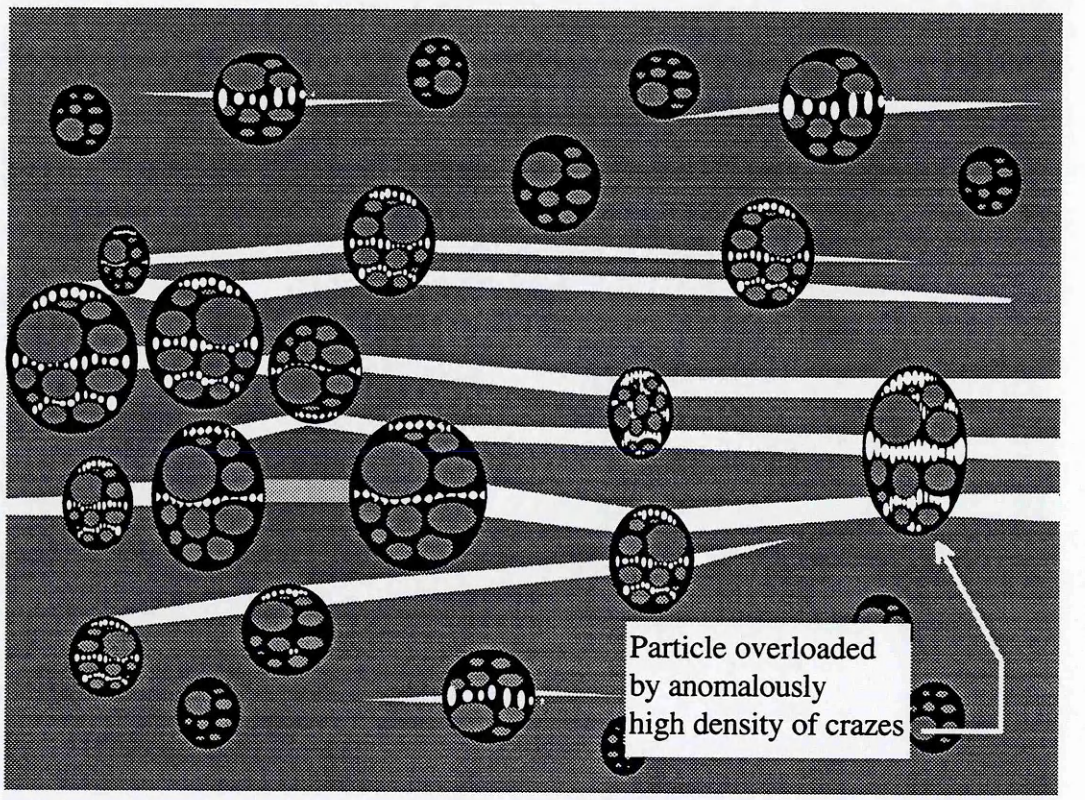

Figure 11-5. Schematic drawing illustrating the importance of a uniform distribution of particles.

strain of HIPS, is determined by the average volume of rubber adjoining the crazes, and the spatial distribution of particle sizes.

11.1.4 Rubber shear modulus

The critical stress to cavitate a rubber particle is dependent on particle size and the rubber shear modulus (Bucknall, 1997). Thus for a given applied stress, increase in rubber shear modulus, decreases the number of particles which will cavitate. Also when a fibrillated particle extends, the strain-hardening extension

decreases with increasing shear modulus. Consequently the average craze thickness should decrease, reducing the overall dilatation in the material.

It was discussed earlier how the shear modulus of the rubber will affect the percolation of deformation through the material (section 10.2). In a similar fashion to decreasing the rubber content, increasing the rubber shear modulus increases the percolation stress, i.e. the stress necessary to produce dilatation in neighbouring material. If the percolation stress is increased, then the extension of the existing rubber fibrils will also increase. Thus at a given strain, the stability of this composite, is lower than the stability of a composite with a lower rubber shear modulus. Indeed as the sulfur blending experiments have shown (see Figure 5.5, H2:0.50), the percolation stress can increase to such an extent that before deformation initiates nearby, the existing rubber fibrils are stretched past their extension at break λ_{max}, resulting in failure at low strain. This experiment demonstrates the importance of stable percolation.

In summation, during plastic flow, an increase in the rubber shear modulus makes deformation percolation more difficult and when deformation does initiate, dilatation is depressed by the lower strain-hardening extension of the rubber.

11.2 Effect of preload on failure strain

The effect of applied stress on the number of particles that cavitate is well demonstrated in Figure 5.8. In this plot, we are interested in H8:0.56 which was extended in creep at an applied stress σ_{app}, of 13.7 MPa. In these vulcanised blends, because the rubber T_g is approximately the same, the only variables in the experiment are the rubber contents and the applied stress. We also introduce the term χ ($=\sigma_{app}/\sigma_y$, where σ_y is the material yield stress) and this is discussed in

greater detail in section 12.1, suffice to say that it is a crude estimation of the effect of stress on the fraction of rubber particles which can dilatate and initiate crazes. In other words the higher the applied stress the greater the fraction of rubber contributing to composite dilatation. For example for H8:0.56 at 13.7 MPa, χ = 0.66, therefore the fraction of rubber contributing to the dilatation is estimated as only $\chi C_r = 0.66 \times 0.08 = 0.053$. To produce the same concentration of rubber contributing to dilatation in H6:0.50, χC_r is kept the same at 0.053. Thus

$$0.053 = \chi C_r \text{ therefore } \chi = \frac{0.053}{0.06} = 0.89$$

hence $\sigma_{app} = \sigma_y \chi = (25.8 \times 0.89) = 23 \text{MPa}$

Consequently H6:0.50 was extended at a constant stress of 23 MPa. It can be seen from Figure 5.8, that the mean failure strain for the two batches is approximately the same. Thus it appears that while the rubber content of H8:0.56 is higher than H6:0.50, owing to the level of applied stress, the effective rubber content is the same.

The effect of the level of applied stress was also examined through applying an initial preload to the material, and observing the effects on the kinetics of deformation, and probability of failure of the material. HIPS8 was loaded at 2mm.min^{-1} to a stress of 16 MPa, this was maintained for 10 seconds and unloaded to a stress of 15 MPa, which was maintained until failure resulted. This stress sequence is displayed in Figure 6.5. Also shown is the creep extension curve, compared with a creep curve which was loaded conventionally to 15 MPa. It can be seen that the initiation kinetics are severely affected by preloading the material. It is again reiterated that the preload was applied before

widespread crazing had formed, thus suggesting that the initiation rate determining step in deformation of HIPS, is an activated process sensitive to stress. The effects of preload on the kinetic processes of HIPS8 in creep, are plotted in Figure 6.3 and 6.4 according to the Eyring equation (Bucknall et al. 1972, 1986b). It can be seen that the preload has a significant effect on the induction time, which may indicate a perturbation to the initiation rate determining mechanism, but it has no effect on the maximum strain rate. Thus it appears that the maximum strain rate is only affected by the level of applied stress during widespread material dilatation.

The effect of preload on the probability of failure of HIPS is shown in Figure 6.6. It was found that the mean failure strain is slightly higher for the preloaded batch. If a greater number of particles have cavitated, then the percolation stress is lower, which reduces the chances of overloading a particle. Also the maximum strain at break is higher for the preloaded specimens, which, while obviously may be an aberration of the scatter of failure strains, does support the hypothesis that the application of a high stress cavitates a greater number of particles than a lower stress, hence increasing the effective concentration of rubber. The effect of stress on the maximum possible strain at failure, is discussed again later.

The failure time distribution of HIPS8 is seen to be significantly affected by the preload. Figure 6.7 shows that the mean failure time is reduced through application of a preload. Clearly, this is due in part to the shorter induction time, i.e. the mechanisms producing creep in the material are effectively advanced to earlier times. Thus the rate of failure with respect to time of the first 50 % of the specimens is approximately the same for both preloaded and no preload specimens. This is apparent as the similar slopes of the two plots between survival probabilities of 1 and 0.5. Subsequently the latter 50 % of the no

preload specimens fail at approximately the same rate as the initial 50 %, but intriguingly, the preloaded specimens begin to become more and more stable. This is an interesting observation, because it indicates a perturbation to the mechanism controlling failure. One possible explanation for this effect is that as mentioned, there are more particles cavitated in the preloaded specimens, thus the percolation stress is decreased, and more particles are available to unload the crazes. Both features increase the stability of the material.

11.3 Irradiation experiment

One problem with normalising the effect of rubber shear modulus on the high strain deformation of HIPS, is the effect of increased cross-link density on the initiation of crazes. It is difficult to say that at a given strain, there are the same number of crazes in a material with a high rubber cross-link density, as in a material with a low rubber cross-link density. However if the same number of crazes are formed in two specimens of the same material, and in one of the specimens the rubber shear modulus is subsequently increased, the resulting difference in behaviour of the materials in creep, may yield important information. Such an experiment is possible through the use of prestraining and high energy irradiation.

A batch of HIPS8 specimens were prestrained to 0.2, and half the batch were irradiated with 20 Mrad gamma irradiation. The effects of gamma irradiation on HIPS, were extensively investigated recently by Soares (1994), who concluded that the changes observed in the mechanical behaviour, were due primarily to an increase in the rubber cross-link density, rather than due to slight changes in the matrix molecular weight. The effect of irradiation on the creep behaviour of HIPS is shown in Figure 6.8. It is apparent that following the initial loading, the increased rubber cross-link density drastically reduces the strain rate

of the material. Even more significant, is that half of the irradiated specimens fractured before reaching the pre-strain level, to which they had been previously subjected. This is in comparison with the fact that none of the non-irradiated specimens fail before reaching the pre-strain level. Reiterated, upon reloading, the strain at break of the irradiated rubber particles is now reduced, and thus now may be surpassed before the craze fibrils strain-harden and become load bearing. This underlines the point that even if the rubber particles unload the crazes, the majority of the load is still carried by the crazes. In some irradiated specimens (which survived reloading), the strained rubber was relieved through strain-hardening of the craze fibrils, and fresh deformation initiated nearby.

11.4 Advanced Impact Modifier

The morphology of the AIM rubber particles is either single, double or triple core shell, i.e. double core shell consists of a hard inclusion, surrounded by a rubber shell surrounded by a hard shell surrounded by a rubber shell. The rubber is of the grade known as labyrinth or 'can of worms' morphology which consists of rod-like or threadlike rubbery elements localised in a glassy polymer domain (Bucknall, 1997). Three processes appear to dominate in the deformation of this material, rubber fibrillation, matrix crazing and matrix shear yielding. The most fundamental difference between the mechanical behaviour of AIM and HIPS or ABS is that while all three materials reach similar strains, AIM fails before it macroscopically strain-hardens. Thus in a standard tensile test, the flow stress progressively decreases, see Figure 9.1, and in a creep test, the strain rate continually increases, see Figure 9.3 and Figure 9.4.

It is difficult to isolate the reason why AIM fails before strain-hardening, because the particle morphology and the rubber grade is different from the other materials studied. Figure 11-6 illustrates a micrograph of a thin film of AIM

extended in-situ. It may be the case that the rubber cross-link density is higher in AIM than in HIPS, therefore the stress to produce cavitation of the rubber particles may be higher. This hypothesis is supported by evidence shown in Figure 9.4, where it can seen that the induction time of HIPS at an applied stress of 14 MPa, is lower than the induction time of AIM at an applied stress of 17 MPa. The mean failure strain of the materials may be similar because of the possibility that the rubber content of AIM is higher. This proposal is quite possible when Figure 11-7(a) is compared with Figure 11-7(b). There is also evidence of a high stress on the matrix, as illustrated by the presence of shear yielding, as seen in Figure 11-7(a). Matrix shear yielding is not synonymous with polystyrene, which crazes at lower applied stresses (Bucknall, 1977).

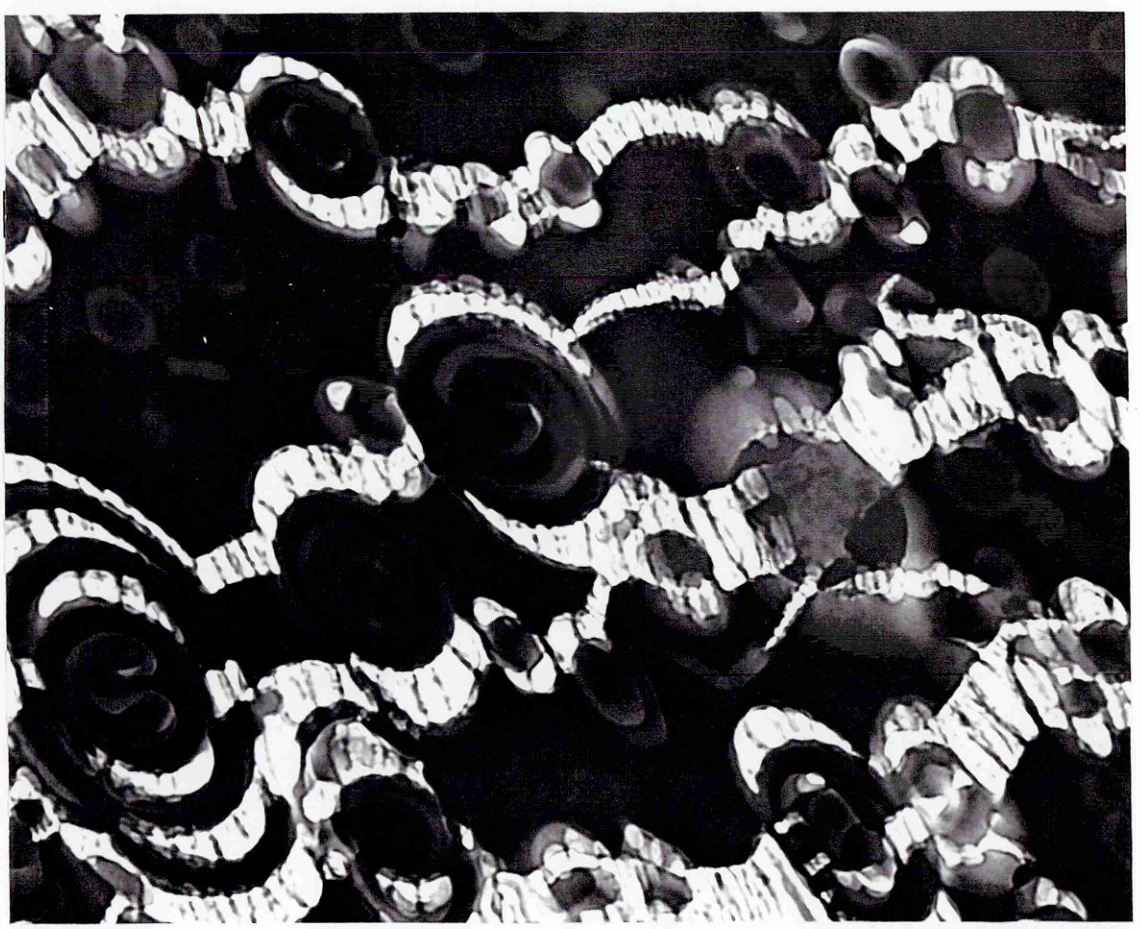

Figure 11-6. Thin film of AIM extended in situ. Note thick crazes, and extensive fibrillation of the rubber shells. (0.1 μm ▬). (Cieslinksi, 1997)

AIM was blended with sulfur, thus increasing the cross-link density of the rubber phase. It was found that the higher rubber cross-link density increased the yield, flow and breaking stresses, and decreased the strain at break in a similar fashion as observed with HIPS and ABS. The stress to produce cavitation in the rubber particles also increased as evidenced by the increased induction time and decreased maximum strain rate, see Figure 9.3. It was again observed that the material fails before macroscopic strain-hardening occurs. As with the unvulcanised material, this may be a result of the particle morphology or the rubber morphology or rubber cross-link density, or all of these.

At the beginning of Chapter 10, it was discussed how it is impossible to determine how a material fails, without first knowing how the material deforms. The number of parameters in AIM which are different from those in HIPS is such, that it is difficult to confidently and directly translate conclusions drawn from the deformation of HIPS, directly to AIM. However, assuming that the arguments given above are correct, how does the material fail ? The conclusions which have been drawn from deformation of HIPS, will possibly apply to many rubber toughened polymers, and it is also possible that they will apply to AIM. Therefore the fraction of rubber unfibrillated; the mean stress on the rubber fibrils; and the statistical arrangement of the particles, all play a critical role in determining when the material fails. Again if a low volume fraction of rubber is adjoining the craze, then it is likely that the rubber particles at this point, will be overcome. Also if the volume of unfibrillated rubber is severely depleted, then the existing fibrils will become increasingly stretched until failure occurs.

It was observed that contrary to that observed in HIPS and ABS, increase in the level of creep stress decreases the probability of survival at a given strain, see Figure 9.5. Kramer and Berger (1990) (in developing a model advanced by

Yang et al. (1986), see Chapter 2) proposed that the probability of craze breakdown increases with stress on the craze. Consequently the adverse effect of applied stress on the probability of survival, may suggest that craze breakdown is the dominant mechanism controlling failure. However, it should also be noted that shear bands were seen to 'shear' some rubber particles into two parts. The effects of the interaction of shear with crazes should be investigated, to clarify the dominant mechanism controlling failure of AIM.

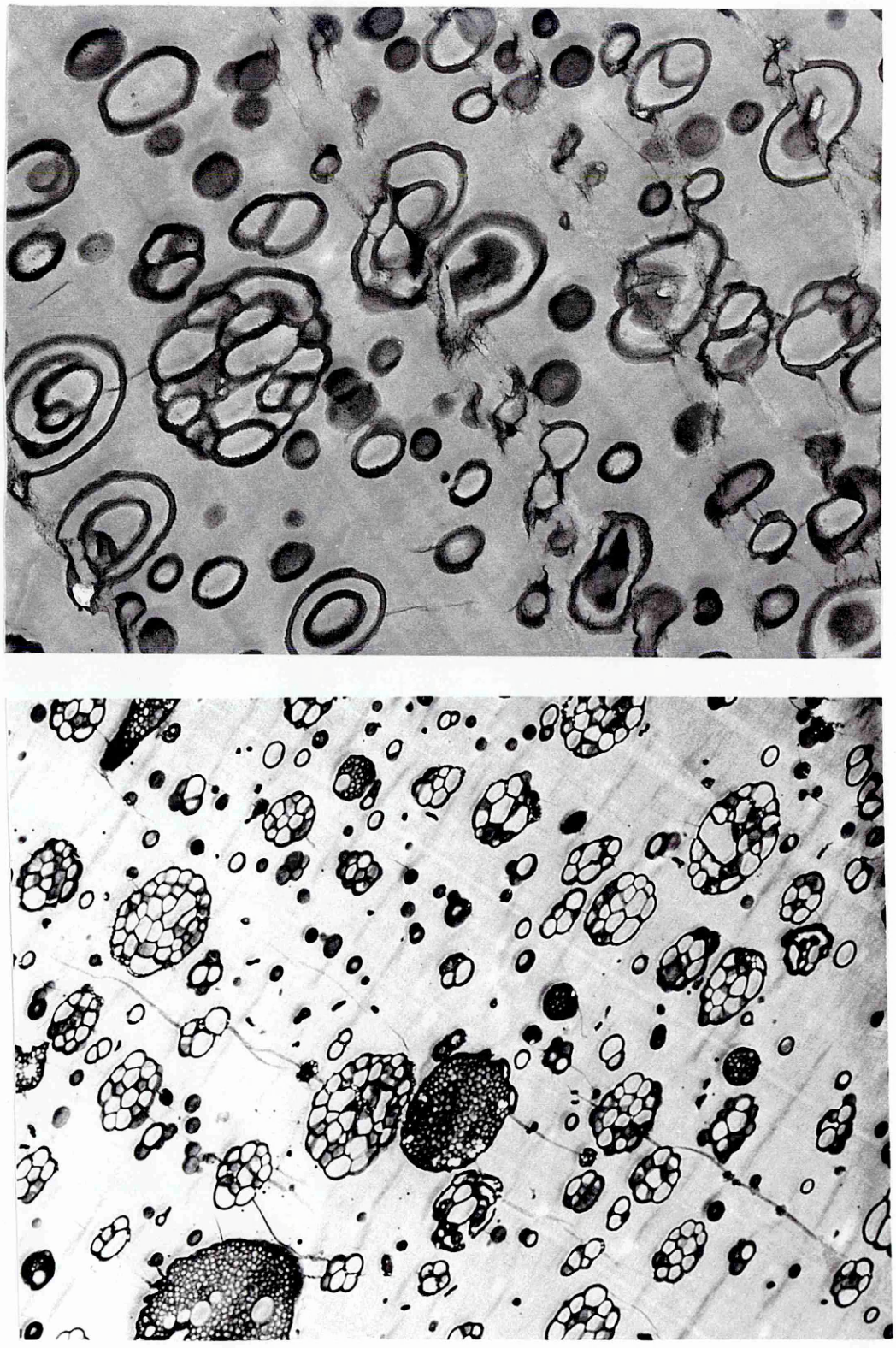

Figure 11-7(a). Post mortem section of AIM in creep at 16 MPa. Note shear yielding of the matrix. (0.1 μm ▬▬). Figure 11-7(b). Post-mortem section of HIPS8. (1μm ▬▬▬) (Cieslinski, 1997)

12. DISCUSSION. Modelling the failure of HIPS and ABS

Clearly, if the mechanism determining failure in HIPS and ABS is known, then steps can be taken to delay fracture until higher strains, thus increasing the toughness of the material. Also, from a renewal theory perspective, a model to predict the probability of failure of the material, would be of considerable use. For some design applications, it may be useful to know the maximum failure strain of the material. Based on the discussion in Chapter 10 and 11, a method to predict the maximum failure strain of HIPS and ABS, is outlined as follows.

12.1 Maximum possible failure strain, ε_{max}

Plastic flow in HIPS and ABS takes place through fibrillation of the matrix and the rubber phase. In a creep test the total change in volume due to cavitation and fibrillation in both matrix and rubber phase can be given by:

$$\Delta V_t = \Delta V_r + \Delta V_c \qquad \textbf{(12-1)}$$

where ΔV_r is the volume change due to non-crazing dilatation, assumed here to be rubber cavitation and ΔV_c is the volume change due to crazing, leading to :

$$1 = \frac{\Delta V_r}{\Delta V_t} + \frac{\Delta V_c}{\Delta V_t} = \delta_r + \delta_c \qquad \textbf{(12-2)}$$

where δ_r and δ_c are the fractional contributions of the rubber dilatation and craze dilatation to the total dilatation. It has recently been shown that the fractional contribution of crazing to the total dilatation δ_c, of HIPS, remains approximately constant throughout a tensile test (~0.45) (Buckley, 1991). Thus the change in volume of the rubber phase is given by

$$\Delta V_r = \Delta V_t \, \delta_r = \Delta V_t . (1 - \delta_c) \qquad \textbf{(12-3)}$$

Since the lateral contraction of HIPS is very small, the total dilatation can be well approximated by $V_t(\varepsilon_t - \varepsilon_{el})$. Thus

$$\Delta V_r = V_t(\varepsilon_t - \varepsilon_{el}).(1 - \delta_c)$$

where ε_t and ε_{el} are the total and elastic longitudinal strains on the material respectively, and V_t is the total volume of the specimen.

Experiments by Wagner and Robeson (1970), Soares (1994), Perche (1996), O'Connor and Bucknall (1997) and Lin (1997) have revealed that increasing the rubber cross-link density, by even a small amount, reduces the extension at failure of HIPS. It appears therefore that the maximum strain at failure is dependent upon the strain at break of the rubber, and as discussed earlier, the rubber's ability to unload the adjoining crazes. Hence the change in volume of the rubber phase can also be given by:

$$\Delta V_r = \sum_{0}^{\chi N} V_L(\lambda_L - 1) \qquad \textbf{(12-4)}$$

where V_L is the volume of the layer of rubber from which the fibrils are formed, and λ_L is the extension ratio of the layer of rubber fibrils. N is the total number of rubber layers in the material and χ ($=\sigma_a / \sigma_y$) is an estimate of the fraction of rubber that can cavitate under the applied stress σ_{app}. Assuming that all the rubber capable of fibrillating, has done so and has reached an extension just less than its extension at break, then equation (12-4) can be well represented by:

$$\Delta V_r = V_t \chi C_r (\lambda_{rx} - 1) \qquad \textbf{(12-5)}$$

where λ_{rx} is the extension at break for polybutadiene. Rearranging equation (12-4) and equation (12-5) gives the maximum strain possible ε_{max}, for HIPS of this rubber content and rubber shear modulus, at the applied stress, σ_{app}:

$$\varepsilon_{max} = \chi \varepsilon_{el} + \frac{\chi C_r (\lambda_{rx} - 1)}{1 - \delta_c} \qquad \textbf{(12-6)}$$

The term χ, crudely incorporates the effects of stress on the craze initiating mechanisms. In the case of neat polystyrene, these include the increase with stress, in the number of crazes initiated from defects, flaws, scratches and other stress concentrating features (Gent, 1970 and Argon, 1977). In the case of HIPS, the minimum particle size which initiates crazes, decreases with increase in applied stress, hence increasing the number of craze initiating particles (Bucknall, 1997). Also because craze thickening will cause drawing of the rubber particles, the volume of fibrillated rubber also increases, thereby increasing dilatation in the material. This favourable feature produces increased crazing and

energy absorption for a given likelihood of failure. Matrix shear yielding is assumed to be negligible.

If the maximum strain ε_{max} attained for HIPS and ABS, is plotted against $\chi C_r/(1-\delta_c)$, a straight line of slope $(\lambda_{rx}-1)$ should result. Figure 12-1 shows the relationship between the effective rubber content χC_r, and the maximum fracture strain of test batches of HIPS8, 6, 4 and 2, and Figure 12-2 shows the same relationship for ABS8, 6, 4 and 2. Linear regression on Figures 12.1 and 12.2, was used to determine the predicted values of λ_{rx} , = 5.3 for HIPS8, and λ_{rx} = 6.26 for ABS8.(from equation (12-6)). This is in good agreement with that calculated by Soares (1994) for polybutadiene in HIPS, (λ_{rx}=5) . The maximum strains attained for vulcanised HIPS and vulcanised ABS, are also plotted in

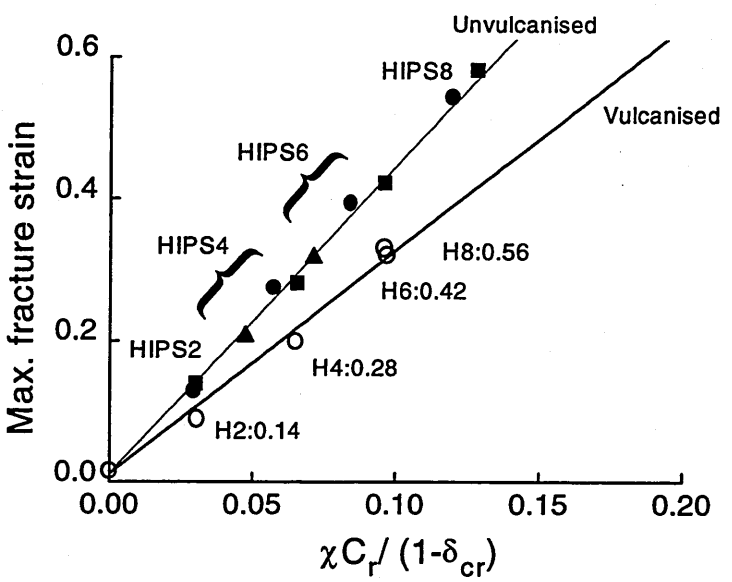

Figure 12-1. Effect of rubber content and rubber shear modulus on maximum strain possible for HIPS. The slope of the solid lines gives λ_{rx}= 5.33 unvulcanised and λ_{rx}= 4.15 vulcanised.

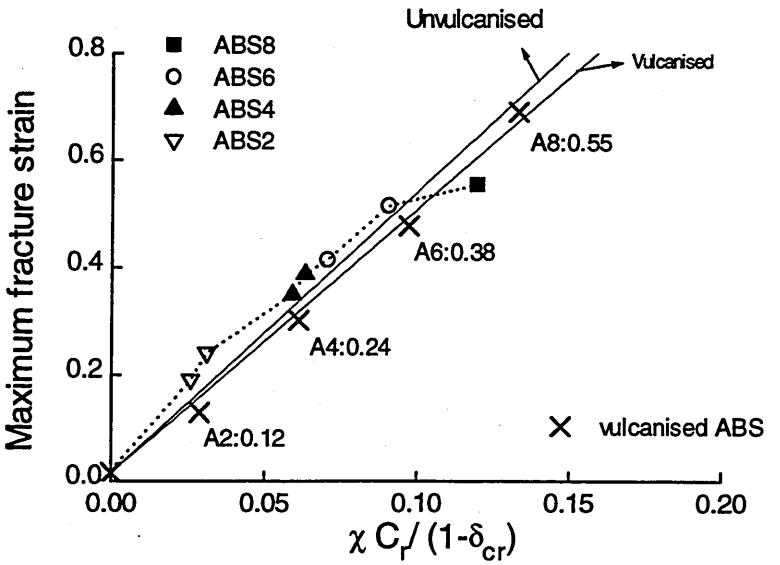

Figure 12-2. Effect of rubber content and rubber shear modulus on maximum strain possible for ABS. The slope of the solid lines gives λ_{rx}= 6.26 unvulcanised and λ_{rx}= 4.95 vulcanised.

Figure 12-1 and Figure 12-2. The maximum extension at failure for vulcanised HIPS was found to be 4.15, and for vulcanised ABS, it was found to be 5.94.

12.2 Weibull statistics

The Weibull distribution introduced earlier, has been used to model many different variable quantities. The two parameter Weibull equation given by equation 4.22, was fitted to the failure strain distributions of HIPS, ABS and AIM. It was found that this equation described reasonably well the failure distributions of these materials. Examples of the Weibull equation fitted to the data are given in Figures 4.9, 4.13, 4.14, 7.4, 7.7, 9.5 and others. Figure 4.15 compares the failure strain data of HIPS6 correlated with the Sjoerdsma equation (4.13), with the same data correlated with the Weibull equation (4.22). It can be seen, that the success Sjoerdsma and Boyens achieved in correlating failure strain data with their model, could not be repeated with the material investigated in this study.

The Sjoerdsma and Boyens model was found to describe reasonably well the failure strain distribution of HIPS2 and AIM (16.7 MPa). It can therefore be asked why does it correlate with these distributions in particular ? This can be explained through examination of the two equations. It can be seen that the Sjoerdsma and Boyens equation is fundamentally a particular Weibull distribution of shape parameter $\beta = 2$ and scale parameter $\alpha = k$ (known particularly as the Rayleigh Distribution). As the name suggests the Weibull shape parameter defines the shape of the distribution. As β increases in value, the distribution becomes increasingly negatively skewed. Skewness is a measure of the asymmetry of the distribution. If a distribution has zero skewness then the distribution is symmetrical about the mean. If a distribution is negatively skewed, the distribution has a tail which tends towards negative values, and vice versa for positively skewed distributions. Values of β below 3.6 give positively skewed distributions and values above 3.6 give negatively skewed distribution. In real terms a negatively skewed failure strain distribution, such as HIPS8 or ABS8, indicates that in the range of failure strains, more specimens fail in the higher strain region than in the lower strain region. In other words, in negatively skewed distributions, the **mode** failure strain is higher than the **mean** failure strain. In positively skewed distributions, the mode value is lower than the mean value. This can be seen in Figure 12-3 and Figure 12-4, where the Weibull shape parameter is plotted against the effective rubber content χC_r, where C_r is the actual rubber content and χ ($=\sigma_{app}/\sigma_y$) is the term defined in section 11.2. The horizontal line marked 'symmetric distribution', defines the transition from positive skewness to negative skewness.

Table 12-1 reveals that the failure strain distributions of HIPS2 and AIM have Weibull shape parameters similar to that of Sjoerdsma's distributions (= 2). Hence the Sjoerdsma equation describes reasonably well the probability of

HIPS2	β
26.5 MPa	2.4
25 MPa	2.3

AIM	β
16.7 MPa	2.3
15.7 MPa	3.4

Table 12-1. Shape parameter of distribution fitted to failure strain data of HIPS2 and AIM

failure of HIPS2 and AIM (16.7 MPa). The distribution of failure strains of AIM at an applied stress of 15.7 MPa yields a value for β of 3.4, consequently Figure 9.6 shows that the Sjoerdsma equation does not fit this data very well. It is therefore clear that the Sjoerdsma and Boyens equation is successful in describing Weibull distributions with shape parameter = 2.

However for the grades of HIPS and ABS investigated in this study, the failure strain data, reveal distributions which become more and more **unlike** a

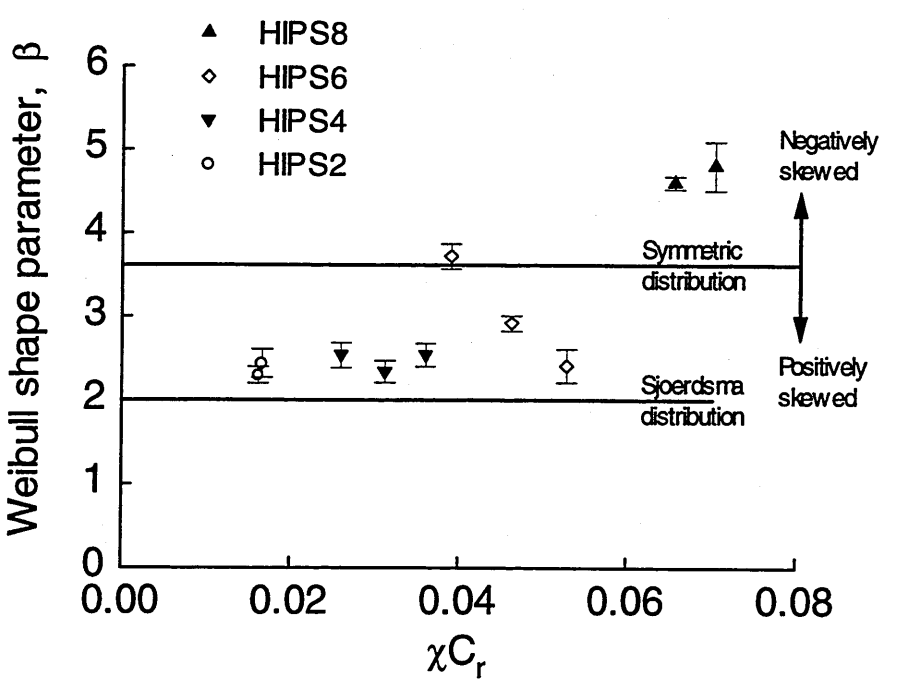

Figure 12-3. Effect of rubber content on the Weibull parameter β fitted to HIPS failure strain data.

Sjoerdsma and Boyens distribution, as the rubber content is increased. This is apparent from Figure 12-3 and Figure 12-4. While there is considerable scatter, there is a general trend towards higher values of β as the rubber content is increased. In the case of HIPS, there is a transition from positively skewed distributions, to negatively skewed distributions, as the rubber content is increased.

The underlying distribution shapes, are perhaps more easily visualised through examination of the sample histogram, and the fitted Weibull probability density function. The probability density function is defined in Section 4.3.1, and essentially it is the probability of failure occurring in the interval ε to ε+Δε, (and = $dP_f/d\varepsilon$). It is apparent from comparison of Figure 4.15 and Figure 4.16 that HIPS8 is more negatively skewed than HIPS6. Figure 4.17 compares the fitted Weibull probability density functions for HIPS8, 6, 4 and 2. The same effect is apparent from Figure 7.9 and Figure 7.10, demonstrating that in ABS, of even

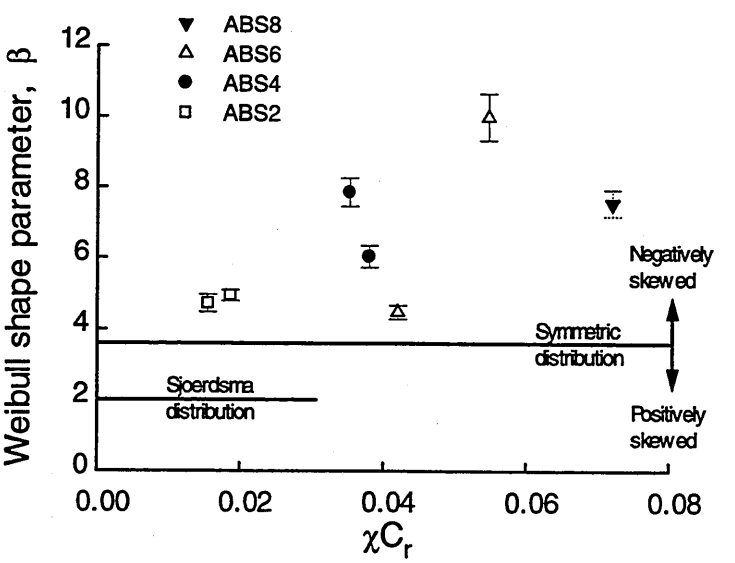

Figure 12-4. Effect of rubber content on the Weibull parameter β fitted to ABS failure strain data.

low rubber content, the material's failure strain distribution is negatively skewed.

It is interesting to note that ABS is more stable than HIPS (i.e. HIPS8 is quite negatively skewed β= 4.8 while ABS8 is significantly negatively skewed, β= 7.5). It was discussed earlier how the standard deviation of the failure strain distribution of ABS8 is narrow in comparison with that of HIPS8. This demonstrates that ABS is more stable at low strains, an observation which is in line with work by Donald and Kramer (1982d). These authors found that large voids in rubber particles in ABS were not sufficient to cause immediate craze breakdown. Of course failure will eventually occur when sufficient rubber particles have ruptured. Thus from a toughness standpoint, a negatively skewed failure strain distribution (high β) with a high mean failure strain (low α) is a favourable feature of a material.

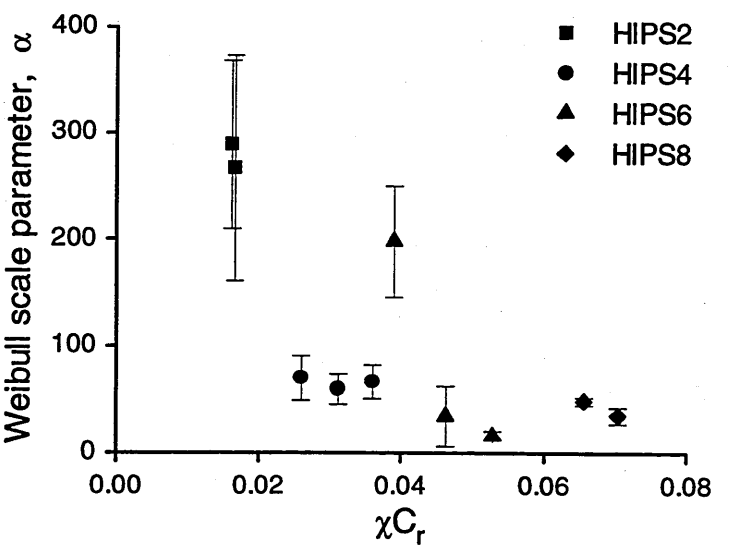

Figure 12-5. Effect of rubber content on the Weibull parameter α fitted to HIPS failure strain data.

The Weibull scale parameter α is a measure of the fracture resistance of the material. If the mean failure strain of the material is low a high value for α

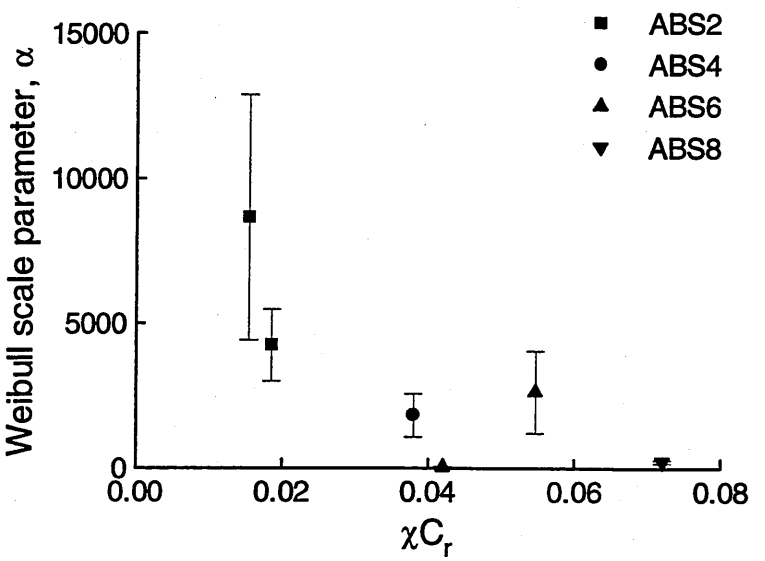

Figure 12-6 Effect of rubber content on the Weibull parameter α fitted to ABS failure strain data.

results and if the mean failure is high, a low value for α results. The relationship between α and the rubber content (and so mean failure strain) is clearly non linear, and very sensitive. A mathematical basis for the relationship between rubber content and the Weibull parameters, does not presently exist, but what follows describes a foundation on which such a task could be undertaken.

12.3 Weibull distribution of rubber stresses at failure

Figure 4.11 shows the logarithm of the cumulative survival probability of HIPS plotted against (fracture strain)$^{\beta}$. If the distribution of fracture strains is well described by the Weibull equation, then a straight line should result. At high strains the slope of the curve increases, indicating an overestimation of the survival probability. If at a given strain, the survival probability is overestimated, then the actual likelihood of failure is greater than that predicted. Obviously from a renewal theory standpoint, this is undesirable. This is also observed for HIPS blended with sulfur, and to a lesser in the ABS blends. Careful examination of these plots, reveals that the Weibull equation also overestimates the probability

of survival at low strains. Hence while a Weibull equation describes the failure strain distribution reasonably well, it does appear limited at low and high strains. This could be construed as resulting from the non-linear relationship between strain on the composite and for example, stress or time. For example, although a parameter such as failure stress or failure time, may follow a Weibull distribution perfectly, the non-linear relationship between strain and stress, or strain and time, will ensure the Weibull equation fails to describe the complete failure strain distribution.

The critical role the rubber particle plays in dictating when failure occurs, logically suggests that a basis for a model which describes the relationship between the rubber content and the probability of failure, may lie in the relationship between stress or strain on the rubber phase, and macroscopic strain on the composite. A fundamental difficulty in determining the stress or strain on the rubber with respect to composite strain, is that, at any stage in the life of the specimen, there exists a distribution of rubber strains and stresses. This is because the crazes do not form simultaneously, thus ensuring that at any strain, crazes and rubber particles exist at different stages of dilatation. A model was advanced earlier which predicted the maximum strain possible on the material with respect to rubber content, and rubber extension at break (equation (12-6)) . This model holds that at the strain just prior to failure, the standard deviation of the distribution of rubber strains is very small, i.e. all the rubber is approximately at the same high strain. At composite strains $< \varepsilon_{max}$ (section 12.1), the assumption that all the rubber layers are at the same strain becomes invalid, λ_{rx} then becomes λ_m, the mean strain on the rubber phase. The term χ refers to the fraction of rubber which can fibrillate, and in the model, this was assumed to be represented by σ_{app}/σ_y. At composite strains $< \varepsilon_{max}$, not all of the rubber which can fibrillate has done so, and so assuming χ is represented by σ_{app}/σ_y at low strains, suggests that all the rubber fibrillates upon application of the creep stress. This is an

unlikely suggestion, rather it is more likely that the large particles cavitate and initiate crazes, thus activating the percolation process. The rate of deformation percolation begins slowly and, as there is an abundance of unfibrillated rubber, progressively increases. However as the unfibrillated rubber decreases, the percolation rate also decreases. It is not unreasonable to suggest that the rate of decrease in the quantity of rubber available to fibrillate, can be likened to a radioactive decay rate or chemical first order reaction rate. Thus in the interval dt, the volume of rubber which is unfibrillated will be dependent on the volume of rubber present and the rubber's propensity to fibrillate. This can be represented by:

$$\frac{dV}{dt} = -kV$$

where V is the volume of rubber, k is a decay constant. The change in total volume of unfibrillated rubber with time is given by

$$\int_{V_{uf}}^{V_r} \frac{dV}{V} = -k\int_0^t dt$$

Hence

$$\ln\frac{V_{uf}}{V_r} = -kt \text{ and } V_{uf} = V_r \exp(-kt)$$

Relating this to the volume of the composite i.e. $V_r/V_t = C_r$ and converting to the fraction of rubber fibrillated gives:

$$C_f = C_r[1-\exp(-kt)]$$

The rate of conversion of rubber to fibrils, only reaches an appreciable rate at the end of the induction period. This period will be defined by the rate at which particles form voids, and the rate at which crazes extend and overcome closure forces at the craze tip. Thus it is assumed that rubber fibril formation is negligible during the induction period, τ. Stress will effect the rate in several ways: one is the significant effect of stress on the rate constant k, and another is the effect of stress on the fraction of rubber available to fibrillate. Thus the term χ introduced earlier, which is dependent on the level of applied stress, imposes an upper limit on the fraction of rubber which can fibrillate:

$$C_f = \chi C_r[1-\exp(-k(t-\tau))] \qquad (12\text{-}7)$$

In determining k, we assume that for a given creep stress, at time t_{max}, almost all the rubber that will fibrillate, has done so. The maximum time to failure t_{max}, is calculated through extending 20 or more specimens at an applied stress of σ, t_{max} is then taken as the time to failure of the specimen that extends the most. Thus the rate constant k in equation (12-7), is selected to produce complete fibrillation of the effective rubber content at time t_{max}. For HIPS4 extended under an applied stress of 16.2 MPa, $k = 2.5 \times 10^{-5}\ s^{-1}$. We can then plot the concentration of fibrillated rubber C_f with respect to time under load, in Figure 12-7. It can be seen that the volume of fibrillated rubber is constantly increasing. Moreover, from the creep curve of the specimen which extended to time t_{max}, we can relate the plastic strain on the composite ε_p, to the concentration of rubber fibrillated, see Figure 12-7. Thus at any given time t, the fractional change in the volume of the composite due to dilatation of the rubber phase, can be given by:

$$\Delta C_r = \varepsilon_p (1 - \delta_{cr}) \qquad \textbf{(12-8)}$$

where ε_p is the plastic strain on the composite and δ_{cr} is the fractional contribution to the dilatation of the material due to crazing. We can then relate the concentration of rubber fibrillated from Figure 12-7, to the dilatation from the fibrillated rubber, to determine the mean strain on the rubber phase ε_{rm} :

$$\varepsilon_{rm}(\varepsilon_p) = \frac{\Delta C_r(\varepsilon_p)}{C_f(\varepsilon_p)} \qquad \textbf{(12-9)}$$

and ε_{rm} is also plotted in Figure 12-7.

Hence we can determine the mean strain on the rubber phase as the macroscopic strain on the composite is increased. It should be reiterated that the mean rubber strain, denoted ε_{rm}, refers to the average rubber strain from the distribution of rubber strains, arises from the different stages of development of craze/rubber particle systems, **in one specimen**. This is as opposed to the mean rubber failure strain for a batch of specimens, denoted $\bar{\varepsilon}_r$.

In this way, for a batch of HIPS4 specimens extended at an applied stress of 16.2 MPa, we can determine ε_{rm} at the point of failure, from ε_{fr} the fracture strain of the composite, as shown in Figure 12-8. It is not surprising that the values of ε_{rm} are distributed about a mean value, $\bar{\varepsilon}_r$. Also as converting ε_p to ε_{rm} is a simple scaling, the shape of the fitted Weibull distribution will be unchanged, thus β remains the same at 2.54 but α changes from 96 to 0.062. It is also

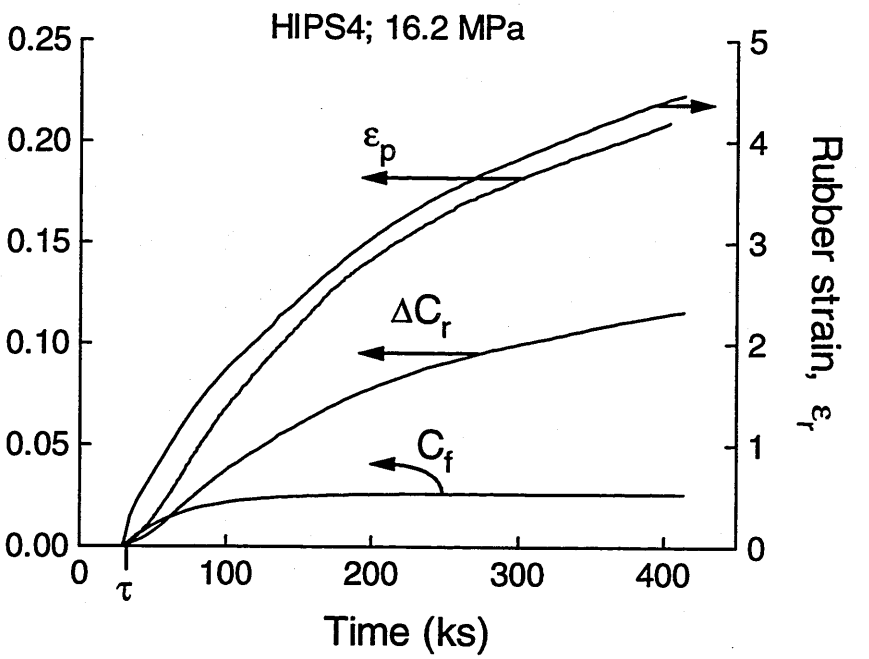

Figure 12-7. Change in concentration of fibrillated rubber with time.

unsurprising that again, the Weibull equation overestimates the survival probability at low and high rubber strains.

If one then assumes that some other parameter such as stress at failure, or time to failure, follows a Weibull distribution perfectly, then would one would expect the stress at failure (or time to failure) data to scatter uniformly about a Weibull curve. In other words, one would still expect scatter, owing to the finite number of specimens used in the experiment, but one would expect the overall trend of the data to be mimicked by the Weibull equation. Assuming stress at failure or time under load follows a Weibull distribution perfectly, then if a linear relationship exists between strain and time, or strain and stress, then one would expect the strain at failure data to also follow a Weibull distribution perfectly. This is not observed for HIPS and ABS. There is however a trend which may reveal information about the relationship between the strain and the quantity which follows the Weibull (if this quantity exists). Having underlined the importance of the stress on the rubber fibrils dominating failure, and considering

the fundamental basis of the Weibull equation, we therefore hypothesise for the following arguments that the mean stress on the rubber phase σ_{rm} at failure, follows a Weibull distribution.

For the following discussion it may serve as a helpful reminder that in graphs such as Figure 12-8, the interval between consecutive values of the survival probability, is determined solely from the number of specimens in the batch. From arguments given in the previous paragraph, for a given survival probability, the degree to which the rubber strain data deviate from the Weibull equation, gives an indication of the non-linearity of the relationship between rubber stress and rubber strain. If we examine the central region of Figure 12-8, from strains of 2 to 3.5, we can see that the data are reasonably well represented by the Weibull equation. This suggests that the relationship between ε_{rm} and σ_{rm} between strains of 2 and 3.5, is approximately linear. Through assuming a value

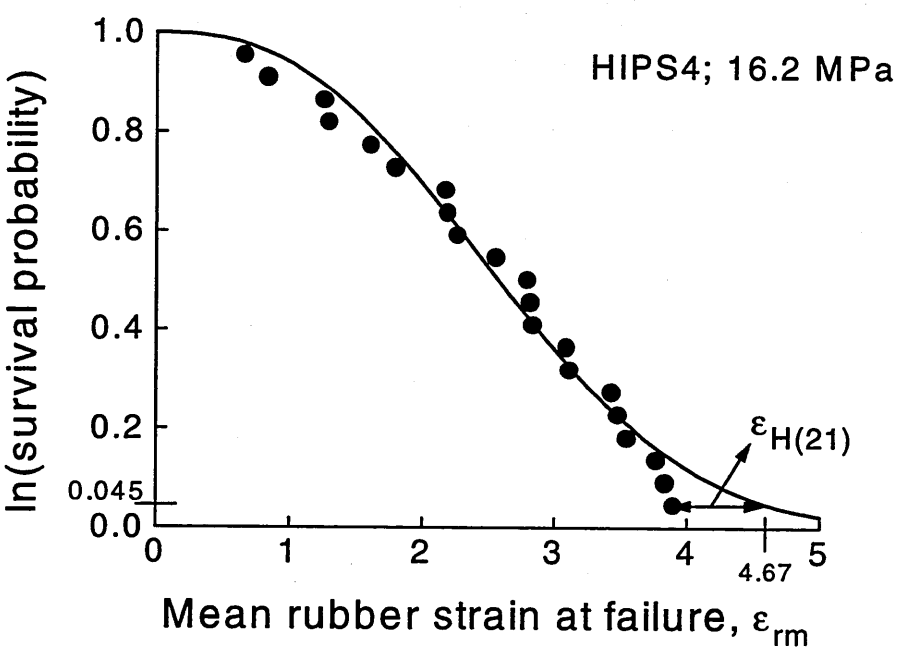

Figure 12-8. Distribution of ε_{rm} for HIPS4 extended under an applied stress of 16.2 MPa. The solid line is the Weibull equation fitted to the data.

of 0.475 MPa, for the modulus of the rubber between strains of 2 and 3.5 (Treloar, 1975), this linear relationship can be plotted, as shown by the dotted line in Figure 12-9. This is a reasonable value for E_r at an intermediate strain, but it should be noted that the absolute value of E_r has little bearing on the result, as it is the trend which is interesting.

At strains lower than 2, the relationship becomes non-linear because for a given survival probability, the material fails at a lower strain than that predicted by the Weibull. This is because at this rubber strain, the stress is in fact higher than that predicted from a linear rubber stress/strain relationship. If one measures $\varepsilon_{H(i)}$, the shift required to fit $\varepsilon_{rm}(i)$ to the Weibull distribution, one also measures the shift from linearity in the rubber stress/strain curve, ($\varepsilon_{rm}(i)$ is the mean rubber strain at failure of specimen i, where i is an integer in the series 1 to N, and where N is the number of specimens). Thus taking as an example, specimen 21 from the HIPS4 batch plotted in Figure 12-8, for a survival probability of 0.045, the Weibull predicts that, if a linear relationship exists between ε_{rm} and σ_{rm}, the strain at failure should be 4.67. As can be seen this is not the case. Instead, for this probability of survival, ε_{rm} has a value of 3.89. Thus the value $\varepsilon_{H(21)} = 0.78$, gives the deviation from linearity at the stress σ_{rm} corresponding to 4.67x(E_r=0.475MPa).

The process of conversion of ε_p to ε_{rm}, and plotting the deviation from linearity of the $\varepsilon_{rm}/\sigma_{rm}$ relationship, was also completed for HIPS6 and HIPS2. The resulting values map a plot which is not unlike the stress/strain curve for rubber (see Figure 12-9). This can be seen in Figure 12-10, where a polynomial fitted to the data in Figure 12-9, is compared with the stress/strain relationship of natural rubber (Treloar, 1975). While this method may be crude, the similarity between the curves plotted in Figure 12-10, indicates that the hypothesis that the

distribution of mean rubber stresses at failure follows a Weibull distribution, is a reasonable one. It is thus proposed that the mean stress on the rubber phase may be a better basis than composite strain for developing a model for lifetime predictions.

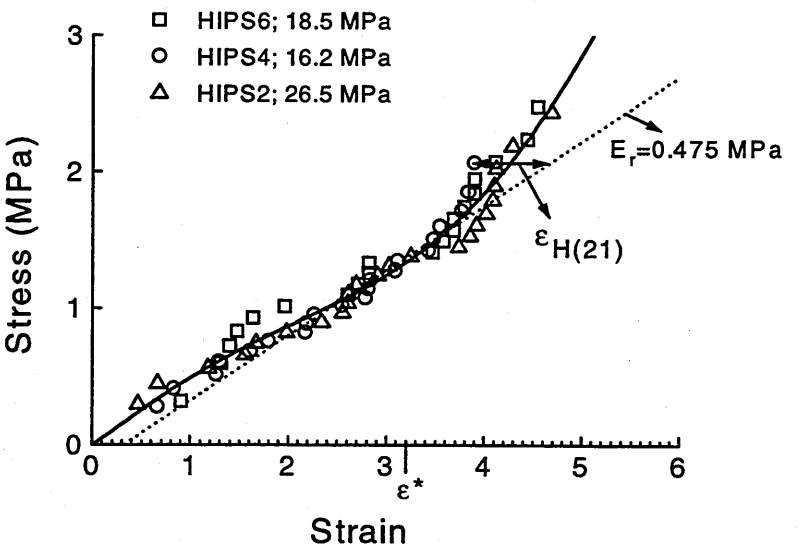

Figure 12-9. Deviation expected from linear rubber stress/strain curve assuming E=0.475 MPa, (as predicted by breakdown statistics)

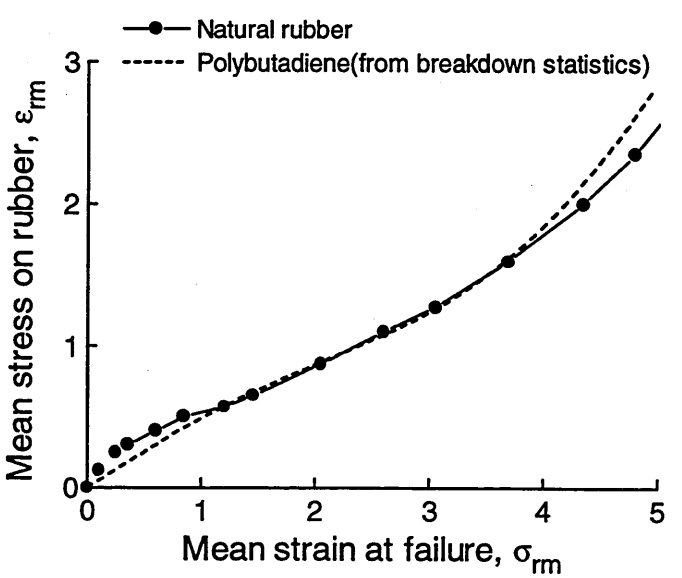

Figure 12-10. Comparison of stress/strain relationship of polybutadiene (as estimated by breakdown statistics) with that of natural rubber (taken from Treloar, 1975).

12.4 Lifetime prediction based on calculation of the volume of rubber at risk from failure

The proposal that the breakdown of the rubber phase determines the lifetime of the material, suggests that a direct relationship may exist between the volume of rubber at high strain, and the probability of composite failure. Thus, as the number of defects (or the volume of material converted to defects) increases, the likelihood of failure also increases. This presents the problem how do we calculate the volume of highly stretched rubber ? This can be achieved through proposing that from Figure 12-9, any rubber fibril at a strain ≥ 3.2 (which is chosen arbitrarily) is at risk from failure, and as such is assumed to be a defect in the material. This proposal can be tested, through comparing the probability of failure estimated by calculating the volume of rubber at risk, with the probability of failure estimated by sampling the parent failure strain distribution.

Through assuming that the volume of rubber which is still unfibrillated decays in a similar manner to a chemical reactant, the rate of conversion of rubber to fibrils can be estimated using equation (12-7). For a given composite strain, the strain on the rubber particles will be spread or distributed about a mean rubber strain. We then have to decide on the shape, and the standard deviation of the distribution of rubber strains. The **Normal distribution** has extremely wide application in the field of engineering and statistics, and has for some time, been used in a standard method to predict the force/extension relationship for a rubber (in McCrum et al., 1988). However, while it is not proposed that the statistics which dictate the force extension curve of a rubber, will be the same as those which dictate the shape of the distribution of rubber strains in a stretched composite, it may indeed be the case that the distribution of rubber strains is Normal in shape.

Assuming the distribution of rubber strains follow a Normal distribution, we can simply calculate the volume of rubber at risk, with respect to the plastic strain on the composite, and compare the results with the experimentally estimated probability of failure.

The Normal distribution is given by

$$f(\varepsilon_r) = \frac{1}{\sqrt{2\pi\, s^2}} \exp\left[-\frac{(\varepsilon_r - \varepsilon_{rm})^2}{2s^2} \right] \qquad \textbf{(12-10)}$$

where ε_r is the strain on the rubber, ε_{rm} is the mean strain on the rubber calculated in the manner described earlier, and s is the standard deviation of the distribution. A value of 0.5 is chosen for the standard deviation of the distribution (this will be discussed further later). Thus the distribution of rubber strains is given by $C_f.f(\varepsilon_r)$, and the probability that ε_r assumes a value between 3.2 and infinity is given by:

$$P(3.2 \le \varepsilon_r \le \infty) = \frac{C_f}{\sqrt{2\pi\, s^2}} \int_{3.2}^{\infty} \exp\left(-\frac{(\varepsilon_r - \varepsilon_{rm})^2}{2s^2} \right) d\varepsilon_r \qquad \textbf{(12-11)}$$

As the Normal distribution cannot be easily integrated, the values are usually normalised using the transformation $z=(\varepsilon_r-\varepsilon_{rm})/s$. In this way all distributions can be normalised to the **Standard Normal distribution,** and Z tables give the resulting probability values. Thus for example, a probability of $P(\varepsilon_r \le 2)$ requires the value 2 to be transformed to z, using $z = (2 - \varepsilon_{rm})/s$. Then the z value can be directly read from a standard statistics textbook z table, which gives the probability that ε_r will assume a value less than or equal to 2.

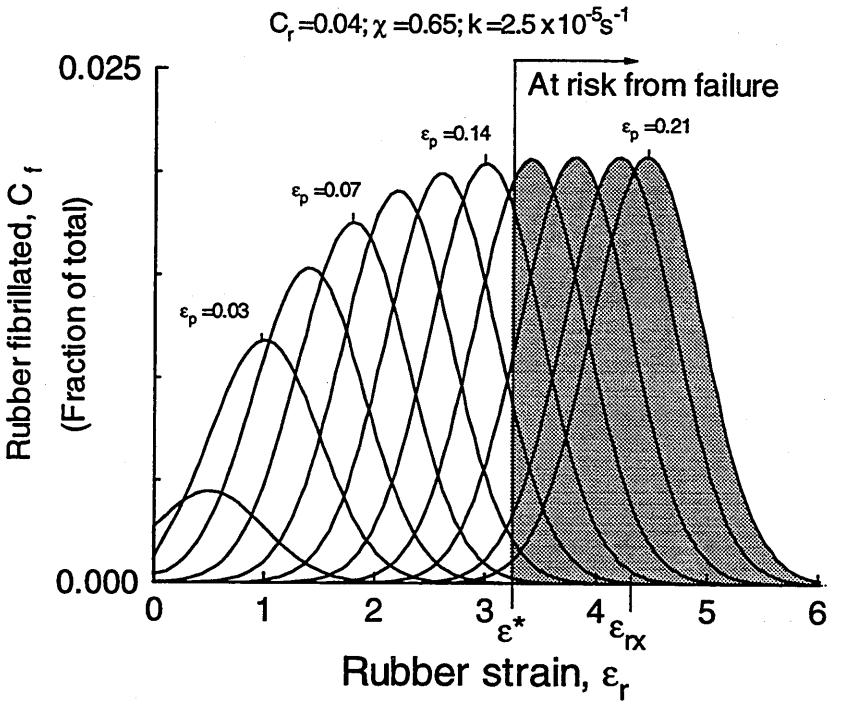

Figure 12-11. Distribution of rubber strains as the composite strain ε_p is increased. Rubber extended to a strain ≥ 3.2 is considered at risk. ε_{rx} is taken from Section 12.1.

Determining the probability that ε_r will assume a value between 3.2 and infinity, simply requires calculation of the probability that ε_r < infinity (=1), and subtracting the probability that ε_r assumes a value less than 3.2.

Figure 12-11 shows the change in the distribution of ε_r as the plastic strain on the composite ε_p increases. From this it can be seen that the volume of rubber fibrillated, and ε_{rm}, increases with the plastic strain of the composite. The shaded area indicates the rubber which is at risk from failure, which increases as the composite strain increases. For a given composite strain ε_p, the concentration of rubber at risk, was calculated using z tables for the distributions shown in Figure 12-11. These values were plotted against ε_p in Figure 12-12 (a). It is apparent that the concentration or rubber at risk, is low at strains ε_p < 10 % but rises rapidly at higher strains. Using the concentration of rubber at risk C_{risk}, we can estimate the probability of failure, through assuming, that when no rubber has fibrillated, the

probability of failure is zero, and when all the rubber has been fibrillated and extended to a strain ≥ 3.2, the probability of failure is 1. Thus with a concentration of rubber at risk C_{risk}, the probability of failure is given by $C_{risk}/\chi C_r$. Hence, in Figure 12-12(b), the probability of failure of the material is plotted against the plastic strain on the material. Also plotted in Figure 12-12(b) is the failure probability of HIPS4, determined experimentally through sampling the parent failure strain distribution (see section 4.3.2). Through comparison of the two data sets, it can be seen that the probability of failure estimated by the volume of rubber at risk method, is underestimated at low strains. This problem arises from assumptions made regarding the standard deviation and shape of the distribution of rubber strains.

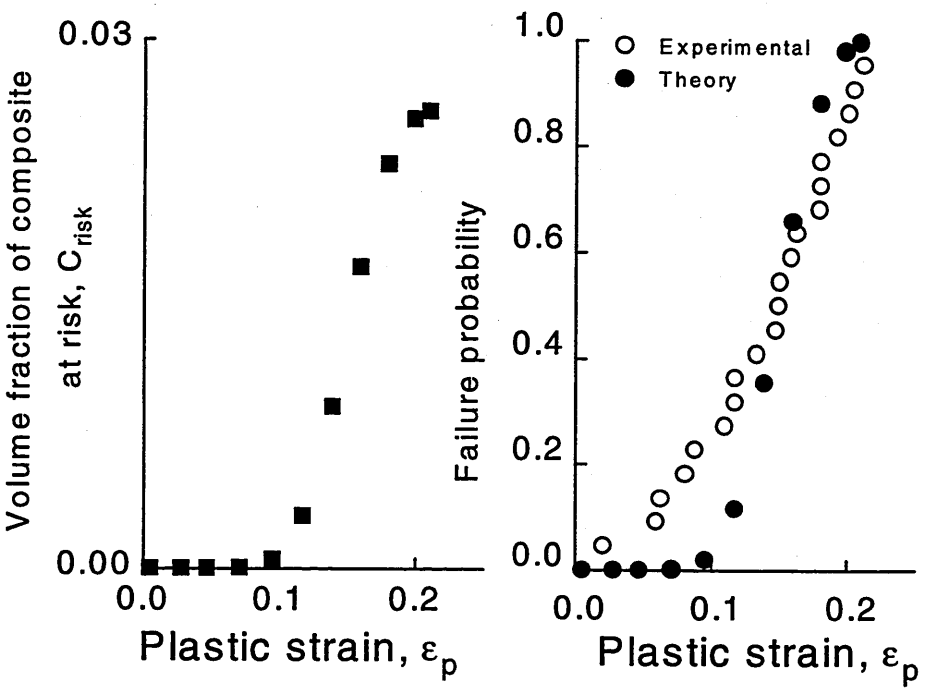

Figure 12-12(a). Plot showing the increase in concentration of rubber at risk with increase in ε_p, calculated from the shaded area of Figure 12-11. **(b)** the increase in failure probability of the composite calculated through measuring the increase in the volume of rubber at risk as ε_p is increased.

When one considers that localised highly deformed regions form at low macroscopic strain, then this infers that at low ε_p, there exists highly stretched rubber particles. This implies that at low ε_p the distribution of rubber strains is broader than shown in Figure 12-13. It may therefore be the case that at small ε_p, the chosen value for the standard deviation is too low. Moreover, considering the mean of the distribution ε_{rm} increases with ε_p, it is clear that the distribution standard deviation cannot remain as wide, because this would force a finite quantity of material to exist at strains greater than ε_{rx} as seen in Figure 12-11. It therefore appears that the standard deviation of the distribution of rubber strains, decreases with increasing plastic strain on the composite.

It is reasonable to suggest that at high ε_p, a large fraction of the fibrillated rubber is at high strain while a small fraction, having just fibrillated is at low strain. This infers a negatively skewed distribution. It is also tentatively assumed that at low ε_p, a large fraction of the rubber is at low strain while a small fraction is at high strain. This infers a positively skewed distribution. This assumption is tentative because of the nature of the action of the rubber, which upon fibrillating, almost instantaneously jumps to intermediate strains (Bucknall, 1997). Upon cavitation in the rubber particle, the void growth is swift thus producing a rapid increase to intermediate rubber strains. However for the purposes of simplifying the calculations, this feature is neglected. The skewed nature of the distribution serves to rule out the possibility of the distribution being Normal so a different distribution is considered. Normal random variables have a set of possible values ranging from $-\infty$ to ∞, and Weibull random variables have a range of values ranging from 0 to ∞. In engineering applications of probability theory, it is occasionally useful to have a function which describes a distribution, whose range of possible values is taken from a finite interval. One

such distribution is the Beta distribution. The Beta distribution over the interval a to (a + b) is a continuous probability distribution with probability density:

$$f(x) = \frac{\Gamma(\alpha+\beta)}{b\Gamma(\alpha)\Gamma(\beta)}\left(\frac{x-a)}{b}\right)^{\alpha-1}\left(\frac{a+b-1}{b}\right)^{\beta-1} \qquad \text{for } a < x\ (a+b)$$

$$= 0 \qquad \text{otherwise}$$

where the parameters α and β control the shape of the distribution over the interval a to a + b, and $\Gamma(x)$ is the Gamma function of advanced calculus given by:

$$\Gamma(x) = \int_0^\infty x^{t-1}e^{-x}dx$$

for $t > 0$ (Vardeman, 1994).

Thus the concentration of rubber fibrillated can be said to be distributed according to:

$$f(\varepsilon_r) = \frac{C_f\ \Gamma(\alpha+\beta)}{b\Gamma(\alpha)\Gamma(\beta)}\left(\frac{\varepsilon_r - a)}{b}\right)^{\alpha-1}\left(\frac{a+b-1}{b}\right)^{\beta-1} \qquad (12\text{-}12)$$

The mean of the distribution is given by:

$$\varepsilon_{rm} = a + b\left[\frac{\alpha}{\alpha+\beta}\right] \qquad (12\text{-}13)$$

The distribution of rubber strains will assume values in the range from 0 to 4.3, thus a = 0 and b = 4.3 = ε_{rx}. Again the value of ε_{rx} is taken from Section 12.1. The value for ε_{rm} is determined in the manner described in section 12.2, and the

values of α and β are used to control the shape of the distribution and the standard deviation.

Thus in the same manner undertaken using the Normal distribution, the rubber strains are distributed according to the Beta distribution. Now however, the standard deviation is allowed to vary and α and β are adjusted to produce distributions of reasonable standard deviation. The resultant distributions are plotted in Figure 12-13, where it can be seen that at low composite strain ε_p, the distribution of rubber strains is positively skewed and at high ε_p, the distribution is negatively skewed. Also it can be seen that the standard deviation of the distribution is low at small ε_p, then increases, and subsequently decreases considerably, at high ε_p. Following each increment of ε_p, the concentration of rubber at risk (i.e. $\varepsilon_r \geq 3.2$) is calculated using a standard spreadsheet software package. The resulting values for C_{risk} are plotted in Figure 12-14(a). It can be seen that the volume of rubber at risk progressively increases, as the plastic strain on the composite increases. The failure probability, which was calculated in the same manner as in Figure 12-12(b), is compared with the results from HIPS4, see Figure 12-14(b). It can be seen that there is good agreement between the probability of failure calculated according to the volume of rubber at risk, and the probability of failure estimated experimentally through sampling the composite failure strain distribution.

The good agreement supports proposals given earlier, that the rubber is the dominating factor controlling failure in HIPS and ABS. It can be conceived that if the concentration of rubber in the composite is increased, then at a given plastic strain the average strain in the rubber phase will be decreased. Compared with the concentration of unfibrillated rubber, the concentration of rubber extended past a strain ≥ 3.2 will be low, thus in order to attain a hazardous volume of

highly stretched rubber fibrils, the overall strain on the composite has to be increased. Hence HIPS8 and ABS8 will extend readily to strains > 0.40 while HIPS4 fails at strains < 0.2. If the rubber cross-link density is increased, both the critical rubber extension ε^* and the rubber strain at break ε_{rx}, shift to a lower strain. Hence, for a given composite strain, the volume of rubber at risk and so the probability of failure will be higher, than in a material with a lower rubber cross-link density.

This method allows for the effects of rubber content, rubber cross-link density, and applied stress on the probability of failure of the composite. The good agreement of theory with experiment also indicates that, in principle at least, correlation of the volume of rubber at risk with strain on the composite, may lead to a more complete method for predicting failure of HIPS and ABS with respect to time under load and composite strain.

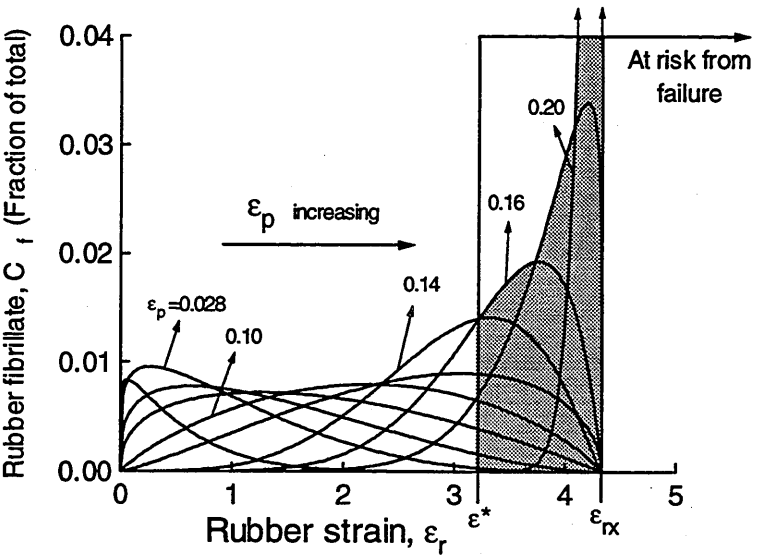

Figure 12-13. Rubber strains distributed according to Beta function. Note at low composite strain ε_p, the distribution is positively skewed and the standard deviation is broad, and at high ε_p the distribution is negatively skewed and the standard deviation is smaller. The shaded area consists of the rubber at risk from failure.

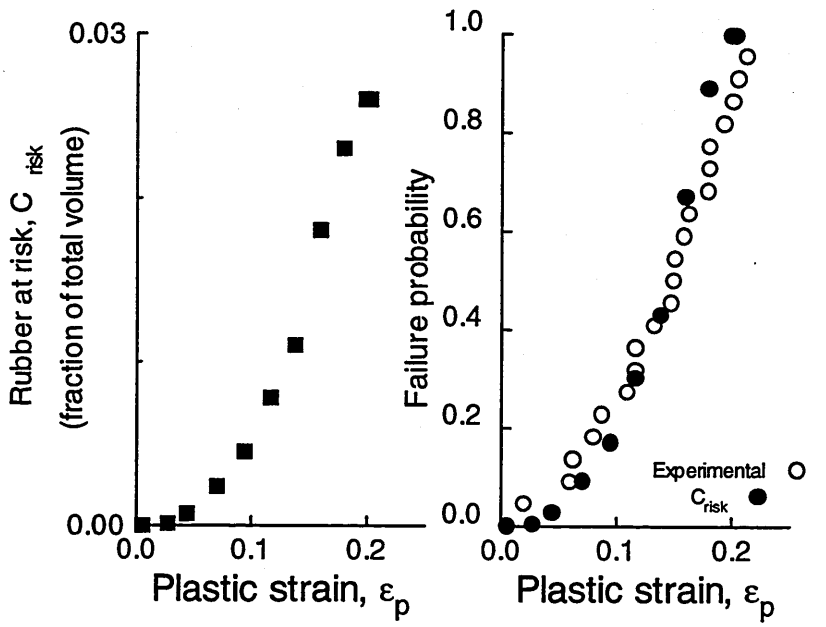

Figure 12-14(a). Plot showing the increase in concentration of rubber at risk with increase in ε_p, calculated from the shaded area of Figure 12-13. (b) the increase in failure probability of the composite calculated through measuring the increase in the volume of rubber at risk as ε_p is increased.

13. CONCLUSIONS

In this study, three commercial grade rubber toughened polymers were examined to: (1) gain information about the deformation mechanics of these materials, and (2) identify the mechanisms controlling final rupture in these materials. The probability of failure of HIPS, ABS and AIM was investigated with respect to applied stress, rubber content and rubber cross-link density. The rubber content was varied through blending HIPS with GPPS, and blending ABS with GPSAN, and the rubber cross-link density was varied through blending the material with sulfur, and it was also varied with gamma irradiation. Changes in the mechanical behaviour, induced through modifying these material properties, were characterised using standard tensile tests and creep tests. Dynamic mechanical analysis revealed that blending the materials with sulfur, increased the rubber T_g, which indicates an increased level of cross-linking in the rubber phase.

In agreement with the work of Sjoerdsma and Boyens (1994) on HIPS, it was found that the probability of failure of HIPS, ABS and AIM scales with the plastic strain on the material. However, when a model advanced by these authors to describe this relationship was tested, it was found to be unsatisfactory in correlating the failure strain data for the materials examined in this study.

The breakdown statistics of HIPS and ABS, revealed that the mean failure strain coincided with the onset of macroscopic strain-hardening. The phenomenon of macroscopic strain-hardening was attributed to the finite number of convenient craze nucleation sites, and an increased load bearing capacity of

the rubber phase at high strain. The rubber fibrils extend in parallel with thickening crazes, therefore they unload the crazes at high strain. In this way, the crazes become increasingly secure from breakdown. In combination with spatially random particle cavitation events, and particle cavitation resulting from collision with bifurcating crazes, both of which may result in craze nucleation, it is proposed that this craze stabilisation mechanism promotes deformation percolation through increasing the number of crazes generated for a given strain.

The load sharing relationship between the rubber and the crazes ensures that the mean stress on the crazes decreases at high strain. Moreover, because the probability of failure increases with increase in composite strain, it is logically concluded that the dominant mechanism controlling failure in HIPS and ABS, is rubber particle rupture. It was illustrated and discussed how the likelihood of material rupture may be dictated by the volume of highly stretched rubber, i.e. the volume of rubber at risk from failure. At any given strain, the volume of rubber at risk will be dependent on the rubber content, and the applied stress. The strain above which the rubber is at risk from failure, decreases with increasing rubber cross-link density. These proposals are supported by evidence that the mean failure strain of the material decreases with decrease in rubber content, decrease in applied stress and increase in rubber cross-link density. The results are discussed in detail, with respect to high strain deformation, breakdown statistics and morphological parameters such as rubber content, particle morphology and interfacial adhesion.

The probability model, advanced by Sjoerdsma and Boyens, was generally unsatisfactory in correlating the fracture strain data for the materials examined in this study. Better correlations between cumulative survival probability and the plastic strain in the composite, are obtained using an alternative model based on the Weibull equation. While reasonable success was

achieved through using the Weibull equation, it was illustrated and discussed how the rubber stress at failure may be a better basis for obtaining a Weibull distribution. A model was also advanced which predicts the maximum strain possible for a rubber toughened polymer, with respect to parameters such as rubber content, rubber cross-link density and applied stress.

It is suggested that one method to minimise the standard deviation of failure strains for these materials, is to use a rubber modifier with an ultimate strength comparable to or greater than the drawing stress of the crazes. In this way, rubber particle rupture should be eliminated, and the crazes are also unloaded, thus forcing deformation to percolate through the material. However it should be noted that this is not a simple matter of increasing the cross-link density of the existing rubber, because this will inhibit particle cavitation and craze nucleation.

Suggestions for Future Work

The conclusions drawn in this work are fundamentally very important from the point of view of designing components made from HIPS and ABS polymers, and also from the point of view of developing fracture resistant materials. Based on the analysis given here, in particular that delineated in Chapter 12, it should be possible to develop a complete model describing the probability of failure of HIPS and ABS. It appears that there exists a fundamental relationship between the probability of failure and the stress on the rubber phase. Therefore, while it will not be easy to measure the stress on the rubber phase, it should be attempted to corroborate (or not) the conclusions arrived at in Chapter 12.

These conclusions should be tested against other rubber toughened polymers to investigate the scope of the hypothesis. Testing at different temperatures should also reveal important information about the failure statistics

of rubber toughened polymers deforming through different micromechanics. The interactions of shear, crazing and rubber cavitation are complicated issues and, as evidenced by the AIM results, should be investigated further to establish the effects of these interactions on the failure initiating mechanism.

7. REFERENCES AND BIBLIOGRAPHY

Argon, A. S. (1975), Pure Appl. Chem. **43**, 247

Argon, A. S., Cohen, R. E., Gebizlioglu, O. S., Brown, H. R. and **Kramer, E. J. (1990),** Macromolecules **23**, 3975

Argon, A. S. and **Hannoosh, J. G. (1977),** Phil. Mag. **36,** 1195

Argon, A. S. and **Salama, M. M. (1977),** Phil. Mag. **36,** 1217

Ball, R., Doi, M., Edwards, S. F. and **Warner, M. (1981),** Polymer **22,** 1010

Beahan, P., Bevis, M., and **Hull, D. (1971),** Phil. Mag. **24**, 1267

Beahan, P., Bevis, M., and **Hull, D. (1972),** J. Mater. Sci. **8**, 162

Beahan, P., Bevis, M., and **Hull, D. (1973),** Polymer **14,** 96

Beahan, P., Bevis, M., and **Hull, D. (1975),** Proc. R. Soc. **A 343**, 525

Berger, L. (1990), Macromolecules **23,** 2926

Berry, J. P. (1961), J. Polym. Sci. **50**, 107

Bevan, L. (1983), Polym. Bul. **10,** 187

Birkinshaw, C., Buggy, M. and **Quigley, F. (1993),** J. Appl. Polym. Sci. **48,** 181

Bowmer, T. N., Cowen, L. K., O'Donnell, J. H. and **Winzor, D. J. (1979),** J. Appl. Polym. Sci. **24,** 425

Borggreve, R. J. M., Gaymans, R. J. and **Schuijer, J. (1989),** Polymer **30**, 71

Braun, D., Klein, M. and **Hellmann, G. P. (1996),** J. Appl. Polymer Sci. **60**, 981

Breuer, H., Haaf, F. and **Stabenow, J. (1977),** J. Macromol. Sci. Phys. **B14**, 387

Brockett, P. and **Levine, A. (1984),** "Statistics and Probability, and Their Applications", Saunders College Publishing, Philadelphia

Brown, H. R. (1979), J. Mater. Sci. -Letters **14,** 237

Brown, H. R., Argon, A. S., Cohen, R.E., Gebizlioglu, O. S., Kramer, E. J. (1989), Macromolecules **22,** 1002

Brown, N. and **Fisher, S. (1975),** J. Polym. Sci. (Phys.), **13,** 1315

Brown, H. R. and **Kramer, E. J. (1981),** J. Macromol. Sci. Phys. **B19**, 487

Brydson, J. A. (1978), "Rubber Chemistry", Applied Science Publishers, London

Bubeck, R. A., Blazy, J. A., Kramer, E. J., Buckley, D. J. and **Brown, H. R. (1986),** Polym. Comm. **27**, 357

Bubeck, R. A., Buckley, D. J., Kramer, E. J., and **Brown, H. R. (1990),** Polym. Prepr. (Am. Chem. Soc. Div. Polym. Sci.), **31**, 116

Bubeck, R. A., Buckley, D. J., Kramer, E. J., and **Brown, H. R. (1991),** J. Mater. Sci. **26**, 6249

Buckley, D. J. (1991), PhD Thesis, Cornell University, Ithaca, USA

Bucknall, C. B. (1967), Bristish Plastics **40,** 118

Bucknall, C. B. (1969), J. Mater. Sci. **4,** 214

Bucknall, C. B. (1977), "Toughened Plastics", Applied Science Publishers Ltd, London

Bucknall, C. B. and **Clayton, D. (1972),** J. Mater. Sci. **7**, 202

Bucknall, C. B., Clayton, D. and **Keast, W. E. (1972),** J. Mater. Sci. **7**, 1443

Bucknall, C. B. and **Smith, R. R. (1965),** Polymer **6**, 437

Bucknall, C. B., Cote, F. P. and **Partridge, I. K. (1986a),** J. Mater. Sci. **21**, 301

Bucknall, C. B., Davies, P. and **Partridge, I. K. (1986b),** J. Mater. Sci. **21**, 307

Bucknall, C. B., Karpodinis, A. and **Zhang, X. C. (1994),** J. Mat. Sci. **29,** 3377

Chan, T., Donald, A. M. and **Kramer, E. J. (1981),** J. Mater. Sci. **16**, 676

Charlesby, A., (1960), "Atomic Radiation and Polymers", Pergamon Press, Oxford

Chatfield, C (1983), "Statistics for Technology" third edition, Chapman and Hall, London

Chen, C. C. and **Sauer, J. A. (1990),** J. Appl. Polym. Sci. **40,** 503

Chorafas, D. N. (1960), "Statistical Processes and Reliability Engineering", Van Nostrand, Princeton, New Jersey

Cieslinski, R. C. (1997), Dow Chemical Company, Midland, USA, private communication

Cook, D. G., Plumtree, A. and **Rudin, A. (1993),** Plasts., Rubb. Compos. Process. App. **20**, 219

Dagli, G., Argon, A. S. and **Cohen, R. E. (1995),** Polymer **36,** 2173

Dekkers, M. E. J. and **Heikens, D. (1985),** J. Mater. Sci. **20,** 3873

Dompas, D., Groeninckx, G. Isogawa, M., Hasegawa, T. and **Kadokura, M. (1994),** Polymer **35,** 4750

Donald, A. M. (1994), in "Rubber Toughened Engineering Plastics" edited by A. A. Collyer, Chapman and Hall, London

Donald, A. M., Chan, T. and **Kramer, E. J. (1981),** J. Mater. Sci. **16,** 669

Donald, A. M. and **Kramer, E. J. (1981),** Phil. Mag. A **43,** 857

Donald, A. M. and **Kramer, E. J. (1982a),** J. Mater. Sci. **17,** 2351

Donald, A. M. and **Kramer, E. J. (1982b),** J. Polym. Sci. Phy. Ed. **20,** 899

Donald, A. M. and **Kramer, E. J. (1982c),** J. Appl. Polym. Sci. **27,** 3729

Donald, A. M. and **Kramer, E. J. (1982d),** J. Mater. Sci. **17,** 1765

Edwards, S. F. and Vilgis, Th. (1986), Polymer **27,** 483

Evans, D. H. (1992), "Probability and its Applications for Engineers", Marcel Dekker, New York

Fedors, R. F. and **Landel, R. F. (1965),** Trans. Soc. Rheol. **9,** 195

Fellers, J. and **Kee, B. F. (1974),** J. Appl. Polym. Sci. **8,** 2355

Ferry, J. D. (1970), "Viscoelastic Properties of Polymers", John Wiley & Sons, Inc. New York

Fond, C., Lobbrecht, A. and **Schirrer, R., (1996),** Int. J. Fract. **77,** 141

Fowler, M. E., Keskkula, H. and **Paul, D. R. (1987),** Polymer **28**, 1703

Fukahori, Y. and **Seki, W. (1992),** Polymer **33,** 502

Gent, A. N. (1970), J. Mater. Sci. **5,** 925

Gent, A. N. and **Wang, C. W. (1991),** J. Mater. Sci. **26,** 3392

Gilbert, D. G. and **Donald, A. M. (1986),** J. Mater. Sci. **21,** 1819

Glandus, J. C., Boch, P. J., (1984), J. Mater. Sci. **24,** 761

Hobbs, S. Y. (1986), Polym. Eng. Sci **26**,74

Hull, D. (1970), J. Mater. Sci. **5,** 357

Ikawa, K., Sakano, H., Tamai, S., Takahashi, K. and **Kojima, H. (1997),** Kobunshi Ronbunshu **54**, 148

Ishai, O. and **Cohen, L. J. (1968),** J. Compos. Mater. **2,** 302

Johnson, R. A. (1994), "Miller and Freund's Probability and Statistics for Engineers", 5th Edition, Prentice-Hall, Englewood Cliffs, New Jersey

Kambour, R. P. (1964), J. Polym. Sci. **A2,** 4159

Kambour, R. P. (1964), Polymer **5,** 143

Kambour, R. P. (1973), J. Polym. Sci. -Macromol. Rev. **7**, 1

Kambour, R. P. and **Holik, A. S. (1969),** J. Polym. Sci. A-2, 7, 1393

Kambour, R. P. and **Robertson, R. E. (1972),** "Polymer Science, a materials handbook", edited by A. D. Jenkins, Chap. 11, Amsterdam, North-Holland

Kambour, R. P. and **Russell, R. R. (1971),** Polymer **12**, 237

Keskkula, H., Turley, S. G. and **Boyer, R. F. (1971)**, J. Appl. Polym. Sci. **15,** 351

Keskkula, H., Schwarz, M. and **Paul, D. R. (1986)**, Polymer **27,** 211

Kinloch, A. J. and **Guild, F. J. (1996)**, Advs. Chem. Series **252,** 1

Kinloch, A. J., Shaw, S. J., Tod, D. A. and **Houston, D. L. (1983)**, Polymer **24,** 1341

Kinloch, A. J. and **Young, R. J. (1983)**, "Fracture Behaviour of Polymers",Applied Science Publishers, London

Kramer, E. J. (1983), "Crazing in Polymers", Advances in Polym. Sci. Series, edited by H. H. Kausch **52/53,** 1

Kramer, E. J. and **Berger, L. (1991)**, "Fundamental Processes of Craze Growth and Fracture", Advances in Polym. Sci. Series, edited by H. H. Kausch **90/91,** 1

Kramer, E. J. and **Hart, E. W. (1984)**, Polymer **25**, 1667

Laatsch, J. and **Michler, G. H. (1997)** Martin-Luther-Universitat, Merseburg, private communication. These workers microtomed 1 μm thick slices of HIPS8 and strained them in-situ, in a 10^6 eV transmission electron microscope

Lapin, L. L. (1990), "Probability and Statistics for Modern Engineering", 2nd Edition, PWS-Kent, Boston

Lauterwasser, B. D. and **Kramer, E. J. (1979)**, Phil. Mag. **A39,** 469

Lavengood, R. E., Nicholais, L. and **Narkis, M. (1973)**, J. Appl. Polym. Sci. **17,** 1173

Lazzeri, A. (1991), PhD Thesis, Cranfield University, Bedford, UK

Lazzeri, A. and **Bucknall, C. B. (1993)**, J. Mat. Sci. **28,** 6799

Lin, C. S. (1997), MPhil. Thesis, Cranfield University, Bedford, UK

Lin, C. S., Ayre, D. S. and **Bucknall, C. B. (1997)**, J. Mater. Sci., submitted

Martin, G. M., Roth, F. L. and **Stiehler, R. D. (1956)**, Trans. Inst. Rubber Ind. **32,** 189

Maestrini, C., Castellani, L., Merlotti, M. and **Vighi, M. (1992)**, Polymer **33,** 1556

Maestrini, C., Monti, L. and **Kausch, H. H. (1996)**, Polymer **37,** 1607

Mason, P. (1964), Polymer **5,** 625

Matsuo, M. (1966), Polymer **7**, 421

Matsuo, M., Wang, T. T. and **Kwei, T. K. (1972)**, J. Polym. Sci. **10 A2,** 1085

Merz, E. H., Claver, G. C. and **Baer, M. (1956)**, J. Polym. Sci. **22**, 325

McCrum, N. G., Buckley, C. P. and **Bucknall, C. B. (1988)**, "Principles of Polymer Engineering", Oxford University Publications, Oxford

Newman, S. and **Strella, S. (1965)**, J. Appl. Polym. Sci. **9,** 2297

O' Connor, B. and **Bucknall, C. B. (1997)**, "Deformation, Yield and Fracture of Polymers" Paper 81, 10th International Conference Churchill College, Cambridge

Oxborough, R. J. and **Bowden, P. B. (1973)**, Phil. Mag. **28**, 547

Pearson, R. A. and **Yee, A.F. (1986)**, J. Mater. Sci. **21,** 2475

Perche, N. (1995), MSc. Thesis, Cranfield University, Bedford, UK

Plummer, C. J. G. and **Donald, A. M. (1991),** Polymer **32,** 409

Prentice, P. (1983), Polymer **24**, 344

Ritter, J. E., Stevens, J. M. and **Jakus, K. (1979),** J. Mater. Sci. **21**, 171

Sauer, J. A., Trent, J. and **Chen, C. C. (1989),** Polym. Eng. Sci. **29,** 69

Silberberg, J. and **Han, C. D. (1978),** J. Appl. Polym Sci. **22,** 599

Sjoerdsma, S. D. and **Boyens, J. P.H (1994),** Polym. Eng. Sci. **34,** 86

Soares, V. L. P. (1994), PhD Thesis, Cranfield University, Bedford, UK

Soares, V. L. P. (1994), "Deformation, Yield and Fracture of Polymers" Paper 71, 9th International Conference Churchill College, Cambridge

Sternstein, S. S. and **Ongchin, L. (1969),** ACS Poly. Prepr. **10,** 1117

Takayanagi, M., Hariam, H. and **Ywata, Y. (1963),** Mem, Fac. Eng. Kyushu Univ. **23,** (1)1

Trassaert, P. and **Schirrer, R. (1983),** J. Mater. Sci. **18**, 3004

Treloar, L. R. G. (1975), "The Physics of Rubber Elasticity", Clarendon Press, Oxford

Trivedi, K. S. (1982), "Probability and Statistics with Reliability, Queuing, and Computer Science Applications",Prentice-Hall, Eaglewood Cliffs, New Jersey

Turley, S. G. and **Keskkula, H. (1980),** Polymer **21,** 466

Verheulpen-Heymans, N. (1984), Polym. Eng. Sci. **24,** 809

Wagner, M. H. (1994), J. Rheol. **38,** 655

Wagner, E. R. and **Robeson, L. M. (1970)**, Rubb. Chem. Tech. **43,** 1129

Weibull, W. (1951), J. Appl. Mech. **18**, 293

Wu, S. (1988), J. Appl. Poly. Sci. **35**, 549

Wu, J. S. and **Mai, Y. W. (1993)**, J. Mater. Sci. 28, 6167

Yang, H. H (1998), PhD Thesis, Cranfield University, Bedford, UK

Yang, H. H. and **Bucknall, C. B. (1996)**, J. Mater Sci. submitted

Yang, A. C-M., Kramer, E. J., Kuo, C. C. and **Phoenix, S. L. (1986)**, Macromolecules **19,** 2010

Yang, A. C-M., Kramer, E. J., Kuo, C. C. and **Phoenix, S. L. (1986)**, Macromolecules **19,** 2020

Zhao, W., Yu, L., Zhong, X, Zhang, Y. and **Sun, J. (1994)**, J. Appl. Polym. Sci. **54,** 1199

Zhurkov, S. N. and **Kursukov, V. E. (1974)**, J. Polym. Sci. (Phys.), **12,** 385

APPENDIX 1

Papers published, and submitted for publication:

1. O'Connor, B, Bucknall, C. B. and Hahnfeld, J. L. (1997), *Criteria for Tensile Failure of HIPS,* "Deformation, Yield and Fracture of Polymers" Paper 81, 10th International Conference, Churchill College, Cambridge

2. O'Connor, B, Bucknall, C. B. and Hahnfeld, J. L. (1997), *Role of the Rubber Particle in Ultimate Tensile Rupture of HIPS,* Plastics, Rubber Compos. Process. Appl. **Accepted**

CRITERIA FOR FRACTURE OF HIGH-IMPACT POLYSTYRENE UNDER UNIAXIAL TENSION

B. O'Connor*, C.B. Bucknall* and J.L. Hahnfeld**

The fracture of High-Impact Polystyrene (HIPS) in tension was investigated following a procedure described in an earlier paper by Sjoerdsma and Boyens[1]. The present study has revealed that fracture of HIPS is initiated not by the coalescence of crazes, as proposed by those authors, but by rubber particle breakdown, which occurs when the fibrillated rubber is stretched past its maximum extension ratio λ_{max}. Criteria for the failure of HIPS materials having a range of rubber cross-link densities and rubber volume fractions are outlined and discussed. Weibull statistics were found to describe reasonably well the probability of fracture of HIPS.

INTRODUCTION

The influence of rubber content, rubber particle morphology and rubber cross-link density on the toughness and failure of HIPS is still not fully understood. Cross-linking in the rubber phase is partly responsible for the familiar effects of outdoor ageing on the failure of rubber toughened materials, an area of primary importance to the industry. The aim of this study is to identify the dominating factors responsible for fracture of HIPS and obtain further insights into the high strain deformation of this material.

To date, the most promising analysis of final rupture in HIPS has been made by Sjoerdsma and Boyens[1], who postulated that HIPS fractures when crazes impinge upon each other, owing to the inevitable misalignment of the craze fibrils. Sjoerdsma and Boyens' model leads to Eq. 1, where the cumulative probability of fracture, P_f, is a function of the square of the craze strain, ε_{cr}, taken by these authors as being the total plastic dilatation of the material, and of A, a parameter dependent on the specimen geometry and on the craze geometry.

$$P_f = 1 - \exp(-A\varepsilon_{cr}^2) \qquad \text{(Eq. 1)}^1$$

For the one HIPS material Sjoerdsma and Boyens investigated, they found that $\ln(P_{sv})$ was linear with ε_{cr}^2, where P_{sv}, the probability of survival, is defined as $(1 - P_f)$.

MATERIALS

The materials investigated in this study were all based on HIPS A, a commercial grade HIPS with approximately 8 wt. % polybutadiene. HIPS B and C were produced by melt blending HIPS A with 0.28 and 0.56 wt. % pure sulfur respectively. HIPS D-F were produced by melt blending 75, 50 and 25 vol. % HIPS A with General Purpose Polystyrene of a similar molecular weight. Compounding was carried out in a double screw co-rotational Werner Pfleiderer

* Cranfield University, Bedford MK43 OAL, UK
** Dow Chemical Company, Midland, Michigan 48667, USA

extruder with a medium shear screw profile and a processing barrel temperature of 200°C. Following the procedure described in the Sjoerdsma and Boyens[1] paper, batches of between 20 and 70 identical creep specimens were tested for each set of test conditions.

The testing was carried out at 23°C on either an Instron screw machine or a custom built creep testing rig. Strains were recorded on the Instron using a clip-on 25mm. gauge length extensometer, and extensions were recorded on the creep rig using linear voltage displacement transducers. A correction factor was applied to the creep rig results to allow for specimen shoulder effects.

Results and Discussion

The constant stress (creep) behaviour of HIPS blended with sulfur is shown in figure 1. Sulfur has the effect of increasing the cross-link density of rubber, decreasing its compliancy and extension at break. With increasing ratio of sulfur/HIPS, the induction time[2] (defined as the time preceding rapid dilatation of the material) increases significantly and the strain rate decreases. HIPS strain-hardens at high strain, the limiting strain decreasing with increasing sulfur content. These results demonstate the influence of rubber cross-link density on strain-hardening in HIPS. The mean strain at fracture is also indicated, showing that the highest probability of fracture coincides with the onset of strain-hardening.

Weibull[3] statistics were used to correlate the fracture strain data for HIPS, which were found to fit Eq. 2.

$$1-P_f = P_{sv} = e^{-\alpha(\varepsilon_f)^{\beta}} \qquad \text{(Eq. 2)}$$

where α and β are Weibull fitting parameters and ε_f is the strain at failure of the material. Figure 2 shows $\ln(P_{sv})$ plotted against (fracture strain)$^{\beta}$ for HIPS B, where $\alpha = 337$ and $\beta = 6.4$. From this it can be seen that Weibull statistics describes reasonably well the failure probability of HIPS.

The proposed mechanism for fracture of HIPS under tensile creep conditions is as follows. Crazes are initiated from cavitated rubber particles[4] and extend laterally until they meet another craze or rubber particle. As the craze thickens (mainly through surface drawing[5] rather than craze fibril creep) it will stretch the adjoining rubber particles with it, causing further cavitation and fibrillation of the rubber phase. Widespread craze extension and thickening, rubber cavitation and fibril extension results in a sharp increase in the strain rate, beyond the percolation threshold. As each craze thickens and 'draws' the associated rubber particle, the rubber fibrils strain-harden and become increasingly load bearing. (See figure 3).

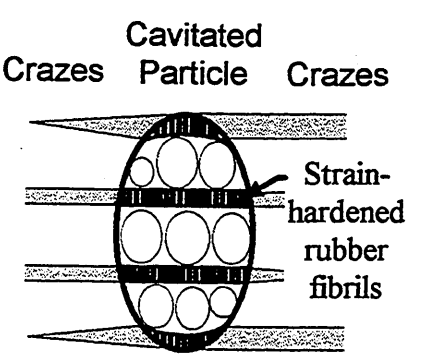

Figure 3: High strain deformation of HIPS.

This causes the observed decrease in strain rate at high strains. Macroscopic strain-hardening occurs in neat HIPS A at $\varepsilon \sim 20$ %. However local strain-hardening almost certainly begins at much lower strains, immediately following the induction period ($\varepsilon > \sim 2$ %). Wherever the rubber fibrils are

fully stretched, fracture is possible. However the probability of fracture increases with the volume of rubber that has fibrillated and stretched.

This explains why the maximum probability of failure of HIPS in tensile creep, as indicated by the open circles in figure 1, occurs not when the mean stress on the crazes is highest (at the point of inflexion in ε vs. t), as would be presumed if the crazes were responsible for final failure, but when the mean stress on the rubber fibrils has increased significantly.

Figure 4 shows the creep behaviour of HIPS A and HIPS D. Reducing the rubber content has similar effects to increasing the rubber cross-link density, i.e. increased induction time, decreased strain rate and limiting deformation. The contribution of the rubber phase to the total volume change can be represented by:

$$\Delta v_r = \Delta v_t \delta_r = \Delta v_t . (1-\delta_c) = (\varepsilon_t - \varepsilon_{el}).(1-\delta_c) \qquad \text{(Eq. 3)}$$

and $$\Delta v_r = \phi_r(\lambda_r - 1) \qquad \text{(Eq. 4)}$$

where Δv_t is the total volume change, ε_{el} is the elastic strain, ϕ_r is the rubber content, δ_c and δ_r are, respectively, the fractional contributions of the crazing and rubber fibrillation to the post-yield dilatation of the material (=0.5 after Bubeck et al.[6]). Combining Eqs 3 and 4 gives Eq. 5:

$$\varepsilon_{max} = \varepsilon_{el} + \frac{\phi_r(\lambda_{max} - 1)}{1-\delta_c} \qquad \text{(Eq. 5)}$$

where ε_{max}, λ_{max} are, respectively, the maximum possible strain and rubber extension ratio. Shear yielding is assumed to be negligible. Figure 5 shows the relationship between the rubber content ϕ_r, λ_{max} and the maximum fracture strains for test batches of HIPS A and HIPS D-F. Linear regression was used to find a value of $\lambda_{max} = 4.3$ for the data in figure 5.

CONCLUSIONS

- Both increasing rubber cross-link density and decreasing rubber volume fraction caused an increase in the induction time, while decreasing, (a) the strain rate, (b) the strain at which strain-hardening takes place, and (c) the fracture strain.
- The probability of failure of HIPS is highest when the material begins to strain harden.
- The two dominant factors controlling fracture in HIPS appear to be the volume of fibrillated rubber and the mean stress on the rubber fibrils.

ACKNOWLEDGEMENTS

We thank the Dow Chemical Company for permission to publish this work.

REFERENCES

1. Sjoerdsma, S.D., Boyens, J.P.H., *Polym. Eng. Sci.*, **34** (1994) 89
2. Bucknall, C.B., Clayton, D., J. *Mater. Sci* , 7 (1972) 202
3. Weibull, W. J., *J. Appl. Mech.*, **18** (1951) 293
4. Yang, H. H., Bucknall, C. B., Poster 79, this conference
5. Lauterwasser, B. D., Kramer, E. J., *Phil. Mag.*, **39A** (1979) 469
6. Bubeck, R. A., Buckley, D. J., Kramer, E. J., Brown, H. R., *J. Mater. Sci.*, **26** (1991) 6249

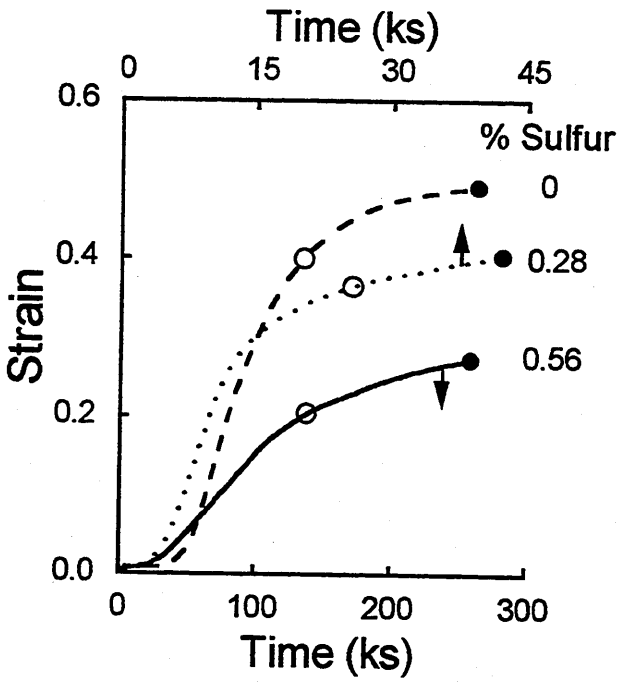

Fig. 1: Creep of HIPS with 0 % S at 14 MPa, 0.28 % S at 13.7 MPa and 0.56 % S at 13.7 MPa. (•), failure strain ε_f for specimen; (O), **mean** failure strain ε_m for **batch**. (See figure 4 for time scale of 100 % HIPS A, 0 % sulfur).

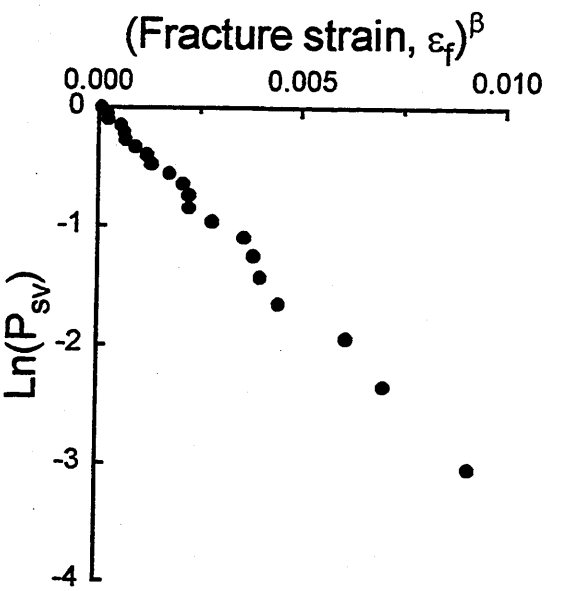

Fig. 2: Survival probability P_{sv} of HIPS B containing 0.28 % sulfur, plotted according to Eq. 2.

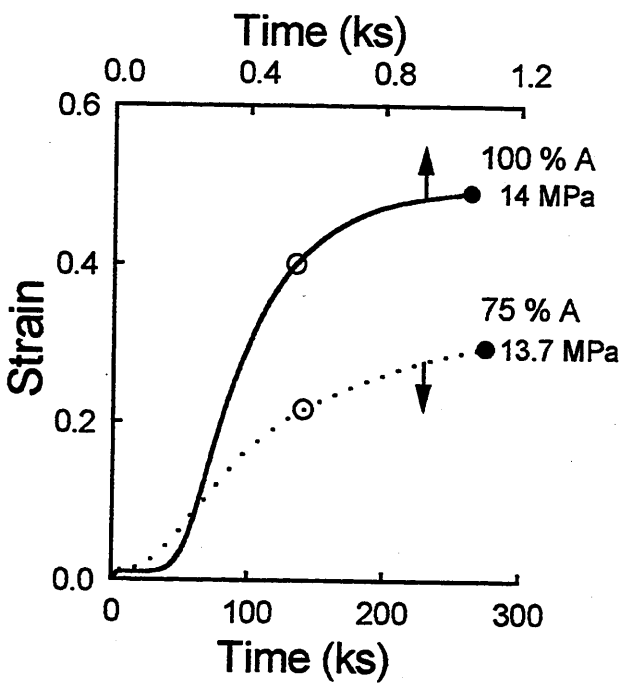

Fig. 4: Effect of rubber content on creep behaviour of HIPS. (•), failure strain ε_f for specimen; (O), **mean** failure strain ε_m for **batch**.

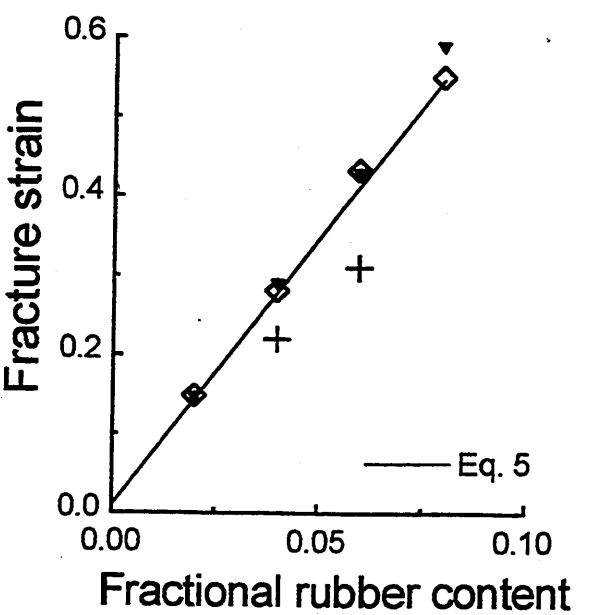

Fig. 5: Effect of rubber content, on maximum fracture strain from batches of HIPS A and HIPS D - F. For each blend $\sigma_{app}(\blacktriangledown) > \sigma_{app}(\Diamond) > \sigma_{app}(+)$.

CRITERIA FOR TENSILE FRACTURE OF HIGH-IMPACT POLYSTYRENE

B. O'Connor, C. B. Bucknall and J. L. Hahnfeld

Cranfield University, Bedford MK43 OAL, UK

Sjoerdsma and Boyens model

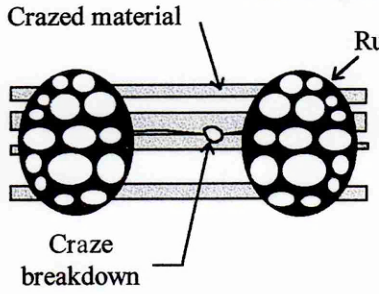

Principle: craze impingement causes fracture

$$\mathrm{Ln}\,(P_{sv}) = -A\varepsilon^2$$

where P_{sv} is the probability of survival (non-fracture), A is a geometrical constant and ε is the plastic strain (total strain – elastic strain).[1]

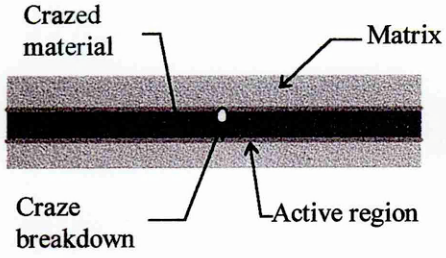

Craze breakdown in Polystyrene

Yang et al[2]. found breakdown in PS initiates in the active region of the craze.

Experimental

Materials: HIPS blended with sulfur, varying rubber cross-link density. HIPS blended with general purpose polystyrene, varying rubber content.

Tests: Tensile creep to failure on batches of between 20 and 70 identical polished specimens.

1. Sjoerdsma, S.D., Boyens, J.P.H., Polym. Eng. Sci., **34** (1994) 89
2. Yang, A.-C. M., Kramer, E. J., Kuo, C. C. and Phoenix, S. L. Macromolecules, **19** (1986) 2010

Results

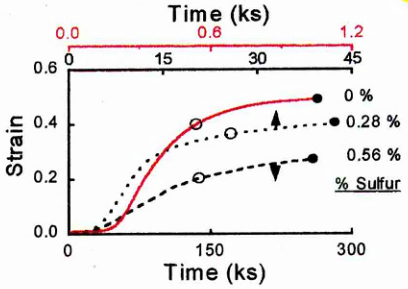

HIPS blended with sulfur, in creep rupture. O: mean fracture strain for batch.

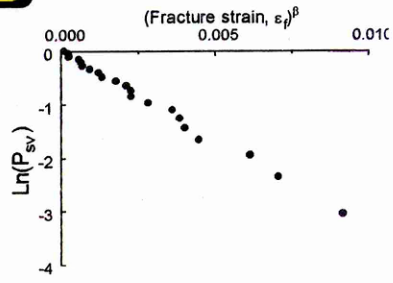

Survival probability of HIPS containing 0.28 % sulfur.

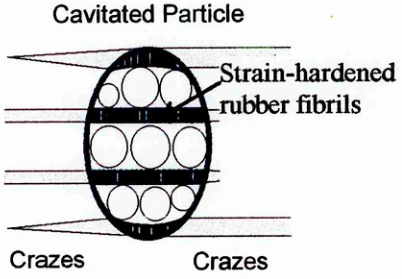

High strain deformation of HIPS.

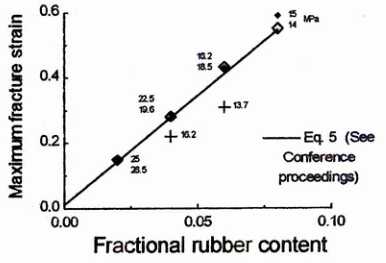

Effect of rubber content on maximum fracture strain from batches of HIPS blended with PS.

Conclusions

- The two dominant parameters in the failure of HIPS, are the **VOLUME OF FIBRILLATED RUBBER** and the **MEAN STRESS ON THE RUBBER FIBRILS**.
- Weibull statistics were found to describe reasonably well the probability of fracture of HIPS.
- It has been shown that the probability of failure of HIPS is highest when the material strain hardens.
- Both increasing rubber cross-link density and decreasing rubber volume fraction caused an increase in the creep induction time, while decreasing, (a) the strain rate, (b) the strain at which strain-hardening takes place, and (c) the fracture strain.

Role of the Rubber Particle in Ultimate Tensile Rupture of HIPS

O' Connor, B.*, Bucknall, C. B.* and Hahnfeld, J. L.#

* Advanced Materials Group, Cranfield University, Bedford, MK43 0AL, UK

Dow Chemical Company, Midland, Michigan, 48667, USA

Abstract

Creep rupture measurements have been made at 23 °C on a commercial grade of HIPS with a rubber content of 8 wt. %. The mean failure strain is found to increase with applied stress. The failure strain data are used to test a craze impingement model[1], which relates the probability of a specimen's failure to its plastic strain, and it is shown that the model is unsatisfactory in correlating results for the chosen grade of HIPS. Better correlations between cumulative survival probability and the plastic strain in the HIPS are obtained using an alternative model based on the Weibull equation. The load sharing relationships between crazes and rubber particles are examined, and it is concluded that the dominant mechanism controlling final failure of HIPS is rupture of the rubber particles.

Introduction

The effects of rubber content, rubber cross-link density and rubber particle morphology on the toughness and failure of HIPS are still not completely understood. It has been observed that HIPS tensile bars exhibit a wide distribution of failure strains under identical test conditions[1,2], and the aim of the present study is therefore to explain this distribution by examining the deformation mechanics of HIPS, and identifying the mechanisms controlling final rupture.

To date, the most important contribution in the area of lifetime predictions for stressed HIPS components has been the work of Sjoerdsma and Boyens[1]. These authors postulated that failure of HIPS occurs when crazes coalesce or impinge upon each other. According to this view, crazes thicken through surface drawing[3] until they collide with neighbouring crazes, whereupon the inevitable misalignment of craze fibrils causes immediate rupture. Sjoerdsma and Boyens advanced a model based on the weakest link principle, in which the failure point of HIPS is the site with the smallest intercraze distance. The cumulative probability of failure P_f of the material can then be given as:

$$P_f = 1 - \exp(-A\varepsilon_{cr}^2) \quad (1)$$

where ε_{cr} is craze strain, defined as the total plastic dilatational strain, and A is a constant dependent on the geometry of the crazes and of the specimen. Sjoerdsma and Boyens also extended their model in order to correlate failure with time, and demonstrated a good fit between the model and the data for one grade of HIPS, over a range of stresses and temperatures.

Experimental

The majority of experiments in this study were carried out on HIPS A, a commercial grade of HIPS containing approximately 8 wt. % polybutadiene. Image analysis of electron micrographs showed that the volume fraction of 'salami' particles in HIPS A is 35 %. In addition, HIPS B, C and D were produced by melt-blending 75, 50 and 25 vol. % HIPS A with a General Purpose Polystyrene (GPPS) of similar molecular weight. Before compounding, the materials were dried under vacuum at a temperature of 80 °C for 3 hours. Compounding was carried out using a twin-screw co-rotational Werner Pfleiderer extruder model ZSK 30 with a medium shear screw profile and a processing barrel temperature of 200°C. The material became noticeably less opaque as the ratio of GPPS to HIPS A was increased. Granules of each material were compression moulded at 200 °C into 3.5 mm thick plaques. Standard dog-bone specimens with parallel gauge portions measuring 41.5 x 3.5 x 5.5 mm were machined from these plaques and polished with 1200 grade aluminium oxide paper. For experiments at any one stress level, batches of between 20 to 70 specimens were tested.

All experiments were carried out on either an Instron screw machine, or a custom-designed creep rig. In tests using the Instron equipment, strain measurements were made using a 20 g clip–on extensometer. In order to prevent the extensometer blades from damaging the surface of the specimen, they were covered with double sided sticky tape. The tape was renewed for every specimen, minimising damage inflicted by the blades, and it was found that fracture did not occur preferentially at the extensometer blades. Constant strain rate tests were also carried out using the Instron machine at a cross head speed of 2 $mm.min^{-1}$.

Because of the large number of specimens involved in this study, and the generally long term nature of creep tests, a dedicated creep rig was designed and built. To avoid the problems of lever loading, loads were applied directly by suspending weights from the lower end of the

specimen. Specimens were loaded by lowering the weights on a lead screw driven by a geared motor. The rig is mounted on rubber cushions and the specimen mounting jig is separated from the rig frame by rubber washers. These two features help prevent cross-talk when specimens fracture. The lower grip is 'channelled' through two guides, with friction minimised to a negligible level by contacting ball-runners. These guides help prevent 'swing' and 'twist' of the specimen. Extension of the specimen is measured using linear voltage displacement transducers, and the data are logged on a computer. Unlike the extensometer used in the Instron machine, this system of strain measurement is non-contacting, and records the full extension of the specimen. This necessitates the application of a correction factor to the creep rig results to allow for shoulder effects.

Results and Discussion

Stress-strain curves for HIPS A, B, C and D at a constant strain rate are shown in Fig. 1. The elastic moduli and the yield, flow and breaking stresses increase with decreasing rubber content, while the strain at break decreases significantly. The upturn in the flow stress at high strains has been attributed to strain-hardening of the rubber phase[4]. A full report containing results on HIPS B, C and D are given in later paper[5].

Work by Bubeck et al.[6] and Buckley[7] has shown that crazing is responsible for no more than half of the dilatational strain developed during tensile testing of HIPS. It follows that cavitation of the rubber particles is the dominant mechanism in the development of large volume strains. From transmission electron microscopy studies, it is known that cavitation of 'salami' particles occurs through fibrillation of the thin rubber membranes that separate the rigid sub-inclusions. There is also considerable evidence suggesting that crazes are capable of supporting considerable loads,[8,9] therefore it is assumed that once cavitation has occurred, crazing controls the rate of extension of the material. As the crazes extend in parallel with the rubber phase, the macroscopic strain rate is kept constant by maintaining a constant average stress on the crazes. Under these conditions, strain-hardening of the rubber phase necessitates an increasing macroscopic stress, to maintain the required drawing stress on the crazes.

It is not immediately clear, however, why the strain at break should decrease as the rubber content is decreased. As long as there is a reasonable number of craze initiation sites, surface drawing of crazes could theoretically continue until the entire specimen is fibrillated, resulting in almost the same overall strain at failure for materials with different rubber contents.

It is well known that this is not the case. How then does the volume fraction of rubber particles control the overall failure strain of the material ?

Figure 2 shows typical creep curves for HIPS A. The material exhibits an initial elastic response to the applied stress, which is followed by a period in which little dilatation occurs, denoted the 'induction period'[10]. The rate then increases in a non-linear manner to a maximum, after which it decreases. Indeed the post-induction period curve of strain-rate against time for HIPS A is almost bell-shaped. Bucknall and Clayton[10] modelled the creep behaviour of HIPS in terms of craze initiation and craze termination, but in their experiments the tensile strain was limited to 0.06, whereas HIPS A fails at strains exceeding 0.5, and gives creep curves that are significantly non-linear. This contrasts with previous observations[1,10] of a constant (post induction period) creep rate for HIPS. The non-linearity of the creep curves for this material complicates any attempt to predict its lifetime. The reasons for this non-linearity, and for the importance of the rubber phase in optimising the strain at failure of toughened polystyrene, are discussed below.

In HIPS A the decrease in strain rate at high strains indicates an upper limit on the attainable strain. The mean fracture strain for a set of specimens, indicated by the solid circles in Fig. 2, occurs after the onset of macroscopic strain-hardening. As mentioned earlier, the characteristic upturn in stress in the late stages of the stress/strain curve for HIPS (see Fig. 1) can be attributed to strain-hardening of the rubber phase[5] and the decreasing number of unfibrillated rubber particles. It is therefore clear that as a creep specimen extends, the mean stress on the rubber phase increases, while the mean stress on the crazes decreases. Many workers[10,11,12,13] have shown that craze kinetics under creep conditions obey the Eyring rate equation, which describes an exponential dependence of the rate of crazing upon the applied stress. Consequently, strain-hardening rubber particles need take only a small share of the applied load to reduce the rate of crazing considerably. Kramer and Berger[14] found that the probability of craze breakdown, due to disentanglement in the fibrils, decreases with decreasing stress on the craze. This implies that the probability of craze breakdown in HIPS during a creep test, due to fibril disentanglement, decreases at high strain because the mean stress on the crazes is decreasing. Also, the proposal advanced by Sjoerdsma and Boyens, that rupture results from the high density of crazes, implies that reducing the number of crazes, through for example a reduction in the rubber content, produces a more fracture resistant material. The well documented effects of rubber content on fracture strain cast doubt on this proposal.

Given the values of the mean failure strain of HIPS, it can be seen from the shape of the creep curve that the conditional probability of specimen failure increases rapidly after the onset of macroscopic strain-hardening. (The conditional probability, $(dP/d\varepsilon)/P$ is the probability at strain ε that a surviving specimen will fail before reaching strain $(\varepsilon + d\varepsilon)$). If the average stress on the rubber is increasing with strain, and the conditional probability of failure is also increasing with strain, then it follows logically that there is a connection between the two variables. Fundamentally, this relationship could be a direct result of rubber fibrils becoming stressed to the point of failure, resulting in rupture of the particle to form a defect in the material. It is unlikely that failure of a single particle would result in an immediate and catastrophic crack, but rupture of enough particles in close proximity would constitute crack initiation culminating in failure of the specimen.

In a material such as HIPS A, which has a particle volume fraction of 0.35, the area occupied by crazed material is approximately 2/3 that of the adjoining coplanar layer of fibrillated rubber, assuming that the crazes follow the path of least resistance. If the area occupied by rubber particles is large enough in comparison with the area occupied by crazes, the crazes can be stabilised to such an extent that their rate of thickening becomes negligible. This is sometimes observed in creep tests on HIPS A, where the material extends and strain-hardens until the strain rate is almost zero. In the later stages of such a creep test, the rubber becomes increasingly secure against rupture because its rate of extension tends towards zero. The relevance of this observation becomes more apparent as one examines the deformation of materials with lower rubber contents.

With respect to the stabilisation of crazes there are four possibilities, (see Fig. 3)

(1) The rubber particle extends and strain-hardens, but the stress on the surface of the craze is still sufficient for it to continue drawing, taking the adjoining rubber layer with it. Eventually the rubber will rupture, thereby contributing to the ultimate failure of the specimen.

(2) During craze thickening, craze fibril breakdown occurs, resulting in overloading of the adjoining rubber particles. This would again culminate in crack initiation and propagation and failure of the specimen.

(3) Under conditions of medium (or lower) stress applied to a material with a high rubber content, the rubber particle extends, strain-hardens and unloads the adjoining craze, to the

extent that the local strain rate is reduced to zero. The rubber particle should remain intact under these conditions.

(4) At higher applied stresses, the same high rubber content material as in case (3) may deform as in case (1), but if the engineering stress to break the rubber fibrils is higher than the craze drawing stress, the rubber will remain intact and the crazes will continue thickening. As the volume of unfibrillated rubber in the material decreases, the crazes may completely envelop the rubber particles. Under these conditions the stress on the rubber may also be sufficient to fibrillate the hard glassy inclusions in the rubber particles.

The behaviour described in case (4) above has been reported by Maestrini et al.[15] who showed that a multiple inclusion rubber particle can become completely enveloped by a thickening craze, without causing significant craze breakdown. This demonstrates that rubber particles are capable of sustaining loads sufficient to cause craze drawing at the particle's poles. Indeed Starke et al.[16] have recently shown that the stresses within rubber/poly(methyl methacrylate) core-shell particles embedded in a poly(styrene acrylonitrile) matrix can reach levels sufficient to fibrillate the PMMA inclusions. The importance of rubber fibrillation was illustrated by Donald and Kramer[17], who showed that solid rubber particles, which do not fibrillate to a great extent, contract at the equator resulting in breakdown at the craze/rubber interface.

Cases (3) and (4) above represent the ideal situation, where the drawing stress of the crazes is not sufficient to break rubber fibrils. Thus at low macroscopic creep stresses, as the rubber strain hardens it becomes capable of reducing the stress on the surface of the crazes below the drawing stress of the craze. However at high macroscopic stresses, because the ultimate strength of the rubber is greater than the craze drawing stress, when the rubber strain hardens the crazes will continue to thicken, thus enveloping the particle.

The stabilisation of crazes in this way is also important from the point of view of energy absorption. As the stress on the rubber fibrils increases, so the stress on the unfibrillated rubber membranes in series with the rubber fibrils also increases. As a result of this increased stress, fresh craze nucleation can take place. Crazes nucleated at these sites will extend and thicken until the adjoining rubber strain-hardens and promotes new nucleation sites. Thus deformation percolates through the material in a 'slip-stick' manner, resulting in the excellent energy dissipation that is characteristic of these materials.

While existing evidence supports the conclusion that rubber particles stabilise crazes[18,19,20], it should be noted that for deformation to percolate through HIPS, the rubber particle must stabilise the adjoining craze. If this occurs, then the particle survives, as in case (3). However, if the rubber particle does not stabilise the adjoining craze, then the load on the rubber particle will continue to increase, rubber fibril extension will continue, and particle rupture becomes more likely, as in case (1). This hypothesis is supported by evidence presented earlier, which showed that the probability of tensile failure of HIPS increases with increasing mean stress on the rubber phase. It is therefore concluded that rubber particle rupture is the dominant mechanism responsible for tensile failure in HIPS.

It follows from this conclusion that every stressed particle is a potential defect. The volume of rubber fibrillated will increase as the plastic strain in the material increases, thereby increasing the 'risk volume'. The decreasing volume of unfibrillated rubber in the material results in a decreasing number of craze initiation sites and this explains why the strain rate decreases after reaching a maximum. Later discussion will consider how, for a given strain, the fraction of rubber fibrillated (and therefore the risk volume) depends on the level of applied stress. Reducing the number of particles will reduce the number of potential failure points, but it will also reduce the area of rubber relative to that of adjoining crazes, and hence it will increase the load that has to be supported by the fibrillated particle in order to reduce the rate of craze thickening. Examination of the creep curves and the fracture statistics for HIPS A indicates that, on average, the volume fraction of rubber present in the material is enough to produce considerable macroscopic strain hardening. However the wide distribution of failure strains ($\varepsilon_{min}/\varepsilon_{max}$ = 0.3), indicates that the stability of the rubber fibrils might in part be governed by some statistical factor. One such statistical but quasi-random characteristic of rubber toughened polymers is the spatial arrangement of the particles. The positions of the particles are only quasi-random, because of the obvious constraint that the centre to centre distance between two adjacent particles must be greater than the sum of the two particle radii.

The effects of the spatial distribution of the particles on the probability of rubber particle rupture should therefore be addressed. Owing to variations in the spatial distribution of rubber particles, the local deformation behaviour will be governed by the local volume fraction of rubber. Thus an anomalously low local volume fraction of rubber particles in HIPS A will produce behaviour that is more representative of HIPS B or HIPS C or even HIPS D. The probability of failure for this segment of the material will obviously be different from that of a

segment with a higher volume fraction of rubber. From this and earlier arguments, the likelihood of failure of the material will be governed by:

(a) the fraction of the rubber that has fibrillated;

(b) the mean stress on the rubber fibrils;

and (c) the spatial distribution of the rubber particles.

Breakdown Statistics

Figure 4 shows that for HIPS with rubber contents ranging from 2 to 8 wt. %, failure almost never occurs before the induction time is reached. This demonstrates two important points:

- in order for failure to occur, some dilatation is necessary, presumably in the form of crazing and/or rubber cavitation;
- the induction period conveniently defines a lower time limit for failure of HIPS, below which the probability of failure is negligible.

However, materials such as HIPS A are designed to absorb large amounts of energy in impact and creep, well in excess of that absorbed during the induction period. Therefore for most design situations, an understanding of the statistics governing final rupture would be of far more practical value than identifying a lower time limit for fracture, and would serve a real purpose in component design.

In the present study, the Sjoerdsma and Boyens[1] model was compared with failure strain data for specimens of HIPS A extended under different applied stresses. According to Eq. 1, plotting the plastic fracture strain (total strain minus elastic strain) against the logarithm of the probability of survival should yield a straight line. The results shown in Fig. 5 exhibit a distinct non-linearity, which indicates that this model is ineffective in correlating failure data for HIPS A. The plastic failure strains for samples of HIPS A, under applied stresses of 14 MPa and 15 MPa, are plotted against the cumulative probability of survival in Fig. 6. The difference in applied stress appears to have a discernible effect on the failure strain distribution in HIPS, as at a given failure strain the probability of survival increases with increasing creep stress. This implies one of two things: either the mechanism responsible for failure in HIPS is inhibited by the increase in stress, or the number of deformation initiating sites (for a given strain) increases

with increase in applied stress, so that there is an increased concentration of fibrillated rubber, with a lower average strain in the fibrils. It seems more likely that the number of craze initiating sites would increase with applied stress: according to the energy-balance model[21], the number of cavitated rubber particles increases with applied stress, thus producing a greater volume of crazed material.

Several workers[14,22,23] have used Weibull statistics[24] in the general form of Eq. 2 to describe the failure statistics of crazes in cast thin films of polystyrene, and Ritter et al.[25] have demonstrated that the failure strengths of polystyrene samples also follow the two–parameter Weibull equation:

$$P_{sv} = \exp[-\alpha(\varepsilon_p)^{\beta}] \qquad (2)$$

where P_{sv} is the cumulative probability of survival, ε_p is the dilatational strain at failure and α and β are Weibull constants. Sjoerdsma and Boyens considered whether Weibull statistics might be suitable for making lifetime predictions for general purpose polystyrene, and whether a similar approach might also be productive in making lifetime predictions for HIPS. The latter proposal was based on the assumption that homogenous or ungrafted rubber particles act as flaws or crack initiating sites. They discounted the proposal because rubber particles are usually well bonded and serve to stabilise crazes[18,19,20]. Yang et al.[22] have identified the Weibull parameters α and β as measures of the craze strength and of the distribution of craze breakdown strains respectively. Comparison of Eq. 1 with Eq. 2 reveals that the failure distributions predicted by Sjoerdsma and Boyens' model are particular Weibull distributions with scale parameter α (A in Eq. 1) and with shape parameter $\beta = 2$.

Equation 2 is fitted to the failure strain data of HIPS A in Fig. 6. The observed wide distribution of failure strains underlines the difficulty in predicting the lifetime of a single HIPS component. The physical limitation on the number of specimens feasible for any one sample produces bunching of the failure strains, as is noticeable in the results for HIPS A tested at 15 MPa. The origin of this bunching was investigated to determine whether it is a characteristic of the underlying distribution, or a trait of the sampling process and sample size.

Figure 7 shows the results of a computer-based experiment, similar to that of Glandus and Boch[26], in which the survival probabilities were calculated for 30 'specimens' sampled

randomly from a perfect Weibull distribution. The solid line in Fig. 7 represents the probability of survival, P_{sv}, for the perfect Weibull distribution represented by Eq. 2, which was sampled by generating a random sequence of 30 values of P_{sv} in the range $0 < P_{sv} < 1$. The 'fracture strain' values corresponding to the selected survival probabilities, which can be read directly from the ideal population distribution, are arranged in descending order, and the probability of survival for each specimen is estimated in the usual manner, i.e. $P_{sv}(i) = 1 - (i)/(N+1)$, where P_{sv} is the probability of survival of the i^{th} specimen and N is the number of specimens[27]. For example, for 'specimen' i = 10, the survival probability $P_{sv} = 1 - 10/(30+1) = 0.68$. The population distribution was chosen to be similar in breadth and range of 'failure strains' to the failure strain values of HIPS A. The resulting data are plotted in Fig. 7. It can be seen that they bunch around specific strain values, in a fashion similar to that observed for HIPS. This bunching is a feature of the sample size, indicating that the evident bunching observed in the upper curve in Fig. 6 can be attributed to the limited number of specimens, rather than to an actual increased probability of failure at specific strains. This point is substantiated by examining results for HIPS A tested under an applied stress of 14 MPa, also shown in Fig. 6. A larger sample size (68) was used in this test, resulting in increased smoothness of the data. Thus while testing a sample of only 30 specimens does produce some scatter and bunching, this method should give a reasonable representation of the underlying population distribution.

Another notable feature of Fig. 6 is the overestimation given by Eq. 2 of the survival probability at high strains. This characteristic, which is reproducible, was also observed for other grades of HIPS[4]. It seems reasonable to conclude that it is a result of macroscopic strain-hardening, which serves to produce a sharp failure strain cut-off point i.e. the distribution is significantly negatively skewed. The skewness of a distribution gives a measure of its asymmetry i.e. a negatively skewed distribution is one that has a concentration of values at the more positive end of the distribution. It is postulated that, given the non-linear stress-strain relationship for rubbers, the stress on the rubber phase may provide a better basis for obtaining a Weibull distribution. This hypothesis is discussed in a later paper.

Conclusions

It has been shown that plastic dilatation is necessary for failure to occur at room temperature in HIPS. Consequently, calculation of the induction time as a function of stress (using the Eyring equation) defines a lower limit below which the probability of failure under creep conditions is

negligible. However, for practical design purposes, prediction of the mean failure time for the material would be of much greater value. Following the onset of macroscopic strain-hardening, there is a rapid increase in the conditional probability of failure of HIPS, which has been attributed to a sudden increase in the mean stress on the fibrillated rubber phase. Consequently it has been concluded that the dominant factors controlling failure of HIPS are: (a) the fraction of rubber fibrillated; (b) the mean stress on the rubber fibrils; and (c) the spatial distribution of the rubber particles.

It was found that the success achieved by Sjoerdsma and Boyens, in correlating failure strain data for a single grade of HIPS, could not be repeated when their model was applied to another grade of HIPS. The two–parameter Weibull equation gave an improved correlation between the failure of HIPS A and the strain on the material. However, the treatment has two weaknesses: (a) the fitted Weibull parameters are purely empirical; and (b) the probability of survival is overestimated by Eq. 2 at high strains. This latter feature, coupled with the observation that strain is non-linear with both time and stress, suggests that the mean stress on the rubber phase might be a better basis than mean strain for obtaining a Weibull distribution. This is examined in a subsequent publication[4].

Acknowledgements

The authors thank the Dow Chemical Company for permission to publish this work.

References

1. Sjoerdsma, S. D. and Boyens, J. P.H, Polym. Eng. Sci., **34** (1994) 86
2. O' Connor, B., Bucknall, C. B. and Hahnfeld, J. L., *"Deformation Yield and Fracture of Polymers"* Paper 81, 10th International Conference Churchill College, Cambridge (1997)
3. Lauterwasser, B. D., Kramer, E. J., Phil. Mag., **A39** (1979) 469
4. Soares, V.L.P., PhD thesis, Cranfield University, Bedford. UK (1994)
5. O' Connor, B., Bucknall, C. B. and Hahnfeld, J. L., to be published.
6. Bubeck, R. A., Buckley, D. J., Kramer, E. J., and Brown, H. R. J., Mater. Sci. **26** (1991) 6249
7. Buckley, D. J. PhD thesis, Cornell University, New York (1991)
8. Sauer, J. A., J. Appl. Phys., **20** (1949) 507
9. Donald, A. M. and Kramer, E. J., **27** (1982) 3729

10. Bucknall, C. B. and Clayton, D., J. Mater. Sci., **7** (1972) 202
11. Bucknall, C. B., Davies, P. and Partridge, I. K., J. Mater. Sci., **21** (1986) 307
12. Regel, V. R., Sov. Phys. Tech. Phys., **1** (1956) 353
13. Kambour, R. P., J. Polym. Sci., **D7** (1973) 1
14. Kramer, E.J., Berger, L.L., Adv. Polymer Sci., **91/92** (1990) 1
15. Maestrini, C, Castellani, L., Merlotti, M. and Vighi, M., Polymer **33** (1992) 1556
16. Starke, J. U., Godehardt, R., Michler, G. H. and Bucknall, C. B., J. Mater. Sci. **32** (1996)
17. Donald, A. M. and Kramer, E. J., J. Mater. Sci., **17** (1982) 2351
18. Cook, D. G., Plumtree, A. and Rudin, A., Plastics, Rubber Compos. Process. Appl., **20** (1993) 219
19. Hobbs, S. Y., Polym. Eng. Sci, **26** (1986) 74
20. Manson, J. A., Hertzberg, R. W., J. Polym. Sci., **11** (1973) 2483
21. Bucknall, C. B. in *"The Physics of Glassy Polymers"* editors R. N. Haward and R. J. Young, Chapman and Hall, London, (1997)
22. Yang, A. C-M., Kramer, E. J., Kuo, C. C. and Phoenix, S. L., Macromolecules, **19** (1986) 2010
23. Berger, L.L., Macromolecules., **23** (1990) 2926
24. Weibull, W., J. Appl. Mech., **18** (1951) 293
25. Ritter, J. E., Stevens, J. M. and Jakus, K., J. Mater. Sci., **21** (1979) 171
26. Glandus, J. C., Boch, P. J., J. Mater. Sci., **24** (1984) 761
27. Johnson, R. A. *"Miller and Freund's Probability and Statistics for Engineers"* fifth ed. Prentice-Hall International, Inc., Englewood Cliffs, (1994)

List of Figures

Fig. 1

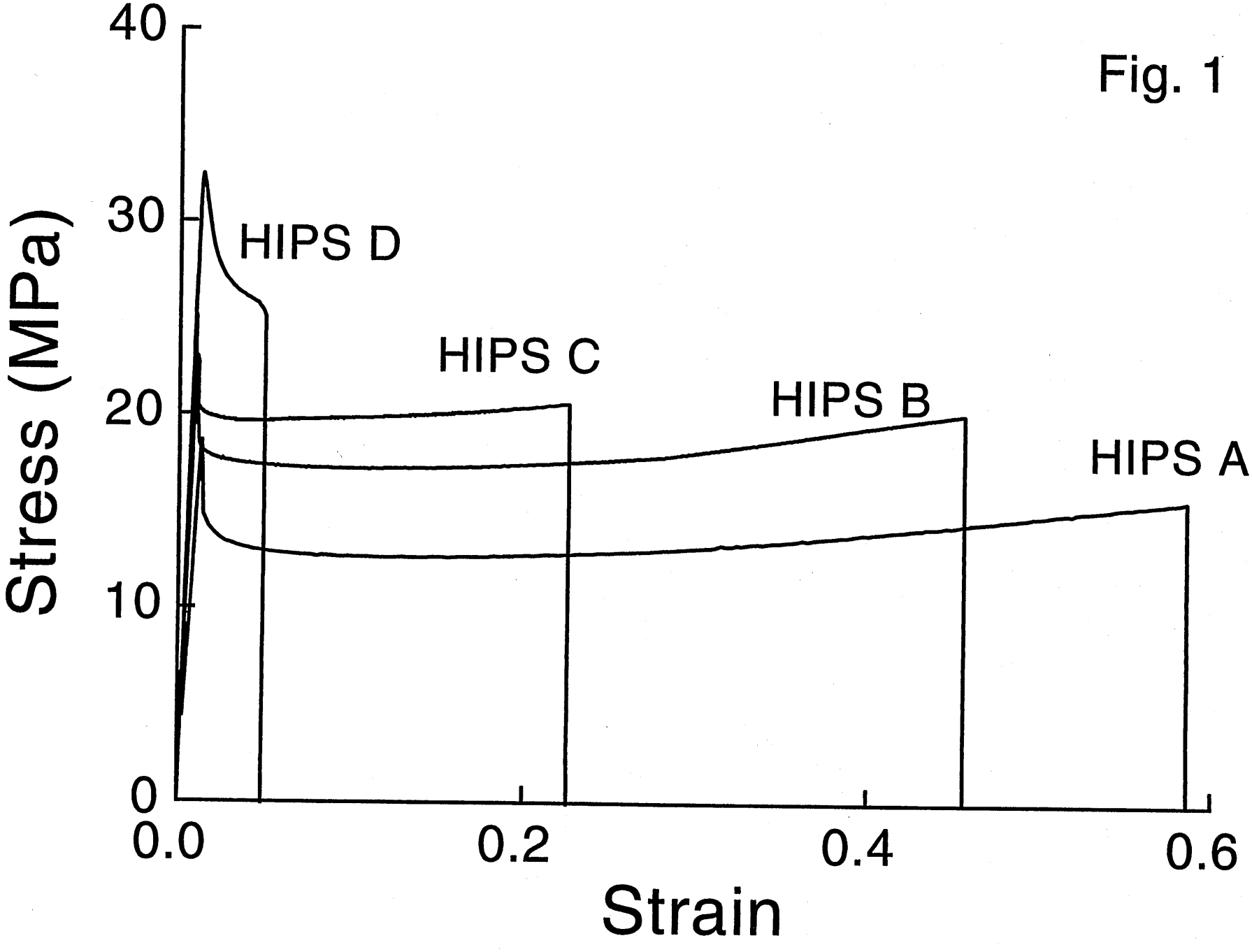
40
30
20
10
0
Stress (MPa)
HIPS D
HIPS C
HIPS B
HIPS A
0.0
0.2
0.4
0.6
Strain

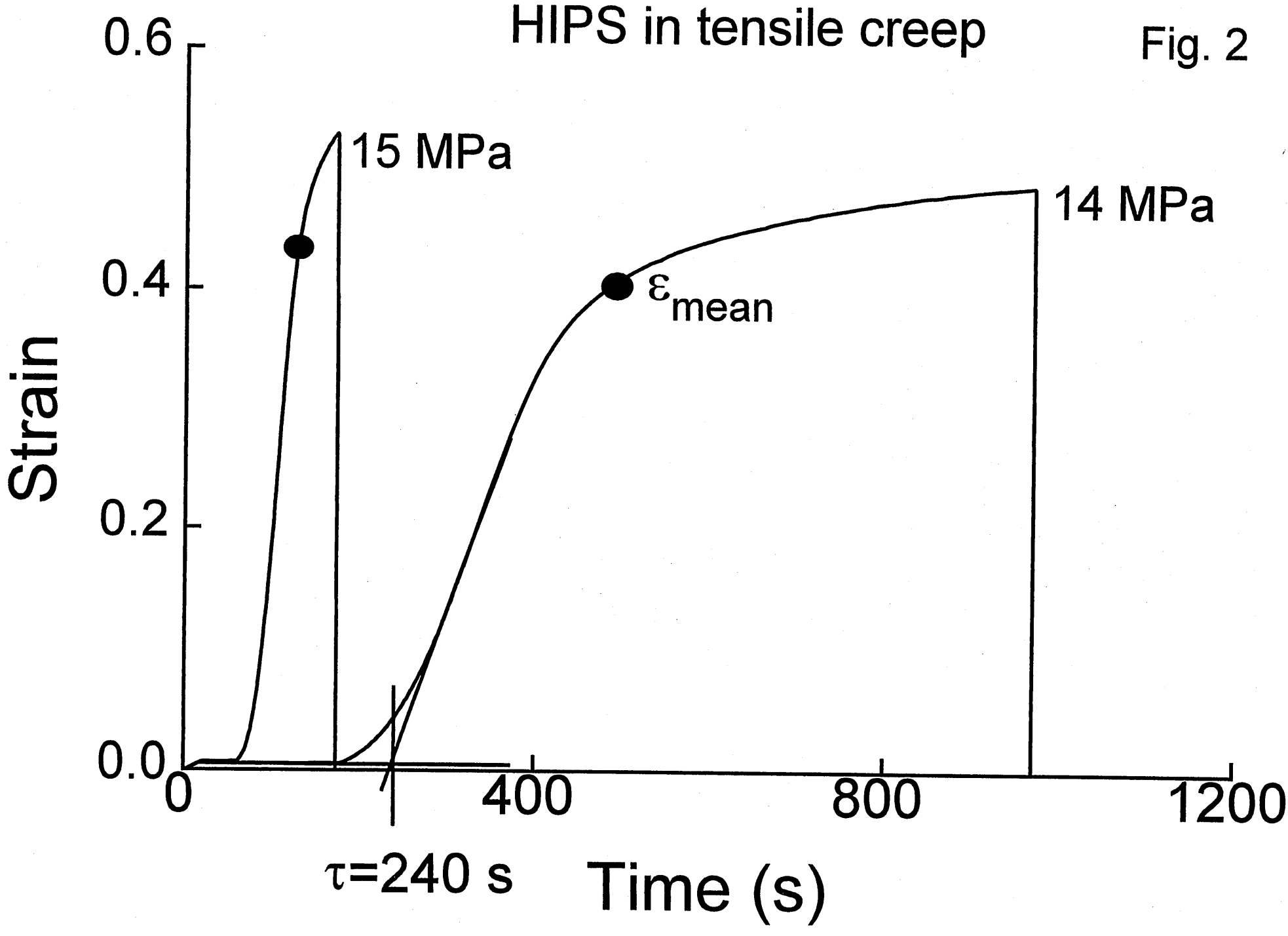
HIPS in tensile creep
Fig. 2
0.6
0.4
0.2
0.0
Strain
15 MPa
14 MPa
ε_{mean}
0
400
800
1200
τ=240 s
Time (s)

Fig. 3

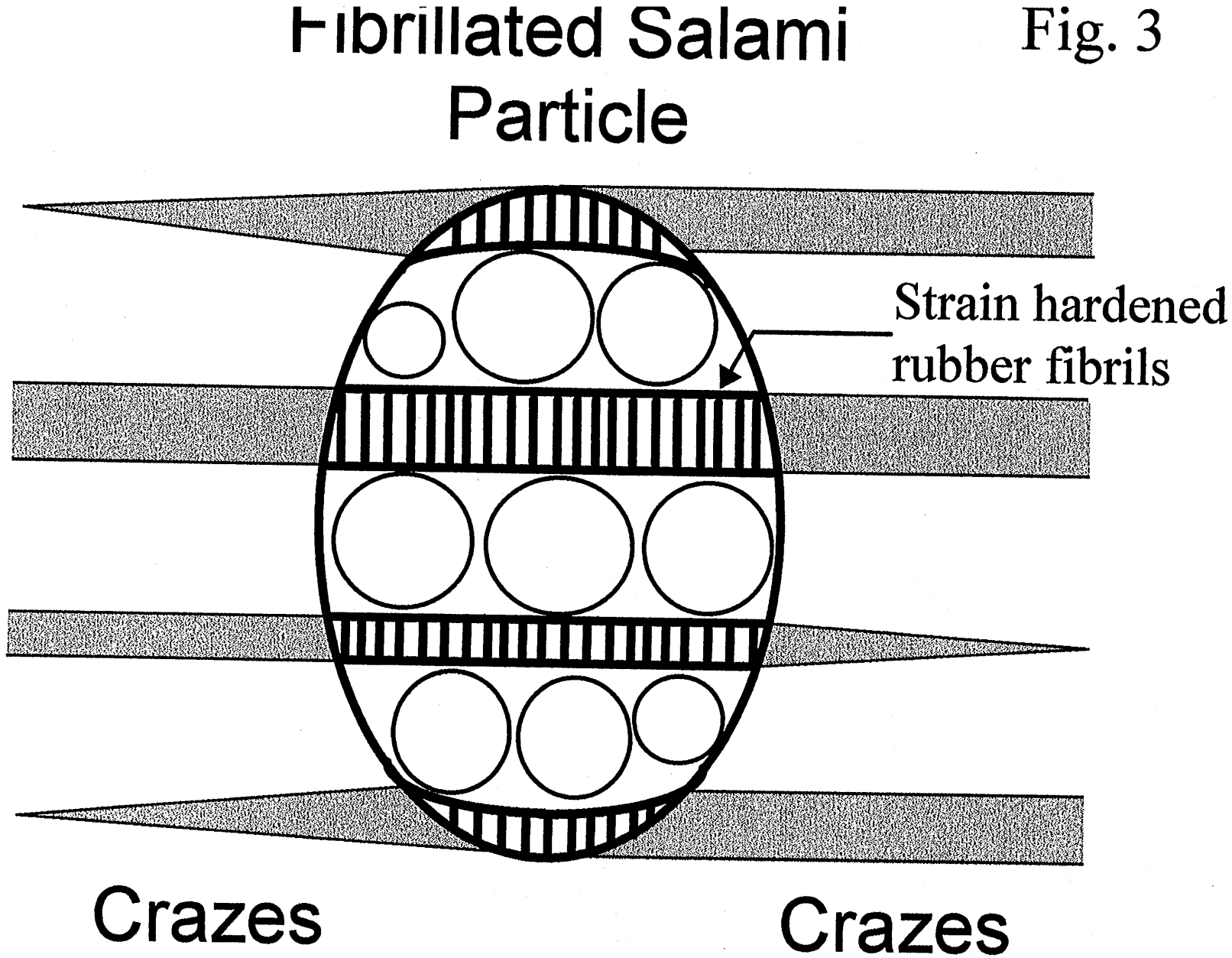
Fibrillated Salami Particle
Strain hardened rubber fibrils
Crazes
Crazes

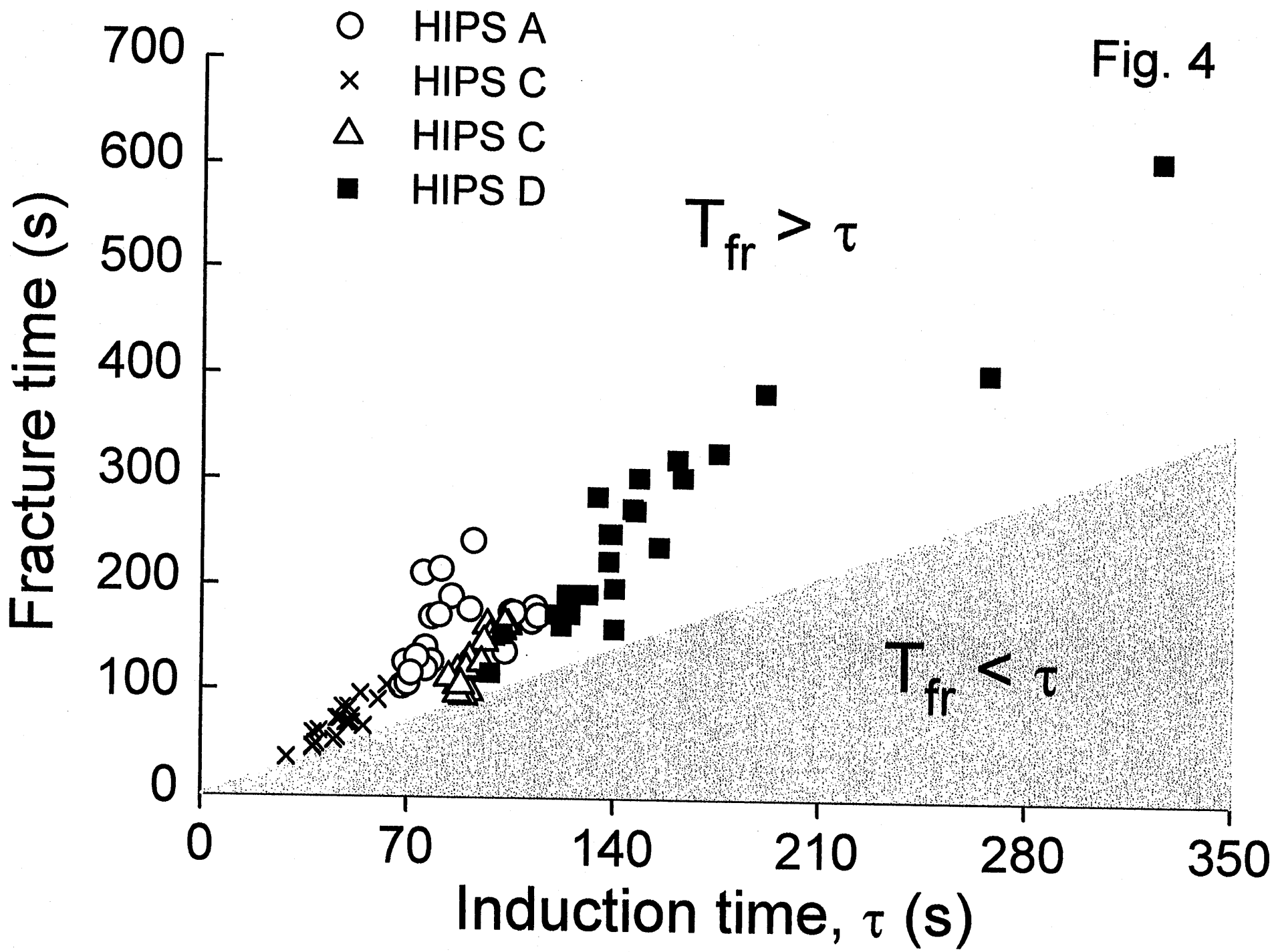
HIPS A
HIPS C
HIPS C
HIPS D
$T_{fr} > \tau$
$T_{fr} < \tau$
Fracture time (s)
Induction time, τ (s)
0
100
200
300
400
500
600
700
0
70
140
210
280
350

Fig. 4

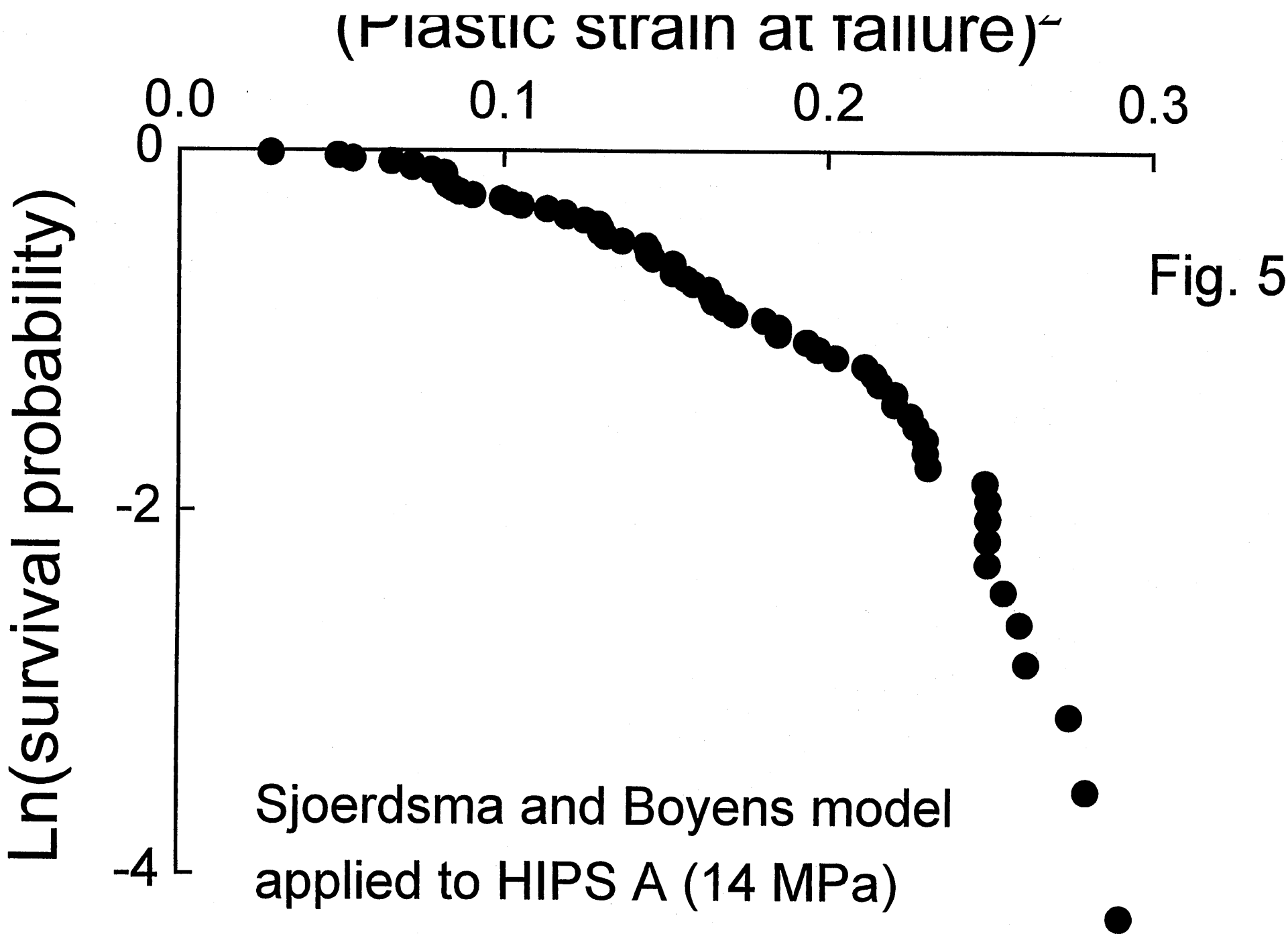
(Plastic strain at failure)²
0.0
0.1
0.2
0.3
0
-2
-4
Ln(survival probability)
Sjoerdsma and Boyens model
applied to HIPS A (14 MPa)

Fig. 5

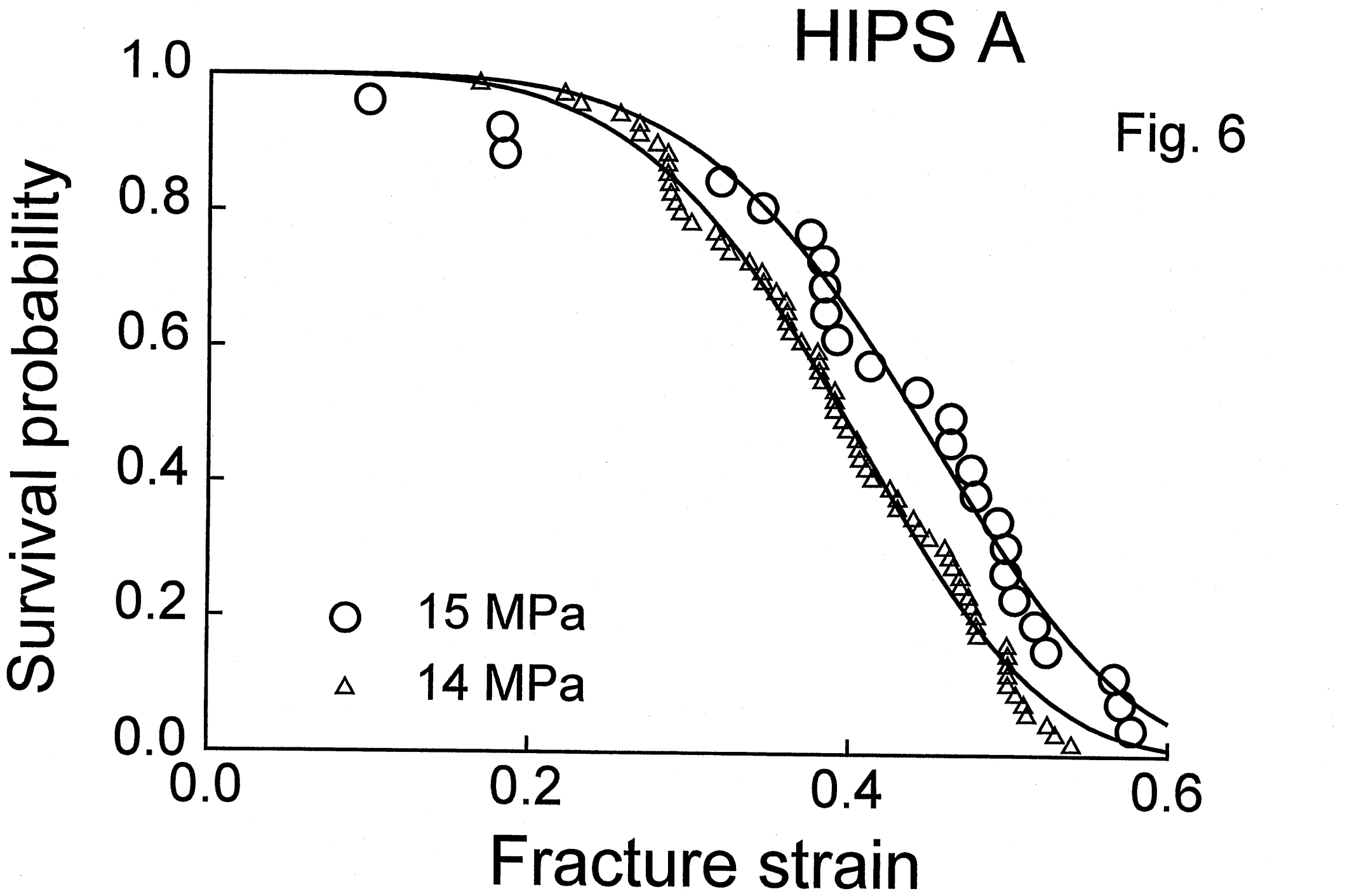
HIPS A
Survival probability
1.0
0.8
0.6
0.4
0.2
0.0
0.0
0.2
0.4
0.6
Fracture strain
15 MPa
14 MPa

Fig. 6

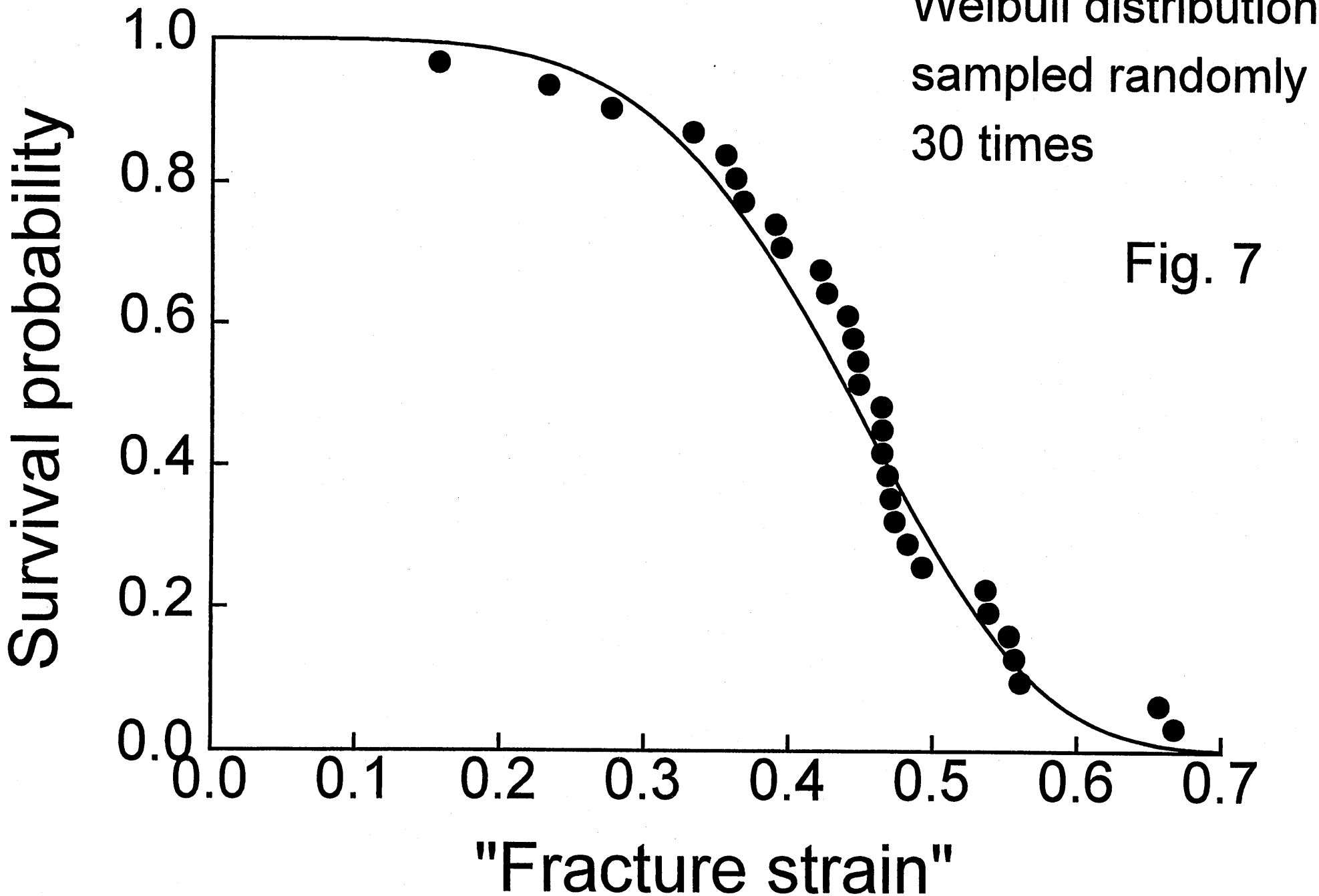
Weibull distribution
sampled randomly
30 times
Survival probability
1.0
0.8
0.6
0.4
0.2
0.0
0.0
0.1
0.2
0.3
0.4
0.5
0.6
0.7
"Fracture strain"

Fig. 7

APPENDIX 2

The following tables contain the fracture strain results for the materials investigated in uni-axial creep in this study. Absolute values of fracture strain are quoted, and fracture strain is taken as the plastic strain at failure, defined as the total strain at failure minus the initial elastic response: $\varepsilon_{fr} = (\varepsilon_t - (\sigma_{app}/E))$. Tests carried out in the creep rig have had a correction factor of 1.2 applied to the results.

HIPS8; 15 MPa
0.09942
0.18188
0.18387
0.31899
0.34482
0.37463
0.38258
0.38357
0.38456
0.39152
0.41238
0.44219
0.46305
0.46305
0.47597
0.47895
0.49286
0.49783
0.49783
0.50379
0.5167
0.52366
0.56638
0.57035
0.57731

HIPS8; 14 MPa	
0.16804	0.43004
0.22084	0.43004
0.2308	0.44
0.25571	0.44399
0.26766	0.44996
0.26766	0.45993
0.27862	0.46291
0.28559	0.46491
0.28559	0.46989
0.28559	0.46989
0.28659	0.47487
0.28759	0.47686
0.29057	0.47985
0.29356	0.47985
0.30054	0.48085
0.31548	0.49878
0.31847	0.49977
0.32444	0.49977
0.3364	0.49977
0.34437	0.49977
0.34536	0.50475
0.35333	0.50974
0.35931	0.51173
0.36031	0.52468
0.36031	0.52966
0.3623	0.53962
0.36927	
0.37923	
0.38023	
0.38023	
0.38222	
0.39019	
0.39019	
0.39019	
0.39517	
0.39816	
0.40414	
0.40514	
0.40613	
0.41012	
0.4141	
0.42506	

HIP6; 18.5 MPa
0.08354
0.12104
0.12902
0.136
0.15096
0.18087
0.24071
0.25068
0.26066
0.26066
0.32049
0.33046
0.34044
0.34044
0.35041
0.36038
0.36038
0.38033
0.41024
0.42022

HIPS6; 16.2 MPa
0.06072
0.13197
0.13747
0.14022
0.14163
0.16497
0.1658
0.1918
0.1958
0.21163
0.21447
0.2233
0.2308
0.2518
0.2533
0.2658
0.27163
0.28413
0.2883
0.28913
0.3133
0.31697
0.31747
0.31747
0.34913
0.35472
0.35538
0.3633
0.3758
0.3858
0.38722
0.39405

HIPS6; 13.7 MPa
0.04013
0.10946
0.11046
0.14446
0.14655
0.15363
0.17213
0.18446
0.19513
0.1978
0.19863
0.19946
0.21955
0.22196
0.22696
0.22946
0.23863
0.25363
0.2558
0.2603
0.28113
0.28863
0.3103

HIPS4; 22.5 MPa
0.03266
0.0408
0.04375
0.04966
0.05064
0.05389
0.05457
0.06835
0.0834

HIPS4; 19.6 MPa
0.0734
0.0868
0.09169
0.09354
0.10786
0.11376
0.1152
0.11747
0.12194

HIPS4; 16.2 MPa
0.03668
0.04643
0.07023
0.07229
0.08981
0.10034
0.12129
0.12228
0.12666

0.09589
0.10967
0.11557
0.12934
0.13918
0.14902
0.14902
0.15492
0.15885
0.16869
0.16869
0.16869
0.16869
0.17656
0.17853
0.17853
0.17853
0.19525
0.19821
0.19821
0.19821
0.19821
0.19821
0.20312
0.21788
0.21985
0.22772
0.24739
0.24739
0.25526
0.25723
0.26707
0.27691
0.27691

0.1227
0.12295
0.13163
0.14115
0.14882
0.15506
0.16036
0.17966
0.18337
0.18472
0.21404
0.22028
0.22289
0.22837
0.23562
0.23595
0.23705
0.24775
0.25534
0.28399

0.14277
0.15615
0.15731
0.15846
0.17268
0.174
0.19176
0.19449
0.19829
0.21068
0.21456
0.21787

HIPS2; 26.5 MPa
0.01333
0.01923
0.03473
0.04583
0.04923
0.05853
0.06933

HIPS2;25 MPa
0.0119
0.01459
0.01663
0.02201
0.02397
0.02446
0.03473

H8:0.56; 13.7 MPa
0.08639
0.09356
0.10972
0.11181
0.11347
0.16039
0.18189

0.07573
0.07723
0.07733
0.07983
0.08623
0.08973
0.09633
0.11093
0.11433
0.11633
0.11933
0.12133
0.12183
0.12233
0.12733
0.13933

0.0375
0.04239
0.04647
0.05788
0.05788
0.05813
0.06522
0.06563
0.06767
0.07011
0.07011
0.07191
0.07337
0.07769
0.08291
0.08479
0.08691
0.08968
0.09294
0.09392
0.09408
0.09865
0.10028
0.10085
0.10395
0.10696
0.10965
0.11006
0.11128
0.11283
0.12278
0.1421
0.14512

0.19056
0.20056
0.20206
0.21306
0.21706
0.21806
0.22489
0.23081
0.23139
0.23431
0.24389
0.26806
0.27156

H6:0.42; 23 MPa
0.03678
0.06098
0.06998
0.11478
0.13758
0.14978
0.15678
0.15678
0.16578

H4:0.28; 26.5 MPa
0.03022
0.04112
0.04632
0.05592
0.06852
0.08002
0.09032
0.09062
0.09822

H2:0.14; 31.5 MPa
0.01201
0.01221
0.01431
0.01651
0.01881
0.02061
0.02171
0.02641
0.02831

0.16998
0.17578
0.18778
0.19578
0.21278
0.22878
0.23378
0.23378
0.24578
0.24778
0.24778
0.24878
0.25678
0.26978
0.28378
0.29078
0.31878

0.10862
0.11542
0.13252
0.14022
0.14482
0.14722
0.14752
0.14882
0.14942
0.15222
0.15782
0.16322
0.17442
0.18142
0.18922
0.19992

0.02881
0.02901
0.03161
0.03311
0.03451
0.03741
0.04251
0.04501
0.04591
0.05621
0.05781
0.06211
0.06501
0.06551
0.07431
0.07491
0.08991

H6:0.50; 22.5 MPa
0.06776
0.07056
0.07106
0.10554
0.10584
0.11683
0.12093
0.13092
0.13772
0.14861
0.15461
0.1579
0.1584
0.16
0.1674
0.18079
0.18839
0.19458
0.20717
0.20957
0.23076
0.23176
0.23486
0.24965

H6:0.50; 21 MPa
0.05169
0.06299
0.06419
0.06659
0.08698
0.09168
0.10178
0.10968
0.12287
0.12397
0.12797
0.13277
0.14947
0.15287
0.17026
0.17286
0.17456
0.17626
0.18096
0.19206
0.19866
0.21295
0.24995

H4:0.50; 33 MPa
0.247
0.253
0.271
0.306
0.319
0.329
0.331
0.37
0.375
0.398
0.423
0.457
0.458
0.463
0.491
0.503
0.551
0.59
0.623

H4:0.50; 28 MPa
0.29053
0.3125
0.32747
0.34145
0.35742
0.36841
0.40335
0.40934
0.4333
0.4353
0.4363
0.47124
0.48522
0.55011
0.55311
0.5571
0.56509
0.69588

HIPS8: 15 MPa Pre-loaded to 16.5 MPa
0.17172
0.21572
0.23572
0.24172
0.31672
0.34172
0.37172
0.39872
0.41272
0.43172
0.44172
0.45672
0.47172
0.47172
0.48172
0.48172
0.48472
0.49172
0.50572
0.51172
0.55172
0.56172
0.56972
0.58172
0.59172

ABS8; 26 MPa
0.32541
0.34541
0.3654
0.3844
0.3854
0.3954
0.40539
0.43539
0.43539
0.45538
0.45538
0.46538
0.47538
0.47538
0.48538
0.49538
0.50537
0.50537
0.50537
0.52337
0.52537
0.52537
0.52737
0.55448

ABS6; 31.5 MPa
0.2922
0.36927
0.3766
0.37747
0.37817
0.38793
0.40101
0.41757
0.42647
0.43152
0.43501
0.4358
0.44443
0.44547
0.44957

ABS6; 24.5 MPa
0.07406
0.11122
0.16822
0.16964
0.23322
0.24656
0.25822
0.26972
0.27406
0.28989
0.29739
0.29989
0.31072
0.33572
0.34531

ABS4; 37.5 MPa
0.14312
0.17637
0.22224
0.22624
0.23115
0.24827
0.25048
0.25689
0.25869
0.25939
0.2649
0.2704
0.28573
0.28833
0.29534

0.45123
0.45419
0.48907
0.4943
0.49604
0.50563
0.52307

0.34556
0.35656
0.36656
0.36706
0.37822
0.39322
0.39989
0.40906
0.41572
0.43497

0.30085
0.30676
0.31607
0.33139
0.3404
0.37445

ABS4; 35 MPa
0.1477
0.20272
0.21192
0.24113
0.24493
0.25214
0.25364
0.26284
0.26294
0.26904
0.27925
0.28395
0.28765
0.29285
0.29585
0.29625
0.29675
0.30746
0.30866
0.31196
0.33436
0.33727

ABS2; 47.5 MPa
0.08655
0.09025
0.11825
0.13325
0.13525
0.14125
0.14225
0.14525
0.15425
0.15425
0.16525
0.16525
0.17125
0.17125
0.17225
0.17725
0.18425
0.18725
0.18925
0.19325
0.19525
0.19625
0.20725
0.21425
0.22025
0.23825
0.24025

ABS2; 39.5 MPa
0.06833
0.07863
0.10903
0.10923
0.11353
0.11703
0.11893
0.12343
0.12653
0.12843
0.13223
0.13563
0.13843
0.14353
0.14973
0.15083
0.15453
0.16603
0.17113
0.17473
0.18033
0.19053

A8:0.55; 34 MPa
0.26552
0.27852

A6:0.38; 37.5 MPa
0.14784
0.18484

A4:0.24; 42 MPa
0.08727
0.10327

0.33052
0.34952
0.35852
0.36352
0.38852
0.40452
0.40752
0.40852
0.41452
0.42652
0.43652
0.45752
0.46352
0.46752
0.47752
0.53752
0.54352
0.54752
0.54952
0.59152
0.60712
0.64152
0.65852
0.66552
0.69052

0.20284
0.23284
0.27284
0.28384
0.30684
0.33184
0.35184
0.35284
0.36284
0.36984
0.38984
0.39084
0.39684
0.41484
0.43184
0.43384
0.43884
0.44784
0.45184
0.46184

0.10427
0.12727
0.14927
0.15127
0.16127
0.17127
0.18427
0.19327
0.20027
0.20227
0.20227
0.21327
0.21627
0.21627
0.21927
0.22027
0.22327
0.22927
0.22927
0.23627
0.24627
0.24627
0.25227
0.28627

A2:0.12; 57.5 MPa
0.01202
0.01292
0.01602
0.02102
0.02602
0.02702
0.03602
0.04102
0.04202
0.04402
0.04802
0.05102
0.06002
0.06202
0.06502
0.06602
0.07702

0.07702
0.07802
0.07902
0.09302
0.11002
0.11332

AIM; 16.7 MPa
0.07871
0.11628
0.1401
0.14093
0.14195
0.18272
0.20233
0.21022
0.21022
0.21219
0.21813
0.2211
0.2211
0.22507
0.23402
0.26952
0.28228
0.28431
0.28634
0.33971
0.35531
0.36304
0.36681
0.36786
0.3731
0.39524
0.42397
0.45085
0.46059
0.57122

AIM; 15.7 MPa
0.08852
0.17281
0.23906
0.24101
0.24701
0.25302
0.25402
0.26307
0.27114
0.28025
0.28634
0.31392
0.33972
0.34283
0.34491
0.35219
0.37206
0.38363
0.40054
0.4197
0.42612
0.43469
0.4541
0.46494
0.50211

AIM:0.55; 20 MPa
0.01389
0.02989
0.04589
0.05889
0.06089
0.06189
0.06289
0.07289
0.08589
0.08889
0.13089
0.13189
0.13889
0.14189
0.15389
0.18289
0.18489
0.20989
0.21089
0.21889
0.23689
0.23989
0.24689
0.28889
0.30189
0.30489
0.32889